Dissertation

submitted to the

Combined Faculties for the Natural Sciences and for Mathematics

of the Ruperto-Carola University of Heidelberg, Germany

for the degree of

Doctor of Natural Sciences

presented by:

Diplom-Biologe Stefan Reuscher

born in: Bergisch Gladbach

Functional characterization of the *Arabidopsis thaliana* gene *Cysteine Three Histidine 2*

Referees: Prof. Dr. Ute Krämer

Prof. Dr. Rüdiger Hell

Date of oral exam:

Summary

The aim of this thesis was to functionally characterize the *Cysteine Three Histidine 2* (*CTH2*) gene in the model plant *Arabidopsis thaliana*, which is a candidate for a role in plant iron homeostasis. *At*CTH2 belongs to the family of tandem zinc-finger proteins (TZF) which are known to bind and initiate the degradation of mRNAs in other organisms. The closest homologue of *At*CTH2 in yeast is negatively regulating the stability of a group of specific transcripts under iron-deficient conditions. Heterologous expression of an *Arabidopsis CTH2* cDNA can complement a yeast *cth1Δcth2Δ* mutant.

Here it was shown that *At*CTH2 partly co-localizes with a marker of plant stress-granules in *Arabidopsis* protoplasts. Localization to these sites of transcript degradation is an indication that CTH2 plays a role in post-transcriptional regulation of gene expression by influencing transcript stability. Two mutants carrying T-DNA insertions in *CTH2* were identified and characterized. The two mutants showed different phenotypes, which was attributed to different partial *CTH2* transcripts originating at the *CTH2* locus.

The results suggested that the partial transcript found in *cth2-1* caused a dominant hyper-sensitivity to iron deficiency, and possibly represents a gain-of-function allele. Most affected were the youngest leaves, which showed a drastic reduction of chlorophyll concentrations and reduced growth, when compared to wild-type plants grown under the same conditions. The total content of iron in the youngest leaves was not affected by the *cth2-1* mutation, which showed that long-distance iron reallocation under Fe-deficient conditions is not disturbed.

The *cth2-2* allele caused sporophytic male sterility, and is recessive. In homozygous *cth2-2* plants tetrads of microspores are found, but instead of separating into individual microspores, the cells enlarged, showed granular structures, and eventually degenerated. In accordance with this, the activity of the *CTH2* promoter was localized to the connective tissue during the release of microspores from tetrads. The developmental defect might be caused by a disturbed iron homeostasis, since iron content was lower in *cth2-2* anthers then in wild-type anthers. A microarray analysis identified several candidate pathways and categories of genes, in which transcript levels are over-proportionately misregulated in *cth2-2* anthers compared to wild-type anthers.

In summary, it was shown that *CTH2* has a role in *Arabidopsis thaliana* iron homeostasis and is critical for anther development. In both roles *CTH2* is the first described RNA-binding protein in a plant to act in these roles.

Zusammenfassung

Das Ziel dieser Arbeit war es das *Cysteine Three Histidine 2* (*CTH2*) Gen der Modellpflanze *Arabidopsis thaliana*, mit Hinblick auf eine mögliche Rolle in der pflanzlichen Eisenhomöostase funktionell zu charakterisieren. *At*CTH2 gehört zur Familie der Tandem Zink-Finger Proteine (TZF), von denen aus anderen Spezies bekannt ist, dass sie an mRNAs binden können und so deren Abbau einleiten. Dass am nächsten verwandte Protein aus Hefe, *Sc*CTH2 reguliert die Genexpression in Hefe unter Eisenmangelbedingungen durch den Abbau einer spezifischen Gruppe von Transkripten. Eine *cth1Δcth2Δ* Hefemutante kann durch heterologe Expression einer *Arabidopsis CTH2* cDNA funktionell komplementiert werden.

Durch transiente Expression in *Arabidopsis* Protoplasten konnte gezeigt werden, dass *At*CTH2 teilweise in „plant stress granules“ lokalisiert ist. Die teilweise Lokalisierung an Orten des Transkript-Abbaus ist ein Indiz dafür, dass CTH2 die Transkript-Stabilität negativ beeinflusst. In dieser Arbeit wurden zwei T-DNA Insertionsmutanten mit Insertionen im *CTH2* Lokus identifiziert und charakterisiert. Es stellte sich heraus, dass diese Mutanten unterschiedliche Phänotypen zeigen, was auf unterschiedliche partielle *CTH2* Transkripte zurückgeführt werden konnte.

Ein partielles *CTH2* Transkript, welches in der *cth2-1* Mutante gefunden wurde, verursachte eine dominante Hypersensitivität gegenüber Eisenmangel, und repräsentiert möglicherweise ein „gain-of-function“ Allel. Am stärksten betroffen waren die jüngsten Blätter, welche eine drastische Verringerung des Chlorophyllgehaltes und ein verringertes Wachstum im Vergleich zum Wildtyp zeigten. Es konnte ferner gezeigt werden, das der Gehalt an Fe in den jüngsten Blättern durch die *cth2-1* Mutation nicht beeinflusst wurde, was zeigt, dass die Reallokation von Eisen unter Eisenmangelbedingungen nicht gestört war.

Das rezessive *cth2-2* Allel bewirkte die sporophytische männliche Sterilitat der Pflanzen. In homozygoten *cth2-2* Pflanzen wurden zwar Mikrosporen gefunden, allerdings entwickelten sich diese nicht zu reifem Pollen. Stattdessen wurden vergrößerte Zellen mit granulären Strukturen gefunden, die später degnerierten. Dazu passend war der *CTH2* Promoter während der Freisetzung der Mikrosporen aus den Tetraden aktiv im Konnektivgewebe. Die Antheren von *cth2-2* Pflanzen enthielten weniger Eisen als Antheren von WT oder *cth2-1* Pflanzen, was auf eine mögliche Rolle von *CTH2* in der Eisenhomöostase während der Antherenentwicklung hinweist. Durch Transkriptmengenanalyse in Antheren mittels „Microarrays“ konnten verschiedene Stoffwechselwege und Kategorien von Genen gefunden werden, die im Vergleich zum Wildtyp in *cth2-2* Antheren dereguliert sind.

Zusammenfassed wurde gezeigt, dass *CTH2* eine Rolle beim Wachstum unter Eisenmangelbedingungen spielt und für die Entwicklung des männlichen Gametophyten erforderlich ist. In beiden Funktionen ist es das erste beschriebene RNA-bindende Protein in Pflanzen.

List of Abbreviations and short gene names

AA	amino acid
ABA	abscisic acid
amiRNA	artificial microRNA
ARE	AU-rich element
bp	base pairs
CaMV	cauliflower mosaic virus
CHX	Cation H^+ exchanger
CLSM	confocal laser-scanning microscopy
CTH	Cysteine three histidine
DNA	deoxyribonucleic acid
e^-	electron
EDTA	ethylen-diamine-tetraacetate
EDDHA	ethylene-diamine-N,N'-bis(2-hydroxyphenylacetic acid)
g	standard gravity, 9.80665 m s^{-2}
GA	giberrellic acid
GFP	Green fluorescent protein
GUS	Glucuronidase
h	hour
HBED	N,N′-bis(2-hydroxybenzyl)-ethylene-diamine-N,N′-diacetic acid
HG	Hoagland's medium
HS	heat shock
ICP-AES	inductively-coupled plasma atomic emission spectrometry
kb	kilobases
KO	knockout
LB	lysogeny broth medium
MES	2-(*N*-morpholino)ethanesulfonic acid
min	minute
mRNP	messenger ribonucleoprotein
MS	Murashige and Skoog medium
NA	nicotianamine
NAS	Nicotianaminesynthase
NADH	nicotinamid adenine dinucleotide, reduced form
NPTII	Neomycin Phosphotransferase II
OD	optical density
ON	overnight (12-16 h)
p.a.	*pro analysi* (for analysis)
PB	processing body
PCR	polymerase chain reaction
PEG	polyethylene glycol
ppm	part per million
PPT	phosphinothricin
qPCR	quantitative PCR
RFP	Red fluorescent protein
RNA	ribonucleic acid
ROS	reactive oxygen species

rpm	revolutions per minute
rps	revolutions per second
RT	room temperature (*ca.* 20 °C)
RTL	relative transcript level
s	second
SD	standard deviation
SE	standard error
SG	stress granules
SL	sphingolipid
TAE	tris-acetate EDTA
T-DNA	transfer DNA
TTP	Tristetraprolin
Tris	2-amino-2-hydroxymethyl-propane-1,3-diol
TZF	tandem zinc finger
UTR	untranslated region
v/v	volume per volume
w/v	weight per volume
WT	wild type
X-Gluc	5-Bromo-4-chloro-3-indolyl-β-D-glucuronide
Y3H	yeast three-hybrid

Table of contents

1 Introduction

1.1 Origin and chemical properties of iron

Iron (Fe) is a chemical element with the atomic number 26 and belongs to the first transition metal series. The most abundant stable isotope is ^{56}Fe. All Fe in the universe was produced by nucleosynthesis in stars (Burbidge, 1957). In this process ^{56}Fe is the last stable element in a series of nuclear fusion reactions. Fe is the sixth most abundant element in the universe. Since the inner and outer parts of the core of the earth are thought to consist of an Fe-Ni alloy, Fe is the most abundant element on Earth. However, in the Earth's crust it is only the fourth most abundant element, constituting 5% after O, Si and Al (Scheffer et al., 2002). Naturally, Fe is almost never found in its metallic form because it readily oxidizes in the presence of O_2. Most Fe is found in the form of oxides, of which 16 different species exist (Cornell and Schwertmann, 2003). Oxidation states of Fe from -2 to +6 are known, with ferrous (Fe^{II}) and ferric (Fe^{III}) Fe being the most abundant oxidation states in nature. Fe oxides form common minerals such as goethite (α-FeO(OH)) or hematite (γ-FeO(OH)), which differ by their crystal structure (Scheffer et al., 2002).

Fe is also by far the most abundantly used metal in industry. Fe is primarily used in the form of steel, which contains 0.2% to 2.1 % C, or as alloy with other metals like Cr, Vn or Mn for constructing machines, tools, cars, ships, weapons and buildings. The worldwide estimated production of steel in 2010 was 1,414 kt (worldsteelorganisation.com).

1.2 Iron availability to plants is often limited

Fe is an essential micronutrient for all plants. The total content of Fe in soils ranges from 0.2% to 5% of soil mass. Under aerobic conditions, most Fe is found as minerals composed of Fe^{III} oxides. These minerals are of very low solubility, so that only a very small fraction of the total Fe is available to plants (< 25 µg Fe l^{-1} soil solution) (Scheffer et al., 2002). Factors that influence Fe availability include soil pH, aeration, microbial activity and the presence of

organic compounds like humic acid (Stevenson, 1994). Of these factors soil pH is most influential. In calcareous soils, with high concentrations of $CaCO_3$ and a pH in the range of 7.4 to 8.5, concentration of hydrated Fe^{III} is around 0.1 nM. As available Fe is often limited, Fe deficiency occurs on more than 30% of the Earth's arable land (Shenker and Chen, 2005). Agricultural strategies to prevent Fe deficiency often aim at increasing the availability of Fe, for example by application of Fe-chelates including EDTA or EDDHA (Wallace and Wallace, 1992). Another approach is to decrease soil pH, either by direct application of concentrated acids, or by application of S, which is oxidized in soils to SO_4^{2-},which results in the release of protons (Wallace, 1991). Most angiosperms, including *Arabidopsis thaliana*, take up Fe from the soil primarily as Fe^{2+} *via* the roots (Strategy I) (see chapter 1.5.1). Only graminaceous plants take up Fe predominantly in the form of organic Fe^{III} complexes (Römheld and Marschner, 1986)

1.3 Iron is an essential micronutrient for humans

Since Fe is an essential micronutrient, humans also have to take up Fe through nutrition. The body of an adult contains about 4 to 5 g of Fe. Out of the total body Fe, 60% is bound to hemoglobin in erythrocytes, 10% is bound to myoglobin and 30% is bound to a variety of Fe containing proteins, such as ferritin, or transferrin (Reilly, 2004). In humans, Fe deficiency causes anemia. When internal Fe stores are depleted, O_2 transport by hemoglobin is impaired. This in turn affects all organs and can ultimately be fatal if severe. Typical symptoms of Fe deficiency-induced anemia are pallor, fatigue and weakness, but more severe symptoms will develop if no countermeasures are taken. The World Health Organization recognizes Fe deficiency as the most common and widespread nutritional disorder with *ca.* 25% of the global population being affected (DeMaeyer and Adiels-Tegman, 1985). It is more prevalent in developing countries but also found in industrialized countries. Children and pregnant women are most affected (de Benoist, 2008).

Because Fe deficiency is a challenge in both agriculture and human nutrition, it is important to understand Fe homeostasis mechanisms in plants. Knowledge of plant Fe homeostasis is expected to lead to novel strategies for the bio-fortification of crops with Fe and increased yields, especially on soils with low Fe availability. Additionally, nutrition strategies can be designed that maximize the bioavailability of Fe in a plant-based diet.

1.4 Essential biological redox reactions are dependent on iron

In all cells, Fe is found as a co-factor or part of co-factors of proteins as ferrous or ferric Fe. Fe is utilized in prosthetic groups, because it can reversibly change its oxidation state under physiological conditions. This makes it an ideal e^- donor/acceptor.

There are three major groups of Fe-containing proteins, which differ by their prosthetic group. One group contains Fe bound to a heme group. Heme groups contain one Fe atom in the center of a heterocyclic, aromatic porphyrin ring. In a porphyrin ring the Fe^{2+} cation is bound by four N atoms from the porphyrin ring and one histidine residue from the protein which incorporates the heme. This leaves one coordination site of the Fe^{2+} cation free for interaction with reaction partners. The best studied examples of heme proteins are in the globin family and transport gases in animals (Berg et al., 2007). Other examples for proteins with heme groups are catalase (Kirkman and Gaetani, 1984) and members of the cytochrome c family of proteins (Bertini et al., 2006). Catalase is found in nearly all aerobic organisms and decomposes H_2O_2, which is a toxic byproduct of cellular metabolism, to H_2O and O_2. Cytochrome c is an e^- shuttle protein and transfers one e^- from Complex III to Complex IV in the oxidative phosphorylation pathway.

The second group of Fe proteins holds Fe as Fe-S clusters. In these, Fe^{II} and Fe^{III} atoms are linked by sulfides. The stoichiometries of these clusters can vary, and 2Fe-2S, 4Fe-4S and also 4Fe-3S clusters are found (Johnson et al., 2005). Similar to heme-containing proteins, Fe-S cluster-containing proteins also play a major role in the transfer of e^- between the protein complexes in the oxidative phosphorylation pathway in mitochondria and chloroplasts (Lill, 2009). For example, NADH-dehydrogenase is located in the inner mitochondrial membrane and catalyzes the transfer of e^- from NADH to ubiquinone (Brandt, 2006). In chloroplasts, the 2Fe-2S cluster-containing protein ferredoxin accepts e^- from photosystem I for either cyclic or non-cyclic e^- transport. Ferredoxin-type proteins also function as e^- shuttles in a range of other biological reactions, such as glutamate synthesis, nitrate reduction and sulfite reduction (Fukuyama, 2004).

In a third group of Fe containing proteins Fe is directly bound to amino acid residues. The transferrin protein, which controls the levels of free Fe in the blood of mammals, belongs to this group. Transferrin has two high affinity (K_d ~10^{-23} M^{-1}) binding sites for Fe^{3+} to keep free

Fe concentration in the blood at very low levels (Anderson and Vulpe, 2009). Once Fe^{3+} is bound, transferrin docks to the transferrin-receptor and is internalized by the cells (Chen and Paw, 2012). Also ferritins, a family of intracellular Fe storage proteins bind Fe directly and not *via* co-factors. Ferritin can store up to 4,000 Fe^{III} atoms in an accessible, nontoxic form (Briat et al., 2010).

Under normal conditions, Fe is not found as a free ion in the cytosol. Because it can so readily participate in redox reactions, free Fe ions may generate free radicals, especially reactive oxygen species (ROS) *via* Fenton's reactions (Valko et al., 2005). In the first reaction, H_2O_2 disproportionates in the presence of Fe^{2+}, resulting in oxidation of Fe^{2+} to Fe^{3+} and the production of a hydroxyl radical and a hydroxyl anion ($Fe^{2+} + H_2O_2 \rightarrow Fe^{3+} + OH\cdot + OH^-$). In the second reaction Fe^{3+} is reduced again to Fe^{2+} by another molecule of H_2O_2 resulting in the production of a peroxide radical and proton ($Fe^{3+} + H_2O_2 \rightarrow Fe^{2+} + OOH\cdot + H^+$). In these reactions Fe acts catalytically. The radicals produced in these reactions can damage cellular components. Consequently, since free Fe is both essential and harmful, organisms need to tightly regulate cellular Fe compartmentalization, concentrations and availability.

1.5 Iron homeostasis in plants

1.5.1 **Uptake of iron into the roots**

Plants control the internal concentrations of micronutrients through a complex network of genes and utilize a set of strategies to acclimatize to changing environmental conditions. The homeostasis of metals involves different aspects including mobilization in the rhizosphere, uptake into the roots, long distance transport from root to shoot, intercellular distribution and subcellular sequestration (Clemens et al., 2002). For Fe, genes involved in each aspect have been identified. Many of these genes encode proteins, which transport Fe across biomembranes.

The uptake of Fe is particularly well understood. Most higher plants, except Graminaceous plants, use a combination of soil acidification, enzymatic reduction of extracellular Fe^{III} and subsequent uptake of Fe^{II} to acquire Fe (strategy I) (Römheld and Marschner, 1986). In *Arabidopsis thaliana*, the proteins required for these steps have been identified and characterized in detail. Soil acidification increases the solubility of Fe^{III} and is achieved by

extruding protons from the root epidermis *via* plasma membrane H^+-ATPases from the P-type ATPase superfamily (Santi and Schmidt, 2009). The reduction step is accomplished by the activity of the membrane-bound FAD-containing reductase FRO2 (Ferric Reduction Oxidase 2), which likely uses NADPH to reduce Fe^{III} to Fe^{II} (Robinson et al., 1999). The primary uptake system for Fe^{II} in *Arabidopsis thaliana* is IRT1 (Iron Regulated Transporter 1), a member of the ZIP (ZRT1/IRT1-Related Protein) family of transporters (Eide et al., 1996; Vert, 2002). As part of the Fe-deficiency response in roots, transcript levels encoding two plasma-membrane H^+-ATPases (AHA2 and AHA7) are strongly induced in Fe-deficient plants, leading to increased proton extrusion (Santi and Schmidt, 2009). Also transcript level of *FRO2* and root surface reductase activity increase under Fe-deficient conditions compared to Fe sufficiency (Robinson et al., 1999). Transcript levels of *IRT1* in roots increase after exposure to Fe deficiency. In addition, IRT1 protein levels are negatively regulated by ubiquitin-dependent endocytosis (Connolly et al., 2002; Kerkeb et al., 2008; Barberon et al., 2011).

Graminaceous plants acquire Fe in the form of Fe^{III}-chelates (strategy II) (Römheld and Marschner, 1986). This strategy is characterized by secretion of phytosiderophores and subsequent of uptake of Fe^{III}-phytosiderphore complexes. Phytosiderophores, such as mugineic acid, are organic Fe-chelators synthesized from nicotianamine (Mori, 1999).

1.5.2 **Long distance transport**

Subsequent to their uptake, nutrients are either used in the roots or transported from the roots to the shoots. In the xylem, nutrients are transported with the transpiration stream (Tyree and Zimmermann, 2002). In the phloem nutrients can move from source to sink organs (Atkins, 2000; Tsukamoto et al., 2009). To increase mobility of Fe it is transported in a chelated form. Likely chelators of Fe are citrate or nicotianamine. In addition, also a protein was found to act as a chelator of Fe in the phloem sap of *Ricinus* (Krüger et al., 2002).

Evidence for the importance of citrate as a chelator includes citrate and Fe concentrations in the xylem sap of soybean correlating well when the plants are exposed to a range of Fe concentrations (Brown and Tiffin, 1965) and a Fe_3Cit_3 complex representing the major citrate complex in xylem sap of tomato (Rellan-Alvarez et al., 2010). An *Arabidopsis thaliana* mutant defective in the MATE (Multidrug and Toxic Compound Extrusion) family transporter

FRD3 (Ferric Chelate Reductase Defective 3) highlights the importance of citrate in long-distance and intercellular mobility of Fe in the apoplast (Rogers, 2002). FRD3 was shown to act as a cellular exporter of citrate in *Xenopus* oocytes (Durrett et al., 2007). The *frd3* mutant (originally termed *man1*) was identified as an accumulator of Mn in shoots in a mutant screen (Delhaize, 1996). Further studies showed that the *frd3* mutant is impaired in the transport of Fe in the xylem as indicated by lower Fe concentrations in xylem sap exudates. Additionally, *frd3* plants show accumulations of apoplastic Fe in the shoots (Green, 2004). This leads to a gradual build-up of higher Fe concentrations in shoots, but the constitutive up-regulation of Fe deficiency response genes shows that *frd3* shoots are in fact physiologically Fe deficient. Thus, decreased xylem and leaf apoplastic mobility of Fe in *frd3* prevents Fe from arriving at intracellular target sites and leads to cellular Fe deficiency. Recently, *FRD3* was shown to be essential for the supply of Fe to the developing pollen (Roschzttardtz et al., 2011b).

Another chelator important for Fe homeostasis is nicotianamine (NA). For NA synthesis, three molecules of S-adenosyl methionine are enzymatically condensed to form one NA molecule. This reaction is catalyzed by the enzyme nicotianamine synthase (NAS). NA is the precursor molecule of phytosiderophores (PS), which are used by graminaceous plants to mobilize and take up Fe from the soil. NA is a high-affinity chelator of Fe, but can also bind other transition metal ions (von Wiren et al., 1999). Fe-NA complexes are thought to be transported by members of the YSL (Yellow stripe-like) family of transporters (Schaaf et al., 2005). Eight *YSL* genes in *Arabidopsis* were identified by their sequence similarity to *YS1* (*Yellow Stripe 1*), a maize Fe^{III}-PS transporter (Curie et al., 2001). In a number of reports YSL proteins have been implicated in lateral movement of Fe-NA in leaf veins (DiDonato et al., 2004), mineral partitioning during the life cycle (Waters and Grusak, 2007) and mobilization of metals from the leaves during senescence (Waters et al., 2006). Another role for YSL transporters is apparently the delivery of Fe-NA to the developing seed (Le Jean et al., 2005; Chu et al., 2010). An additional line of evidence for the role of NA in Fe homeostasis comes from the analysis of plants defective in NA bio-synthesis. The tomato mutant *chloronerva* shows constitutively high root-surface Fe-reduction activity and strong intercostal chlorosis in young leaves, indicating an impaired mobility of Fe. Map based cloning identified the mutation to be in a gene encoding a NAS enzyme (Ling et al., 1996; Ling et al., 1999). The genome of *Arabidopsis thaliana* contains four *NAS* gene copies. A quadruple mutant showed a *chloronerva*-like phenotype and was also impaired in fertility due to reduced translocation of Fe to reproductive tissues (Klatte et al., 2009). When endogenous NA levels are depleted by overexpressing a gene encoding a NA-aminotransferase (NAAT), tobacco plants

developed interveinal chlorosis in the young leaves and abnormally shaped, sterile flowers (Takahashi et al., 2003).

1.5.3 **Intracellular homeostasis of iron**

In addition to distributing Fe to different organs, there is also a need to supply Fe to different organelles within the cell. In mitochondria, Fe is the most abundant micronutrient with the ratio of Fe:Zn:Cu:Mn being 26:8:6:1 (Tan et al., 2010). However, the proteins involved in mitochondrial Fe import are unknown in plants (Nouet et al., 2011). Fe-S cluster and heme biosynthesis occur partially in the mitochondria (Lill, 2009). Frataxin was identified as a possible metal chaperone which supplies Fe to Fe-S cluster and heme biosynthesis in many eukaryotes including plants (Maliandi et al., 2011). Frataxin was also implicated in protection against ROS produced by free Fe (Busi et al., 2006).

As in mitochondria, heme and Fe-S cluster biosynthesis also partially takes place in the chloroplasts and many e^- transport proteins in the photosynthetic apparatus contain Fe in hemes or in Fe-S clusters. This make the chloroplast are major subcellular sink for Fe in plant cells (Ye et al., 2006) since up to 80% of cellular Fe is found in chloroplasts (Terry and Abadia, 1986). *At*NAP14 (Non-Intrinsic ABC-Type Protein 14) was proposed to be an importer of Fe-S clusters into the chloroplast (Shimoni-Shor et al., 2010). Another candidate gene for chloroplastidal Fe import is *PIC1* (*Permease in Chloroplasts 1*) which resembles a cyanobacteria-like permease (Duy et al., 2011; Duy et al., 2007). A member of the Ferric Reduction Oxidase Family (FRO7) might also be involved in Fe acquisition of chloroplasts (Jeong et al., 2008).

An important protein in intracellular Fe homeostasis is ferritin (*Fer*). In mammals, ferritin represents the main cellular storage form of Fe (Eisenstein, 2000). Initially it was thought that this was also the case in plants. However, in seeds of *Arabidopsis thaliana* only 5% of the total Fe is bound to ferritin (Ravet et al., 2009) and the major Fe store is the vacuole, as indicated by studies on vacuolar membrane transporters like VIT1 (Vacuolar Iron Transporter 1) (Kim et al., 2006), and NRAMP 3 and 4 (Natural-Resistance Associated Macrophage Protein 3 and 4) (Lanquar et al., 2005). In mammals, ferritins are found in the cytosol and the mitochondria (Chen and Paw, 2012). In contrast to this, plant ferritins are not cytosolic, but localized to the mitochondria and the chloroplasts (Nouet et al., 2011). The current model

invokes ferritins as an intracellular protection mechanism against the production of ROS by free Fe ions in *Arabidopsis* (Ravet et al., 2009). Both, transcript and protein levels of ferritins decrease, when plants are subjected to Fe deficiency.

FER1 is also regulated at the level of mRNA stability (Ravet et al., 2011). There are conserved sequence elements found in the 3'-UTR of the ferritin transcript which influence transcript stability *via* unknown factors. These downstream *cis*-acting elements (*DST* elements) were identified in a group of small auxin-upregulated transcripts (*SAUR* transcripts) in soybean (McClure et al., 1989) and shown to shorten the half-life of *reporter:DST* fusion transcripts in tobacco (Newman et al., 1993). Two *Arabidopsis* mutants (*dst1* and *dst2*) that showed elevated transcript levels of a transgenic reporter construct containing a *DST*-element were isolated in a forward genetic screen (Johnson et al., 2000), but there is no information about the affected genes.

A pair of transporters were identified to function in the mobilization of Fe from the vacuole during germination. NRAMP3 and 4 are localized to the vacuolar membrane (Thomine et al., 2003) and are crucial for germination under Fe-deficient conditions (Lanquar et al., 2005). Later it was shown that NRAMP3 and NRAMP4 also act in Mn release from the vacuole in vegetative plants (Lanquar et al., 2010). VIT1 is an *Arabidopsis* homologue of the yeast CCC1 (Ca^{2+}-sensitive cross-complementer 1) transporter and critical for early seedling development. Seeds of *vit1-1* plants do not accumulate Fe stocks in their vacuoles during embryo development so that seedlings grow poorly when Fe is limiting (Kim et al., 2006).

Recently, the nucleolus was also identified as a pool of cellular Fe, but it remains unclear what functions Fe could have in the nucleolus (Roschzttardtz et al., 2011a). The authors propose that Fe is bound directly to rRNA molecules.

1.5.4 **Regulation of iron homeostasis**

A number of genes contributing to the regulation of the homeostasis of Fe have been identified. Most of the characterized genes regulate root responses to Fe deficiency (increased *IRT1* transcript levels, increased root-surface Fe-chelate reductase activity). The best studied regulatory protein is the basic helix-loop-helix (bHLH) transcription factor FIT (FER-Like Iron Deficiency-Induced Transcription Factor; also named FIT1/BHLH29/FRU) (Bauer et al., 2007). FIT activity is necessary to activate the Fe-deficiency response in roots of *Arabidopsis*

thaliana (Colangelo and Guerinot, 2004; Jakoby et al., 2004; Yuan et al., 2005). Activation of the Fe-deficiency response requires dimerization of FIT with bHLH38 or bHLH39 (Yuan et al., 2008). The transcript levels of *FIT* are increased under Fe-deficient conditions compared to Fe-sufficient conditions. However, stability of FIT protein is at the same time decreased (Sivitz et al., 2011). In Fe-deficient conditions, FIT protein is turned over at a high rate by the proteasome. Presumably, this is a protective mechanism against the accumulation of toxic amounts of Fe. FIT also seems to be a link between nitric oxide (NO) and ethylene signaling in the Fe deficiency response (Lingam et al., 2011; Meiser et al., 2011). NO was shown to positively regulated the Fe deficiency response (Chen et al., 2010; Graziano and Lamattina, 2007; Graziano et al., 2002). Ethylene production was shown to induce NO production and being induced by NO itself, which makes ethylene another positive regulator of the Fe deficiency response (Lucena et al., 2006; Garcia et al., 2010).

1.6 Post-transcriptional regulation of transcript stability

Regulation at the post-transcriptional level provides a possibility to rapidly shut off the expression of a gene. It also acts as another level of regulation to integrate gene expression into more complex regulatory networks. There are several ways by which gene expression can be regulated after transcription, and both the rate of translation and the stability of mRNAs are generally known to be regulated in eukaryotes (Balagopal and Parker, 2009).

Small RNA molecules play an essential role in post-transcriptional regulation of gene expression. MicroRNAs (miRNAs) (Jones-Rhoades et al., 2006) and small interfering RNAs (siRNAs) (Baulcombe, 2004) form ribonucleoprotein silencing complexes together with argonaute proteins (Liu et al., 2004; Joshua-Tor, 2006). The base sequence of the RNA partner then guides this complex to its target transcripts, which are either degraded or translationally repressed. Both events supposedly trigger the complete degradation of the transcript *via* transcript decay pathways.

A committing step for the degradation of transcripts is the removal of the poly(A) sequence from the 3’ end of the transcript. In mammals, this step is carried out by deadenylases, namely the CCR4-NOT complex (Carbon Catabolite Repression 4-NOT), PARN (Poly(A)-Specific Ribonuclease) and PAN2-PAN3 (Poly(A) Nuclease) (Garneau et al., 2007). There is evidence that at least parts of the CCR4-NOT complex and PARN are conserved in plants and have

similar functions. In *Arabidopsis thaliana*, CCR4 Associated Factor 1 (*At*CAF1) was found to have *in vitro* deadenylation activity (Liang et al., 2009). Deadenylation by *At*PARN is essential for embryo development (Chiba et al., 2004; Reverdatto et al., 2004) and also seems to play a role in abscisic-acid (ABA) signaling (Nishimura et al., 2005). After deadenylation, transcripts can be degraded from the 5'- or from the 3'-end as described below.

One pathway is characterized by enzymatic removal of the 7-methylguanosine cap at the 5'-end by a decapping protein-complex. Some essential components of the decapping complex found in mammals, such as DCP1 (Decapping Enzyme 1), DCP2 and HEDLS (Human Enhancer of Decapping Large Subunit) are conserved in plants. In *Arabidopsis, At*DCP2 has decapping activity *in vitro*, which is stimulated by *At*DCP1 and *At*VCS (*At*Varicose) (Xu et al., 2006). *At*VCS is the *Arabidopsis* homologue of HEDLS. The 5' decapping of transcripts seems to be a very common transcript degradation pathway in plants, as suggested by a transcriptome-wide analysis of uncapped RNAs (Jiao et al., 2008). After decapping, transcripts are cleaved by XRN1 (Exoribonuclease 1), the major cytosolic 5'→3' exoribonuclease in mammals and yeast (Garneau et al., 2007). There are three homologues of XRN1 in *Arabidopsis* (*AtXRN2*, *AtXRN3*, *AtXRN4*) (Kastenmayer and Green, 2000). Of these, *At*XRN4 was shown to be able to degrade uncapped transcripts (Souret et al., 2004).

Another pathway for transcript degradation after deadenylation is the 3'→5' cleavage by a multi-subunit complex called the exosome. This protein complex is also involved in RNA quality control (Houseley et al., 2006; Vanacova and Stefl, 2007) *via* the nonsense-mediated decay pathway and in processing of the 5.8S rRNA (Allmang et al., 2000). Although the general structure of the exosome seems to be conserved in plants, there are differences in comparison to mammals in certain subunits (Chekanova et al., 2007). In exosome-mediated cleavage of transcripts the 5' cap is removed by the Scavenger Decapping Enzyme (DcpS) in mammals (Liu et al., 2002). In plants, no homologue of DcpS was found.

Sequence motifs and three-dimensional structures at both ends of mature transcripts can act as determinants of stability or instability, although it seems that the 3'-UTR is more often involved in the regulation of degradation than the 5'-UTR. A mostly destabilizing sequence motif from mammals and yeast, found in the 3'-UTR, is rich in A and U nucleotides (Chen and Shyu, 1995). These AU-Rich Elements (AREs) stimulate transcript turnover. In mammals several of ARE-binding proteins have been identified and characterized extensively (Barreau et al., 2005). One well characterized group of ARE-binding proteins in mammals and yeast

contains a Tandem Zinc-Finger (TZF) domain and represents a distinct class of RNA binding proteins.

1.7 Cytoplasmic foci are places of transcript metabolism

From studies in mammalian cells it is known that granular structures in the cytoplasm are a major site of both transcript degradation and regulation of translation rates. The current research focuses on two distinct, but probably functionally overlapping structures.

The key enzymes of the mammalian and yeast 5'→3' decay pathway (DCP1, DCP2, HEDLS, XRN1), are localized in granular cytoplasmic foci, called processing bodies (PBs), reviewed in Anderson and Kedersha, 2006; Eulalio et al., 2007 and Parker and Sheth, 2007. Also Argonaute 2 and transcripts targeted by the miRNA degradation pathway are found in PBs (Liu et al., 2005; Sen and Blau, 2005). The number and sizes of PBs increase in mutants defective in RNA degradation (Sheth and Parker, 2003) and after various stresses, such as heat-shock (Weber et al., 2008) or arsenite treatment (Kedersha et al., 2005). A decrease in the number and sizes of PBs can be observed in the presence of transcriptional or translational inhibitors, supposedly because the formation of PBs is dependent on the presence of non-translated mRNAs in the cytosol (Cougot et al., 2004). PBs are transient structures and are thought to contain translationally inactive mRNAs that are destined for degradation (Teixeira et al., 2005). PBs are also found in plant cells and it seems that their functionality and composition are comparable to those found in mammalian cells (Goeres et al., 2007; Iwasaki et al., 2007; Xu et al., 2006).

Another subcellular structure of similar appearance and function are stress granules (SGs) (Anderson, 2006; Buchan and Parker, 2009). SGs contain RNA-binding proteins, translation initiation factors and messenger ribonucleoproteins. It is believed that they act as a reservoir for transcripts with halted translation. SGs seem to interact transiently with PBs and it is possible that transcripts can shuttle between both structures (Kedersha et al., 2005; Balagopal and Parker, 2009). SGs are also present in plants, concluded from the dynamic localization of plant homologues of mammalian SG components in *Arabidopsis* protoplasts (Weber et al., 2008).

1.8 Tandem zinc finger proteins regulate transcript stability

Tandem zinc finger (TZF) proteins are characterized by two zinc-binding motifs; each consisting of a $CX_8CX_5CX_3H$ motif (CCCH motif), separated by a conserved sequence of 15 to 18 amino acids. They belong to a super family of proteins that contain up to six zinc fingers of the CCCH type in total.

1.8.1 **Tristetraprolin controls the inflammatory response in mammals**

In humans, three TZF proteins are found: Tristetraprolin (TTP), Butyrate Response Factor 1 and 2 (BRF1 and 2). Especially TTP has been studied in detail (Sanduja et al., 2011; Baou et al., 2009). It was shown that TTP is able to bind specifically to AREs (Carballo et al., 1998) with the consensus sequence 5'-WWAUUUAWW-3'. Mutation studies identified the cysteine and histidine residues in the zinc fingers (Fig. 1b) as critical for the RNA-binding function (Lai et al., 1999). The same residues are also critical for the zinc-binding capability (Worthington et al., 1996). Knockout mice for TTP show a complex phenotype of inflammatory diseases, which is explained by elevated levels of TNFα. It was then found that the *TNFα* transcript is hyperstabilized in macrophages derived from these mice (Carballo et al., 1997). Additional studies established TTP as a negative regulator of *TNFα* mRNA stability. TTP can bind AREs in the 3'-UTR of the *TNFα* transcript *via* its TZF domain and thereby promotes the 5'- to 3' decay of the transcript by recruiting decapping and deadenylation factors (Lykke-Andersen and Wagner, 2005) to the transcript. Additional target transcripts of TTP-dependent regulation have been found in *in vitro* assays (Carballo et al., 2000; Ogilvie et al., 2005) and in global transcriptome analyses of transcripts (Lai et al., 2006). When overexpressed, TTP localizes to SGs (Kedersha et al., 2005), but further studies revealed that it can be found in both SGs and PBs (Franks and Lykke-Andersen, 2007).

1.8.2 Two TZF proteins in yeast are required for WT growth under Fe deficiency conditions

In *Saccharomyces cerevisiae*, the regulation of transcript stability by TTP homologues is critical for Fe homeostasis. When yeast cells are grown in Fe-deficient conditions, they respond by up-regulating the expression of a number of genes through the transcription factors AFT1 and AFT2 (Rutherford et al., 2001; Yamaguchi-Iwai et al., 1995). The AFT1 regulon encodes proteins that increase the uptake of Fe and the mobilization of intracellular Fe stores. Also, two genes encoding yeast TZF proteins, named *Cysteine Three Histidine 1* and *2* (*CTH1*/*CTH2*), are part of the AFT1/AFT2 regulon (Shakoury-Elizeh et al., 2004; Puig et al., 2005).

Both CTH1 and CTH2 contain TZF domains with high sequence similarity to TTP. Also, similar to TTP, they can bind to AREs of transcripts, which decreases the stability of these target transcripts (Puig et al., 2005). Known target transcripts of *Sc*CTH1 and *Sc*CTH2 mostly encode Fe-containing proteins. It is thought that this change in transcript stability leads to a cellular protein complement that is less dependent on Fe. This idea is supported by the fact that compared to WT cells, *cth1Δcth2Δ* cells show a growth defect when grown in Fe-deficient conditions. *Sc*CTH2 has a dynamic localization in PBs in the cytosol and in the nucleus (Vergara et al., 2011) and accelerates the degradation of transcripts, supposedly *via* the 5'- to 3'- pathway, by interacting with DExD/H-Box Helicase 1 (DHH1) (Pedro-Segura et al., 2008), an RNA helicase involved in removal of the 5'- cap structure of transcripts (Fischer and Weis, 2002).

1.9 CCCH-superfamily and TZF-family proteins in plants are regulators of development and responses to environmental cues

In *Arabidopsis thaliana* and *Oryza sativa* there are 68 and 67 proteins, respectively, that feature at least one CCCH-type zinc-finger (Wang et al., 2008a). Interestingly, in both species, there are also pairs of proteins with high similarity to the mammalian TTP-like proteins and the yeast CTH1 and CTH2 proteins. Several studies have been published that focus on proteins containing CCCH-type zinc-fingers. For example the six CCCH-type zinc-finger protein *At*HUA1 was shown to bind the *AGAMOUS* preRNA *in vitro* and to play a role

in determination of floral organ identity (Cheng et al., 2003). *At*CPSF30, an *Arabidopsis* homologue of the mammalian CPSF (cleavage and polyadenylation specificity factor), which has three CCCH motifs, was shown to bind to the polyadenylation signal from the pea *rbcS* gene (Delaney et al., 2006). It was also shown that *At*CPFS30 has endonuclease activity *in vitro* (Addepalli and Hunt, 2007). The same group also found that at least five other CCCH proteins exhibit RNase activity *in-vitro* (Addepalli and Hunt, 2008). Transcript levels of two genes encoding a pair of homologous proteins containing two zinc fingers (*At*SZF1 and *At*SZF2) are induced under salt stress, and knockout of mutants of these display an enhanced sensitivity to salt stress (Sun et al., 2007). Their biochemical roles, especially in RNA-binding, are not clear. The *At*SOM protein contains three CCCH motifs and is thought to play a role in light signaling (Kim et al., 2008). *At*SOM is expressed specifically in the seeds and is a negative regulator of phytochrome-mediated initiation of germination. Through an unknown mechanism *At*SOM regulates transcript levels of a set of genes involved in GA and ABA metabolism. *At*FES1 contains one CCCH motif and seems to control flowering time *via* FRI and FRL1 (Schmitz et al., 2005). Another protein with one CCCH motif in *Arabidopsis* is *At*PEI1, which is required for embryo development (Li and Thomas, 1998). In rice, the *Os*LIC protein, which contains one CCCH motif, controls the architecture of the plant (Wang et al., 2008b). Also in rice, the *Os*DOS protein is thought to be a negative regulator of leaf senescence (Kong et al., 2006). However, no protein with a TZF domain similar to TTP was included in these prior studies. Also, no evidence for the regulation of transcript stability by proteins with a CCCH-type zinc finger was identified in these studies.

In Pomeranz et al., 2010a and Pomeranz et al., 2010b the presence of eleven TZF proteins in *Arabidopsis thaliana* (*At*TZF1 to 11) is reported, but the loci At1g66810 (*AtCTH1*) and At1g68200 (*AtCTH2*) were not described as members of this family. *At*TZF1 to 11 contain a TZF domain unique to plants ($CX_{7/8}CX_5CX_3HX_{16}CX_5CX_4CX_3H$), which slightly differs from the TZF domain found in TTP ($CX_8CX_5CX_3HX_{18}CX_8CX_5CX_3H$). However, *At*CTH1 and *At*CTH2 contain TZF domains, which are more similar to that found in *Hs*TTP, *Sc*CTH1 and *Sc*CTH2. Studies on *At*TZF1 revealed that it is a positive regulator of ABA responses and a negative regulator of GA responses. Overexpression of *AtTZF1* results in a pleiotropic phenotype and most notably an increased tolerance to drought stress (Lin et al., 2010). A *TZF1-GFP* fusion, expressed from the CaMV 35S promoter, co-localized with marker proteins for PBs in maize protoplasts (Pomeranz et al., 2010a). Later, it was reported that all eleven *Arabidopsis* TZF-proteins, as well as *At*CTH1 and *At*CTH2, localize to cytoplasmic foci which resemble PBs or SGs, although no co-localization with a marker protein was

shown (Pomeranz et al., 2010b). Since the amino acid sequences of the TZF domains of *At*TZF1 to 11 are similar to the TZF domain of TTP, an interaction of *At*TZF proteins with specific RNA sequences seemed likely. However, by RNA mobility gel shift assays it was shown that *At*TZF1 did not bind to an ARE-containing target transcript of *Hs*TTP (Pomeranz et al., 2010a).

1.10 Two direct homologues of TTP and *Sc*CTH2 are found in *Arabidopsis thaliana*

Out of all plant TZF proteins, the proteins encoded by the loci At1g66810 and At1g68200 showed the highest overall amino acid sequence similarity to the human TTP or yeast CTH2. Especially the TZF domain was highly conserved between TZF proteins of different species (Fig. 1). It is therefore reasonable to explore the possibility that these proteins share functional similarities. Although acting in distinct regulatory pathways, human TTP-like TZF proteins and *Sc*CTH1 and *Sc*CTH2 work *via* a conserved molecular mechanism, and their respective interaction partners are conserved across organisms. However, their physiological roles seem unrelated in both organisms. TTP is best characterized as a negative regulator of *TNFα* in the inflammatory-response pathway. *Sc*CTH1 and *Sc*CTH2 are regulators in the response of yeast to Fe deficiency and act to post-transcriptionally down-regulate transcript levels of a set of genes encoding Fe-containing proteins. However, it is known that human Fe homeostasis is strongly altered in response to infections, involving the peptide hormone hepcidin (Nemeth and Ganz, 2006). Extremely low concentrations of free Fe in tissue fluids restrict bacterial growth (Weinberg, 1999). Cellular Fe uptake in humans is known to be controlled post-transcriptionally by regulating translation rates of ferritin transcripts and by regulating the *Transferrin Receptor* transcript stability. These mechanisms function through Iron-responsive elements (IREs) in the 5'- and 3'-UTR of the respective transcripts and their recognition by Iron-Regulatory Proteins (IRPs) that sense cytosolic Fe concentrations (Rouault, 2006). It is possible that TTP also contributes to human Fe homeostasis, probably in response to infections. Also, it has been suggested that TTP activity is regulated by the exchange of Zn for Fe in the RNA-binding domain (diTargiani et al., 2006) or by oxidation of the Zn-binding cysteines *via* ROS (Lee and Michel, 2010).

1.11 Aim of this thesis

In this thesis, the *Arabidopsis thaliana* gene At1G68200 encoding *At*CTH2 is functionally characterized. *At*CTH2 has a slightly higher sequence similarity to *Sc*CTH2 than to *At*CTH1. Moreover *AtCTH2*, but not *AtCTH1*, transcript levels increased when plants were grown under Fe-deficient conditions (Leonard Krall & Ute Krämer, unpublished results). One aim of this thesis is to explore the role of *At*CTH2 in Fe homeostasis. It will be shown that expression of full-length *AtCTH2* from its native promoter is indeed important for plant growth under Fe-deficient conditions. Evidence will be presented indicating a function for *AtCTH2* in transcript metabolism. By characterizing the *Arabidopsis cth2-2* mutant, it became evident that *AtCTH2* is essential for the development of the male gametophyte. The analysis of this developmental defect and a possible link to Fe homeostasis and altered stability of transcripts is the second aim of this thesis.

2 Material

2.1 Plant material

All *Arabidopsis thaliana* plants were of the ecotype Columbia (Col-0). Two T-DNA insertion lines were made available by the Salk Institute Genomic Analysis Laboratory (La Jolla, CA, USA). SALK line 045897 was designated *cth2-1*; SALK line 065040 was designated *cth2-2*. Seeds were ordered *via* the Nottingham Arabidopsis Stock Centre (NASC, Nottingham, UK).

2.2 Bacteria

For cloning and for handling of plasmid vectors two *Escherichia coli* strains were used. For most purposes DH5α cells (F^- φ80*lacZ*ΔM15 Δ(*lacZYA-arg*F)U169 *rec*A1 *end*A1 *hsd*R17(r_k^-, m_k^+) *pho*A *sup*E44 *thi*-1 *gyr*A96 *rel*A1 λ^-) were used. To handle GATEWAY destination vectors containing the *ccdB* gene DB3.1 cells (F^- *mcr*A Δ(*mrr-hsd*RMS-*mcr*BC) Φ80*lac*ZΔM15 Δ*lac*X74 *rec*A1 *ara*Δ139 Δ(*ara-leu*)7697 *gal*U *gal*K *rps*L (Str^R) *end*A1 *nup*G *fhu*A-*IS*2) were used. For stable transformation of *Arabidopsis thaliana* plants the *Agrobacterium tumefaciens* strain GV3101 pMP90 (Rif^r, $Gent^r$) (Koncz and Schell, 1986) was used.

2.3 Plasmid Vectors

Plasmid vector maps can be found in the Appendix in chapter 7.3.

2.3.1 **Cloning Vectors**

pENTR/D-TOPO (Life Technologies, Darmstadt, Germany): A cloning vector which is supplied as a linear plasmid with Topoisomerase enzyme attached to both ends. It confers

kanamycin resistance to bacteria. It allows directional cloning *via* a CACC overhang of the insert at the 5'- end to generate an entry vector, which can be used to introduce inserts into GATEWAY destination vectors by *in vitro* recombination.

pGEM-T Easy (Promega, Madison WI, USA): A cloning vector supplied as a linearized plasmid with 3'-T overhangs. It is used in T/A cloning of inserts carrying 3'-A overhangs. It confers ampicillin resistance to bacteria and allows blue/white screening of transformants.

2.3.2 **Binary vectors**

pMDC99 (Curtis and Grossniklaus, 2003): A GATEWAY destination binary vector with no functional sequences adjacent to the recombination sites, designed for genetic complementation experiments using genomic fragments. It is suitable for stable transformation of *Arabidopsis thaliana*. It confers kanamycin resistance to bacteria and hygromycin resistance to plants.

pMDC107 (Curtis and Grossniklaus, 2003): A GATEWAY destination binary vector designed for the expression of *GFP::(His)*$_6$ fusion constructs. No promoter sequences are located upstream of the recombination sites so expression of fusion constructs can be driven by endogenous promoters. It is suitable for stable transformation of *Arabidopsis thaliana*. It confers kanamycin resistance to bacteria and hygromycin resistance to plants.

pMDC163 (Curtis and Grossniklaus, 2003): A GATEWAY destination binary vector designed for the fusion of promoter sequences to the *uidA* gene. It is suitable for stable transformation of *Arabidopsis thaliana*. It confers kanamycin resistance to bacteria and hygromycin resistance to plants.

pGREENII 35S-Bar (Hellens et al., 2000): This binary vector allows expression from the CaMV 35S promoter. It is suitable for stable transformation of *Arabidopsis thaliana*. It requires the pSOUP plasmid for replication in *A. tumefaciens*. It confers kanamycin resistance to bacteria and phosphinotricine resistance to plants.

pSOUP (Hellens et al., 2000): This binary vector is required for replication of pGREEN-derived vectors in *A. tumefaciens*. It was co-transformed together with pGREEN vectors into *A. tumefaciens*. It confers resistance to tetracycline in bacteria.

pGWB402Ω (Nakagawa et al., 2007): A GATEWAY destination binary vector which allows expression from the CaMV 35S promoter. It is suitable for stable transformation of *Arabidopsis thaliana*. It confers spectinomycin resistance to bacteria and kanamycin resistance to plants.

2.3.3 **Localization Vectors**

pRTds-XRN4-GFP; pRTds-DCP1-GFP; pRTds-DCP1-Cherry; pRTds-RBP47-tdtomato (Weber et al., 2008): These vectors allow expression of the respective fusion constructs (*Decapping Enzyme 1; DCP1;* At1g08370, *Ribonucleotide-Binding Protein 47; RBP47*, At1g19130, *Exoribonuclease 4, XRN4*, At1g54490) from the CaMV 35S promoter. They can be used for transient transformation of *Arabidopsis thaliana* protoplasts. They confer ampicillin resistance to bacteria. They were kindly provided by Dr. Markus Fauth (Goethe Universität, Frankfurt am Main, Germany). The pRTds backbone is a modified version of pCK-GFP S65C (Reichel et al., 1996).

35Ω-sGFP(S65T)-CTH2 (Sergi Puig, unpublished): This vector allows expression of a translational *CTH2::GFP* fusion construct from the CaMV 35S promoter. It can be used for transient transformation of *Arabidopsis thaliana* protoplasts. It confers ampicillin resistance to bacteria. It was kindly provided by Sergi Puig (Instituto de Agroquímica y Tecnología de Alimentos, Valencia, Spain). The vector backbone is described in (Chiu et al., 1996).

2.4 Chemicals

Unless stated otherwise, chemicals were obtained as p.a. grade from the following companies/brands: Applichem (Gatersleben, Germany), Becton Dickinson (Franklin Lakes, NJ, USA), J. T. Baker (Center Valley, PA, USA), Merck (Darmstadt, Germany), Roth (Karlsruhe, Germany), Riedel-de Haën (Seelze, Germany), Sigma-Aldrich (St. Louis, MO, USA). All solutions were prepared using ultrapure water (18.2 MΩ system, Merck Millipore, Billerica, MA, USA).

2.5 Equipment

Atomic emission spectrometry	iCAP 6500 DUO (Thermo Scientific, Waltham, MA, USA) with ASX-520 Autosampler (Cetac, Omaha, NE, USA)
Balances	Model 470 and Model 770 (Kern, Balingen-Frommern, Germany)
Bead mill	MM200 (Retsch, Haan, Germany)
Centrifuges	Sorvall RC5B plus with SS34 rotor (Thermo Scientific, Waltham, MA, USA)
	Heraeus Multifuge XR3 with TX750 rotor (Thermo Scientific, Waltham, MA, USA)
	Microcentrifuge 5417C (Eppendorf, Hamburg, Germany)
	Microfuge 22R (Beckman Coulter, Indianapolis, IN, USA)
Confocal microscope	TCS SP5 (Leica Microsystems, Wetzlar, Germany)
Controlled environment shaker	G25 and 4230 New Brunswick Scientific (Edison, NJ, USA)
Drying cabinet	TK/L E117 (EHRET, Emmendingen, Germany)
Electric dispensing pipettes	Research Pro (Eppendorf, Hamburg, Germany)
Electroporation	Gene Pulser II (BioRad, Hercules, CA, USA)
Gel documentation	GelDoc XR+ (BioRad, Hercules, CA, USA)
Gel electrophoresis	i-My Run (Cosmo Bio, Tokyo, Japan)
Heating block	HBT130 HLC and EC2 (VLM, Bielefeld, Germany)
Light microscope	Axioskop (Carl Zeiss, Göttingen, Germany)
Magnetic stirrers	MR3002 (Heidolph, Schwabach, Germany)
	IKAMAG RCT (IKA Werke, Staufen, Germany)
Microtome	RM 2065 (Leica Microsystems, Wetzlar, Germany)
PCR machine	DNA Engine Peltier Thermo Cycler (BioRad Hercules, CA, USA)
Photometers	Biomate 3 (Thermo Scientific, Waltham, MA, USA)
	Nanodrop 2000 (Thermo Scientific, Waltham, MA, USA)
qPCR machine	LightCycler 480 (Roche Applied Science, Indianapolis, IN, USA)
Shaker	Model 3005 (GFL, Burgwedel, Germany)

Stereo microscope	M212 (Leica Microsystems, Wetzlar, Germany)
Sterile workbench	Fortuna Sterile Cabinet (LaboGene, Lynge, Denmark)
Ultrapure Water Filtration	18.2 MΩ system (Merck Millipore, Billerica, MA, USA)
Vortex mixer	Vortex Genie 2 (Scientific Industries, Bohemia, NY, USA)

2.6 Molecular biology reagents

For restriction enzyme digests, enzymes from Fermentas (St. Leon-Rot, Germany) and NEB (Ipswich, MA, USA) were used. T4 DNA ligase and desoxynucleotide-triphosphate solutions for PCR were supplied by NEB (Ipswich, MA, USA). PCRs for the purpose of cloning were performed with PHUSION DNA Polymerase (Finnzymes, Vantaa, Finland). PCRs, in which high fidelity was not needed were carried out using RedTaq supplied by Bioline (Luckenwalde, Germany). Oligonucleotide primers for PCR and qPCR were supplied by Eurogentec (Köln, Germany). Reagents for GATEWAY cloning were supplied by Life Technologies (Darmstadt, Germany). All reagents were used according to the specifications given by the respective manufacturer.

2.7 Media

2.7.1 **Medium for bacterial culture**

For growth of *E. coli* and *A. tumefaciens* lysogeny broth (LB) medium (5 g l^{-1} yeast extract, 10 g l^{-1} tryptone, 10 g l^{-1} NaCl) (Bertani, 1951) was used. For solid media, 1% (w/v) Bacto Agar (DIFCO, Lawrence, KA, USA) was added to the media before autoclaving. Antibiotics were added to *ca.* 60°C warm medium after autoclaving as sterile-filtered 1000x stock solutions. The final concentrations were: ampicillin 100 µg ml^{-1}, gentamycin 25 µg ml^{-1}, kanamycin 50 µg ml^{-1}, rifampicin 100 µg ml^{-1}, spectinomycin 100 µg ml^{-1}, tetracycline 10 µg ml^{-1}.

2.7.2 **Medium for plant culture**

For sterile culture of *Arabidopsis thaliana* 0.5x MS medium (Murashige and Skoog, 1962) and modified 0.25x Hoagland's medium (HG medium) (Hoagland and Arnon, 1938) was used. 0.5x MS medium was used to germinate seeds for propagation and selecting transgenic plants using antibiotics. HG medium was used to culture plants for metal treatment experiments. Liquid HG medium was used for hydroponic culture.

0.5x MS medium

2.2 g l^{-1} MS salts with vitamins (Duchefa, Haarlem, Netherlands; the exact composition is given in Supplemental Table 1)
10 g l^{-1} sucrose
3 ml l^{-1} 1 M MES adjusted to pH 5.7 with KOH

For solid medium 1% (w/v) Agar M, plant cell culture tested (Sigma-Aldrich, St. Louis, MO, USA), was added to the media before autoclaving. Antibiotics were added to *ca*. 60°C warm medium after autoclaving as sterile-filtered 1000x stock solutions. The final concentrations were: 50 µg ml^{-1} cefotaxim, 15 µg ml^{-1} hygromycin, 50 µg ml^{-1} kanamycin, 10 µg ml^{-1} phosphinothricin.

HG medium

HG medium was prepared from autoclaved stock solutions (Table 1). The stock solutions were added in the indicated sequence to a large volume of ultrapure water (*ca*. 80% of the final volume) to avoid precipitation. After stirring, the final volume was adjusted.

N,N′-bis(2-hydroxybenzyl)-ethylenediamine-N,N′-diacetic acid (HBED) (Chaney, 1988) was ordered from Strem Chemicals (Kehl, Germany). The FeHBED stock solution contained 10 mM $Fe(NO_3)_3$ and 10.5 mM HBED. An excess of chelator is used to make sure all Fe is chelated. The pH of the solution was adjusted to pH 5.7 with KOH.

For hydroponic culture, HG medium was prepared fresh. For sterile culture 10 g l^{-1} sucrose and 10 g l^{-1} Agar M were added prior to autoclaving.

Table 1: Composition of HG medium.

Stock solution	Final concentration	ml stock solution l^{-1} of media
1 M $Ca(NO_3)_2$	1.5 mM	1.5 ml
1 M KH_2PO_4	0.28 mM	0.28 ml
1 M $MgSO_4$	0.75 mM	0.75 ml
1 M KNO_3	1.25 mM	1.25 ml
1000 x micronutrient stock solution: 0.5 mM $CuSO_4$ 1 mM $ZnSO_4$ 5 mM $MnSO_4$ 25 mM H_3BO_3 0.1 mM Na_2MoO_4 50 mM KCl	 0.5 µM 1 µM 5 µM 25 µM 0.1 µM 50 µM	1 ml
1 M MES pH 5.7 with KOH	3 mM	3 ml
10 mM FeHBED	5 µM	0.5 ml

3 Methods

3.1 Standard methods

Standard methods of microbiology and molecular biology were used according to Sambrook et al., 2001. These included handling of *Escherichia coli* and *Agrobacterium tumefaciens*, restriction digests of plasmid vectors, ligations, and PCRs. A typical PCR program is given in Table 2. Specific conditions for reactions are given in the main text when appropriate.

Table 2: Typical steps of a PCR program.

T_a is the annealing temperature, t_e is the extension time, x is the number of cycles.

95°C	3 min	Initial denaturation	
95°C	30 s	Denaturation	x cycles
T_a	30 s	Annealing	
72°C	t_e	Extension	
72°C	3 min	Final elongation	

GATEWAY cloning technology was used according to protocols provided by Life Technology (Darmstadt, Germany). In this thesis, topoisomerase-assisted cloning into pENTR/D was used to create entry vectors. Inserts were then transferred to destination vectors using GATEWAY recombination sites and LR-clonase (LR-reaction) (Hartley, 2000).

3.2 Bacterial methods

3.2.1 Transformation of *Escherichia coli* by heat shock

To transform *E. coli* with plasmid vectors, chemically competent cells were prepared by the RbCl method (Hanahan, 1983) and stored at -80°C. For each transformation a 50-µl aliquot was thawed on ice. Plasmid DNA (100 ng), 5 µl of a ligation reaction or 5 µl of a

GATEWAY LR-reaction were added to the tube and mixed by tapping the tube. A heat-shock treatment was performed by incubation of the cells at 42°C for 30 s. Afterwards, the cells were immediately placed on ice, and 250 µl of LB medium without antibiotics were added. The cells were incubated with shaking at 37°C for 30 min to 1 h and plated on solid LB medium containing the appropriate antibiotic. Colonies were visible after incubation at 37°C for 8 h.

3.2.2 **Transformation of *Agrobacterium tumefaciens* by electroporation**

Agrobacterium tumefaciens was transformed with binary plasmid vectors by electroporation for later transformation of *Arabidopsis thaliana*. Fifty µl of electroporation-competent cells were thawed on ice. 1 µl of a 1:20 dilution of a plasmid DNA preparation was added to the cells and mixed. After incubation on ice for 5 minutes the cells were transferred to a cold 1 mm electroporation cuvette on ice. Electroporation was performed with the following settings: voltage: 1.8 kV, resistance: 400 ohm, capacity: 25 µF. Immediately after electroporation 250 µl of LB medium without antibiotics were added to the cuvette. The bacteria were then transferred to a 2 ml tube and allowed to grow at 28°C, with shaking at 200 rpm for 1 h. Then the bacteria were spread on LB medium containing gentamycin (to select against *E. coli* and for the presence of the helper plasmid pMP90) and the antibiotic required to select for the transformed binary plasmid. The plates were incubated at 28°C, and colonies were visible after 48 h days.

3.3 Cloning procedures

3.3.1 ***pCTH2:GUS* in pMDC163**

To generate a *pCTH2:GUS* construct, a fragment was amplified by PCR (T_a 55°C, t_e 90 s, 35 cycles) from the *CTH2* locus, using genomic DNA as a template and the primers 5'-CACCAATCTTTCATCCACTAC-3' and 5'-GATTTTGTTTTCCATTTTTC CCG-3'. The fragment contained the 1518 bases upstream of the translational start and the first 5 codons of the *CTH2* open-reading frame. After PCR amplification, the fragment was cloned into

pENTR/D, using the CACC overhang for directional cloning, and subsequently transferred into pMDC163 by *in vitro* recombination. The generated plasmid was used for *Agrobacterium*-mediated transformation of *Arabidopsis thaliana*.

3.3.2 *pCTH2:CTH2-GFP-(HIS)$_6$* in pMDC107

To generate a *pCTH2:CTH2-GFP-(HIS)$_6$* construct, a fragment of 1518 bases upstream of the translational start to the end of the open-reading frame excluding the translational stop from the *CTH2* locus was amplified by PCR (T_a 55°C, t_e 3.5 min, 35 cycles), using genomic DNA as a template, and the primers 5'-CACCAATCTT TCATCCACTAC-3' and 5'-GATTTTGTTTTCCATTTTTCCCG-3'. The fragment was cloned into pENTR/D using the CACC overhang for directional cloning and subsequently transferred into pMDC107 by *in vitro* recombination. The generated plasmid was used for *Agrobacterium*-mediated transformation of *Arabidopsis thaliana*.

3.3.3 *pCTH2:CTH2* in pDMC99

The vector pMDC99 (Curtis and Grossniklaus, 2003) was used to generate a genomic complementation construct. pMDC99 was used because it confers resistance to hygromycin, whereas the T-DNA insertion mutants characterized in this work carry a resistance to kanamycin. To generate a genomic complementation construct, a fragment from 1518 bases upstream of the translational start to 359 bases downstream of the translational stop was amplified by PCR (T_a 55°C, t_e 4 min, 35 cycles) from the *CTH2* locus, using genomic DNA as a template, and the primers 5'-CACCAATCTTTCATCCACTAC-3' and 5'-ACATAATTGGTAAAACTATATCAA-3'. The fragment was cloned into pENTR/D using the CACC overhang for directional cloning and subsequently transferred to pMDC99 by *in vitro* recombination. The generated plasmid was used for *Agrobacterium*-mediated transformation of *Arabidopsis thaliana*.

3.3.4 *35S:CTH2, 35S:CTH2_Nterm, 35S:CTH2_Cterm* in pGWB402Ω

Three different *CTH2* overexpression constructs were made, containing the full-length coding sequence, the part encoding the N-terminal 170 amino acids of the CTH2 protein or the part encoding the C-terminal 103 amino acids. cDNA from 45-day-old WT plants was used as a template for PCR (T_a 65°C, t_e 22 s, 30 cycles). To amplify the full-length coding sequence the primers 5'-CACCATGGAAAACAAAATCGC-3' and 5'-TGTGATCAGCTTGAGG GATGAC-3' were used. To amplify the part of the cDNA encoding the N-terminal part of CTH2 the primers 5'-CACCATGGAAAACAAAATCGC-3' and 5'-CTCCTGATCTTC TTTCTTCCCTCC-3' were used. To amplify the part of the cDNA encoding the C-terminal part of CTH2 the primers 5'-CACCGAAGATCAGGAGGAAGAGATAGAAGTG-3' and 5'-TGTGATCAGCTTGAGG GATGAC-3' were used. Each fragment was cloned into pENTR/D, using the CACC overhang for directional cloning, and subsequently transferred to pGWB402Ω by *in vitro* recombination. The generated plasmids were used for *Agrobacterium*-mediated transformation of *Arabidopsis thaliana*.

3.3.5 *amiRNACTH1/CTH2* in pGREENII-35S-Bar

pGreenII-35S-Bar (Hellens et al., 2000) allows ectopic overexpression in plants. It was used to generate plants expressing an artificial microRNA (amiRNA) (Schwab et al., 2006) directed against the *CTH1* and *CTH2* transcripts in an attempt to silence both genes simultaneously. Three different amiRNAs were designed and named amiRNA A, amiRNA B, and amiRNA C (Supplemental Fig. 3, Appendix). To generate the amiRNA constructs. the MIR319a precursor sequence was subjected to site-directed mutagenesis following the protocol published on wmd3.weigelworld.org (Max Planck Institute for Developmental Biology, Tübingen, Germany). In a first round of PCR, overlapping fragments, in which the bases that determine the target specificity of the mature miRNA are mutagenized, were amplified from the MIR319a precursor. In a second round of PCR, the mutagenized fragments are joined using flanking primer to generate the final amiRNA. Primer sequences used for generation of the amiRNA constructs are listed in Table 3. The products of the second round of PCR were cloned into pGEM-T Easy by ligation and subcloned into pGREENII-35S-Bar by restriction and ligation using *Xba*I and *Xho*I restriction sites. The resulting *35S:amiRNA* constructs were used for *Agrobacterium*-mediated transformation of *Arabidopsis thaliana*.

Table 3: Oligonucleotides used to generate amiRNAs targeting *CTH1* and *CTH2*.

amiRNA	Oligo name	Sequence
A	CTH1_2AImir-s	GATCATTCTGCAAACGTCAGTTTTCTCTCTTTTGTATTCC
	CTH1_2AIImir-a	GAAAACTGACGTTTGCAGAATGATCAAAGAGAATCAATGA
	CTH1_2AIIImir*s	GAAACCTGACGTTTGGAGAATGTTCACAGGTCGTGATATG
	CTH1_2AIVmir*a	GAACATTCTCCAAACGTCAGGTTTCTACATATATATTCCT
B	CTH1_2BImir-s	GATTTCTGCAAACCTCAGTCGTGTCTCTCTTTTGTATTCC
	CTH1_2BIImir-a	GACACGACTGAGGTTTGCAGAAATCAAAGAGAATCAATGA
	CTH1_2BIIImir*s	GACAAGACTGAGGTTAGCAGAATTCACAGGTCGTGATATG
	CTH1_2BIVmir*a	GAATTCTGCTAACCTCAGTCTTGTCTACATATATATTCCT
C	CTH1_2CImir-s	GATCTCAGTTTTGTAGCGTGGAATCTCTCTTTTGTATTCC
	CTH1_2CIImir-a	GATTCCACGCTACAAAACTGAGATCAAAGAGAATCAATGA
	CTH1_2CIIImir*s	GATTACACGCTACAATACTGAGTTCACAGGTCGTGATATG
	CTH1_2CIVmir*a	GAACTCAGTATTGTAGCGTGTAATCTACATATATATTCCT
Flanking primers	A	CTGCAAGGCGATTAAGTTGGGTAAC
	B	GCGGATAACAATTTCACACAGGAAACAG

3.4 Molecular biology methods

3.4.1 **Sequencing**

Sequencing of PCR products and inserts in vectors was performed by Seqlab (Göttingen, Germany), Starseq (Mainz, Germany) and the sequencing service of the University of Bochum (Bochum, Germany) using the chain termination method (Sanger et al., 1977). The inserts of all constructs which were generated by restriction and ligation were sequenced. Also the inserts of entry vectors of the GATEWAY cloning system were sequenced in full. For this, universal vector-specific primers and insert specific primers were used. GATEWAY destination vectors with inserts recovered from LR reactions were sequenced across the recombination sites to ensure success of recombination.

3.4.2 **Plasmid DNA isolation**

3.4.2.1 Small scale

Small quantities (ca. 50 µg) of plasmid DNA were isolated using the Plasmid Mini Kit from QIAGEN (Hilden, Germany) following the manufacturer's manual. Two ml of LB medium were inoculated with a single colony of *E. coli* and grown at 37°C with shaking at 200 rpm for 12 h to 16 h. Cells were harvested by centrifugation at 8,000 rpm for 2 minutes in a benchtop centrifuge. The pellet was resuspended and the bacteria were subjected to alkaline lysis. After neutralizing with K acetate the lysate was centrifuged at 10,000 rpm for 10 min. The supernatant was passed through the provided silica gel column, so that plasmid DNA could bind to the column. After washing the column to remove contaminants, the plasmid DNA was eluted in 50 µl of the provided elution buffer (10 mM Tris-HCl, pH 8.5).

3.4.2.2 Large scale

Up to 500 µg of plasmid DNA was isolated using the Plasmid Maxi Kit from QIAGEN (Hilden, Germany) following the manufacturer's instructions. Five ml of LB medium containing the appropriate antibiotic were inoculated with a single colony of *E. coli* and grown at 37 °C with shaking at 200 rpm for 8 h. 2.5 ml of the culture were used to inoculate 100 ml of fresh LB medium with antibiotic. After culturing at 37°C with shaking at 200 rpm for 16 h the cells were harvested by centrifugation at 6000 x *g* at 4°C for 15 min. The pellet was resuspended and the bacteria were subjected to alkaline lysis. After neutralizing with K acetate, the lysate was centrifuged at 20,000 x *g* at 4°C for 30 min, transferred to a new tube and centrifuged again for 15 min. The supernatant was passed through a QIAGEN-tip 500 anion-exchange column by gravity flow. After washing the column with the supplied washing buffers to remove contaminants, plasmid DNA was eluted in a high-salt buffer. To concentrate and desalt the DNA, it was precipitated by adding isopropyl alcohol, washed with 70% (v/v) ethanol and resuspended in 300 µl of TE buffer (10 mM Tris-HCl, 1 mM EDTA, pH 8).

3.4.2.3 Quantification and storage

The concentration of plasmid DNA was quantified using a spectrophotometer. Plasmid DNA was used for restriction digests, sequencing, as a template in PCRs or for transformation of bacteria or protoplasts. Plasmid DNA was stored at -20°C.

3.4.3 Total RNA isolation

Total RNA from *Arabidopsis thaliana* tissues was isolated using the RNeasy Plant Mini Kit from QIAGEN (Hilden, Germany) following the manufacturer's manual. Depending on the type and amount of tissues from which RNA was isolated harvesting was performed differently. When large amounts (> 100 mg) of tissues were harvested, the tissue was flash-frozen in liquid N_2 and ground with a mortar and pestle for homogenization. Then, an aliquot of *ca*. 75 mg was taken for RNA isolation. For amounts less than 100 mg all tissue was flash-frozen in a 2 ml reaction tube and disrupted using a bead mill (25 rps, 30 s). For both methods it was ensured that the tissue did not thaw until addition of the provided denaturing buffer. The denaturing buffer ensures immediate inactivation of RNases to keep the RNA intact. After adding 0.5 volumes of ethanol, the sample was passed through the provided column to allow RNA molecules longer than 200 bases to bind to a silica-based membrane. Impurities were washed off the column by a high-salt buffer. When following the isolation protocol, the optional step of on-column DNase treatment was performed. For this, RNase-free DNase solution from the same manufacturer was applied directly onto the membrane to digest DNA contaminations. RNA was eluted in 50 µl RNase free water. When a low yield was expected, for example when isolating from small samples, the elution volume was decreased to as few as 20 µl to reach concentrations of RNA suitable for cDNA synthesis. The concentration of the obtained total RNA was quantified using a spectrophotometer. RNA was used directly for cDNA synthesis or stored at -80°C.

3.4.4 Quantification of nucleic acids

To determine the concentration of nucleic acids, especially from plasmid DNA isolations, gel-eluted PCR products or total RNA isolations, a spectrophotometer was used. The absorbance of a nucleic acid solution at 260 nm and 280 nm was compared against the appropriate blank

solution. When a cuvette-based spectrophotometer was used, the absorbance at 260 nm was used to calculate concentrations according to the Beer-Lambert Law:

$$c\ (\mu g\ ml^{-1}) = A_{260}/[\varepsilon\ (\mu g\ ml^{-1}\ cm^{-1}) * D\ (cm)]$$

ε is the average extinction coefficient of nucleic acids (≥ 20 bases) and 0.02 µg ml^{-1} cm^{-1} for dsDNA and 0.025 µg ml^{-1} cm^{-1} for RNA. The path-length D was 1 cm. The ratio of A_{260} / A_{280} shows potential contamination with proteins and is between 1.8 and 2.2 in a pure nucleic acid solution. All samples were measured diluted, so that A_{260} did not exceed 1. Alternatively, a cuvette-less spectrophotometer (Nanodrop 2000) was used and concentrations and absorbance ratios were calculated directly by the controlling software.

3.4.5 **cDNA synthesis**

To quantify transcript abundance and to clone transcript sequences into plasmid vectors, RNA was reverse transcribed to complementary DNA (cDNA). For the synthesis of oligo(dT) primed cDNA, the RevertAid cDNA Kit from Fermentas (St. Leon-Rot, Germany) was used. In short, 1 µg of total RNA was mixed with 100 pmol oligo(dT_{18}) primer and filled up to a volume of 12 µl. The mixture was heated to 65°C for 5 min to melt potential secondary structures. After cooling on ice, the reaction was filled up to a volume of 20 µl by adding reaction buffer and dATP, dCTP, dGTP and dTTP to a final concentration of 1 mM each, 20 u RNase Inhibitor and 200 u reverse transcriptase. cDNA synthesis was performed at 42°C for 1 h. The reverse transcriptase was then inactivated by heating to 70°C for 5 min. The reaction was used directly as a template in PCR and qPCR or stored at -80°C for later use.

3.4.6 **Quantitative real-time PCR**

To quantify the abundance of specific transcripts quantitative real-time PCR (qPCR) was used. A SYBR-Green based detection system was used here. SYBR-Green is a fluorescent dye which binds specifically to double stranded DNA (dsDNA). Upon binding the fluorescence is dramatically increased. SYBR-Green can thus be used to detect a double-stranded PCR product in a quantitative manner. oligo(dT_{18})-primed cDNA synthesized from total RNA was used as a template. A qPCR reaction contained 1 µl of primer mix (2.5 µM of

each primer), 4 µl cDNA-mix (1:50 dilution of a cDNA synthesis reaction) and 5 µl of a 2x qPCR mastermix (Applied Biosystems, Carlsbad, CA, USA). Pipetting into 384-well plates was done using electric dispensing pipettes to minimize pipetting errors and filter pipette tips to avoid contamination. After preparation of a 384-well plate, the plate was sealed using a transparent adhesive cover. The plate was briefly vortexed and centrifuged before the qPCR program (Table 4) was started. Fluorescence intensity was recorded during both the amplification and melting curve phases.

Table 4: Program used for quantification of relative transcript levels by qPCR.

2 min 50°C 10 min 95°C	Denaturation
15 s 95°C 1 min 60°C	40 amplification cycles
5 s 65°C Increase to 95°C at 0.11°C s^{-1}	Melting curve analysis

After the program ended, the fluorescence data was exported to MS-Excel using the Roche LightCycler 480 Software. The linregPCR software (Ramakers et al., 2003) was used to determine reaction efficiencies (*re*) and cycle thresholds (C_T). The C_T value is the number of the PCR cycle at which the threshold fluorescence intensity is reached. The threshold was set to 0.5 arbitrary fluorescence units to allow comparisons between experiments. Reaction efficiencies were calculated as arithmetic means of all reactions using the same primer pair in the respective qPCR run. Relative transcript levels (ΔC_T) were determined using the following formula:

$$\Delta C_T = re_{GOI}^{-\mathrm{C_T GOI}} / re_{HK}^{-\mathrm{C_T} HK}$$

GOI is the gene of interest. HK is a housekeeping gene. *Elongation factor 1α* (*EF1α*, At5g60390) and *Helicase* (*HEL*, At1g58050) were used as constitutively expressed housekeeping genes to normalize target transcript levels (Czechowski et al., 2005). Depending on the target transcript level different housekeeping genes were used, so that the difference between C_T*GOI* and C_T*HK* never exceeded five. All reactions were performed with two technical replicates and two ΔC_T-values were calculated, each using one C_T*GOI*-value and one C_T*HK*-value.

Melting curve analysis was done to ensure the amplification of a single PCR product. Since SYBR-Green can bind to any dsDNA it is important to rule out the possibility of primer dimers or amplification from misannealed primers. A single PCR product is indicated by a single peak in the curve of the first derivative of the fluorescence value plotted against the temperature in the melting curve analysis. In addition, all amplicons were analysed by agarose gel electrophoresis at least once to verify amplification of a single product.

Primers for qPCR were designed using the PrimerExpress software V3 (Applied Biosystems) to ensure high reaction efficiencies. The parameters used to design primer pairs were: T_M between 59°C and 61°C and amplicon length between 50 and 150 bp. Primer pairs with a low penalty score were preferred. Also, primers binding close to the 3' end of a transcript were preferred. A summary of all qPCR primer pairs can be found in Supplemental Table 5.

3.4.7 **Genomic DNA isolation from *Arabidopsis thaliana***

To prepare genomic DNA from *Arabidopsis thaliana* for the purpose of PCR-based genotyping, DNA was isolated according to Edwards et al., 1991. A piece of shoot tissue, *ca*. 3 mm in diameter, was ground in a 1.5 ml reaction tube using a plastic pestle. Then 400 µl extraction buffer (200 mM Tris-HCl pH 7.5, 250 mM NaCl, 25 mM EDTA, 0.5% (w/v) SDS) was added. The tube was centrifuged at 13,000 rpm for 1 min in a benchtop centrifuge. 300 µl of the supernatant was transferred to another tube and mixed with 300 µl isopropyl alcohol. After 2 min of incubation at RT the sample was centrifuged at 13,000 rpm for 5 min. The supernatant was carefully decanted, and remaining was buffer was aspirated using a pipette without disturbing the pellet. After 30 min of air-drying, the pellet was resuspended in 25 µl TE buffer pH 8 by vigorous vortexing. The preparations were stored at -20°C. One µl was used as a PCR template in 25 µl PCR reactions for genotyping. Genomic DNA of higher purity and integrity was used as a PCR template for cloning procedures and was kindly provided by Dr. Ina Talke.

3.4.8 **Agarose gel electrophoresis of DNA fragments**

To separate DNA fragments of different sizes agarose gel electrophoresis was used. Gels were prepared by adding 0.8 to 3% (w/v) agarose to 1 x TAE buffer (40 mM Tris, 20 mM acetic acid, 1 mM EDTA, pH 8). The agarose suspension was heated in a microwave until all agarose was in solution. After cooling, SYBR-Safe DNA stain (Life Technologies, Darmstadt, Germany) was added to obtain a 1 : 20,000 dilution. After mixing, the gel was poured into a mold and a comb was used to create wells. If necessary, samples were mixed with a loading dye (PEQLAB, Erlangen, Germany) to increase the density of the sample and to monitor gel electrophoresis. To analyze the size of DNA fragments a size standard (PEQGOLD 1kB ladder, PEQLAB) was run along with the samples. Gel electrophoresis was carried out in 0.5 x TAE buffer at 100 V for *ca*. 30 min.

3.4.9 **Transient transformation of *Arabidopsis thaliana* protoplasts**

Arabidopsis thaliana mesophyll protoplasts were transiently transformed using the protocol described in Yoo et al., 2007 with slight modifications. For each series of transformations leaves were harvest from 3 to 5 4-week-old *Arabidopsis* plants grown in the greenhouse. Only expanded leaves with no visible signs of senescence were used, to generate a homogeneous population of protoplasts. Typically, the leaves number four to ten, counting from the youngest visible leaf, were used.

After harvest, attached soil particles were carefully rinsed off, and leaves were blotted dry on Whatman paper. Then, strips of *ca*. 0.5 to1 mm width were cut with a fresh razorblade, in the direction perpendicular to the petiole. The petiole itself was discarded. The strips were submerged in 30 ml enzyme solution (see below) in a plant tissue culture container (53 mm diameter x 100 mm height) immediately after cutting. After harvesting was complete the leaf strips were vacuum infiltrated at 100 mbar for 1 min. The vacuum was released slowly for *ca.* 1 min. Then the leaf strips were incubated in the dark without shaking for 3 h. Protoplasts were released by gently swirling the suspension. $CaNO_3$ was added to the suspension to a final concentration of 50 mM. The protoplast suspension was filtered through a 41-µm nylon net filter (Merck Millipore, Billerica, MA, USA) to remove cell debris and undigested leaf material. Protoplasts were kept on ice after release from the leaf and handled with care.

Unnecessary pipetting was avoided. All centrifugation steps were performed at RT. The filtrate was centrifuged at 300 x *g* for 5 min. The supernatant was carefully aspirated, and the pelleted protoplasts were gently resuspended in 20 ml WI solution (see below). After centrifugation at 300 x *g* for 5 min, the supernatant was removed, and the pellet was carefully resuspended in *ca*. 2 ml of WI solution. The suspension was pipetted on top of 5 ml of a 21% (w/v) sucrose solution in a 15 ml tube. After centrifugation at 300 x *g* for 10 min, *ca.* 2 ml of intact protoplasts were collected from the interphase and incubated on ice for 30 min. For each transformation, an aliquot of 200 µl protoplast suspension was transferred to a new 2 ml reaction tube, centrifuged at 1000 x g for 3 min, and resuspended in 100 µl Man/Mg solution (see below). Fifty µg of each plasmid DNA of a concentration of at least 1 µg μl^{-1} and 110 µl PEG solution (see below) were added, and the contents of the tube were gently mixed by tapping the tube. After 15 min at RT, 440 µl W5 solution (see below) was added, followed by gently mixing the tube by tapping. The reaction was then centrifuged at 1000 x g for 3 min and the pellet was resuspended in 100 µl WI solution. Each transformation reaction was transferred to 500 µl of WI solution in a 24-well plate. The transformed protoplasts were incubated at RT in constant light in a standard laboratory fume hood for 12 to 16 h before observation. Wavelengths used in confocal microscopy can be found in Supplemental Table 3 in the Appendix.

Enzyme solution: 0.4 M Mannitol, 20 mM KCl, 10 mM $CaCl_2$, 0.1% (w/v) BSA fraction IV, 20 mM MES pH 5.7 with KOH, 1% (w/v) cellulase Onozuka R-10, 0.25% (w/v) Macerozyme R-10. Enzymes were purchased from SERVA (Heidelberg, Germany) and added freshly.

WI solution: 0.5 M Mannitol, 4 mM MES pH 5.7 with KOH

Man/Mg solution: 0.5 Mannitol, 15 mM $MgCl_2$

PEG solution: For 10 ml: 4 g Polyethylenglycol (PEG) 4000, 3 ml H_2O, 2.5 ml 0.8 M Mannitol, 1 ml 1 M $CaNO_3$. PEG was purchased from Merck, (Darmstadt, Germany). After preparation, PEG solution was stored at RT for a maximum of one week.

W5 solution: 0.5 M Mannitol, 154 mM NaCl, 125 mM $CaCl_2$, 5 mM KCl, 5 mM glucose, adjusted to pH 5.8 with KOH

Solutions were made directly by dissolving chemicals in ultrapure water except for MES solution, which was used as an autoclaved 1 M stock solution. All solutions were stored and used at 4°C, with the exception of enzyme solution and PEG solution, which were used at RT.

3.5 Analytical methods

3.5.1 **Chlorophyll extraction and quantification**

Total chlorophyll was extracted and quantified according to Porra et al., 1989. For plant tissues cultivated in sterile culture, whole shoots were used for extractions. In the case of hydroponically grown tissues, leaf discs of 3 mm diameter or whole leaves were used. The fresh weight (5 to 50 mg) was recorded immediately after sampling. To extract chlorophylls *a* and *b*, tissues were incubated in 1 ml methanol at 70°C with shaking at 300 rpm for 15 min. Subsequently, the samples were kept on ice until measuring.

Absorbance of the extracts was measured at 450 nm, 652 nm, 665 nm and 750 nm. The absorbance at 450 nm can be used to quantify anthocyanins. The absorbance at 652 nm and 665 nm is used to quantify chlorophyll *a* and *b*, respectively. The absorbance at 750 nm is used to correct for turbidity of the extract. If the absorbance was above 1, the extract was diluted with methanol and measured again. Chlorophyll concentrations were calculated according to the following formula:

$$c(Chl_{a+b})(\mu M) = 22.12 * (A_{652} - A_{750}) + 2.71 * (A_{665} - A_{750})$$

3.5.2 **Element analysis**

Multi-element analysis was done by completely mineralizing plant tissues and subsequent analysis by inductively-coupled plasma atomic emission spectrometry (ICP-AES).

To remove metals bound to the cell wall in the apoplast of root tissues, whole root systems were desorbed before mineralizing. For this, the roots were incubate in 5 mM $CaSO_4$, 1 mM MES pH 5.7 for 10 min, followed by incubation in 10 mM Na_2EDTA, 5 mM $CaSO_4$, 1 mM MES pH 5.7 for 5 min. After this the roots were incubated twice in ultrapure H_2O for 1 min

each. All solutions were ice-cold. For each step a volume of 30 to 45 ml was used. After desorbtion, the roots were blotted dry on Whatman paper.

To completely mineralize plant tissues, they were dried at 70°C in a drying cabinet for at least two days. After recording the dry biomass, tissues were placed in DURAN glass tubes (washed over night in 0.2 M HCl and rinsed twice with ultrapure water) or 15 ml disposable polypropylene tubes and covered with up to 4 ml of 65% (w/v) HNO_3. After incubation at room temperature for at least 12 h, the samples were heated to 100°C in a heating block for at least 3 h with occasional manual shaking. When the development of orange-brown gas (NO_x) stopped, the samples were allowed to cool to room temperature and 1 ml 30% (w/v) H_2O_2 was added. After mixing, the samples were heated to 80°C to completely oxidize any remaining C and NO_x. When the gas development stopped, samples were again allowed to cool down to room temperature. The volume was adjusted to 10 ml with ultrapure water. Samples were mixed by inverting and stored at 4°C until measurement.

For measurement of elemental concentrations in anthers, the protocol was slightly modified because of the small sample size. For each sample, anthers from ten flowers (n = 60) were collected using titanium forceps to avoid contamination with Fe. Anthers were collected in 0.5 ml reaction tubes filled with ultrapure water to facilitate removal of samples from the tips of the forceps. The water was evaporated in a drying cabinet set to 70°C over night. Then 200 µl of 65% (w/v) HNO_3 was added. Care was taken that all anthers were covered with acid. Then the samples were heated to 90°C for 3 h, cooled to RT and 100 µl of 30% (w/v) H_2O_2 was added. The samples were again heated to 80°C for 30 min. Then the samples were transferred to 15 ml disposable plastic tubes. The 0.5 ml tube was rinsed once with ultrapure water and the rinse was added to the 15 ml tube. Then the samples were filled up to 3 ml with ultrapure water. After inverting the tubes to mix the contents, samples were either measured immediately or stored at 4°C.

The liquid samples were supplied to the ICP-AES instrument as an Ar-aerosol, using a concentric glass nebulizer (Thermo Scientific, Waltham, MA, USA). All elements were quantified through axial observation of the plasma, except K and Mg, which were quantified radially. The ICP-AES instrument was calibrated with a series of multi-element standards made from analytical grade chemicals (Supplemental Table 2, Appendix). Quality control was performed by measuring calibration standard 3 and certified reference material made from tobacco leaves (CTA-VTL2, Dybczyński et al., 1998).

3.6 Microarray transcriptome analysis

To simultaneously measure expression levels of ca. 22,000 genes, the ATH1 microarray (Affymetrix, Santa Clara, CA, USA) was used. Total RNA was isolated using the QIAGEN RNeasy Plant Kit. The RNA was quantified using a spectrophotometer and analyzed for integrity by denaturing gel electrophoresis. Furthermore, an aliquot of the RNA was used for cDNA synthesis and a 1-kb amplicon (At2g46800, *AtMTP1*) was amplified by PCR using the primers 5'-ATGGAGTCTTCAAGTC-3' and 5'-CTTAGCGCTCGATTTGTATCG-3'. Five µg quality-controlled RNA was send to the EMBL Genomics Core Facility (Heidelberg, Germany) for hybridizing to ATH1 arrays.

For the analysis of shoots and roots of WT and *cth2-1* plants (chapter 4.17) data processing and statistical analysis was performed using Genespring Version 10 (Agilent Technologies, Santa Clara, CA, USA). Data were normalized by the robust multi-array average method. Genes, with signal intensities in the lower 20%-tile of all signal intensities were considered not expressed and excluded from the analysis. Differences between genotypes or treatments were calculated separately for each replicate experiment. Genes showing differential transcript levels by at least 1.25-fold in both replicates were tested for significance ($p \leq 0.2$) by a paired Student's *t*-test, corrected by the Benjamini-Hochberg method. Lists with all possible combinations of transcripts present at levels higher or lower levels under Fe deficiency than under control conditions, or in the *cth2-1* mutant compared to WT, were generated (

Table 9). Also, the presence of an ARE consensus sequence (WATTTAW) in the 3'-UTRs of genes was annotated.

For the analysis of anthers of WT and *cth2-2* anthers (chapter 4.23) the affy (Gautier et al., 2004) and limma (Smyth, 2005) packages of Bioconductor (Gentleman et al., 2004) were used. Data were normalized by the robust multi-array average method. Subsequently, present calls were assigned to transcripts using the MAS5 algorithm. Arithmetic means of transcript levels of both replicates were used to find genes with significantly different transcript levels. Transcript levels were considered significantly different between WT and *cth2-2*, when the

difference in signal intensity between the two genotypes was at least two-fold in either direction, and the *p*-value, calculated by the ebayes function (part of the affy package), corrected for multiple comparisons with the Benjamini-Hochberg method, was ≤ 0.05.

3.7 Plant growth

All *Arabidopsis thaliana* seeds were germinated and grown in sterile conditions for the first 7 to 10 days. Depending on the purpose, plants were then either kept in sterile culture or transferred to soil. All sterile culture was done in a controlled environment incubator (Percival CU-41L4, CLF Plant Climatics, Wertingen, Germany). Plants on soil were either cultured in a controlled environment (GroBank BB-XXL^3, CLF Plant Climatics, Wertingen, Germany) or in a greenhouse. Soil was prepared by mixing 4 parts compost, 1.5 parts gravel, 1.5 parts sand, 1 part peat and 1 part vermiculite (all volume parts). Hydroponic culture was performed in a climate controlled room built by the University of Bochum. Growth conditions are summarized in Table 5.

Table 5: List of growth conditions.

	Settings
Sterile culture, Hydroponic culture	11 h 22°C day / 13 h 18°C night, 70% relative humidity, light intensity *ca*. 120 µmol s^{-1} cm^{-1}
Controlled environment for soil-grown plants	11 h 22°C day / 13 h 18°C night, 70% relative humidity, light intensity *ca*. 120 µmol s^{-1} cm^{-1}
Greenhouse	Natural light complemented by artificial illumination to achieve 16 h of light regardless of the season. Conditions were set to 22°C and 40% relative humidity in winter and 30°C and 70% relative humidity in summer.

3.7.1 **Sterile culture of Arabidopsis thaliana**

Arabidopsis thaliana was grown under sterile conditions on solid HG or 0.5x MS media in square (12 mm x 12 mm, containing 50 ml media) or round (90 mm diameter, containing 25 ml media) Petri-dishes. For seed sterilization, the desired number of seeds was aliquoted into

a 1.5 ml tube and incubated with 500 µl sterilization solution (10% (v/v) NaOCl, 0.01% (v/v) Tween20) for 15 min with occasional manual mixing. The sterilization solution was aspirated under sterile conditions, and the seeds were washed 3 times with 500 µl sterile ultrapure water. After the last washing step the seeds were singled out onto solid media, using a 1 ml pipette tip. After placing the seeds onto the media the Petri-dish was left open until residual water had evaporated. The plates were closed, sealed with semi-permeable tape (Leukopor, BSN medical, Hamburg, Germany) and transferred to 4°C in the dark for 2-3 days to synchronize germination. Subsequently, the plates were moved to a controlled environment and plants were cultured at conditions noted in Table 5. For transfer of seedlings (e.g. to start a treatment) autoclaved wooden toothpicks were used under sterile conditions.

3.7.2 **Preparation of EDTA-washed Agar for metal deficiency experiments**

For growing *Arabidopsis thaliana* in sterile culture under metal deficient conditions Agar M was washed with EDTA to remove bound divalent cations. To prepare 1 l of HG medium, 11 g of Agar M (10% excess compared to non-washed media) were weighed into a 1 l beaker. The agar was suspended in 1 l 50 mM EDTA, pH 8 and stirred at the minimum speed sufficient to keep all agar in suspension for 8 h to overnight. Then the agar was allowed to settle for *ca*. 1 h and the supernatant was decanted. The EDTA washing was repeated twice to a total of three EDTA washes. Then the agar was washed six times with ultrapure water for 30 min each. After the last washing step, the agar was used immediately to prepare 1 l of HG medium. To achieve metal deficiency the desired metal was omitted from the media. This procedure was successfully carried out to achieve Fe (Haydon et al., 2012) and Cu deficiency (Bernal et al., 2012) in a sterile cultivation system.

3.7.3 **Hydroponic culture of *Arabidopsis thaliana***

For hydroponic culture of *Arabidopsis thaliana*, 4-week-old-plants grown on soil under controlled environmental conditions were transferred to liquid medium. During transfer, all soil particles were removed from the plant by washing in tap water two times in two different beakers with in a volume of at least 3 l. Plants were transferred to 400 ml boxes with two plants per box. To avoid microbial contamination, plants were first transferred to HG medium

containing 0.025% (v/v) Plant Preservative Mixture (Plant Cell Technology, Washington, DC, USA). After 2 to 3 days, plants were transferred to HG medium, and experimental treatments were started. For deficiency treatments, the roots were washed in deionized water prior to transfer into deficiency medium. The medium was thereafter changed weekly.

3.8 Molecular biology methods in *Arabidopsis thaliana*

3.8.1 **Stable transformation of *Arabidopsis thaliana***

To generate stable transformants of *Arabidopsis thaliana* a modified floral dip method (Clough and Bent, 1998) was employed. To prepare transformants, *Arabidopsis thaliana* was grown on soil in short-day conditions for 4 weeks and then shifted to long-day conditions to induce flowering. The primary inflorescence was removed to encourage the growth of secondary inflorescences and thus the formation of a larger number of flowering buds. When the secondary inflorescence reached a length of *ca*. 5 cm (approximately four days after cutting the primary bolt) the plants were used for transformation. To prepare an *Agrobacterium tumefaciens* culture, a single colony of *Agrobacterium tumefaciens*, which had been shown to contain the required binary plasmid, was used to inoculate a starter culture of 5 ml LB medium with the appropriate antibiotics and gentamycin to avoid contamination with *E. coli*. The culture was incubated at 28°C with shaking at 200 rpm for 24 h. The entire starter culture was used to inoculated 45 ml of fresh LB medium and incubated again for 24 h. The cells were harvested by centrifugation at 6000 x g for 10 min and resuspended to an OD_{600} of *ca.* 0.8 in a 5% (w/v sucrose), 0.05% (v/v) Silwet L-77 (Lehle Seeds, Round Rock, TE, USA) solution.

The transformation was carried out using a soft paintbrush. The paintbrush was sterilized with ethanol and allowed to dry. For transformation, the bacterial suspension was painted generously onto the shoot apical meristem, the stem, the flowering buds and the axial buds. After application of the suspension, the plants were covered with plastic wrap to increase humidity and promote survival of the bacteria. After two days the plastic wrap was removed and plants were allowed to set T1 seeds. For each construct at least 12 plants in two different pots were transformed.

3.8.2 **Screening and propagation of stable *Arabidopsis thaliana* transformants**

To screen T1 seeds of *Arabidopsis thaliana* for successful genomic integration of the T-DNA 100 mg of seeds (*ca*. 5000 seeds) were sterilized according the aforementioned protocol (chapter 3.7.1) with the following modifications: The procedure was carried out in 15 ml disposable tubes. 5 ml of each the sterilization solution and ultrapure water were used. After the last washing step, the seeds were resuspended in 5 ml 0.1% (w/v) autoclaved agarose solution and evenly spread on two square Petri-dishes. The medium for T1 screenings was 0.5x MS with 1% sucrose and 50 mg l^{-1} cefotaxim to inhibit growth of *Agrobacterium tumefaciens* and the antibiotic appropriate to select for the transformed construct. Seeds were then stratified and germinated as described. *Ca*. ten days after germination, at least 12 resistant T1 plants were transferred to soil and allowed to self, to generate 12 independent T2 populations. From *ca*. 5000 seeds 10 to 25 seedlings were resistant, indicating a transformation rate of at least 0.2% of the seeds.

To determine the number of independently segregating T-DNAs, T2 seeds were germinated on 0.5x MS medium with 1% (w/v) sucrose and the appropriate antibiotic to assay segregation rates. A population, in which 25% of all individuals were sensitive to the antibiotic (1 in 4) indicated a single locus of insertion. A population in which 6.25% of all individuals were sensitive to the antibiotic (1 in 16) indicated two independent loci of insertion. When possible, single-locus insertion lines were selected and propagated to the T3 generation. For the generation of T3 populations, six T2 plants from a single T1 population were allowed to self. The segregation rates of the obtained T3 populations were analyzed. A population with no apparent segregation was considered to be homozygous for the transgene. For each construct, T3 populations from three independent lines were generated and analyzed when possible.

3.8.3 **Genotyping and analysis of partial transcripts of T-DNA insertion mutants**

To genotype T-DNA insertion mutants genomic DNA was isolated as described in chapter 3.4.7. The genomic DNA was then used as a template in PCR reactions. By using gene-specific primers that anneal to the genomic DNA sequence upstream or downstream of a putative insertion site, a WT allele can be detected. By using a combination of a gene-specific primer and a primer annealing to the left (LB) or right (RB) border sequence of the T-DNA an insertion can be detected. Primers used for genotyping are given in Table 6. The reaction-specific PCR conditions for all reactions were: T_a 55°C, t_e 1 min, 30 cycles.

Table 6: Primers used for PCR-based genotyping of T-DNA insertion mutants.

Name	Sequence 5' to 3'	Annealing region
CTH2-1_FWD	TTCTGATTTCTCTGTGGCGATTT	upstream of the *cth2-1* T-DNA
CTH2-1_REV	CACGAGGTTTTCCACTTTGAGC	downstream of *cth2-1* T-DNA
CTH2-2_FWD	ATCAGGAG GAAGAGATAGAAG	upstream of *cth2-2* T-DNA
CTH2-2_REV	TGTGATCAGCTTGAGGGATGAC	downstream of *cth2-2* T-DNA
LBa1	TGGTTCACGTAGTGGGCCATCG	left border-region of the T-DNA
RBa1	GGGTTGGGGTTTCTACAGGACGTAAC	right border-region of the T-DNA

To detect partial transcripts, generated at the *CTH2* locus in the *cth2-1*and *cth2-2* T-DNA mutants, RNA was isolated from WT and homozygous mutant plants and reverse transcribed to cDNA. It was then tried to amplify different fragments of the *CTH2* transcript from this cDNA preparation (Table 7). To demonstrate successful cDNA synthesis a product was amplified from the *Elongation Factor 1α* (*EF1α)* transcript. For primer pairs I, II and IV PCR conditions were: T_a 55°C, t_e 1 min, 35 cycles. For primer pairs III and V PCR conditions were: T_a 59°C, t_e 1 min, 35 cycles. For *EF1α* PCR conditions were: T_a 55°C, t_e 1 min, 25 cycles.

Table 7: Primer pairs used to detect partial transcripts in *cth2* T-DNA mutants.

Name	Sequences 5' to 3'
I	GCGTCAAGATATGGTGAATCG TGTGATCAGCTTGAGGGATGAC
II	GCGTCAAGATATGGTGAATCG CACGAGGTTTTCCACTTTGAGC
III	ATCAGGAGGAAGAGATAGAAG TGTGATCAGCTTGAGGGATGAC
IV	GCGTCAAGATATGGTGAATCG CTCCTGATCTTCTTTCTTCCC
V	ATCAGGAGGAAGAGATAGAAG TGTGATCAGCTTGAGGGATGAC
EF1α	TAAGGATGGTCAGACCCGTGA GAGACTCGTGGTGCATCTCAAC

3.8.4 **Detection of overexpressed *CTH2* cDNAs by semi-quantitative RT-PCR.**

To detect overexpressed *CTH2* cDNAs in transgenic *Arabidopsis* plants (chapter 3.3.4) RNA was extracted and reverse transcribed to cDNA in a 20 µl reaction (chapter 3.4.5). One µl of a cDNA-synthesis reaction was then used as a template for a 25 µl PCR reactions. By using different combination of primers (Table 8) it was attempted to amplify the overexpressed *CTH2* cDNA. To demonstrate the success of cDNA synthesis, a product was amplified from the *Elongation Factor 1α* (*EF1α)* transcript. The reaction-specific PCR conditions for all reactions were: T_a 55°C, t_e 1 min, 25 cycles. After amplification, 10 µl of the PCR reactions were analyzed by agarose-gelelectrophoresis, so that transcript levels could be compared semi-quantitatively.

Table 8: Primer pairs used to detect overexpressed *CTH2* cDNAs by semiquantitative RT-PCR.

Name	Sequences 5' to 3'
CTH2_FL	GCGTCAAGATATGGTGAATCG TGTGATCAGCTTG AGGGATGAC
CTH2_Nterm	GCGTC AAGATATGGTGAATC CTCCTGATCTTCTTTCTTCCC
CTH2_Cterm	ATCAGG AGGAAGAGATAGAAG TGTGATCAGCTGAGGGATGAC
EF1α	TAAGGATGGTCAGACCCGTGA GAG ACTCGTGGTGCATCTCAAC

3.9 Histological Methods

3.9.1 **Histochemical staining of transgenic plants expressing β-Glucuronidase**

To visualize domains of promoter activity, *Arabidopsis thaliana* was stably transformed with constructs allowing expression of the bacterial *uidA* gene under the control of the promoter of interest (Jefferson et al., 1987). The *uidA* gene from *E. coli* encodes a β-glucuronidase (GUS) which can cleave off the glucuronic acid residue from 5-Brom-4-chlor-3-indolyl-β-D-glucuronic acid (X-Gluc). The indoxyl residue dimerizes in the presence of O_2 to form 5, 5'-Dibrom-4, 4'-dichlor-indigo, which is a blue dye.

Tissues from transgenic *Arabidopsis thaliana* plants were immersed in GUS-staining solution (50 mM Na_3PO_4, 2 mM $K_4Fe(CN)_6$, 2 mM $K_3Fe(CN)_6$, 0.2% (v/v) Triton X-100, 2 mM X-Gluc), and a vacuum of at least 100 mbar was applied for 5 min. The vacuum was released slowly, and tissues were incubated at 37°C until the intensity of the staining was considered sufficient. The staining solution was then removed and the tissue was incubated in 70% (v/v) ethanol to remove chlorophyll. The ethanol was changed daily until the tissue was cleared sufficiently for observation of GUS staining. Images were taken with a digital SLR camera, or in the case of smaller samples with a binocular or a light-microscope.

Similar to X-Gluc, also C_{12}-fluorescein-di-β-D-galactopyranoside (Imagene-Green, Life Technologies, Darmstadt, Germany) was used as a substrate for the GUS enzyme. The fluorescence of the fluorescein residue is activated after cleavage of the sugar residues by GUS. The C_{12} lipophilic residue allows Imagene-Green to pass through membranes of living cells. It allows the visualization of promoter activity with a higher spatial resolution by confocal laser scanning microscopy (CLSM). Tissues from *Arabidopsis thaliana* were submerged in staining solution (33 µM Imagene Green, 0.2% (v/v) Triton X-100 in PBS, pH 7.4) and vacuum infiltrated for 5 min. The vacuum was released slowly and staining was performed at 37°C for 30 min. Then the staining solution was replaced with PBS and samples were observed with a confocal laser-scanning microscope. Wavelengths can be found in Supplemental Table3.

3.9.2 **Alexander's stain**

To stain viable pollen, Alexander's stain (Alexander, 1969) was used. Anthers from opened flowers of *Arabidopsis thaliana* were placed on a microscopy glass slide using forceps. A drop of Alexander's staining solution (see below) was applied to the glass slide, and a cover slip was placed on the slide. The sample was observed immediately using a light microscope. Viable pollen appeared in magenta-red color.

Alexander's staining solution: 50 ml ultrapure water, 10 ml ethanol, 25 ml glycerol, 1 ml glacial acetic acid, 5 g phenol, 5 g chloral hydrate, 1 ml 1% (w/v) malachite green (4-[(4-dimethylaminophenyl)phenyl-methyl]-*N*,*N*-dimethylaniline) in 95% (v/v) ethanol, 5 ml 1% (w/v) fuchsine (4-[(4-Aminophenyl)-(4-imino-1-cyclohexa-2,5-dienylidene)methyl]aniline hydrochloride), 0.5 ml 1% (w/v) orange G (Na_2(8Z)-7-oxo-8-(phenylhydrazinylidene) naphthalene- 1,3-disulfonate)

3.9.3 **Fixing and embedding of plant tissues in resin**

To fix plant organs for later embedding and sectioning, the tissues were completely submerged in phosphate buffer pH 7.4 containing 20 g l^{-1} sucrose and 35 g l^{-1} para-formaldehyde. A vacuum of at least 100 mbar was applied for 15 min and released slowly twice. Then the buffer was renewed and vacuum-infiltration was repeated once. Then the buffer was changed again, this time omitting the para-formaldehyde. A vacuum of at least 100 mbar was applied for 5 min and released slowly twice. After this, the samples were incubated for 2 h at room temperature. Then the samples were dehydrated using an ascending series of ethanol concentrations (50%, 70%, 80%, 90%, 99.5% (v/v) in water). A vacuum was applied for 10 min and released slowly after each increase in ethanol concentration. After fixing, the samples were placed in embedding forms (Histoform S) and embedded in Technovit 7100 according to the manufacturer's protocol. The polymerized resin was then mounted onto a microtome adaptor (Histoblocks) using household two-component glue. Technovit 7100, Histoform S, and Histoblocks were suppliedfrom Heraeus Kulzer, Wehrheim/Taunus, Germany.

3.9.4 **Thin sectioning of resin-embedded plant tissues**

Sectioning of resin-embedded tissues was performed on a rotary microtome (RM 2065, Leica Microsystems, Wetzlar, Germany). Series of sections of 3 µm thickness were prepared. While cutting, consecutive sections stayed attached to each other, forming a ribbon of sections. Immediately after sectioning, the ribbon was placed on a water surface to expand the individual sections. After *ca*. 1 min the sections were transferred to a microscope glass slide and warmed to ca. 60 °C on a hot plate until dry. Then section were ready for observation or further staining procedures.

3.9.5 **Toluidine blue stain of resin-embedded sections**

Resin-embedded sections of tissues were stained using toluidine blue. For this, individual sections on a microscope glass slide were covered with a drop of a solution of 1% (w/v) toluidine blue in ultrapure water for 1 min. After incubation in the staining solution, the sections were carefully rinsed with water for destaining and subsequently observed using a light microscope.

4 Results

4.1 Identification of homologues of *Hs*TTP and *Sc*CTH2 in *Arabidopsis thaliana*

A database consisting of translated nucleotide sequences of the *Arabidopsis thaliana* reference RNA sequences (refseq_rna), provided by the National Center for Biotechnology Information (NCBI, Rockville Pike, MD, USA), was queried by the TBLASTN algorithm (Altschul et al., 1990) using the *Saccharomyces cerevisiae* Cysteine Three Histidine 2 (*Sc*CTH2) amino acid sequence (285 amino acids in total) as an input.

The two sequences producing the most significant alignments were the amino acid sequences of the proteins encoded by the loci At1g68200 (three consecutive hits covering amino acid positions 169 to 233 of the query, BLAST E-value 1e-13) and At1g66810 (three consecutive hits covering amino acid positions 169 to 235 of the query, BLAST E-value 4e-13). At1g66810 was named *AtCTH1* and At1G68200 was named *AtCTH2*. The proteins encoded by these two genes also represented a distinct pair in the genome-wide, phylogenetic analysis of all proteins containing a CCCH-type zinc finger in *Arabidopsis* (Wang et al., 2008a), suggesting that these two proteins might belong to a distinct protein family within the CCCH superfamily that exists in human, yeast and plants. Out of all *Arabidopsis* proteins with at least one CCCH motif, these two proteins were the only proteins containing a tandem zinc finger (TZF) domain characteristic of *Hs*TTP, *Sc*CTH1 and *Sc*CTH2. The next best hit of the TBLASTN search was the protein encoded by the locus At2g35430 (BLAST E-value 1e-9). This protein also had two CCCH motifs, but these were not in a close tandem arrangement and are thus unlikely to constitute a TZF domain.

Alignment of the amino acid sequences of *Hs*TTP, the two yeast TZF proteins and the two *Arabidopsis thaliana* TZF proteins showed that the TZF domain is highly conserved, whereas the sequences outside the TZF domain are less conserved (Supplemental Fig. 1). *At*CTH2 exhibited 21.1% amino acid identity to *Sc*CTH2 over the entire length of the protein (Fig. 1a). However, between the 62 amino acids forming the TZF domains, the amino acid sequence identity was 45.2%. Since the TZF domain is highly conserved across species, its amino acid sequence was analyzed in more detail. Conserved residues included the C and H residues of

each zinc finger, as well as a KTEL motif upstream of the first zinc finger (Fig. 1b). Overall, 13 out of the 15 residues, which were identified by (Hudson et al., 2004) to interact directly with RNA bases, were strictly conserved between TZF proteins from human, yeast and plants. Interestingly, some residues in the TZF domain are unique to the plant kingdom and distinct from yeast or human TZF proteins. These plant specific motifs were: an NKW motif in the first zinc finger, an MVL motif in the second zinc finger and a PVI motif in between the two zinc fingers. This indicated that the RNA-recognition sequence of the two identified plant TZF proteins might slightly differ from *Hs*TTP or *Sc*CTH2.

No other domain was identified in the amino acid sequence of any of the plant TZF proteins by comparison to the PFAM database (Punta et al., 2011). To identify putative uncharacterized domains, the evolutionary conservation of each amino acid position was analyzed. First, amino acid sequences from *At*CTH2-homologues from 20 angiosperm species were identified by a BLASTP search using the interface provided on www.phytozome.org (Goodstein et al., 2011) and the *At*CTH2 amino acid sequence as a query. After manually removing duplicate hits and proteins with non-TZF CCCH domains, 43 amino acid sequences were aligned using Jalview 2.7 (Waterhouse et al., 2009). For each column of the alignment the percentage of amino acids identical to the modal amino acid was calculated to identify sequence regions with high conservation. As expected, the TZF domain was the most conserved region (Fig. 1c). The majority of the remaining sequence showed little conservation between species. However, two conserved regions (CRs) located N-terminally of the TZF domain could be identified by high consensus scores (75% to 100%). CR1 covered amino acids 39 to 88 of the *At*CTH2 protein and CR2 covered amino acids 150 to 170, respectively. This indicated that these sequence regions might be of functional importance, for example for the interaction with other component of the transcript degradation machinery.

(a)

Full-length protein					
	*Hs*TTP	*Sc*CTH1	*Sc*CTH2	*At*CTH1	*At*CTH2
*Hs*TTP		19.7	19.3	19.0	16.6
*Sc*CTH1	**36.5**		41.3	22.7	20.6
*Sc*CTH2	**34.0**	**56.9**		21.2	21.1
*At*CTH1	**35.0**	**41.5**	**38.1**		37.1
*At*CTH2	**30.7**	**42.2**	**40.3**	**58.4**	

TZF domain					
	*Hs*TTP	*Sc*CTH1	*Sc*CTH2	*At*CTH1	*At*CTH2
*Hs*TTP		51.6	51.6	58.1	58.1
*Sc*CTH1	**64.5**		79.0	45.2	45.2
*Sc*CTH2	**64.5**	**87.1**		43.5	45.2
*At*CTH1	**66.1**	**59.7**	**56.5**		85.5
*At*CTH2	**66.1**	**58.1**	**58.1**	**90.3**	

(b)

```
                 **          *↓   **↓                ***          *↓   **↓
HsTTP       KTELCRTFSESGRCRYGAKCQFAHGLGELRQANRHPKYKTELCHKFYLQGRCPYGSRCHFIH
HsBRF1      KTELCRPFEENGACKYGDKCQFAHGIHELRSLTRHPKYKTELCRTFHTIGFCPYGPRCHFIH
HsBRF2      KTELCRPFEESGTCKYGEKCQFAHGFHELRSLTRHPKYKTELCRTFHTIGFCPYGPRCHFIH
ScCTH1      KTELCESFTIKGYCKYGNKCQFAHGLNELKFKKKSNNYRTKPCINWSKLGYCPYGKRCCFKH
ScCTH2      KTELCESFTLKGSCPYGSKCQFAHGLGELKVKKSCKNFRTKPCVNWEKLGYCPYGRRCCFKH
Os1G45730   KTELCNKWEETGDCPYGDQCQFAHGVTELRPVIRHPRYKTAVCRMVLAGDVCPYGHRCHFRH
Os5G50080   KTELCNKWEETGACPYGDQCQFAHGVAELRPVIRHPRYKTQVCRMVLAGGVCPYGHRCHFRH
AtCTH1      KTELCNKWQETGACCYGDNCQFAHGIDELRPVIRHPRYKTEVCRMMVTGAMCPYGHRCHFRH
AtCTH2      KTELCNKWQETGTCPYGDHCQFAHGIKELRPVIRHPRYKTEVCRMVLAGDNCPYGHRCHFRH
AlCTH1      KTELCNKWQETGACPYGDNCQFAHGIGELRPVIRHPRYKTEVCRMIVTGAMCPYGHRCHFRH
AlCTH2      KTELCNKWQETGTCPYGDHCQFAHGIKELRPVIRHPRYKTEVCRMVLAGDNCPYGHRCHFRH
              CX8         CX5     CX3  H                  CX8         CX5     CX3  H
```

(c)

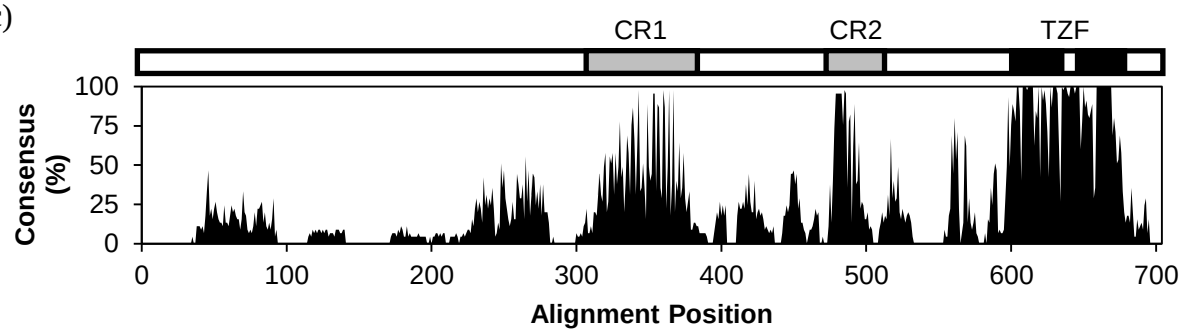

Figure 1: Sequence analysis of tandem zinc finger (TZF) proteins reveals high evolutionary conservation of the TZF domain.

Shown are (a) tables of percentage similarity (bold type) and percentage identity (normal type), calculated using MatGAT 2.02 (Campanella et al., 2003), based on pair-wise alignments of full-length amino acid sequences or the 62 amino acids forming the TZF domain from *Hs*TTP, two yeast and two *Arabidopsis thaliana* TZF proteins. (b) Sequence alignment of the TZF domains of proteins from human, yeast, rice and two *Arabidopsis* species. *Arabidopsis lyrata* locus Al475777 was named *Al*CTH1 and Al475938 was named *Al*CTH2. White-on-black characters were used to highlight the cysteine and histidine residues of the two CCCH-type zinc fingers, each involved in binding one Zn^{2+} cation. Underscored characters were used to highlight residues partially conserved in plants, but distinct from the TZF proteins of other organisms presented here. Arrows show residues intercalating between RNA bases and asterisks mark residues interacting with RNA bases *via* hydrogen bonds in *Hs*BRF1 (Hudson et al., 2004). (c) The percentage of amino acids identical to the modal amino acid (Consensus [%]) is plotted for each column of an alignment of 43 TZF proteins from 20 plant species (Supplemental Table 6, Appendix). Sequences were identified by a BLASTP search using the PHYTOZOME web interface

(Goodstein et al., 2011) and the *At*CTH2 amino acid sequence as a query. Jalview 2.7 (Waterhouse et al., 2009) was used to generate the alignment and to calculate consensus scores (in %). Black boxes show the position of the two CCCH-type zinc fingers in the TZF domain and grey boxes show conserved regions (CR) 1 and 2.

4.2 Functional analysis of *At*CTH2 by heterologous expression in *Saccharomyces cerevisiae*[1]

Saccharomyces cerevisiae CTH2 can negatively regulate transcript stability upon binding to AU-rich elements (AREs) in the 3'-untranslated regions (3'-UTRs) of target transcripts (Puig et al., 2005). To test, if *At*CTH2 has a similar function, its ability to physically interact with *Sc*CTH2 target transcripts was analyzed using the yeast three-hybrid system (Y3H) (SenGupta et al., 1996). This system consists of three chimeric constructs expressed in yeast (Fig. 2a). The first construct encodes a fusion protein consisting of a DNA-binding domain (LEXA) fused to an RNA-binding domain (MS2 CP). The second construct is a hybrid RNA, which consists of an RNA sequence (*MS2*) that is recognized by the RNA-binding domain of the first construct, and the RNA sequence of interest (in this case the 3'-UTRs of the *SDH4* and *ACO1* transcripts from yeast). The third construct encodes for a fusion protein which consists of the protein of interest (in this case *Sc*CTH2 and *At*CTH2) and a transcriptional activation domain (GAL4 AD). Upon interaction of the RNA and the protein of interest, transcription of a reporter gene is activated. The reporter gene was *Imidazole Glycerol-Phosphate Dehydratase* (*HIS3)*, which allows growth of *his3Δ* cells on histidine-free media (-His). To increase the specificity of the assay, 3-amino-1,2,4-triazole (3-AT) was used as a specific inhibitor of the HIS3 protein.

The interaction of *Sc*CTH2 with the 3'-UTRs of two *Sc*CTH2 target transcripts, *Succinate Dehydrogenase Subunit 4* (*SDH4*) and *Aconitase 1* (*ACO1*) (Puig et al., 2005), was used as a positive control. An interaction of *Sc*CTH2 with the *SDH4* and *ACO1* 3'-UTRs was

[1] Unpublished data shown in Fig. 2 and Fig. 3 were kindly provided by Dr. Sergi Puig (Instituto de Agroquímica y Tecnología de Alimentos, Valencia, Spain).

confirmed, as indicated by growth of cells on -His media (Fig. 2b). *At*CTH2 also seemed to interact with these 3'-UTRs. A mutated *At*CTH2-C243R, in which the third cysteine residue of the first CCCH domain, critical for RNA binding in the corresponding yeast and human proteins, was changed to arginine, could not activate reporter gene expression. This indicated that the interaction between *At*CTH2 and *Sc*CTH2 target transcripts in yeast is dependent on an intact TZF domain. The 3'-UTR of the yeast *SDH4* transcript contains two ARE-consensus sequences (UUAUUUAUUAUUAUUUAUU and UUAUUUAUU). When the first ARE was mutagenized to UU**C**UUUAUU**C**UUAUUU**C**UU, interaction with *Sc*CTH2 and *At*CTH2 was weaker compared to the non-mutated *SDH4* transcript, as indicated by the impaired growth on -His medium containing 100 µM or more 3-AT. When the second ARE was mutagenized additionally (UU**C**UUUAUU), no interaction was found, as indicated by the inability of growth on -His medium. This showed that the detected RNA-protein interaction was dependent on the presence of AREs in target transcripts.

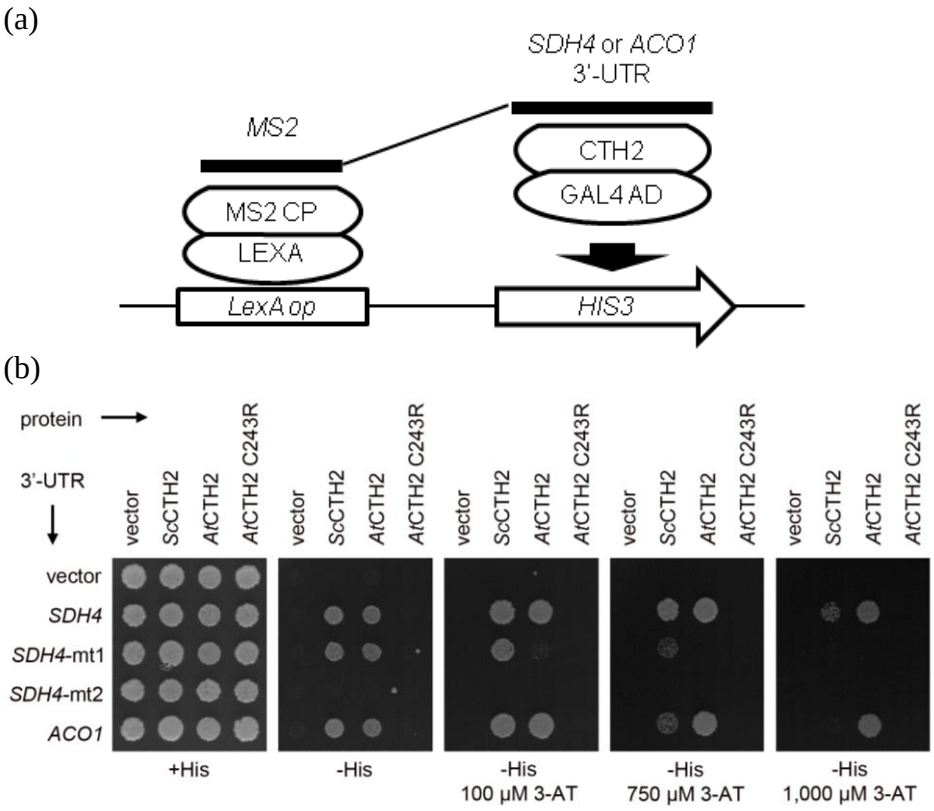

Figure 2: *Arabidopsis CTH2* can interact with target transcripts of yeast *CTH2*.

Shown is (a) a schematic overview of the yeast three-hybrid (Y3H) system used to detect interactions of *Sc*CTH2 and *At*CTH2 with the 3'-UTRs of the *ScSDH4* and *ScACO1* transcripts and (b) drop tests of Y3H assays for

protein-RNA interaction. In (a), *LexA op* is the DNA target sequence for binding of the *E. Coli* LEXA binding domain. MS2 CP is a bacteriophage coat protein that binds to the *MS2* RNA sequence. GAL4 AD is the transcriptional activation domain of the *E. coli* GAL4 protein. *Imidazole Glycerol-Phosphate Dehydratase* (*HIS3)* is encoding an enzyme required for histidine biosynthesis used here as a reporter for protein-RNA interaction in a *his3Δ* genetic background. In (b), the interactions of *Sc*CTH2, *At*CTH2 and a *At*CTH2 C243R mutant with the 3'-UTR of the *SDH4* transcript, two mutated versions of the 3'-UTR of the *SDH4* transcript with deletions of one (*SDH4-mt1*) or two (*SDH4-mt2*) AREs, and the 3'-UTR from the *ACO1* transcript are analyzed in the Y3H system. Cultures in the exponential growth phase were spotted in serial dilutions starting at A_{600} = 0.1 on SC medium with (+His) or without (-His) histidine and grown at 30°C for 4 days. 3-amino-1,2,4-triazole (3-AT) was used as a competitive inhibitor of HIS3 and added as indicated.

The transcript-destabilizing activity of *At*CTH2 was examined in a *cth1Δcth2Δ* yeast mutant. In this mutant, *SDH4* transcript levels are not reduced under Fe-deficient conditions, as opposed to WT cells (Fig. 3). Expression of either *ScCTH2* or *AtCTH2* from the *ScCTH2* promoter was able to restore Fe deficiency-dependent down-regulation of *SDH4* transcript levels. In accordance with the Y3H assays, a mutated *At*CTH2-C243R was unable to cause a reduction in *SDH4* transcript levels under Fe-deficient conditions. In summary, heterologous *At*CTH2 can substitute for *Sc*CTH2 function in yeast.

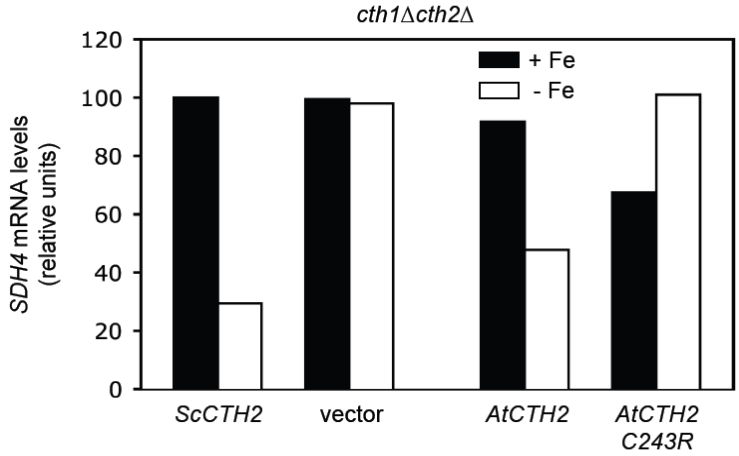

Figure 3: *Arabidopsis CTH2* is able to reduce *ScSDH4* transcript levels in a *cth1Δcth2Δ* yeast mutant in response to Fe deficiency.

Shown are relative *SDH4* transcript levels, as determined by RNA-blotting using RNA isolated from *cth1Δcth2Δ* cells, grown in Fe-sufficient (+Fe) or Fe-deficient (-Fe) conditions. Cells were transformed with an empty vector or vector containing expression constructs for *ScCTH2*, *AtCTH2*, or *AtCTH2-C243R* cDNAs. All constructs were

expressed from the *ScCTH2* promoter, which is induced in response to Fe deficiency. *SDH4* signal intensities were normalized to *Actin1* signal intensities.

4.3 Subcellular localization of *At*CTH2

4.3.1 Stable transformation of *Arabidopsis thaliana* with a chimeric *CTH2-GFP* fusion construct

To determine the subcellular localization of the CTH2 protein, *CTH2* was translationally fused to *GFP* (*Green Fluorescent Protein*) and placed downstream of the endogenous *CTH2* promoter in the binary plasmid pMDC107 (see chapter 3.3.2 and vector map in the Appendix). This construct was then used for the stable transformation of *Arabidopsis thaliana* WT (Col-0) plants. Twenty-two independent lines were generated and analyzed by fluorescence microscopy and confocal laser-scanning microscopy in the T2 and T3 generations. All plants were analyzed following selection on hygromycin-containing media, to ensure the presence of the T-DNA. No GFP signal was observed in any of the lines. This might be due to the fact that the promoter of *CTH2* does not sustain expression levels sufficient to generate a detectable GFP signal. It was attempted to observe fluorescence in roots and shoots of plants grown in sterile culture, hydroponic culture and soil culture. Since promoter activity was localized to anthers using a *pCTH2:GUS* construct (see Fig. 31), it was also unsuccessfully attempted to detect a GFP signal in anthers. The analysis of *pCTH2:GUS* lines also showed an induction of promoter activity after wounding of leaves (Fig. 12), so it was also tried to detect a GFP signal in shoots after wounding. Additionally, plants grown under Fe-deficient conditions in sterile and hydroponic culture were also analyzed. Since the subcellular localization of CTH2-GFP was not successful in stably transformed plants, a transient approach was pursued.

4.3.2 **Transient transformation of *Arabidopsis thaliana* mesophyll protoplasts**

A *35S:CTH2-GFP* construct for transient expression (chapter 2.3.3) was kindly supplied by Dr. Sergi Puig (Instituto de Agroquímica y Tecnología de Alimentos, Valencia, Spain). It contained the complete *CTH2* coding sequence as a C-terminal translational fusion with a *GFP*-encoding sequence. For the subcellular localization of CTH2, *Arabidopsis thaliana* mesophyll protoplasts were then used as a transient expression system. The fluorescent signal from a CTH2-GFP fusion protein was observed in granular structures in the cytosol (Figure 4b, c). These structures resembled the aggregates of messenger ribonucleoproteins (mRNPs) that can be observed in mammalian (Balagopal and Parker, 2009) and plant cells (Goeres et al., 2007; Weber et al., 2008). Since there are at least two different types of such structures, namely processing bodies (PBs) and stress granules (SGs), it was important to determine the exact type of structure CTH2 is localized to.

For this, the *35S:CTH2-GFP* construct was cotransformed with marker constructs for PBs (*XRN4-GFP*, *DCP1-Cherry*) and SGs (*RBP47-tdtomato*) (Weber et al., 2008 and chapter 2.3.3), which were kindly supplied by Dr. Markus Fauth (Göthe Universität, Frankfurt am Main, Germany). They contained the respective coding sequences as N-terminal translational fusions with GFP or the RFP variants mCherry and tdtomato in the pRTdS plasmid backbone (see vector maps in the Appendix). All marker constructs contained the CaMV 35S promoter to drive expression.

To test for the correct localization of known PB markers, the *XRN4-GFP* (*Exoribonuclease 4*) and *DCP1-mCherry* (*Decapping Enzyme 1*) constructs were co-transformed. DCP1 is part of the mRNA decapping complex and described as a component of PBs (Xu et al., 2006). XRN4 is an *Arabidopsis* homologue of *Sc*XRN1, the main RNA-degrading exoribonuclease in yeast (Souret et al., 2004). Both fusion proteins co-localized in granules in the cytosol (Fig. 4a). The number of granules and the fluorescence signal intensity increased after a heat-shock (HS) treatment (40°C, 30 min). This is in accordance with published results (Weber et al., 2008).

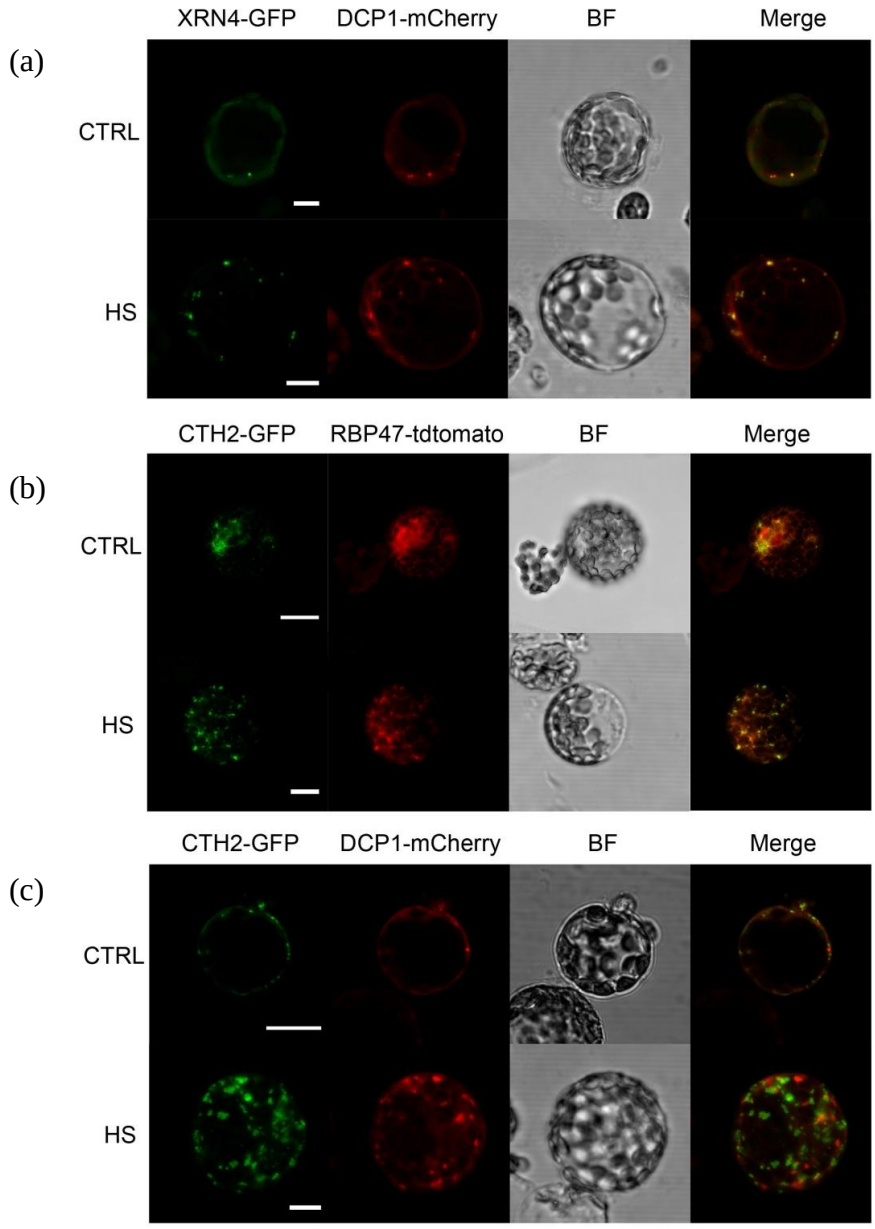

Figure 4: Transiently expressed *35S:CTH2-GFP* co-localizes with markers for plant stress granules, but not with markers for processing bodies in *Arabidopsis* mesophyll protoplasts.

Shown are images obtained with confocal laser-scanning microscopy of protoplasts transiently co-transformed with the indicated constructs. Each image consists of 20 superimposed *z*-slices covering a distance of *ca.* 30 µm in total. (a) Co-localization of processing body markers XRN4 and DCP1. (b) Partial co-localization of CTH2 and plant stress granule marker RBP47. (c) CTH2 does not co-localize with processing body marker DCP1. At least two independent transformations were performed for each combination of constructs, and representative images of five to ten recorded image sets per transformation are shown. BF shows a bright-field image. Merge shows an overlay of the GFP and the RFP channel. CTRL indicates no treatment prior to observation. HS indicates a heat-shock treatment (40°C, 30 min) prior to observation. Exoribonuclease 4 (XRN4) and Decapping

Enzyme 1 (DCP1) were used as markers for processing bodies. Ribonucleotide-Binding Protein 47 (RBP47) was used as a marker for plant stress granules. Scale bars: 25 µm.

The *CTH2-GFP* construct was then co-transformed with RFP fusions of marker proteins for PBs or SGs. First, *CTH2-GFP* was co-transformed with *RBP47-tdtomato*. RBP47 (Ribonucleotide-Binding Protein 47) was first described as a nuclear localized protein, which is associated with poly(A) mRNAs (Lorkovic et al., 2000). It contains three RNA-recognition motifs (Lorkovic and Barta, 2002), which are essential for localization to SGs during HS treatment (Weber et al., 2008). RBP47 is an *Arabidopsis* homologue of the human T-Cell Intracellular Antigen 1 (TIA-1) and TIA-related proteins, which are components of mammalian SGs (Kedersha et al., 2000). TIA-1 mediates the aggregation of mRNPs to SGs through a prion-like mechanism (Gilks et al., 2004). The CTH2-GFP signal was localized partly in granular structures and partly in diffuse structures, presumably in the cytosol (Fig. 4b). After an HS treatment, the number of GFP-fluorescent granules increased compared to untreated protoplasts. RBP47-tdtomato was localized diffusely in the cytosol and in what appears to be the nuclear region in untreated cells, which is in accordance with published data (Weber et al., 2008). After HS treatment, RBP47-tdtomato was localized to granular structures. In untreated protoplasts, diffusely localized CTH2-GFP partially co-localized with diffusely localized RBP47-tdtomato. In HS-treated protoplasts, CTH2-GFP and RBP47-tdtomato co-localized in granular structures, indicating that CTH2 is a component of SGs. *CTH2-GFP* was also co-transformed with *DCP1-mCherry*, a marker for PBs (Fig. 4c). CTH2-GFP and DCP1-mCherry localized to structures of similar size and outline, but did not co-localize. However, the fluorescent signals of the two fusion proteins were sometimes found in close proximity to one another, so it is possible that CTH2 is a peripheral component of PBs. When protoplasts were isolated from hydroponically grown, Fe-deficient plants, the localization of CTH2-GFP was similar as in Fe-sufficient plants shown in Fig 4 (data not shown), although no co-localization experiments were performed.

The translational inhibitor cycloheximide stabilizes polysomes by trapping ribosomes on translating mRNAs and prevents the aggregation of RBP47-tdtomato in SGs after HS treatment (Fig. 5 and Weber et al., 2008). In human cells, aggregation of the SG marker TIA-1 is dependent on the release of mRNAs from polysomes and free, non-translating mRNAs (Kedersha et al., 2000). Consequently, the inhibition of RBP47-tdtomato aggregation in SGs is probably due to the absence of non-ribosome associated mRNAs in the cytosol after

cycloheximide treatment (100 µg ml^{-1}, 15 min). However, granular localization of CTH2-GFP could still be observed following cycloheximide treatment. This indicated that the localization of CTH2-GFP to *bona fide* SGs is not dependent on the release of non-translated mRNAs from polysomes.

The co-localization experiments showed that CTH2 is partially localized to plant stress granules, which is in agreement with the hypothesized role of CTH2 in transcript degradation. The fact that the localization of CTH2 to plant SGs is not dependent on untranslated transcripts indicates that CTH2 might be involved in the degradation of specific transcripts rather than being part of a general RNA degradation mechanism that removes non-translating mRNAs from the cytosol.

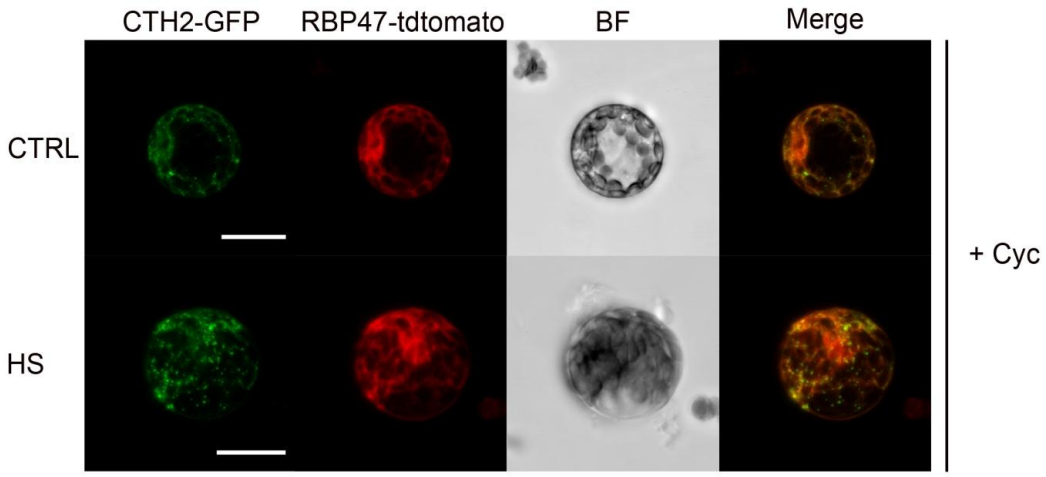

Figure 5: Localization of CTH2-GFP to granular structures is not inhibited by cycloheximide.

Shown are images obtained with confocal laser-scanning microscopy of protoplasts transiently cotransformed with the indicated constructs. Each image consists of 20 superimposed *z*-slices covering a distance of *ca.* 30 µm in total. Two independent transformations were performed and representative images of five to ten recorded images sets per transformation are shown. BF indicates a bright-field image. Merge shows an overlay of the GFP and the RFP channel. Cycloheximide treatment (+ Cyc) was performed by adding cycloheximide to the protoplast suspension to a final concentration of 100 µg ml^{-1} and incubation for 15 min. HS indicates a heat-shock treatment (40°C, 30 min), immediately after + Cyc treatment, prior to observation. CTRL indicates no further treatment prior to observation.Ribonucleotide-Binding Protein (RBP47) was used as a marker for plant stress granules. Scale bars: 25 µm.

4.4 Transcript levels of *AtCTH2* in different plant tissues

Relative transcript levels of *AtCTH2* were determined by qRT-PCR, using RNA extracted from different tissues of *Arabidopsis thaliana* WT (Col-0) plants. *CTH2* transcript was detected in all tissues (Fig. 6). Transcript levels were generally low, in the range of those for *Helicase*, the control gene expressed at low levels in all tissues. *CTH2* transcript levels were highest in stems of inflorescences and flower buds of stage 9 to 10 and lowest in roots. This was in agreement with data obtained from publicly available microarray data sets (Schmid et al., 2005b).

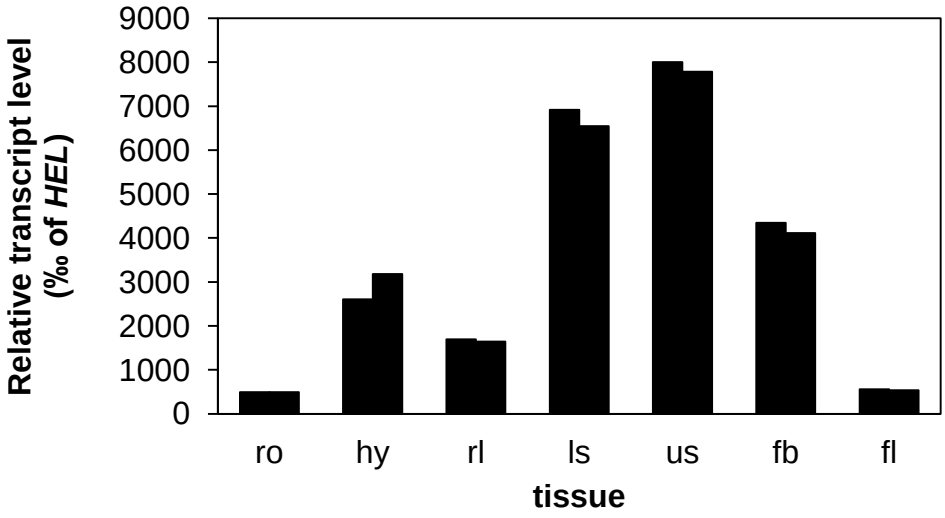

Figure 6: Relative transcript levels of *Arabidopsis CTH2* are low in all tissues.

Shown are relative transcript levels of *AtCTH2* in different tissues. Plants were grown in hydroponic culture for 45 days to harvest roots (ro) or on soil to harvest hypocotyls (hy), rosette leaves (rl), stem tissue without cauline leaves or reproductive organs from the lower (ls) or upper (us) half of the inflorescence stem, flower buds (floral stage 9 to 10) (fb) and flowers during anthesis (floral stage 13) (fl). For each type of tissue, material from at least five individual WT plants was pooled. RNA was extracted, reverse transcribed to cDNA, and relative transcript levels were determined by qPCR with two technical replicates of each reaction. Each bar represents one technical replicate. *Helicase* (*HEL*), a constitutively expressed control gene, was used for normalization of *CTH2* transcript levels.

4.5 Transcript levels of *AtCTH2* in shoots respond to iron status in an age-dependent manner

Based on preliminary results obtained by Leonard Krall and Ute Krämer, it was tested whether transcript levels of *CTH2* respond to Fe supply. For this, qRT-PCR was used to measure the relative transcript levels of *CTH2* in WT plants of different ages grown under Fe-sufficient or Fe-deficient conditions. First, plants were grown in a sterile cultivation system on agar-based solid HG medium and analyzed after 28 days of growth, with the final 14 days of cultivation on medium with no added Fe. No Fe-dependent regulation of *CTH2* transcript levels was observed in roots or shoots (Fig. 7a). When 45-day-old plants grown in hydroponic culture in liquid HG medium were analyzed, *CTH2* transcript levels were found to be up-regulated in shoots four-fold under Fe-deficient conditions compared to Fe-sufficient conditions (Fig. 8a). No Fe-dependent regulation of *CTH2* transcript levels was observed in the roots of 45-day-old plants. The transcript levels of the closest homologue of *AtCTH2*, *AtCTH1* were not found to be regulated in response to Fe supply regardless of age (data not shown). The analysis of *CTH2* transcript levels indicated a role of *CTH2* in the homeostasis of Fe, probably restricted to shoots of mature, 45-day-old plants.

To ensure that the Fe-deficient growth conditions employed did cause a Fe-deficiency response in the plants, transcript levels of Fe-deficiency marker genes were also analyzed in 28 and 45-day-old plants. When plants are subjected to Fe-deficient conditions, transcript levels of *Ferritin 1* (*FER1*), encoding a shoot Fe-storage protein (chapter 1.5.3), are known to decrease. Transcript levels of *Ferric Reduction Oxidase 3* (*FRO3*), encoding a Fe^{III} chelate reductase, probably contributing to Fe reduction in shoots, are reported to increase when plants are subjected to Fe deficiency (Mukherjee et al., 2006). As expected, transcript levels of *FER1* decreased *ca.* ten-fold under Fe-deficient conditions compared to Fe-sufficient conditions in plants of both ages (Figs. 7b, and 8b). Transcript levels of *FRO3* increased about three-fold and nine-fold under Fe-deficient conditions, compared to Fe-deficient conditions in shoots of younger and older vegetative plants, respectively (Figs. 7c and 8c). In root tissues, transcript levels of *Iron-Regulated Transporter 1* (*IRT1)* and *Ferric Reduction Oxidase 2* (*FRO2)*, two main components of the Fe-uptake system (chapter 1.5.1) were determined. As expected, transcript levels of *IRT1* and *FRO2* were increased under Fe-deficient conditions in plants of both analyzed ages up to 30-fold in 28-day-old plants and about 5 to 6-fold in 45-

day-old plants compared to Fe-sufficient conditions (Figs. 7d, e and 8d, e). These results showed that all analyzed tissues were Fe-deficient.

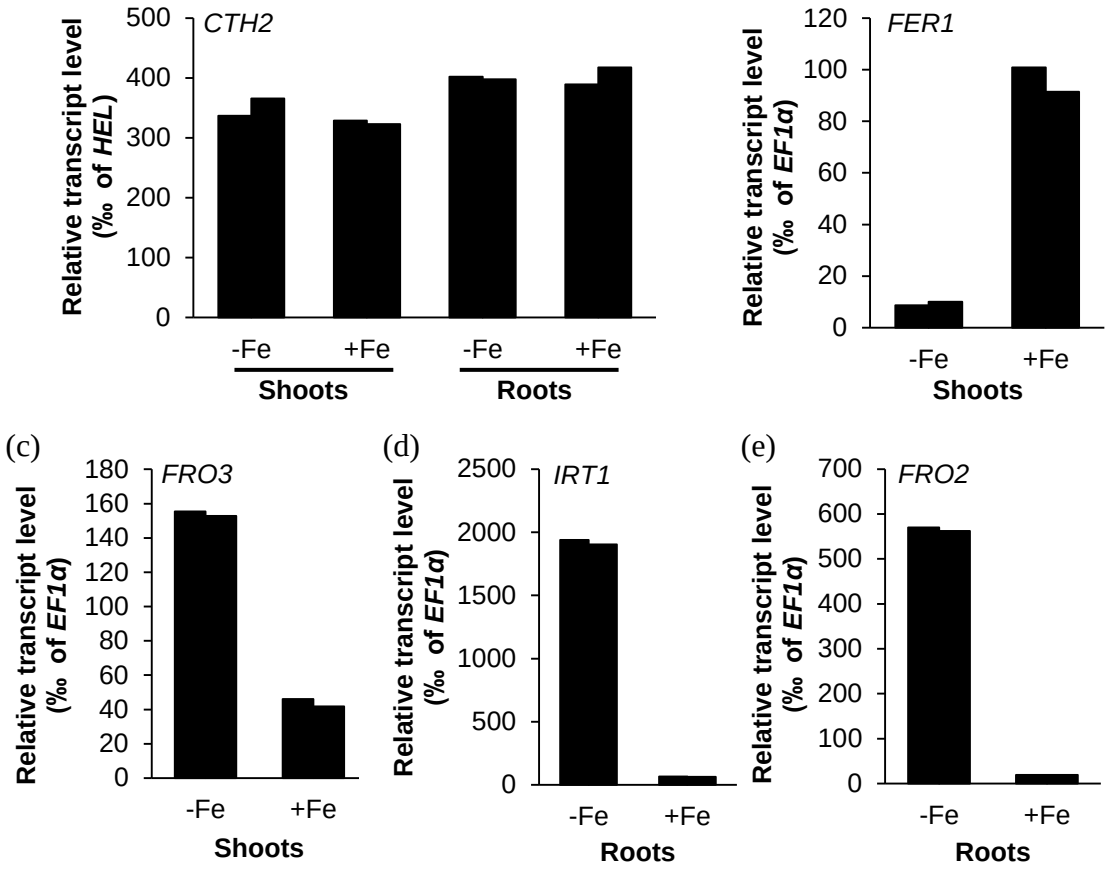

Figure 7: In 28-day-old plants *CTH2* transcript levels do not respond to Fe status.

Shown are relative transcript levels in 28-day-old WT plants grown in sterile culture. Plants were grown in the absence of added Fe (-Fe) for the final 14 days of cultivation. Control plants (+Fe) were grown on media containing 5 µM FeHBED throughout. RNA was extracted from shoot (a, b, c) or root (a, d, e) material pooled from 12 individual plants, reverse transcribed to cDNA, and relative transcript levels were determined by qPCR with two technical replicates of each reaction. Each bar represents one technical replicate. Data are shown from a single experiment representative of a total of two independent experiments. *Helicase* (*HEL*) (a) and *Elongation Factor 1α* (*EF1α) (*b-e) are constitutively expressed control genes and were used for normalization of transcript levels. Fe-status marker transcripts were *Ferritin 1* (*FER1*) (b) and *Ferric Reduction Oxidase 3* (*FRO3*) (c) in shoots and *Iron-Regulated Transporter 1* (*IRT1)* (d) and *Ferric Reduction Oxidase 2* (*FRO2)* (e) in roots.

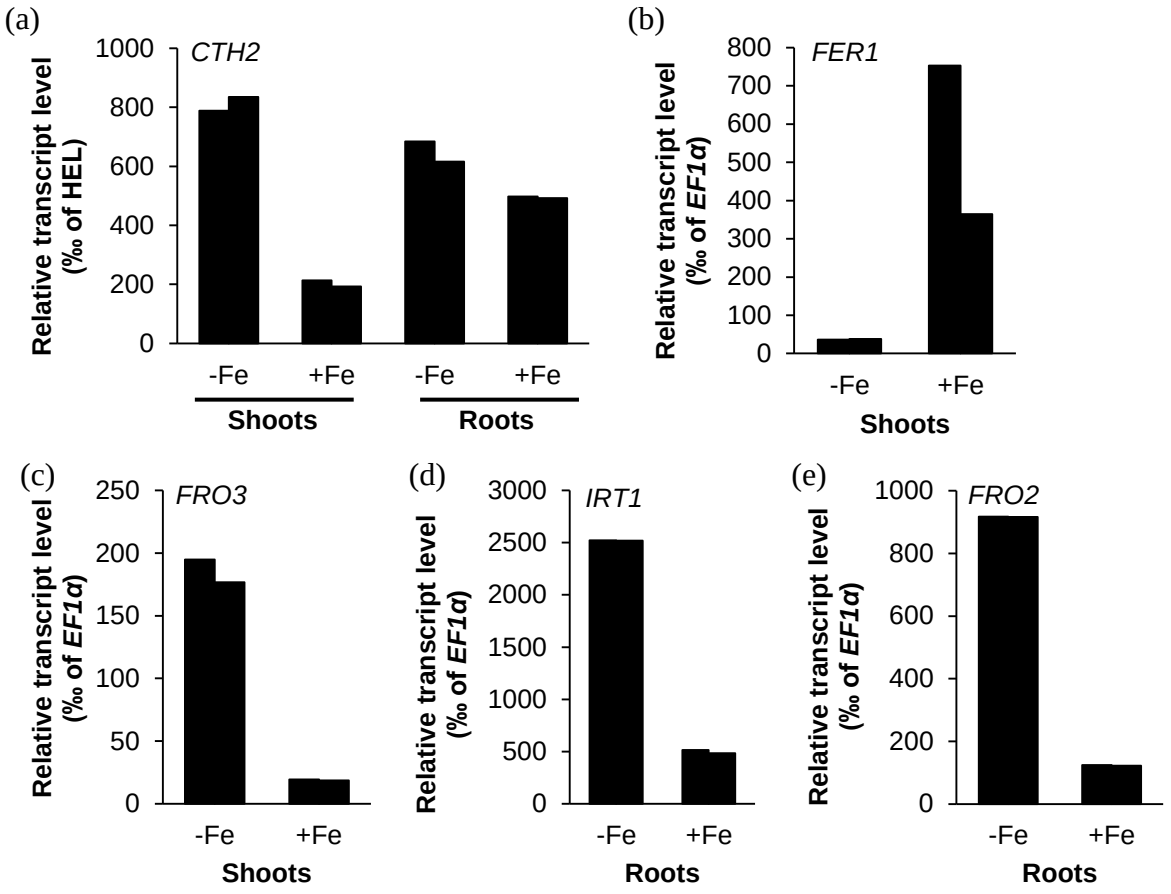

Figure 8: In 45-day-old plants *CTH2* transcript levels respond to Fe status in shoots, but not in roots.

Shown are relative transcript levels in 45-day-old WT plants grown in hydroponic culture. Plants were grown in the absence of added Fe (-Fe) for the final 10 days of cultivation. Control plants (+Fe) were grown in hydroponic solution containing 5 µM FeHBED throughout. RNA was extracted from shoot (a, b, c) or root (a, d, e) material pooled from at least five individual plants, reverse transcribed to cDNA, and relative transcript levels were determined by qPCR with two technical replicates for each reaction. Each bar represents one technical replicate. Data are shown from a single experiment representative of a total of four independent experiments. *Helicase* (*HEL*) (a) and *Elongation Factor 1α* (*EF1α)* (b-e) are constitutively expressed control genes and were used for normalization of transcript levels. Fe-status marker transcripts were *Ferritin 1* (*FER1*) (b) and *Ferric Reduction Oxidase 3* (*FRO3*) (c) in shoots and *Iron-Regulated Transporter 1* (*IRT1)* (d) and *Ferric Reduction Oxidase 2* (*FRO2)* (e) in roots.

4.6 Localization of *CTH2* promoter activity

4.6.1 Stable transformation of *Arabidopsis thaliana* with a chimeric *CTH2*-promoter reporter gene fusion construct

A 1.5-kb fragment of the promoter of *CTH2*, including the bases encoding the first five amino acids of the CTH2 protein, was fused to the bacterial *uidA* reporter gene encoding β-glucuronidase (GUS), using the binary plasmid pMDC163 (see chapter 3.3.1 and vector map in the Appendix). The resulting *pCTH2:GUS* construct was used for stable transformation of *Arabidopsis thaliana* WT (Col-0) plants. The activity of the *CTH2* promoter was then visualized by histochemical staining using 5-Bromo-4-chloro-3-indolyl-β-D-glucuronide (X-Gluc) or C_{12}-fluorescein-di-β-D-galactopyranoside (Imagene Green) as dyes. Since the *pCTH2:GUS* construct is randomly inserted into the genome, observed staining patterns can be influenced by positional effects. To ensure that the observed patterns and responses were independent of positional effects of the insertion of the transgene, 11 independent lines were analyzed in the T2 generation. Three lines that showed a representative staining pattern and in which 75% of all individuals were resistant to hygromycin (the selectable marker of pDMC163 in plants), indicating a single locus of insertion, were selected for further analysis and propagated to the T3 generation. Analysis was performed with hygromycin-resistant plants in the T2 generation or homozygous T3 populations, which showed no segregation for the selectable marker, indicating homozygosity of the introduced transgene.

4.6.2 Localization of *CTH2* promoter activity in roots

In roots, the promoter of *CTH2* was constitutively active. No differences in promoter activity or localization were observed between plants of different ages (7, 28 or 45 days of growth) or grown under different Fe regimes (data not shown). Promoter activity in roots was detected in the central cylinder (Fig. 9a) of the root hair zone. By using Imagene Green, promoter activity could be localized to the pericycle, with possibly minor activity in the endodermis (Fig. 9b).

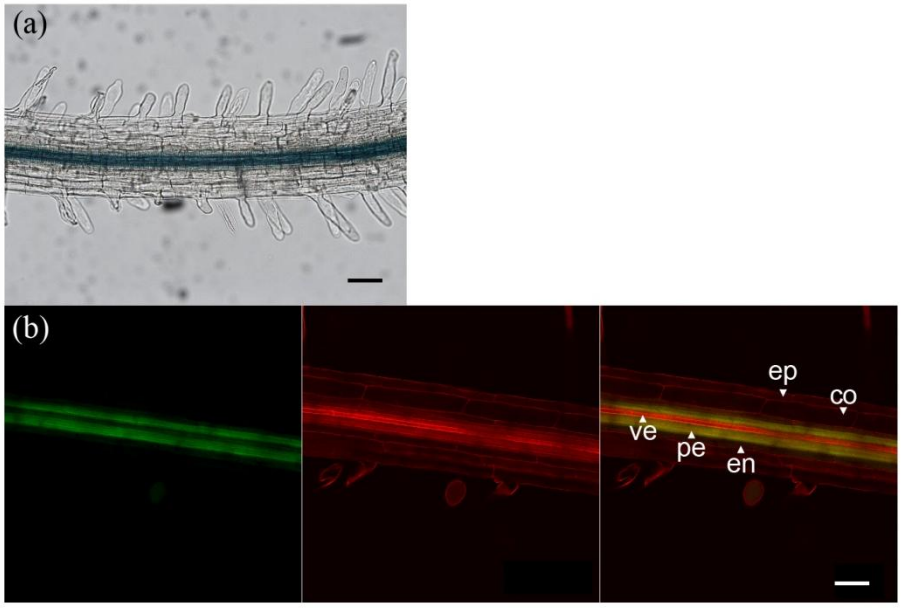

Figure 9: The activity of the *CTH2* promoter in roots is localized to the central cylinder.

Shown are images of roots of 21-day-old plants expressing the *uidA* gene under the control of a 1.5-kb fragment of the *CTH2* promoter. Transformants were generated as described in the main text. Plants were stained using (a) 5-Bromo-4-chloro-3-indolyl-β-D-glucuronide for 4 h and destained using ethanol or (b) stained using Imagene Green for 30 min, followed by Propidiumiodide staining for 1 min, and imaged immediately. Panels in (b) show (from left to right): Imagene Green stain, Propidiumiodide stain, merge. Images were obtained using (a) a conventional light microscope or (b) a confocal laser-scanning microscope. In (b), a single longitudinal optical section is shown. Eleven independent lines were analyzed in the T2 generation after selection on hygromycin, and representative results are shown. ve = xylem vessel, pe = pericycle, en = endodermis, co = cortex, ep = epidermis. Scale bars: 50 µm.

4.6.3 **Localization of *CTH2* promoter activity in shoots**

In shoots, *CTH2* promoter activity was dependent on the developmental stage of the plant. In younger shoot tissues (until 28 days of growth), the *CTH2* promoter exhibited a strong activity. Staining time for a typical GUS experiment was 2 to 6 h. This is short compared to overnight staining, which is used for most promoter-GUS constructs. This observation was in contrast to *CTH2* transcript levels, which were generally very low. In seedlings, the cotyledons and the hypocotyl were stained, indicating *CTH2* promoter activity (Fig. 10a). Strong staining was observed in the vasculature of the cotyledons (Fig. 10b). When the plants

developed true leaves, the staining in the cotyledons was persistent, whereas no staining was observed in true leaves (Fig. 10c). In 28-day-old plants, the staining pattern of the leaves and the number of stained leaves became more variable between individuals (Fig. 10d). In rosette leaves of 45-day-old plants, the promoter activity was strongly reduced compared to younger plants, with the exception of occasional staining of small sectors in older leaves (Fig. 10e). Additionally, staining was observed in the hydathodes of 45-day-old plants (Fig. 10f). The supply with Fe had no reproducible effect on the number of stained leaves or the intensity of staining (Fig. 11).

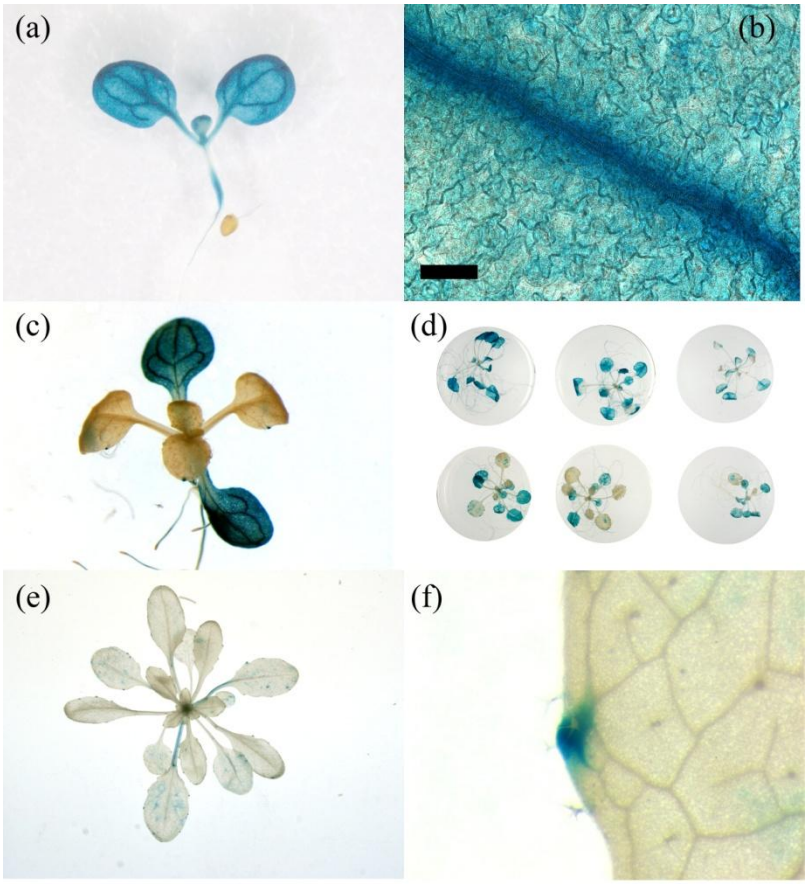

Figure 10: The activity of the *CTH2* promoter changes during vegetative development.

Shown are images of plants expressing the *uidA* gene under the control of 1.5-kb fragment of the *CTH2* promoter. Transformants were generated as described in the main text. Plants were stained using 5-Bromo-4-chloro-3-indolyl-β-D-glucuronide for 4 h (a-d) or 24 h (e and f) and subsequently destained using ethanol. The panels show: (a) a 7-day-old seedling, (b) a microscopic image of the vasculature in cotyledons from a 7-day-old seedling, (c) a 14-day-old plant, (d) six representative 28-day-old plants, (e) a 45-day-old plant and (f) a microscopic image of the margin of a rosette leaf surrounding a hydathode of a 45-day-old plant. Plants in (a)-(d) were grown in sterile culture on solid medium; plants in (e) and (f) were grown on soil under controlled

environmental conditions in short days. Eleven independent lines were analyzed in the T2 generation after selection on hygromycin, and representative results are shown. Scale bar in (b): 50 µm.

Figure 11: The activity of the *CTH2* promoter is not regulated by Fe status.

Shown are 28-day-old plants grown in sterile culture expressing the *uidA* gene under the control of a 1.5-kb fragment of the *CTH2* promoter. Transformants were generated as described in the main text. Plants were grown in sterile culture without added Fe (-Fe) for the final 14 days of cultivation. Control plants (+Fe) were grown on 5 µM FeHBED throughout. Plants were stained using 5-Bromo-4-chloro-3-indolyl-β-D-glucuronide for 4 h and destained using ethanol. For each treatment, three individual plants from three independent transgenic lines (n = 9 plants) were analyzed in the T3 generation. Shown is one representative plant from each line for each treatment. Data shown are from one experiment representative of a total of two experiments.

4.6.4 **Promoter activity in shoots after wounding**

Handling of plant tissues for GUS staining occasionally leads to wounding of the tissues. It was observed that wounding led to strong GUS staining in the shoots of *pCTH2:GUS* lines (Fig. 12). The GUS staining was confined to the site of the wounding and did not spread systemically. No staining was observed when WT plants were wounded and stained for β-glucuronidase activity (data not shown). When WT plants were wounded, and relative transcript levels of *CTH2* were analyzed, a two-fold increase of transcript levels 24 h after wounding was detected (Fig. 13). This contrasting data indicated that *CTH2* transcript levels

might be regulated not only by transcriptional control but also by post-transcriptional mechanisms.

Figure 12: *CTH2* promoter activity is induced in leaves in response to wounding.

Shown are images of leaves from six-week-old plants expressing the *uidA* gene under the control of a 1.5 kb-fragment of the *CTH2* promoter. Transformants were generated as described in the main text. Leaves were wounded with a 3-mm diameter cork borer and stained using 5-Bromo-4-chloro-3-indolyl-β-D-glucuronide (X-Gluc) at the indicated time points after the wounding stimulus and destained using ethanol. Images show representative results of three independent experiments, each performed with two independent transgenic lines in the T3 generation. Scale bar: 2 mm.

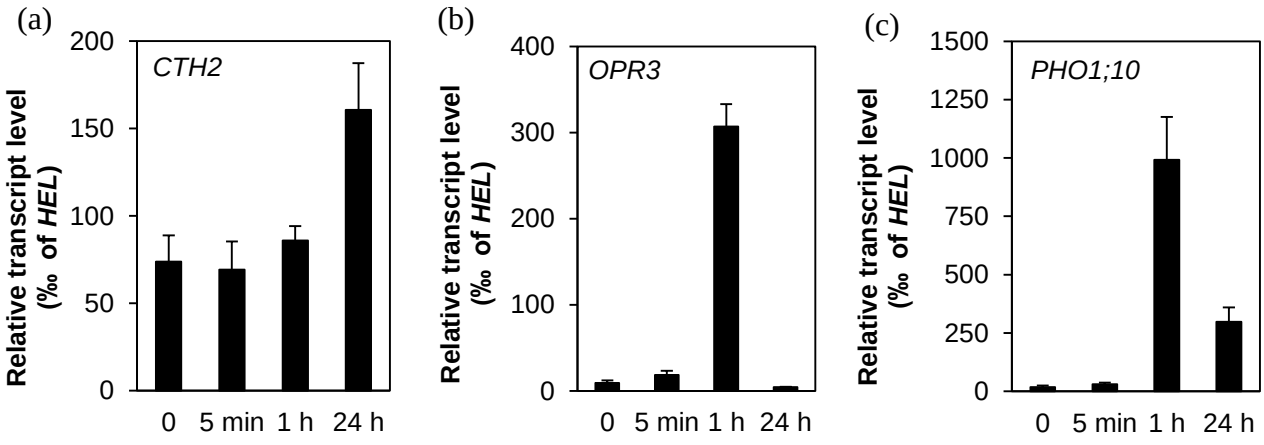

Figure 13: Transcript levels of *CTH2* respond moderately to wounding after 24 h.

Shown are relative transcript levels in 6-week-old WT plants grown on soil. For each time point, five leaves of similar relative position within the rosettes of five different plants were wounded with a 3-mm cork borer. Leaves were harvested for RNA extraction at the indicated time points after wounding. RNA was extracted from

pooled leaves, reverse transcribed into cDNA, and analyzed by qPCR. Bars represent arithmetic means ± SD of three independent experiments. *Helicase* (*HEL*) (a-c) is a constitutively expressed control gene and was used for normalization of transcript levels. Transcript levels of (b) *12-Oxophytodienoate Reductase 3* (*OPR3*) and (c) *Phosphate Transporter 1;10* (*PHO1;10*) were previously published to respond to wounding (Strassner et al., 2002; Ribot et al., 2008).

4.7 Identification of two *Arabidopsis* T-DNA mutants with insertions in the *CTH2* locus

A common approach to characterize gene functions in *Arabidopsis thaliana* is the analysis of T-DNA insertion mutants. In the past, several collections of mutants were generated and made publicly available. For this thesis, the collections were browsed using the T-DNA express tool (http://signal.salk.edu/cgi-bin/tdnaexpress), to identify mutants with a T-DNA insertion in the *CTH2* locus. Two T-DNA insertion lines were found, both from the SALK collection (Alonso, 2003). Insertion line SALK_045597 was named *cth2-1* and line SALK_065040 was named *cth2-2*. Seeds from these lines were ordered from the Nottingham Arabidopsis Stock Centre (Nottingham, UK).

To confirm the insertion site of the T-DNA in both mutant lines, genomic DNA was extracted from individual plants in the T4 (for *cth2-1*) or T3 (for *cth2-2*) generation and PCR-based genotyping was performed (see chapter 3.8.3). For this, attempts were made to amplify different products from genomic DNA isolated from WT, *cth2-1* and *cth2-2* plants by PCR. By using gene-specific primers that anneal upstream and downstream of the putative T-DNA insertion site, a WT allele can be detected through a PCR product of 591 bp (*cth2-1*) or 302 bp (*cth2-2*). By using one gene-specific primer, and one primer annealing at the left (LB) or right (RB) border sequence of the T-DNA, an insertion can be detected.

When using genomic DNA from *cth2-1* plants as a template, PCR products could be obtained with a primer annealing at the LB sequence in combination with either of the two gene-specific primers (Fig. 14a, only one reaction is shown). No PCR products could be obtained, when a primer annealing at the RB sequence was used in combination with either of the gene-specific primers. Sequencing of the PCR products revealed a putative head-to-head insertion in *cth2-1* between position 393 and 407, counting from the translational start site (Fig. 14c).

In addition, 13 bases of the *CTH2* sequence were deleted. When using genomic DNA from *cth2-2* plant as a template, a PCR product could only be obtained with a primer annealing at the LB sequence in combination with one of the two gene-specific primers (Fig. 14b). Sequencing of the PCR product revealed an insertion upstream of position 1649, counting from the translational start site of the *CTH2* sequence (Fig. 14c). Since only one LB sequence was detected by PCR, the sequence of the other border was possibly shortened during insertion of the T-DNA and was not detectable with the primers used. Since it was not possible to detect a WT allele in genomic DNA from both mutants, it was assumed that homozygous mutant plants could be isolated for both insertion lines.

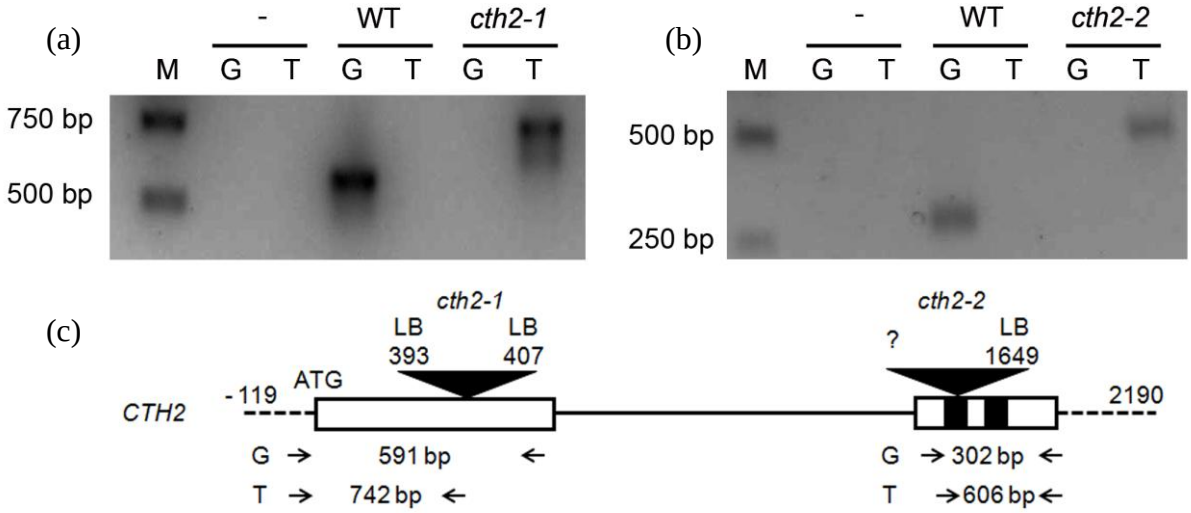

Figure 14: In *cth2-1* and *cth2-2* the *CTH2* locus contains T-DNA insertions.

Shown are images of agarose gels from PCR-based genotyping analysis of (a) *cth2-1* and (b) *cth2-2*, and (c) a schematic representation of the *CTH2* locus showing the positions of both T-DNA insertions. Lanes were loaded with a size standard (M) or PCR reactions with no template (-), genomic DNA extracted from WT, (a) homozygous *cth2-1* or (b) homozygous *cth2-2* plants. Amplification was performed with a pair of gene-specific primers (G) or with one gene-specific primer and one primer specific to the left border of the T-DNA (T). In panel (c) ATG marks the translational start site, dashed black lines represent UTRs with the position of their respective first or last base relative to the translational start site, white boxes represent exons, black boxes represent the sequences encoding the CCCH motifs, a black line represents the intron and black triangles represent the T-DNA insertions in the indicated genotypes. Note a putative head-to-head insertion in *cth2-1*. The numbers above the insertions give the positions of the nucleotides of *CTH2* directly adjacent to the T-DNA insertion site relative to the translational start. LB marks a left border sequence of the T-DNA and ? marks an unidentified border. Arrows show the binding sites of primers used for the gene-specific PCR reactions (G) or the T-DNA-specific PCR reactions shown in (a) and (b). The expected product sizes are shown in between the respective arrows.

Since the T-DNA used to mutagenize the plants confers resistance to kanamycin, the presence of this selectable marker was tested in the plant in the T4 (for *cth2-1*) or T3 (for *cth2-2*) generation. In *cth2-1*, no kanamycin resistance could be detected. However, using PCR-based genotyping, it was possible to isolate populations of homozygous *cth2-1* plants. According to the literature it is not uncommon for a transgene to be silenced (Mlotshwa et al., 2010). Especially expression of transgenes driven by the CaMV 35S promoter seems to be prone to silencing. Probably this is the case for *35S:NPTII* transgene conferring kanamycin resistance. The obtained *cth2-2* population segregated regarding the kanamycin resistance. PCR-based genotyping confirmed that the T-DNA insertion segregated in a Mendelian way. Subsequently it was found that all homozygous *cth2-2* plants were male sterile. Consequently, plants had to be propagated *via* hemizygous individuals. A detailed analysis of the unexpected male sterility phenotype was done and is described later (see chapter 4.18 ff). In the next step, the effects of the T-DNA insertions on transcripts generated at the *CTH2* locus were analyzed in both mutants.

4.8 Analysis of partial *CTH2* transcripts in *cth2-1* and *cth2-2*

Transcripts generated at the *CTH2* locus were analyzed in WT plants and both mutants (see chapter 3.8.3). RNA from WT, *cth2-1* and *cth2-2* plants was isolated and reverse transcribed to cDNA using an oligo$(dT)_{18}$ primer. Using different primer combinations (see Table 7), it was then attempted to amplify different fragments of the *CTH2* transcript by PCR. When cDNA from WT plants was used as a template, PCR products of the expected sizes could be obtained with all primer pairs (Fig. 15a, b).

Primer pair I amplifies a 977 bp long fragment (nucleotides -50 to 977 relative to the translational start site) containing both exons of *CTH2*. With this primer pair, a product could only be obtained with cDNA from WT plants, but not with cDNA from *cth2-1* or *cth2-2* plants. This showed the absence of full-length *CTH2* transcript in both mutants. Primer pair II amplifies a 591 bp long fragment (-50 to 541) containing part of the first exon. With this primer pair, products could be obtained with cDNA from WT and *cth2-2* plants. This showed that the part of the *CTH2* transcript encoding the N-terminal region of CTH2, is still present in *cth2-2,* but absent in *cth2-1*.

Primer pair III amplifies a 354 bp long fragment (623 to 977) containing part of the second exon. With this primer pair, products could be obtained with cDNA from WT and *cth2-1* plants. This showed that the part of the *CTH2* transcript encoding the C-terminal region of CTH2, including the TZF domain, is still present in *cth2-1*, but absent in *cth2-2*. Primer pair IV amplifies a 681 bp long fragment (-50 to 631) containing the first exon and part of the second exon. With this primer pair, products of apparently identical size could be obtained with cDNA from WT and *cth2-2* plants. This shows that the partial transcript found in *cth2-2*, but not in *cth2-1*, is spliced correctly. Primer pair V amplifies a 427 bp long fragment (550 to 977) containing part of the first exon and the second exon. With this primer pair, products of apparently identical size could be obtained with cDNA from WT and *cth2-1* plants. This shows that also the partial transcript found in *cth2-1*, but not in *cth2-2*, is spliced correctly. Amplification of a fragment of the *EF1α* (*Elongation Factor 1α*) transcript as a control confirmed a successful cDNA synthesis.

The analysis showed that partial *CTH2* transcripts can be detected in cDNA from both mutants. In the *cth2-1* mutant, the T-DNA insertion is in the first exon downstream of nucleotide position 393. A partial transcript could be detected, that contains at least the final 16 nucleotides of the first exon and the complete second exon (Fig. 15a). The T-DNA insertion in the *cth2-2* mutant is in the second exon upstream of nucleotide position 704 of the *CTH2* cDNA (position 1649 when referring to genomic DNA, compare Fig. 14c). In cDNA from this mutant, a partial transcript could be detected containing the first exon and at least the first 24 nucleotides of the second exon (Fig. 15b).

To confirm that the PCR products represented partial *CTH2* transcripts they were sequenced. For the partial transcript in *cth2-1*, a PCR product, amplified using a T-DNA LB-specific primer and a primer binding to the 3'-UTR of the *CTH2* transcript, was sequenced. The T-DNA border facing the transcriptional start site of *CTH2* in *cth2-2* could not be detected (see Fig. 14). Consequently, a gene-specific primer annealing to nucleotides 610 to 631 of the *CTH2* coding sequence was used in combination with a primer annealing in the 5'-UTR of *CTH2*, to amplify a PCR product for sequencing. The sequencing results confirmed that different, partial *CTH2* transcripts were detected in both mutants (Supplemental Fig. 2). The 5'-end of the partial transcript in *cth2-1* is located in the LB region of the T-DNA, upstream of the LB primer binding site. The first nucleotide of the *CTH2* sequence in the partial transcript in *cth2-1* was position 407 of the CTH2 coding sequence. The sequence of the 3'-end of the partial transcript in *cth2-2* contains at least nucleotide position 609 of the WT

CTH2 transcript. Since the first nucleotide of the *CTH2* coding sequence after the T-DNA insertion in *cth2-2* is position 704, the longest possible partial transcript in *cth2-2* would include position 703 of the *CTH2* coding sequence. Since both PCR products spanned an exon junction, it could be ruled out that the sequencing results represented genomic DNA.

A putative partial CTH2 protein in *cth2-1* corresponds to a ΔN-CTH2 protein, lacking parts of the N-terminus but containing an intact TZF domain. A putative partial CTH2 protein in *cth2-2* corresponds to a ΔC-CTH2 protein containing the N-terminal region but lacking an intact TZF domain.

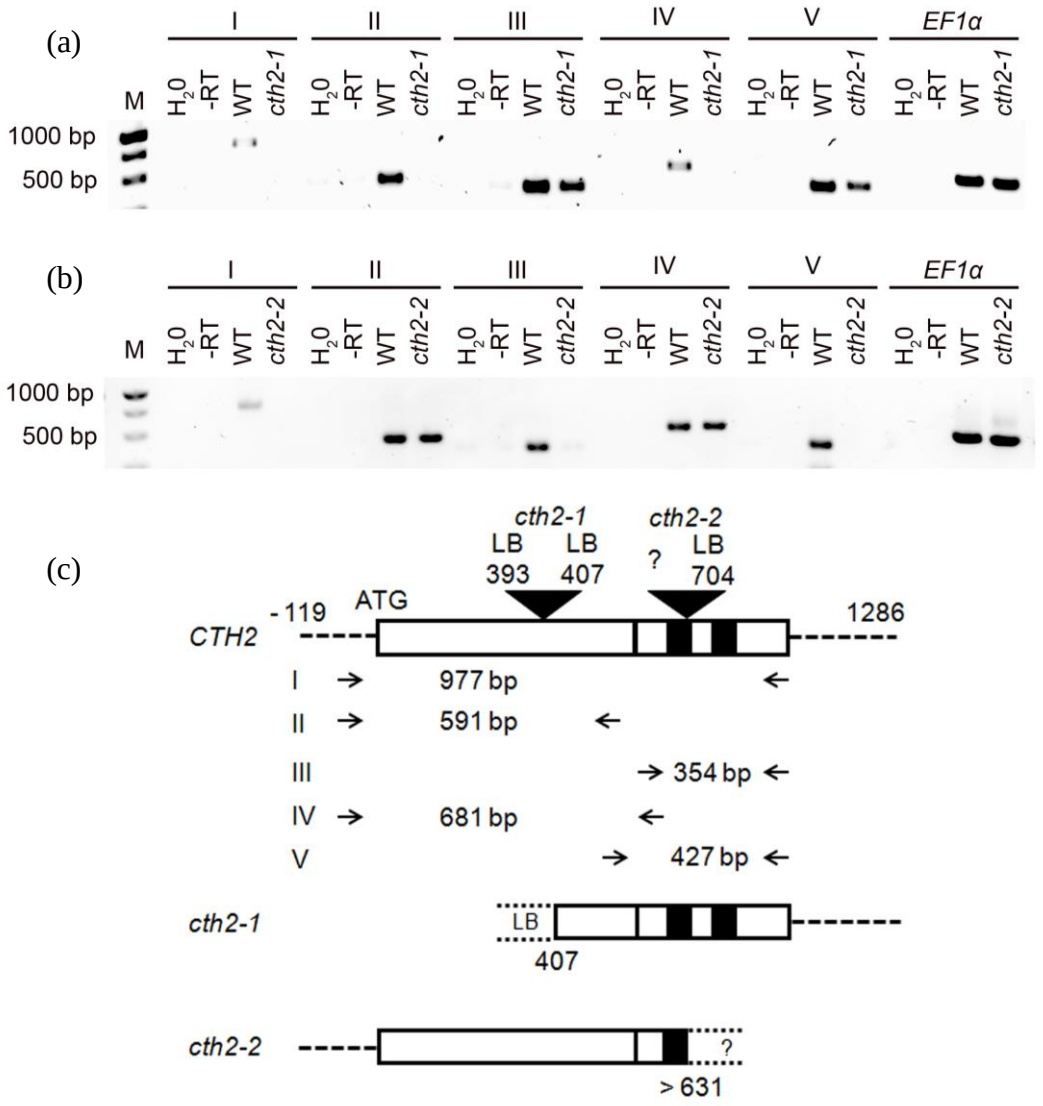

Figure 15: Partial transcripts originating at the *CTH2* locus can be detected in *cth2-1* and *cth2-2* plants.

Shown are (a, b) images of agarose gels of PCR products from reactions using cDNA as a template and (c) a schematic representation of the *CTH2* locus with both T-DNA insertions, the primer pairs (I–V) used in (a) and (b) and the partial transcripts detect in *cth2-1* and *cth2-2* plants. Panel (a) shows results obtained with cDNA

from WT and *cth2-1* plants, panel (b) shows results obtained with cDNA from WT and *cth2-2* plants. Lanes were loaded with a size standard (M), or PCR reactions conducted with no template (H_2O), with RNA extracted from WT plants (-RT) or with 1 µl of a 20-µl cDNA reaction with RNA extracted from WT, homozygous *cth2-1* or homozygous *cth2-2* plants. Amplification was performed with primer pairs I–V to amplify the indicated fragments of the *CTH2* transcript. *Elongation Factor 1α* (*EF1α)* was amplified as a control for successful cDNA synthesis. In panel (c), ATG marks the translational start site, dashed black lines represent predicted UTRs with the position of their respective first or last base relative to the translational start site, white boxes surrounded by black lines represent exons, black boxes represent the sequences encoding the CCCH motifs, and black triangles mark the positions of T-DNA insertions in the mutant genomes for orientation. The numbers given above the insertions indicate the positions of the nucleotides directly adjacent to the position of the T-DNAs relative to the translational start site. LB marks left border sequences of the T-DNA and ? marks an unidentified border sequence. Arrows mark the positions of primers used to amplify fragments of the (partial) *CTH2* cDNAs. The expected product sizes are shown in between the respective arrows.

4.9 Growth of *cth2* mutants in different iron regimes

Since results from studies in yeast (Puig et al., 2005) and analysis of transcript levels (see Fig. 8) in *Arabidopsis* suggest a role of *AtCTH2* in shoot Fe homeostasis under Fe-limiting conditions, *cth2-1*, *cth2-2* and plants in the F1 generation of a *cth2-1* x *cth2-2* cross were grown hydroponically alongside WT plants for 45 days and subjected to Fe deficiency for the final eight days of cultivation. After eight days of growth in Fe-deficient conditions, plants of all genotypes started to show mild symptoms of chlorosis (Fig. 16a). The leaves of *cth2-1* and *cth2-1* x *cth2-2* F1 plants seemed to be more affected by the chlorosis then those of WT and *cth2-2* plants. To quantify the chlorosis, total chlorophyll concentrations in the leaves were measured (Fig. 16b). In WT, *cth2-1* and *cth2-1* x *cth2-2* F1 plants grown under Fe-sufficient conditions chlorophyll concentrations were approximately 1 µg mg^{-1} fresh biomass. In leaves of *cth2-2* plants chlorophyll concentrations were slightly, but significantly higher (1.38 µg mg^{-1} fresh biomass, $p = 0.037$ according to Student`s *t*-test with Bonferroni corrections). Under Fe-deficient conditions, the chlorophyll concentrations were reduced in all genotypes. Leaves of WT and *cth2-2* plants contained 0.56 µg chlorophyll mg^{-1} fresh biomass. In accordance with the visual phenotype, leaves of *cth2-1* and *cth2-1* x *cth2-2* F1 plants contained significantly ($p < 0.001$ according to Student`s *t*-test with Bonferroni corrections) less chlorophyll (0.44 and 0.41 µg mg^{-1} fresh biomass, respectively). Roots of mutant plants showed no obvious difference under Fe-deficient conditions, when compared to WT plants.

Yellowing of leaves and reduced chlorophyll levels are typical symptoms of Fe-deficiency. The Fe deficiency induced-chlorosis started at the base of the lamina and then proceeded over time acropetally to the tip of the leaf. Since *cth2-1* and *cth2-1* x *cth2-2* F1 plants had stronger visual symptoms of Fe deficiency and had significantly reduced chlorophyll concentration in Fe-deficient conditions, it was concluded that 45-day-old plants of these genotypes were hypersensitive to Fe deficiency compared to WT plants. A hypersensitivity to Fe deficiency was not found in 21- or 28-day-old plants grown in sterile culture (data not shown). In contrast to this, 45-day-old *cth2-2* plants reacted to Fe deficiency in a manner comparable to WT plants. The fact that *cth2-1* x *cth2-2* F1 plants behaved phenotypically like *cth2-1* plants showed that the effect of the *cth2-1* allele is dominant over the *cth2-2* allele.

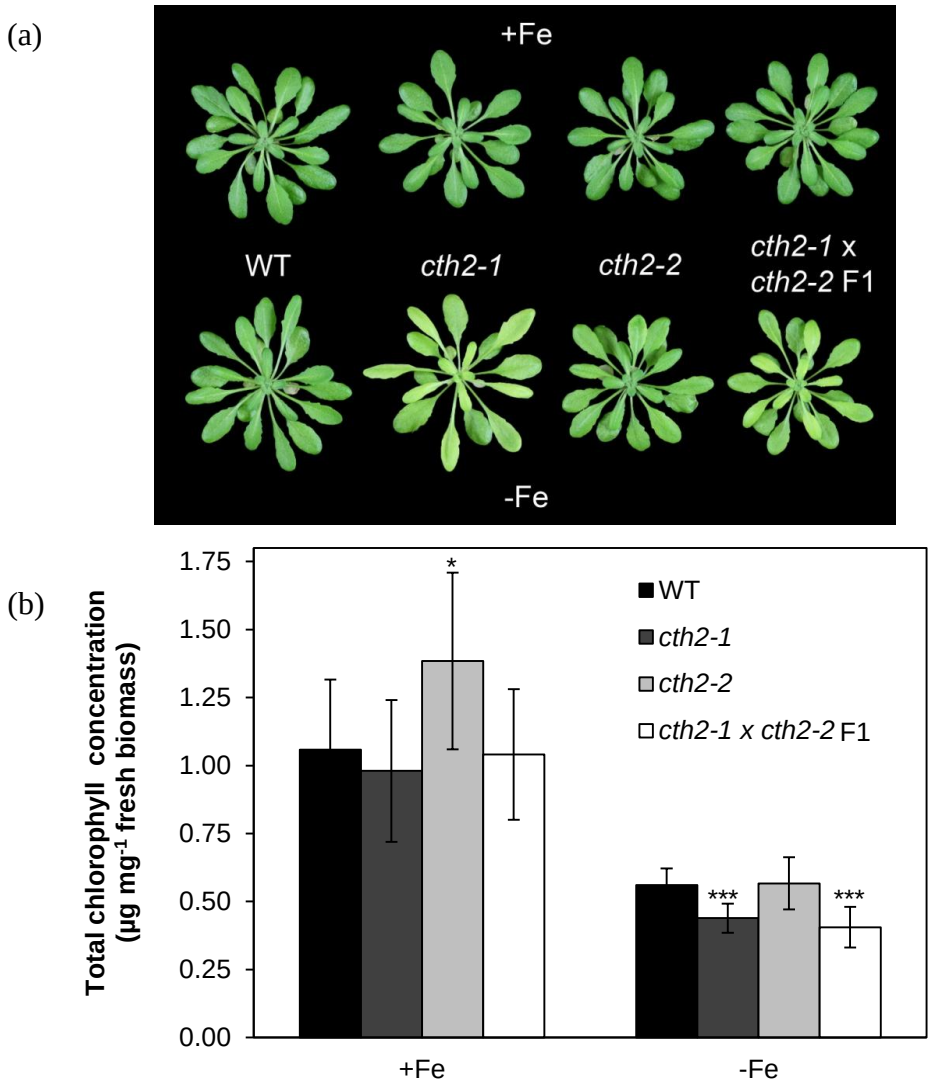

Figure 16: The *cth2-1* mutant is sensitive to Fe deficiency, but the *cth2-2* mutant is not.

Shown are (a) photographs and (b) chlorophyll concentrations of shoots from 45-day-old hydroponically grown plants. Plants were grown in the absence of added Fe (-Fe) for the final eight days of cultivation. Control plants (+Fe) were grown on media containing 5 µM FeHBED throughout. Chlorophyll was extracted from 3-mm leaf

discs from four leaves of three individual plants resulting in $n = 12$ replicate measurements per genotype and treatment. Bars represent arithmetic means ± SD. For WT, *cth2-1* and *cth2-2* at least two independent experiments were done, and data are shown from one representative experiment. For the *cth2-1* x *cth2-2* F1 plants one single experiment was performed. Asterisks mark significant differences compared to the respective WT (* $p \leq 0.05$; *** $p \leq 0.001$) as detected through Student`s *t*-test with Bonferroni corrections for multiple comparisons of means.

4.10 The *cth2-1* insertion causes a dominant phenotype under iron-deficient conditions

The phenotype of *cth2-1* and *cth2-1* x *cth2-2* F1 plants under Fe-deficient conditions became more obvious, when plants were left in Fe-deficient conditions for a longer period of time, so the following experiments were performed with 10 to 12 days of Fe deficiency treatment. After 10 to 12 days of growth in Fe-deficient conditions also a difference in the strength of the chlorosis between rosette leaves of old and young relative age became obvious in *cth2-1* and *cth2-1* x *cth2-2* F1 plants. In WT plants, subjected to Fe deficiency for the final 10 days of cultivation, the strength of the chlorosis was comparable between most leaves of the rosette. Only the youngest, and to a lesser degree also the oldest leaves appeared less chlorotic (Fig. 17a). In *cth2-1* plants the degree of chlorosis increased gradually from the oldest to the youngest leaf.

The chlorophyll concentrations in single leaves of WT plants ranged between 0.3 and 0.98 µg mg^{-1} fresh biomass (Fig. 17b). Highest concentrations of chlorophyll were found in the oldest and youngest leaves. Chlorophyll concentrations in older leaves of *cth2-1* plants were comparable to those in leaves of a comparable relative age of WT plants (*ca.* 0.6 µg mg^{-1} fresh biomass). However, the chlorophyll concentrations in leaves of *cth2-1* plants decreased gradually from the oldest to the youngest leaves. In the youngest leaves of *cth2-1* plants chlorophyll concentrations were as low as 0.1 µg mg^{-1} fresh biomass. These results showed that the younger leaves of *cth2-1* plants were more severely affected by the hypersensitivity to Fe deficiency compared to the older leaves.

As described above, *cth2-1*, but not *cth2-2* mutant plants were more sensitive to Fe deficiency. Also, double hemizygous *cth2-1* x *cth2-2* F1 plants were more sensitive to Fe

deficiency. So the hypothesis was tested that *cth2-1* is a dominant allele. To test this, a segregating *cth2-1* population was generated by backcrossing *cth2-1* to WT. The resulting F1 plants were genotyped by PCR as outlined in Fig. 14 (data not shown). Hemizygous *CTH2*/*cth2-1* plants were identified and allowed to set seed. The resulting segregating F2 population was grown in hydroponic culture for 45 days, with the final 10 days of cultivation on medium without added Fe. The plants were genotyped by PCR to distinguish WT, hemizygous and homozygous *cth2-1* plants. It was found that chlorophyll concentrations in both, hemi- and homozygous *cth2-1* plants decreased gradually from the oldest to the youngest leaves (Fig. 17b). This provided evidence that *cth2-1* is a dominant allele.

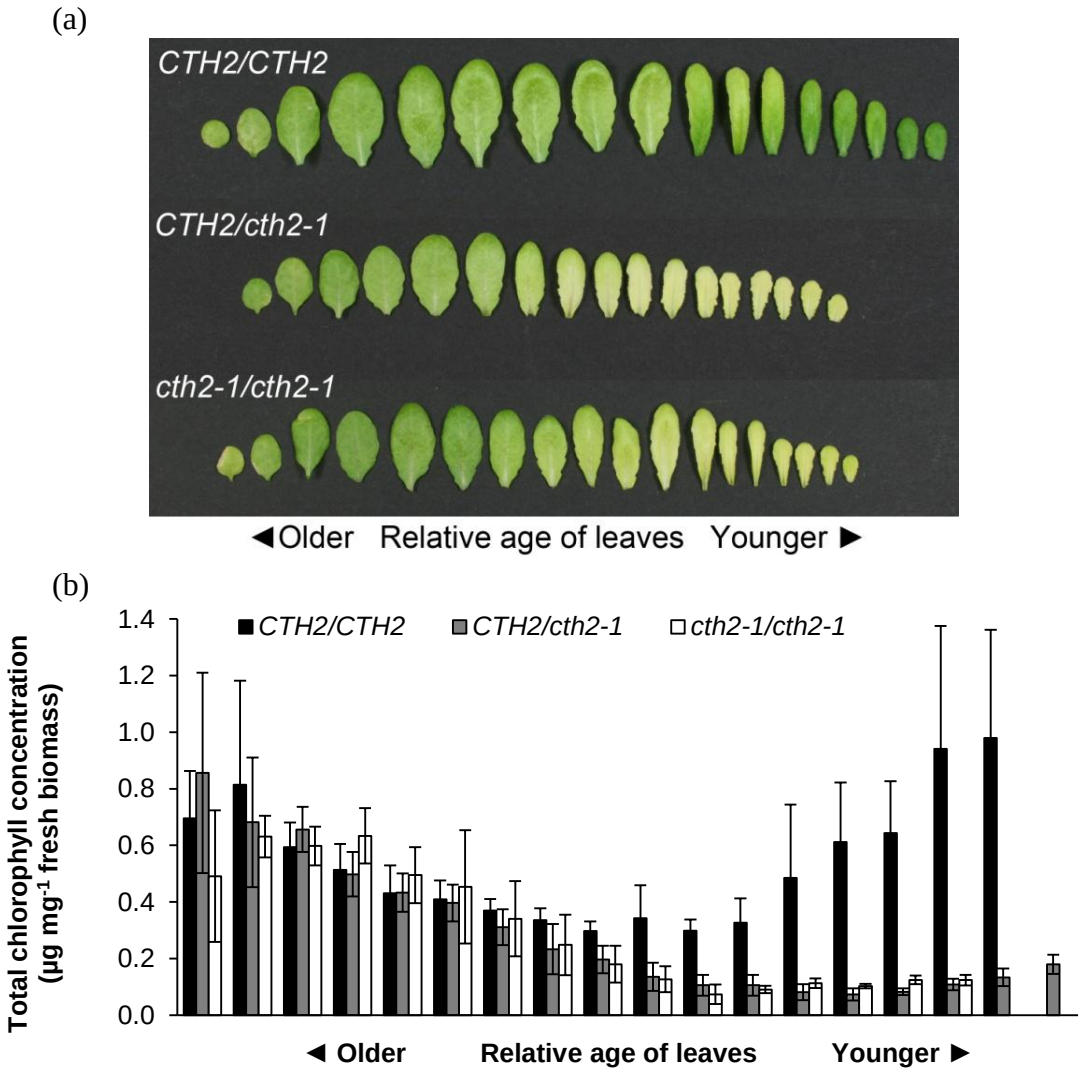

Figure 17: The *cth2-1* allele is dominant over the WT allele and causes increased chlorosis under Fe deficiency.

Shown are (a) photographs and (b) chlorophyll concentrations of series of all individual leaves from 45-day-old hydroponically grown plants. Plants were grown in the absence of added Fe (-Fe) for the final 10 days of cultivation. Panel (a) shows leaves from a representative individual plant of the indicated genotype arranged

from the oldest (left) to the youngest (right) leaf. Bars represent arithmetic means ± SD of three replicate plants. Data shown are from a single experiment.

4.11 Transcript levels of the partial *CTH2* transcript in *cth2-1*

The partial transcript described in chapter 4.8 (see also Fig. 15) might explain the dominance of the Fe-deficiency phenotype found in *cth2-1*. In Fig. 18, relative transcript levels of the partial, 5'-truncated *CTH2* transcript found in *cth2-1* are shown in comparison to full-length *CTH2* transcript levels in WT. The same primer pair could be used to detect both transcripts, since the amplicon is located in a region present in both transcripts, and since it was shown earlier that no full-length *CTH2* transcript is made in *cth2-1*plants. In shoots, the abundance of the partial transcript in *cth2-1* was found to be comparable to levels of the full-length *CTH2* transcript in WT plants (Fig. 15a). Furthermore, the levels of the partial transcript found in the *cth2-1* mutant did not increase in response to Fe deficiency, as was the case for full-length *CTH2* levels in WT plants. In roots of *cth2-1* plants, the abundance of the partial transcript was found to be near to the detection limit ($C_t \approx 39$) and thus considered absent, suggesting that *cth2-1* roots might exhibit a complete loss of *CTH2* function and that the abundance of the *CTH2* transcript might be regulated by different post-transcriptional mechanisms in roots compared to shoots.

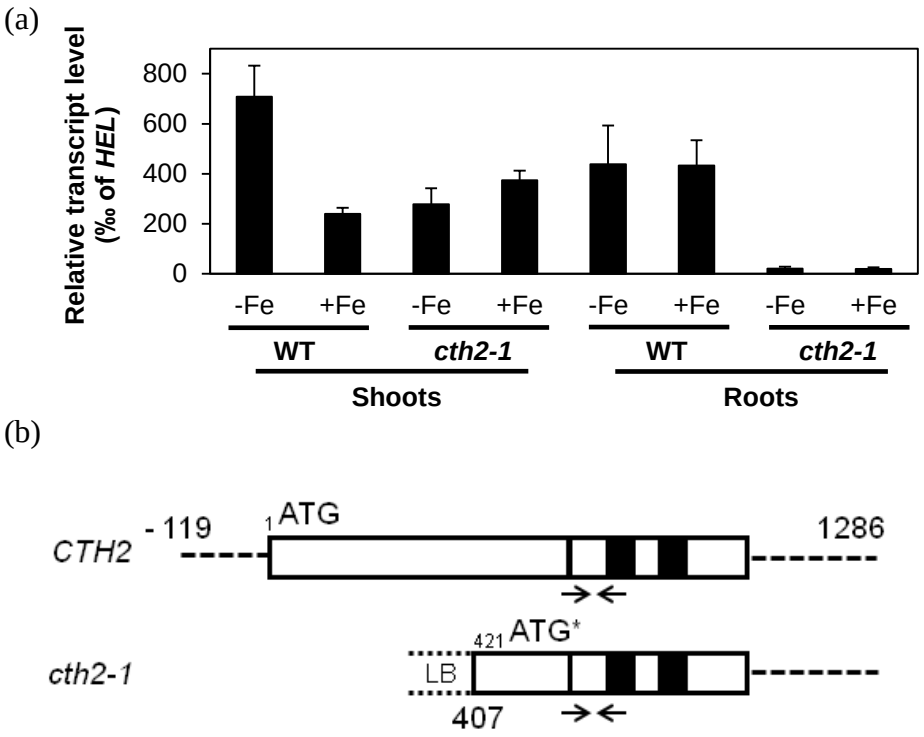

Figure 18: A partial transcript of the *CTH2* locus is accumulated in *cth2-1* plants at levels comparable to the WT.

Shown are (a) relative transcript levels of full-length *CTH2* transcript in WT and of a partial, 5'-truncated *CTH2* transcript in *cth2-1* of 45-day-old plants grown in hydroponic culture and (b) a representation of the *CTH2* transcript found in WT plants and the partial transcript found in *cth2-1* plants. Plants were grown in the absence of added Fe (-Fe) for the final 10 days of cultivation. Control plants (+Fe) were grown in media containing 5 µM FeHBED throughout. RNA was extracted from shoot and root material pooled from at least five individual plants, reverse transcribed to cDNA and relative transcript levels were determined by qPCR with two technical replicates of each reaction. In (a), bars represent arithmetic means from n = 3 independent experiments ± SE. *Helicase* (*HEL*) is a constitutively expressed control gene used for normalization of transcript levels. In (b), dashed black lines represent UTRs with the position of their respective first or last base relative to the translational start site, white boxes represent exons and black boxes represent the sequences encoding the CCCH motifs. LB marks a left border sequence of the T-DNA. Arrows (not drawn to scale) show binding sites of the oligonucleotides used for qPCR in (a). ATG marks the translational start site, ATG* marks a putative alternative translational start site present in the partial transcript in *cth2-1*. Indices show the positions of both putative translational start sites with respect to the translational start site from the WT cDNA.

4.12 Analysis of iron concentrations in bulk tissues of WT and *cth2-1* plants

To find an explanation for the increased sensitivity to Fe deficiency of *cth2-1* plants, element concentrations were analyzed by ICP-AES in shoots and roots of WT and *cth2-1* plants grown in hydroponic culture under Fe-sufficient and -deficient conditions (Fig. 19). Shoot Fe concentrations were reduced by 40% under Fe-deficient conditions compared to Fe sufficiency. No significant difference was detected between WT and *cth2-1*.

In roots of WT plants, Fe concentrations were reduced by 50% under Fe-deficient conditions compared to Fe sufficiency. In roots of *cth2-1* plants, Fe concentrations were reduced by 66% under Fe-deficient conditions compared to Fe sufficiency. This difference comes from the increased Fe concentration in *cth2-1* roots compared to WT under Fe-sufficient conditions, although the data is too variable to show any significant differences. Under Fe-deficient conditions Fe concentrations were comparable in roots of both genotypes.

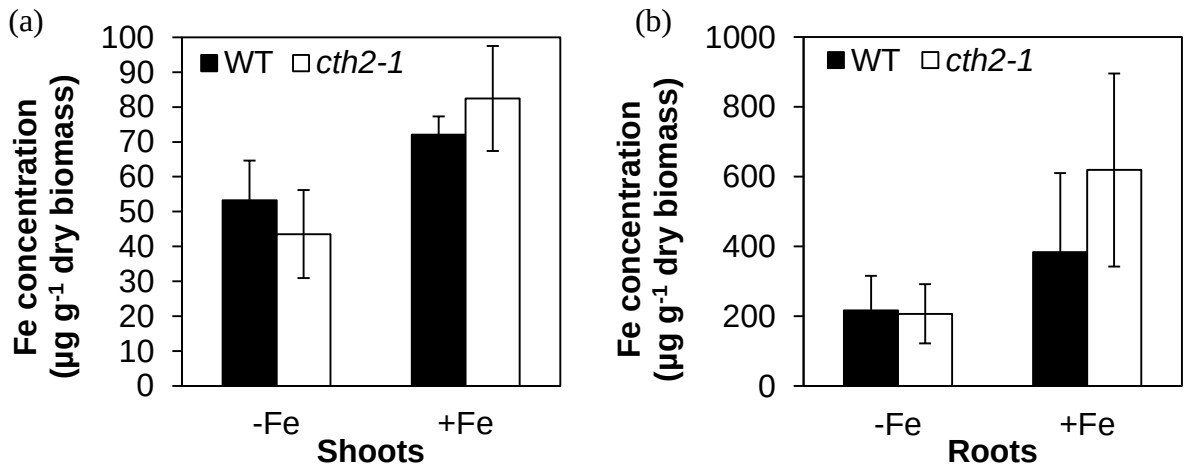

Figure 19: Iron concentrations in *cth2-1* shoots and roots are not significantly different from those in the WT.

Shown are Fe concentrations in (a) shoots and (b) roots of 45-day-old WT and *cth2-1* plants grown in hydroponic culture. Plants were grown in the absence of added Fe (-Fe) for the final eight days of cultivation. Control plants (+Fe) were grown on media containing 5 µM FeHBED throughout. Whole rosettes and root systems were harvested, dried, and completely mineralized for ICP-AES analysis. Bars represent arithmetic means ± SD of five replicate plants. Data are from a single experiment.

These data showed that Fe concentrations in bulk shoot and root tissues are comparable in WT and *cth2-1* plants. The increased Fe-deficiency induced chlorosis of *cth2-1* plants compared to WT plants can thus not be explained by a lack of root Fe uptake or allocation of Fe to the shoot. To further investigate the distribution of Fe within the shoot, element concentrations were analyzed in individual leaves (chapter 4.15).

4.13 Transcript levels of iron deficiency marker genes in shoots of WT and *cth2-1* plants

Even if Fe concentrations in shoots of WT and *cth2-1* plants are comparable, it is possible that misallocation of Fe on the tissue- or cellular level is responsible for the increased sensitivity of *cth2-1* plants to Fe deficiency. If this is the case, one would expect the transcript levels of genes regulating the homeostasis of Fe to be affected. To test this, transcript levels of *Ferric Reduction Oxidase 3* (*FRO3*) and *Ferritin 1* (*FER1*) were analyzed in shoots from WT and *cth2-1* plants grown in hydroponic culture under Fe-sufficient and -deficient conditions. Relative transcript levels of both Fe-deficiency marker genes were comparable in WT and *cth2-1* plants (Fig. 20). Relative transcript levels of *FRO3* were increased by 75% under Fe-deficient conditions compared to Fe sufficiency in both WT and *cth2-1* shoots. Relative shoot transcript levels of *FER1* decreased by 95% in Fe deficient conditions compared to sufficiency in WT and *cth2-1*. This result showed that *cth2-1* plants were not physiologically more or less Fe-deficient than the WT, at least with regard to the analyzed Fe-deficiency marker genes.

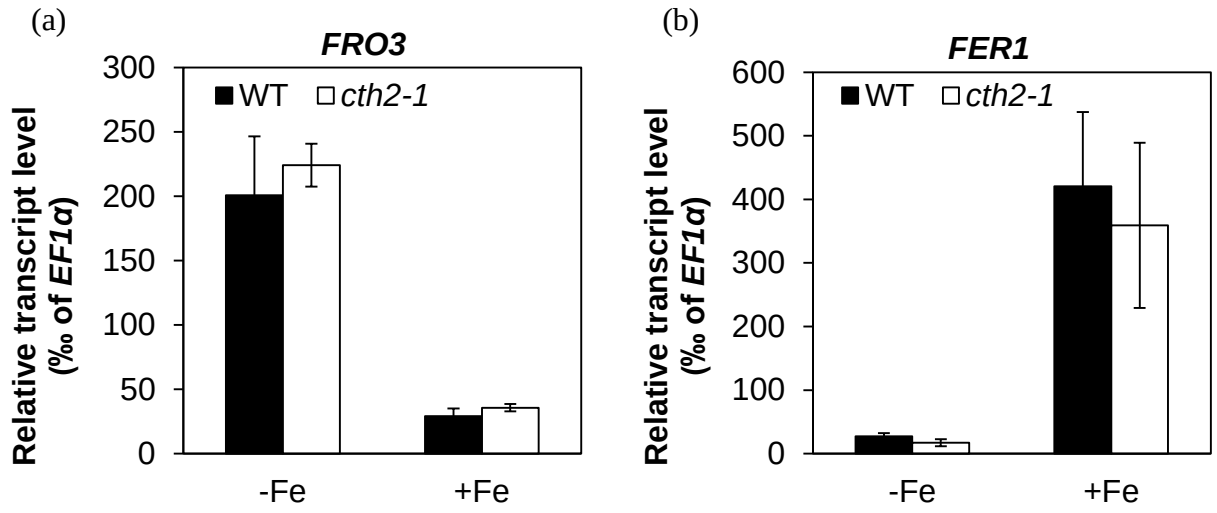

Figure 20: Transcript levels of Fe-deficiency marker genes are not affected in *cth2-1* plants.

Shown are relative transcript levels of (a) *FRO3* and (b) *FER1* in 45-day-old plants grown in hydroponic culture. Plants were grown in the absence of added Fe (-Fe) for the final 10 days of cultivation. Control plants were grown on media containing 5 µM FeHBED throughout. RNA was extracted from shoot material pooled from at least five individual plants, reverse transcribed to cDNA and relative transcript levels were determined by qPCR with two technical replicates of each reaction. Bars represent arithmetic means ± SE from three independent experiments. *Elongation Factor 1α* (*EF1α)* is a constitutively expressed control gene used to normalize transcript levels. *Ferritin 1* (*FER1*) encodes a shoot Fe storage protein and *Ferric Reduction Oxidase 3* (*FRO3*) might contribute to the reduction of Fe^{III} in shoots. Both transcripts were used as markers of Fe status.

4.14 Overexpression of a cDNA fragment encoding the C-terminus of CTH2 leads to a disturbed Fe-homeostasis

To test the effect of constitutively high expression of *CTH2*, transgenic plants were generated, which express either the full-length *CTH2* coding sequence (*35S:CTH2*), the part of the *CTH2* transcript encoding the first 170 amino acids (*35S:CTH2_Nterm*) or the part of the transcript encoding the final 103 amino acids (*35S:CTH2_Cterm*) under the control of the CaMV 35S promoter (chapter 3.3.4). The fragment used for the *35S:CTH2_Cterm* construct represents the partial transcript found in *cth2-1*, including the region encoding the TZF-domain, which caused a dominant sensitivity to Fe deficiency. After transformation of WT plants with all

three constructs, the T1 generation was screened for the presence of the transgene, making use of the selectable marker gene (*NPTII*, conferring resistance to kanamycin). Transcript levels of the introduced transgene were then analyzed in kanamycin-resistant six-week-old plants grown on soil by semi-quantitative RT-PCR. The number of PCR cycles (x = 25) was not sufficient to generate a detectable signal when cDNA from WT plants was used as a template (Fig. 21). However, when cDNA from T1 plants was used, a strong signal was detected in several lines for each construct. Therefore, it was concluded that in the respective lines overexpression was successful for all three constructs.

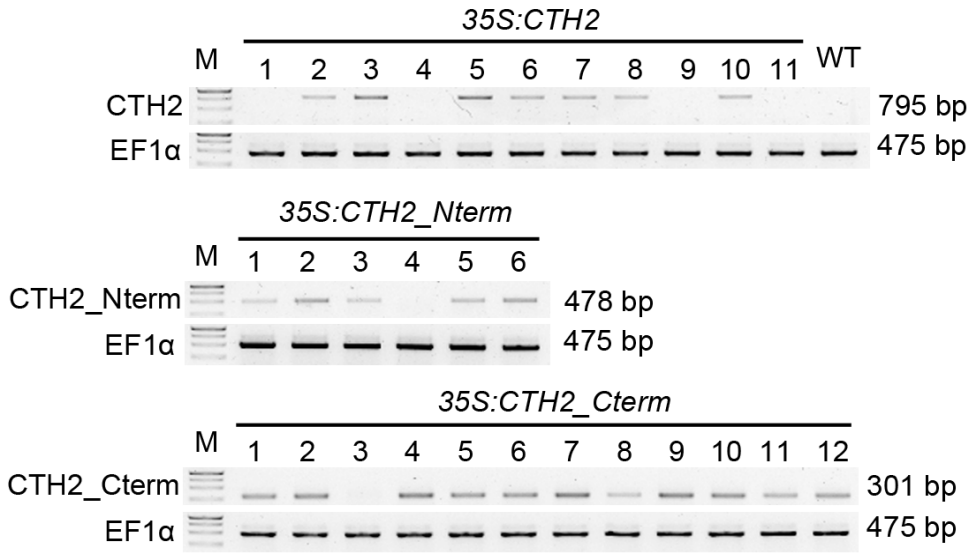

Figure 21: Overexpression of full-length and partial *CTH2* cDNAs in plants of the T1 generation.

Shown are images of agarose gels with products of PCR reactions using cDNA as a template. Kanamycin-selected plants in the T1 generation with the indicated constructs were grown on soil for six weeks. RNA was extracted from rosette leaves and reverse transcribed to cDNA. Three different primer pairs (CTH2, CTH2_Nterm, CTH2_Cterm) were used to detect *CTH2* transcripts. The expected product sizes are given to the right. After amplification, 10 µl out of a 25 µl PCR reaction were analyzed by gelelectrophoresis. *EF1α* was used as a control for successful cDNA synthesis. For each construct 6 to 12 independent transformants were analyzed Sizes of marker bands (M) are (from top to bottom): 1000 bp, 750 bp, 500 bp, 250 bp.

After allowing those lines, showing highest *CTH2* transcript levels in the T1 generation to self, plants of the T2 generation were used to conduct experiments. For each construct, kanamycin-selected plants of three independent lines in the T2 generation were grown in

hydroponic culture for 45 days alongside WT plants, and subjected to Fe deficiency for the final 10 days of cultivation The *35S:CTH2* construct or the *35S:CTH2_Nterm* construct had no evident effect on plant performance under Fe deficiency (Fig. 22). Lines of plants transformed with the *35S:CTH2_Cterm* construct showed an increased sensitivity to Fe deficiency, indicated by the increased chlorosis and the reduced rosette diameter compared to WT plants. The youngest leaves of *35S:CTH2_Cterm* plants suffered from more severe chlorosis compared to the youngest leaves of WT plants (Fig. 23). This finding provides further support for the hypothesis that the *cth2-1* allele causes a dominant phenotype, because *cth2-1* and *35S:CTH2_Cterm* plants show a similar phenotype under Fe deficiency. Under Fe-sufficient conditions, no phenotype for plants carrying any of three constructs was found.

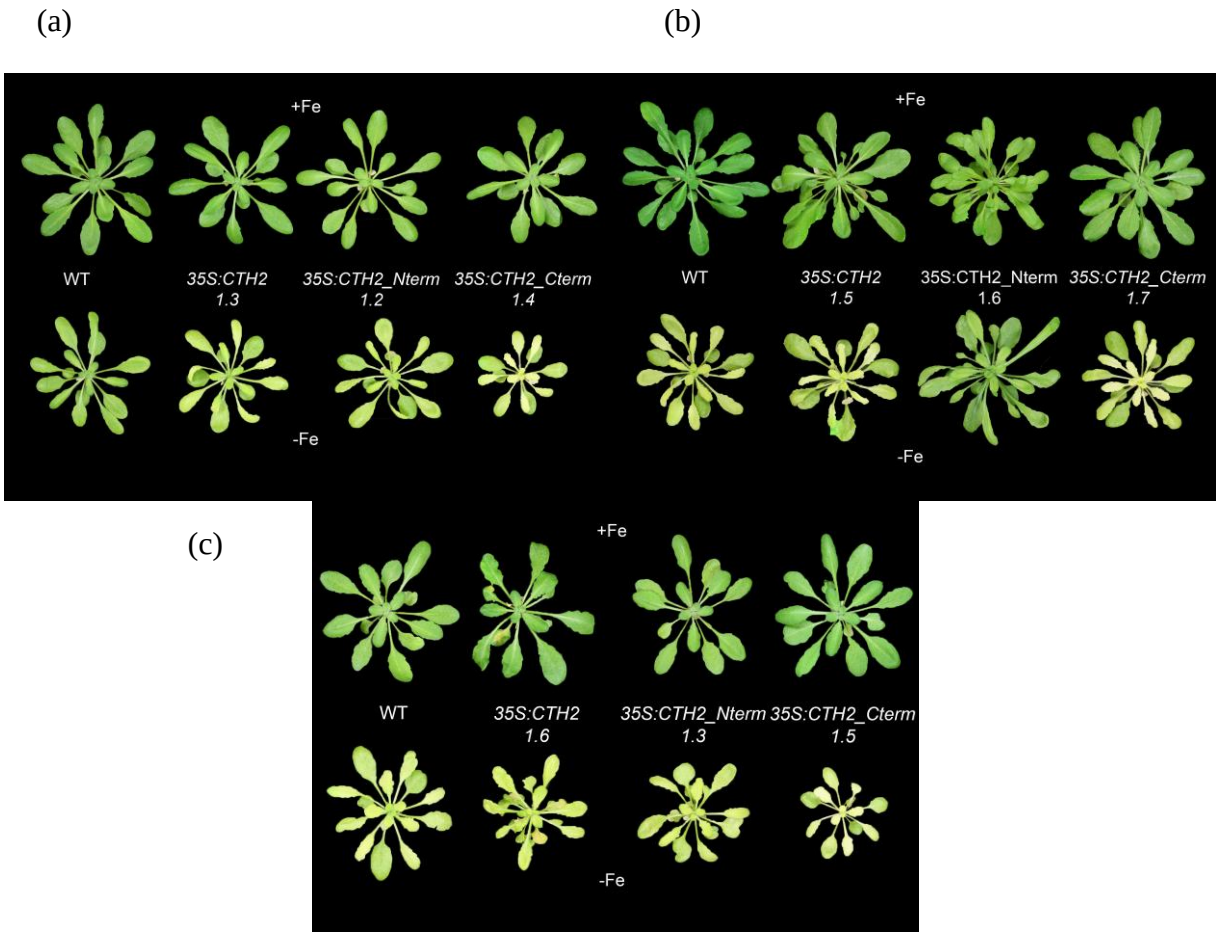

Figure 22: Overexpression of the full-length coding sequence, the 5'-part or the 3'-part of the *CTH2* cDNA has different effects on the development of chlorosis under Fe deficiency.

Shown are photographs of 45-day-old plants grown in hydroponic culture. Plants were grown in the absence of added Fe (-Fe) for the final 10 days of cultivation. Control plants (+Fe) were grown on media containing 5 µM FeHBED throughout. *35S:CTH2* plants overexpress the complete *CTH2* coding sequence. *35S:CTH2_Nterm*

plants overexpress a fragment of *CTH2* encoding the 107 N-terminal amino acids. *35S:CTH2_Cterm* plants overexpress a fragment of *CTH2* encoding the 103 C-terminal amino acids. Data shown are from three (a, b, c) independent experiments. In each experiment, WT plants and kanamycin-selected plants in the T2 generation from one line for each construct were grown in parallel. For each experiment different, independent lines were used and representative plants are shown.

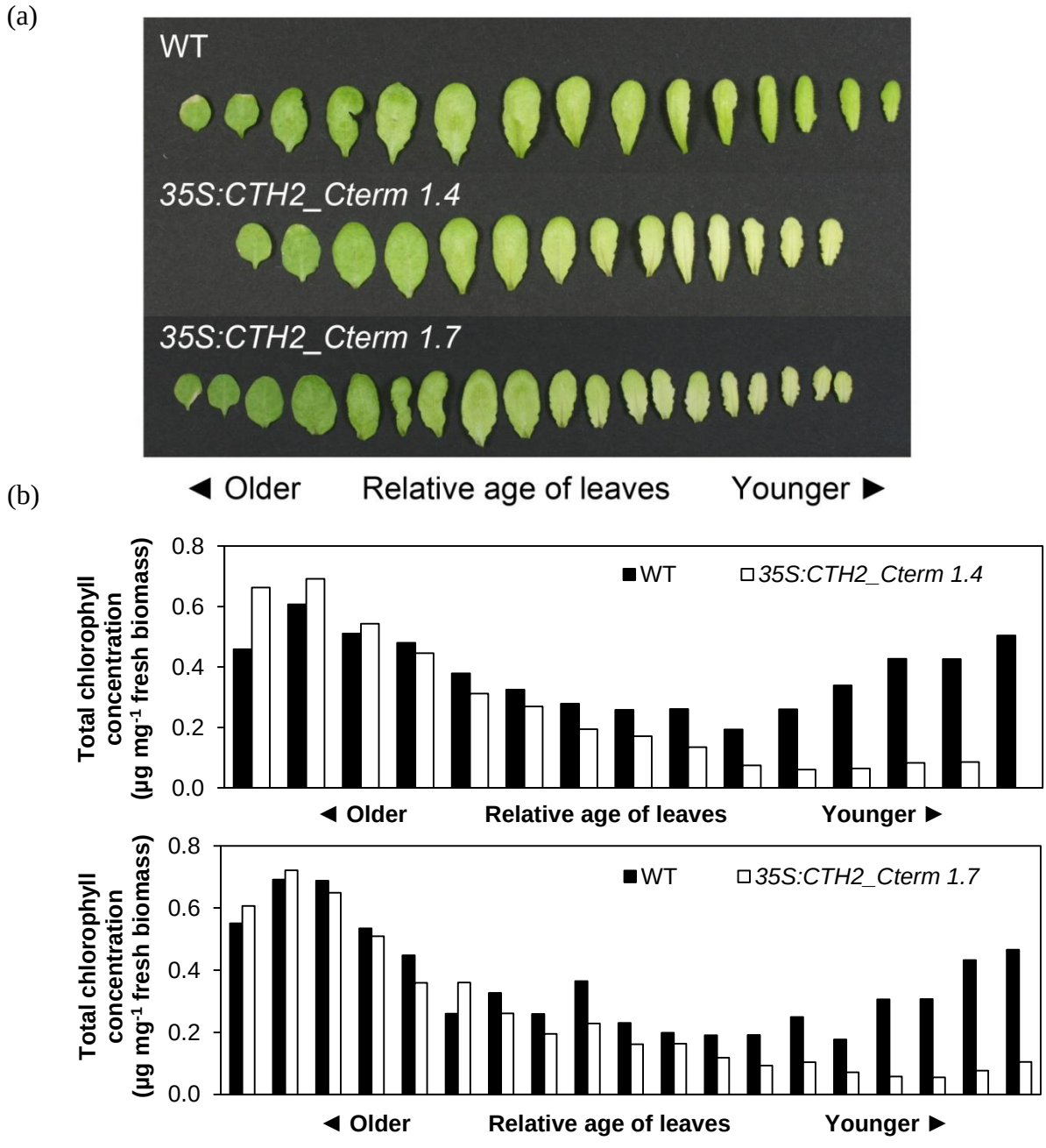

Figure 23: Overexpression of a 3'-fragment of *CTH2*, encoding the 103 C-terminal amino acids, results in reduced chlorophyll concentrations under Fe deficiency.

Shown are (a) photographs and (b) chlorophyll concentrations of individual leaves from 45-day-old hydroponically grown plants. Plants were grown in the absence of added Fe for the final 10 days of cultivation. (a) Leaves were harvested from individual, representative plants of the indicated genotypes and arranged from

the oldest to the youngest leaf for photographing. (b) Chlorophyll was extracted from whole individual leaves. Each bar represents one leaf. Data are from two independent experiments, each conducted with a different independent line in the T2 generation.

4.15 Analysis of iron concentrations in individual leaves

Since the enhanced chlorosis of young leaves of *cth2-1* and *35S:CTH2_Cterm* plants grown in Fe-deficient media suggested the possibility of a decreased supply of Fe to specific leaves, element concentrations were analyzed in single leaves. In WT plants, the concentration of Fe was decreased in all leaves under Fe-deficient conditions, when compared to plants grown under Fe-sufficient conditions (Fig. 24a). Among all individual leaves, Fe concentrations were highest in the oldest and the youngest leaves in WT plants, regardless of the Fe supply. When comparing WT and *cth2-1* or *35S:CTH2_Cterm* plants grown under Fe deficiency, it became evident that the number of leaves is slightly reduced in *cth2-1* and *35S:CTH2_Cterm* plants. This indicated that *cth2-1* and *35S:CTH2_Cterm* plants developed more slowly under Fe-deficient conditions. The Fe concentrations were increased up to ten-fold in the youngest leaves of both *cth2-1* and *35S:CTH2_Cterm* plants grown under Fe-deficient conditions, when compared to WT plants. In leaves of medium-to-old relative age, Fe concentrations were only slightly increased (Fig. 24b). The biomass of the youngest leaves from *cth2-1* and *35S:CTH2_Cterm* plants grown under Fe-deficient conditions was drastically reduced compared to WT plants (Fig. 24c). Also, older leaves from both, *cth2-1* and *35S:CTH2_Cterm* plants showed reduced biomass, although the differences to the WT were smaller than in young leaves. The reduction in biomass was stronger in *35S:CTH2_Cterm* plants then in *cth2-1* plants, which was probably a dosage effect of the partial transcript. The total Fe contents in the young leaves of both, *cth2-1* and *35S:CTH2_Cterm* plants were not reduced in comparison to WT (Fig. 24d). In Fe-sufficient conditions, no differences in biomass or Fe content could be detected between WT and *cth2-1* or *35S:CTH2_Cterm* plants (data not shown).

The severe chlorosis of young leaves of *cth2-1* and *35S:CTH2_Cterm* plants grown under Fe deficiency (Figs. 17 and 23) is apparently not caused by decreased Fe concentrations in these tissues. In fact, Fe concentrations in the young leaves of *cth2-1* and *35S:CTH2_Cterm* plants grown under Fe deficiency were up to ten-fold higher than in leaves of WT plants (Fig. 24b). Since the biomass of the young leaves of *cth2-1* and *35S:CTH2_Cterm* plants grown under

Fe-deficient conditions was also reduced up to ten-fold compared to WT (Fig. 24c), the total Fe content of the young leaves of WT, *cth2-1* and *35S:CTH2_Cterm* plants grown under Fe-deficient conditions was comparable (Fig. 24d). From the analysis of Fe concentrations and total Fe contents in individual leaves no defect in leaf-to-leaf Fe distribution in *cth2-1* and *35S:CTH2_Cterm* plants grown in Fe deficiency can be concluded. The inability of the young leaves of *cth2-1* and *35S:CTH2_Cterm* plants to thrive under Fe deficiency could be explained by a misallocation of Fe on the cellular level. It is possible that *cth2-1* and *35S:CTH2_Cterm* plants waste Fe on non-essential cellular functions, so that when Fe is scarce, essential functions of metabolism cease to work. Another possibility is that young leaves of *cth2-1* and *35S:CTH2_Cterm* plants suffer from Fe toxicity, since Fe concentrations are increased up to ten-fold compared to young leaves of WT plants.

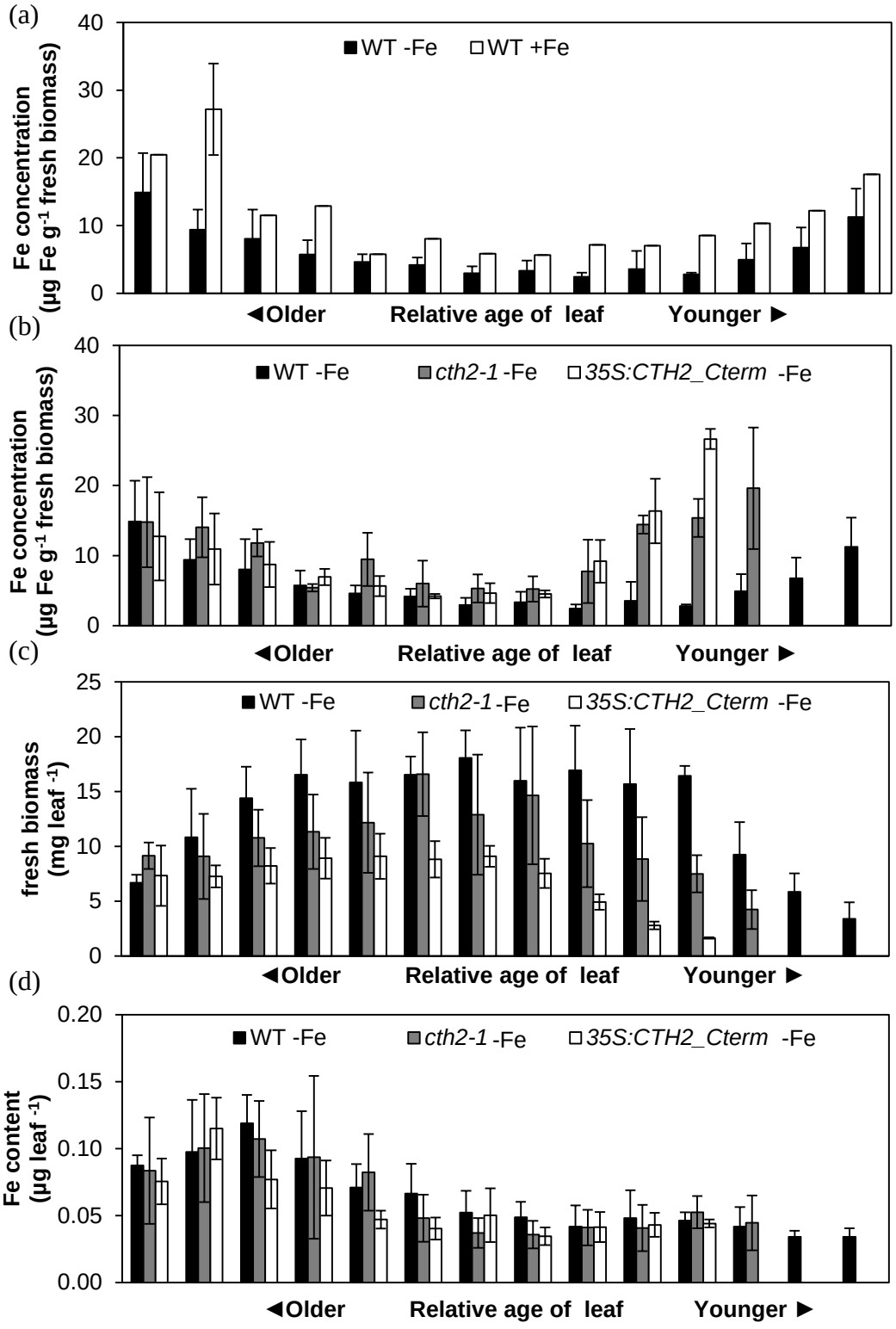

Figure 24: Young leaves of *cth2-1* and *35S:CTH2_Cterm* plants are impaired in growth under Fe-deficient conditions despite adequate leaf Fe contents.

Shown are (a, b) Fe concentrations, (c) biomass and (d) Fe content of leaves from 45-day-old plants grown in hydroponic culture. Plants were grown in the absence of added Fe (-Fe) for 10 days. Control plants (+Fe) were grown on media containing 5 µM FeHBED throughout. Individual leaves were harvested, weighed and analyzed using ICP-AES. Bars represent arithmetic means ± SD. For each +Fe data-point (a) one plant from three independent experiments was analyzed. For each -Fe data-point (a-d) three representative plants were analyzed

and data are shown from one experiment representative of three independent experiments, using two different independent lines in the T2 generation for the *35S:CTH2_Cterm* construct. Data from line *35S:CTH2_Cterm 1.4* are shown. Transformants carrying the *35S:CTH2_Cterm* construct were selected on kanamycin-containing media.

4.16 Transcript levels of iron-deficiency marker genes in leaves of different relative age

Since the analysis of Fe concentrations in individual leaves was more informative than measuring bulk tissues, also transcript levels of Fe-deficiency marker genes were analyzed separately in groups of leaves of different relative age. For this, relative transcript levels of two genes encoding transporters, putatively involved in the leaf-to-leaf movement of Fe, were analyzed in the five oldest and the five youngest leaves from WT and *35S:CTH2_Cterm* plants grown in Fe deficiency and sufficiency. *Yellow Stripe-Like 1 (YSL1)* encodes a Fe-NA transporter with a putative function in remobilization of Fe in senescing leaves (Le Jean et al., 2005). *YSL2* is a closely related gene which is also regulated in response to Fe status and has a putative role in lateral movement of Fe in the vasculature (DiDonato et al., 2004). Also, transcript levels of the Fe-deficiency marker genes *FRO3* and *FER1* were analyzed.

Under Fe-deficient conditions, transcript levels of *YSL1* and *YSL2* were strongly reduced, down to 95% compared those in Fe sufficiency (Fig. 25a, b). Transcript levels of *YSL1* were highest in old leaves from Fe-sufficient plants. Transcript levels of *YSL2* were highest in young leaves from Fe-sufficient plants. No major differences in *YSL1* and *YSL2* transcript levels were found between WT and *35S:CTH2_Cterm* plants. Also, the at least 7-fold increase of *FRO3* transcript levels in Fe-deficient conditions compared to Fe sufficiency was expected and comparable between WT and *35S:CTH2_Cterm* (Fig. 25c). Transcript levels of *FER1*, encoding the Fe-storage protein Ferritin 1, were decreased in leaves of Fe-deficient plants compared to Fe sufficiency (Fig. 25d). Young and old leaves from WT plants grown under Fe deficiency showed comparable *FER1* transcript levels. Interestingly, under Fe-deficient conditions, *FER1* transcript levels were increased five-fold in young leaves and three-fold in old leaves of *35S:CTH2_Cterm* plants compared to WT plants. In Fe-sufficient old leaves, *FER1* transcript levels were 30% lower in *35S:CTH2_Cterm* plants than in the WT.

From the transcript levels of *YSL1*, *YSL2* and *FRO3* it was concluded that the physiological Fe-status of *35S:CTH2_Cterm* plants was comparable to WT plants in both young and old leaves. From the transcript levels of *FER1* a difference in physiological Fe-status between *35S:CTH2_Cterm* plants and WT plants can be concluded. The higher *FER1* transcript levels in both, young and old leaves of *35S:CTH2_Cterm* plants compared to WT plants could be a consequence of the higher concentrations of Fe in leaves of *35S:CTH2_Cterm* plants compared to WT plants. It is also possible that *CTH2* acts to destabilize *FER1* transcript directly, and that *35S:CTH2_Cterm* plants cannot fully down-regulate *FER1* transcript levels.

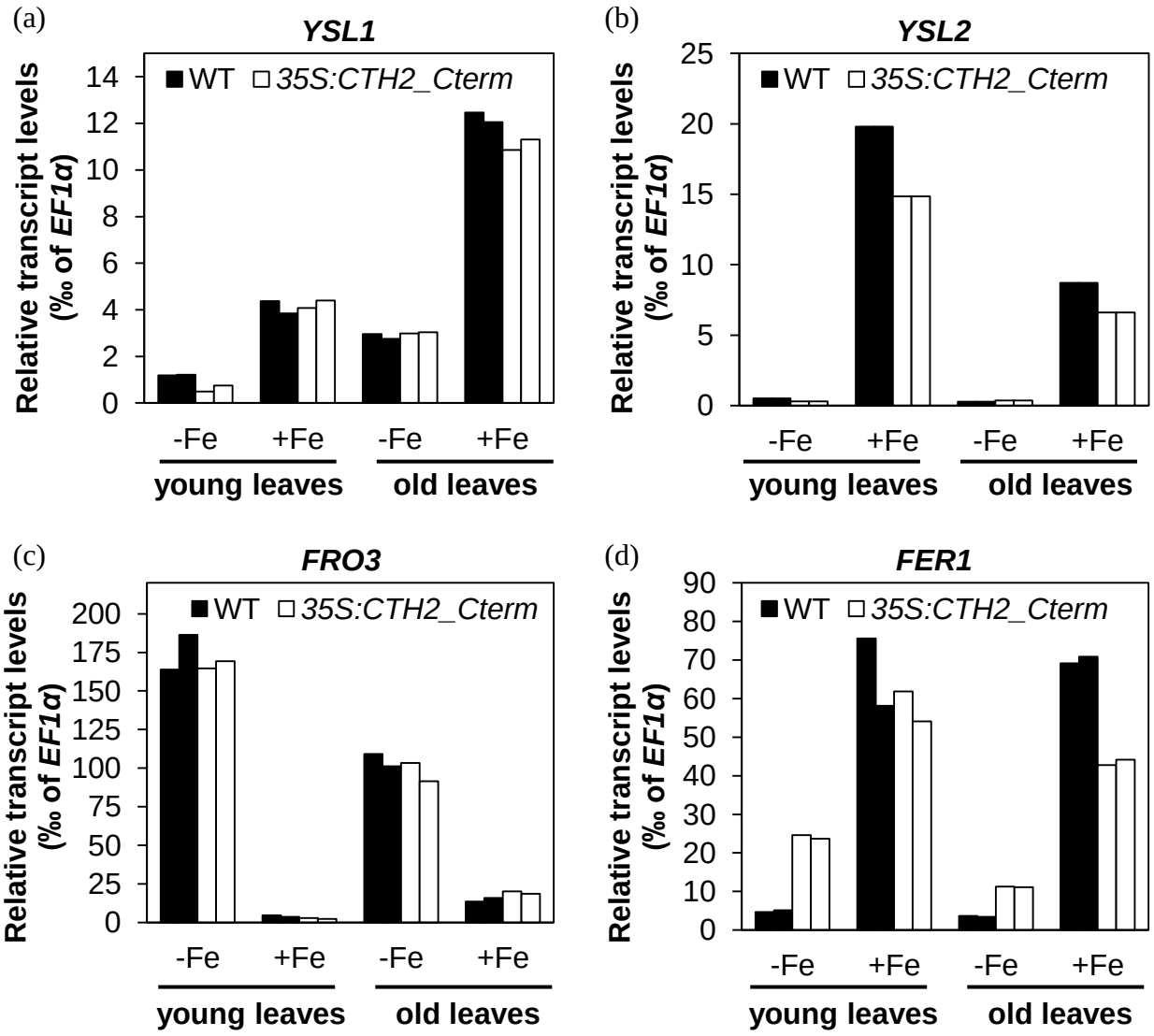

Figure 25: Transcript levels of Fe-status marker genes are similar in WT and *35S:CTH2_Cterm* plants, except for *FER1*.

Shown are relative transcript levels of Fe-deficiency marker genes in 45-day-old plants grown in hydroponic culture. Plants were grown in the absence of added Fe (-Fe) for the final 10 days of cultivation. Control plants

(+Fe) were grown in media containing 5 µM FeHBED throughout. RNA was extracted from the youngest and oldest five leaves, respectively, pooled from at least five representative individuals and reverse transcribed to cDNA. Relative transcript levels were determined by qPCR with two technical replicates of each reaction. Each bar represents one technical replicate. Data are from one experiment representative of two experiments each using one different independent line in the T2 generation (*35S:CTH2_Cterm 1.4* and *1.7*; data from line 1.7 is shown). Plants carrying the transgene were selected on kanamycin-containing media. *Elongation Factor 1α* (*EF1α)* (a-d) is a constitutively expressed control gene used to normalize transcript levels. *Yellow-Stripe-Like 1* and *2* (*YSL1/2*) (a, b) encode Fe transporters with a putative function in re-allocation of Fe between organs. *Ferric Reduction Oxidase 3* (*FRO3*) (c) might contribute to the reduction of Fe^{III} in shoots. *Ferritin 1* (*FER1*) (d) encodes a Fe storage protein.

4.17 Microarray transcriptome analysis comparing WT and *cth2-1* plants

In an attempt to identify transcripts regulated by *CTH2*, a microarray analysis was performed. For this, WT and *cth2-1* plants were grown in hydroponic culture for 45 days and subjected to Fe deficiency for the final eight days of cultivation. Control plants were grown in Fe sufficiency throughout. Shoots and roots were harvested separately. Pooled tissues from at least eight plants for each genotype and treatment of two replicate experiments were used, resulting in a total of $n = 16$ samples. RNA was extracted from each sample and analyzed by microarrays (chapter 3.6). In WT plants, transcript levels of a total of 415 and 331 genes in shoots and in roots respectively changed more than 1.25 fold ($p \leq 0.2$) in either direction in response to Fe deficiency. In contrast, only 216 genes in shoots and 44 genes in roots were found, when WT and *cth2-1* plants grown under Fe-deficient conditions were compared.

The next step involved attempting to find genes, which responded to Fe supply and had different transcript levels in WT and *cth2-1* plants (Fig. 26) and thus represent candidate genes for *CTH2*-dependent regulation. The number of genes, which fulfilled both criteria was small, and also the differences in transcript levels between WT and *cth2-1* were of small magnitudes. Especially in roots, only one combination of criteria (up-regulated in –Fe *vs.* +Fe in WT; higher transcript levels in WT *vs. cth2-1*) yielded 16 putative candidate genes.

Since *cth2-1* showed a Fe deficiency-dependent phenotype in shoots, and more genes fulfilled the criteria for genotype and Fe-supply dependent changes in transcript levels, discussion will be focused on shoot tissue.

Results shown earlier (see chapters 4.11 and 4.14) indicated that *cth2-1* might be a gain-of-allele under Fe-deficient conditions. Assuming that CTH2 de-stabilizes its target transcripts, transcripts that are down-regulated in response to Fe deficiency in WT and are also less abundant in *cth2-1* compared to WT under Fe deficiency would support this hypothesis. Three transcripts were found that matched these criteria (Table 9a). These putative candidate genes were *FER1*, an Fe storage protein and *YSL1*, an Fe transporter with proposed roles in seed-loading and remobilization of Fe during leaf senescence. The third gene (At5G17170) is annotated as rubredoxin and encodes an Fe-sulfur protein putatively involved in the detoxification of ROS. Since also 16 genes were found to be up-regulated under Fe deficiency in WT and had higher transcript level in WT than in *cth2-1* under Fe deficient conditions the possibility was considered that CTH2 acts as a stabilizer of transcripts.

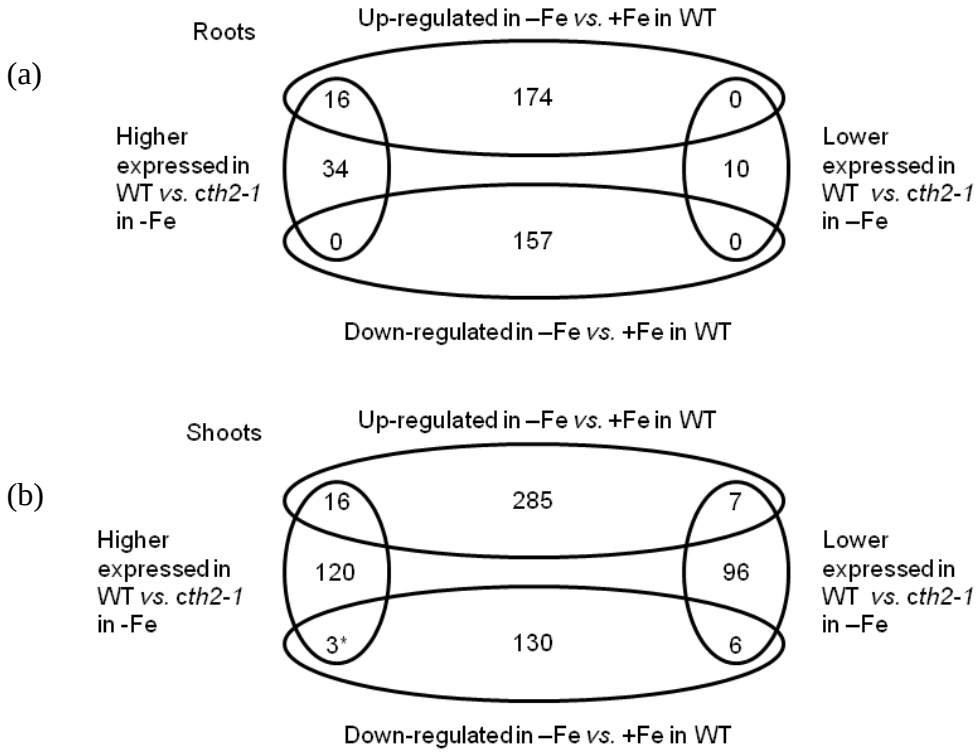

Figure 26: Microarray analysis of WT and *cth2-1* plants grown under different Fe regimes.

Shown is a summary of results from a microarray analysis (chapter 4.17) of transcript levels of (a) roots and (b) shoots. The numbers of genes that passed the fold-change and significance thresholds (fold-change ≥ 1.25; $p \leq$

0.2) are shown. Numbers in overlaps show the number of genes that met the criteria for both, significantly different transcript level in -Fe *vs.* +Fe in WT and WT *vs. cth2-1* under Fe-deficient conditions. The asterisk indicates the criteria which reflect the expected change in target transcript levels based on the hypothesis of CTH2 being a transcript-destabilizing protein in the shoot and *cth2-1* being a hyperactive gain-of-function mutant.

Table 9: Genes with significantly different transcript levels in -Fe *vs.* +Fe in WT shoots and in WT *vs. cth2-1* shoots under Fe deficiency.

Shown are fold-changes, *p*-values and number of AREs (WATTTAW) of genes for which transcriptional signals met the criteria for both, significantly different (fold-change [FC] ≥ 1.25; $p \leq 0.2$) in –Fe *vs.* +Fe in WT and WT *vs. cth2-1* under Fe deficiency (Fig. 26). Tables show genes (a, b) lower or (c, d) higher expressed in –Fe *vs.* +Fe in WT shoots and (a, c) higher or (b, d) lower expressed genes in WT *vs. cth2-1* in Fe deficiency.

(a)

				Corrected *p*-values		
AGI Code	Gene title	FC -Fe/+Fe WT shoots	FC WT/*cth2-1* -Fe shoots	Treatment	Genotype	No. of AREs
At5g17170	*ENH1* (Enhancer of *SOS3-1*)	0.228	1.409	0.116	0.163	-
At5g01600	*FER1* (Ferritin 1)	0.071	1.426	0.062	0.087	-
At4g24120	*YSL1* (Yellow stripe-like 1)	0.484	1.260	0.116	0.099	2

(b)

				Corrected *p*-values		
AGI code	Gene title	FC -Fe/+Fe WTshoots	FC WT/*cth2-1* -Fe shoots	Treatment	Genotype	No. of AREs
At2g19970	Encodes a CAP (cysteine-rich secretory proteins, antigen 5, and pathogenesis-related 1 protein) domain protein	0.584	0.707	0.103	0.197	-
At1g50110	Encodes a aminotransferase class IV	0.462	0.715	0.085	0.074	-
At1g70710	*CEL1* (Cellulase 1)	0.497	0.713	0.086	0.054	-
At1g18250	TLP1 (Thaumatin-like protein 1)	0.568	0.756	0.051	0.084	-
At4g28250	*EXPB3* (Expansin B3)	0.518	0.745	0.153	0.183	1
At3g54260	*TBL36* (Trichome birefringence-like 36)	0.587	0.671	0.090	0.171	-

Table 9, continued.

(c)

				Corrected *p*-values		
AGI code	Gene title	FC -Fe/+Fe WT shoots	FC WT/*cth2-1* -Fe shoots	Treatment	Genotype	No. of AREs
At4g19690	*IRT1* (Iron Regulated Transporter 1)	3.183	1.670	0.187	0.185	-
At5g54490	PINOID-binding protein	2.637	1.460	0.178	0.122	1
At5g02780	Glutathione transferase lambda-1	2.468	1.878	0.195	0.100	-
At1g72920	disease resistance protein (TIR-NBS class)	2.458	1.502	0.191	0.145	-
At3g55970	2OG-Fe(II) oxygenase family protein	2.301	1.538	0.189	0.147	1
At2g32030	GCN5-related N-acetyltransferase	2.194	1.426	0.181	0.197	1
At1g51420	Sucrose-phosphatase-1	2.031	1.377	0.183	0.185	-
At5g08240	Unknown	1.790	1.382	0.181	0.163	1
At5g47220	Ethelyne response factor	1.770	1.608	0.016	0.150	-
At1g72260	Thionin THI2.1	1.679	1.502	0.178	0.120	-
At2g29460	Glutathione transferase tau-4	1.678	1.950	0.199	0.197	-
At3g01260	Aldose 1-epimerase family protein	1.625	1.437	0.194	0.163	-
At4g17245	Zinc finger protein (C3HC4-type RING finger)	1.565	1.501	0.189	0.190	-
At5g66690	UDP-glucosyl transferase family protein	1.586	1.582	0.196	0.152	-
At2g44790	Uclacyanin 2	1.554	1.468	0.189	0.087	-
At1g07135	Glycine-rich protein	1.767	1.400	0.178	0.152	4

(d)

				Corrected *p*-values		
AGI code	Gene title	FC -Fe/+Fe WT shoots	FC WT/*cth2-1* -Fe shoots	Treatment	Genotype	No. of AREs
At3g02480	ABA-responsive, LEA protein-related	2.668	0.676	0.172	0.131	-
At5g02220	unknown protein	2.414	0.642	0.136	0.167	1
At5g01540	Lectin receptor kinase A4.1	2.302	0.706	0.184	0.113	-
At3g45970	*EXPL1* (expansin family protein)	2.244	0.395	0.149	0.116	-
At5g18270	NAC domain-containing protein 87	1.897	0.723	0.007	0.187	1
At5g11510	*MYB3R4* (MYB transcription factor)	1.576	0.794	0.149	0.056	1
At1g20350	*TIM17-1*, putative mitochondrial translocase	1.571	0.700	0.116	0.171	-

4.17.1 **Confirmation of putative candidate transcripts by qRT-PCR**

To confirm the microarray data, the regulation of putative candidate transcripts for CTH2-dependent regulation was confirmed in the same biological material using qPCR for six candidate genes in shoots (Table 10). The data from the microarray could be confirmed by qPCR, showing that microarray hybridizations and data analysis were successful. When the regulation of a set of 12 candidate genes in shoots was analyzed in another independent experiment, it was found that the extent and the direction of both, the Fe-dependent regulation and the difference in transcript levels between WT and *cth2-1* were different compared to the

microarray analysis (Table 11). It was thus concluded that the selected genes could not be confirmed as *CTH2* candidate genes because of too variable transcript levels between experiments.

Table 10: Differential regulation of shoot transcript levels observed using microarrays can be confirmed by qRT-PCR

Shown are fold-changes (FC) of transcript levels between the indicated genotypes and treatments determined by microarrays or qPCR. For both methods the same biological material was used as described in the main text.

		FC by microarray		FC by qPCR	
AGI code	Gene Title	-Fe/+Fe in WT	WT/*cth2-1* under -Fe	-Fe/+Fe in WT	WT/*cth2-1* under -Fe
At4g19690	Iron-Regulated Transporter 1 (IRT1)	3.18	1.67	3.15	1.66
At5g02780	Glutathione transferase lambda-1	2.47	1.88	3.06	2.23
At3g55970	Fe(II)-oxygenase family protein	2.30	1.54	3.10	1.56
At5g47220	Ethylene response factor	1.77	1.61	2.18	1.58
At1g72260	Thionin 2.1	1.68	1.50	2.61	1.60
At2g44790	Uclacyanin 2	1.55	1.47	1.49	1.29

Table 11: Putative candidate genes for *CTH2*-dependent regulation cannot be confirmed in independent experiments.

Shown are fold-changes (FC) of transcript levels between the indicated genotypes and treatments determined by microarrays or qPCR. Microarray analysis was performed as described in the main text. qPCR analysis was conducted with material from an independent replicate experiment.

		FC by microarray		FC qPCR	
AGI code	Gene title	-Fe/+Fe in WT	Col/*cth2-1* under -Fe	-Fe/+Fe in WT	Col/*cth2-1* under -Fe
At4g19690	Iron-regulated transporter 1 (IRT1)	3.18	1.67	40.18	3.60
At5g54490	Pinoid-binding protein 1 (PBP1)	2.64	1.46	0.72	0.83
At5g02780	Glutathione transferase lambda-1	2.47	1.88	0.94	0.64
At3g55970	2OG-Fe(II) oxygenase family protein	2.30	1.54	2.02	0.15
At4g17500	Ethylene responsive element binding factor 1	1.81	1.37	0.33	1.35
At5g47220	Ethelyne response factor	1.77	1.61	0.52	1.28
At1g07135	Glycine-rich protein	1.77	1.40	0.69	0.78
At5g10770	Eukaryotic aspartylprotease family protein	1.76	1.49	0.86	1.53
At1g72260	Thionin 2.1	1.68	1.50	0.52	0.22
At2g44790	Uclacyanin 2	1.55	1.47	1.41	1.33
At1g08940	Phosphoglycerate mutase family protein	1.25	1.48	1.13	1.46
At4g24120	Yellow stripe-like 1 (YSL1)	0.48	1.26	0.13	0.76

4.17.2 *In silico* analysis of putative binding sites for *At*CTH2 in 3'-UTRs

In another approach to find putative candidates for *CTH2*-dependent regulation, the 3'-UTRs of transcripts found at significantly different levels in WT and *cth2-1* plants were analyzed for the presence of AREs. First, all transcripts annotated in the *Arabidopsis thaliana* genome (Version TAIR10), containing at least one ARE in their 3'-UTRs were identified by using the PATMATCH tool found on www.arabidopsis.org. The query sequence used was WATTTAW, which is the minimum consensus sequence necessary for *Hs*TTP binding (Lai et al., 1999; Worthington et al., 2002) and *Sc*CTH2 (Puig et al., 2005). The identified loci were then used to annotate lists of transcripts, showing regulation as described above, with the number of AREs located within the 3'-UTRs. The analysis revealed the presence of at least one ARE in 16.8% of all transcripts expressed significantly different in WT and the *cth2-1* mutant. When all annotated 3'-UTRs from *Arabidopsis thaliana* were analyzed, it was found that the 3'-UTRs of 18.1% of all sequences contained at least one ARE. Since there is the possibility that *At*CTH2 interacts with a different sequence than its homologues, a search for enriched motifs in the transcripts regulated differently between the two genotypes was conducted. For this the MEME algorithm (Bailey et al., 2009) was used. An extensive analysis using different parameters and sets of input revealed no enrichment of AREs or ARE-like motifs in the datasets.

It is very likely that only a fraction of the genes regulated differently in WT and *cth2*-1 represent direct targets of CTH2 and a larger proportion consists of indirectly regulated genes. Moreover, overall small extents of regulation will increase the number of false positives and false negatives in the lists.

4.18 Homozygous *cth2-2* plants are male sterile

Homozygous *cth2-2* plants did not produce any seeds. This made handling of *cth2-2* difficult, because propagation had to be done *via* hemizygous individuals. The resulting offspring was then segregating for the *cth2-2* mutation. A closer inspection revealed that *cth2-2* plants did not present pollen on their anthers during floral stage 13 (Fig. 27, stages of flower development were named according to (Bowman, 1994) and (Smyth et al., 1990) and can be found in Supplemental Table 4). On the anthers of WT plants, pollen was visible as yellow

grains, whereas no pollen was visible on *cth2-2* anthers. Instead, the anthers of *cth2-2* plants appeared swollen and were not dehiscing. Manual opening of the anthers using a needle did not yield any pollen grains. Anthers on senescent *cth2-2* flowers eventually fell off the inflorescence, in a manner comparable to WT anthers. The *cth2-2* mutation seemed to be 100% disruptive of pollen development, since no homozygous *cth2-2* seed population was ever obtained. In the rare case, that a *cth2-2/cth2-2* plant produced seeds, it turned out to be an outcrossing event, since the resulting seeds were segregating for the *cth2-2* insertion again (data not shown). Since pollination did not occur, no siliques developed. Inflorescences of *cth2-2* plants continued to grow and produced new flowers at a stage when WT plants had stopped to produce new flowers when siliques began to ripen. This was likely a consequence of the absence of normal fruit development.

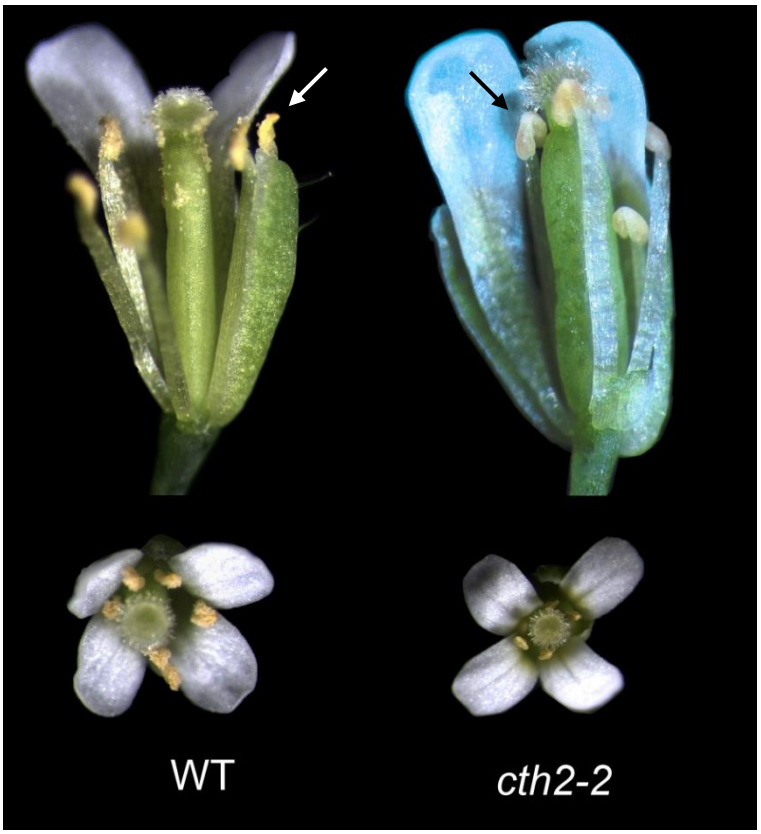

Figure 27: No pollen is presented by *cth2-2* anthers.

Shown are photographs of representative flowers from WT and *cth2-2* plants at anthesis (floral stage 13). For the upper images some sepals and petals were removed for better visibility of anthers. Arrows indicate anthers with (WT) or without (*cth2-2)* visible pollen grains.

To gain evidence that the *cth2-2* mutation is responsible for the male sterility, a population of plants segregating for the *cth2-2* insertion was germinated on media containing kanamycin. From a total of 1397 plants, 329 were sensitive to Kanamycin (1:4.3). The resistant plants were transferred to soil and allowed to flower. 322 plants out of 1062 showed the male sterile phenotype (1:3.3). The segregation rates indicated that the *cth2-2* mutant carries a single insertion (or closely linked multiple insertions) of a kanamycin resistance gene in the genome at the *CTH2* locus and that *cth2-2* is a recessive mutation causing male sterility. Additionally, 36 randomly selected male sterile plants were genotyped using PCR (data not shown). All 36 plants were homozygous for the *cth2-2* T-DNA insertion. This provided further evidence that the T-DNA insertion in the *CTH2* locus of *cth2-2* plants is the cause of male sterility. The fact that it was possible to find 25% homozygous *cth2-2* plants in a segregating population, although *cth2-2* is completely male sterile shows that the male sterile phenotype is caused by the sporophyte, and not the gametophyte. If development of the male gametophyte (the developing pollen) was disrupted by the *cth2-2* mutation, different segregation rates would be observed. Moreover, all pollen grains from heterozygous *CTH2/cth2-2* plants were phenotypically normal (data not shown).

To analyze further, whether the developmental defect is caused by the male or the female reproductive organs, reciprocal crosses were carried out (Table 12). Pollination of *cth2-2* pistils with WT anthers led to normal silique development. When *cth2-2* anthers were used to pollinate WT pistils, no offspring could be obtained. This shows that *cth2-2* is a male sterile mutant. Each direction of crossing was carried out at least ten times. Also WT pollen was used to pollinate WT pistils to determine the rate of success of crosses.

Table 12: Reciprocal crosses of WT and *cth2-2* show a defect in the male organs of *cth2-2*.

	WT ♂ x *cth2-2* ♀	*cth2-2* ♂ x WT ♀	WT ♂ x WT ♀
Total no. of crosses	20	12	10
No. of successful crosses	12	9	7

4.19 Genomic complementation of *cth2-2* plants

To confirm that the T-DNA insertion in the *CTH2* locus is responsible for the male sterile phenotype, a genomic complementation construct, using the vector pMDC99 (see chapter 3.3.3 and vector map in the Appendix), was transformed into CTH2/*cth2-2* hemizygous plants. After screening the T1 generation for the newly introduced transgene using hygromycin, surviving plants were genotyped by PCR for the *cth2-2* mutation, and homozygous *cth2-2* plants carrying the transgene were propagated to the T2 generation (Supplemental Fig. 4). In three independent transgenic lines, in a homozygous *cth2-2* background, a complete restoration of fertility was observed in the T2 generation (Fig. 28). Transcript levels of the transformed, full-length *CTH2* transcript were analyzed by semi-quantitative RT-PCR and found to match WT levels (data not shown). This confirmed that the T-DNA insertion in the *CTH2* locus is the reason for the male sterility in *cth2-2* plants. Also, F1 plants from a cross between *cth2-1* and *cth2-2* did not show the *cth2-2* male sterile phenotype. This was expected, since homozygous *cth2-1* plants did not show a male sterile phenotype.

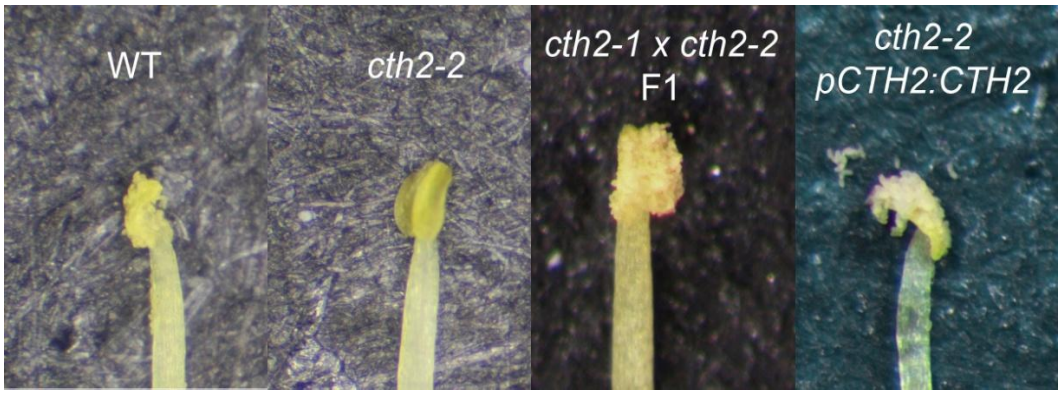

Figure 28: Male sterility of *cth2-2* plants can be complemented by *cth2-1* or by transformation with a wild-type *CTH2* gene.

Shown are images of anthers prepared from stage 13 flowers of the indicated genotypes. For *cth2-1* x *cth2-2* F1 plants, three crosses were performed, and the success of crossing was confirmed by PCR-based genotyping of five plants of each F1 population. For genetically complemented *cth2-2* plants, three independent lines were generated as described in the main text and Supplemental Fig. 4 and analyzed in the T2 generation.

4.20 Histological analysis of anthers of *cth2-2* plants

4.20.1 **Alexander's stain of anthers**

To visualize pollen *in vivo*, Alexander's stain (Alexander, 1969) was used. This stain can be used to distinguish between viable and aborted pollen. Viable *Arabidopsis* pollen from WT plants appeared as well defined, round structures stained in pink (Fig. 29). When *cth2-2* anthers were analyzed, pink structures were observed that did not resemble WT pollen grains. Instead, larger, less delineated, round structures could be observed. No pollen was released from *cth2-2* anthers during sample preparation and observation, as observed for WT anthers.

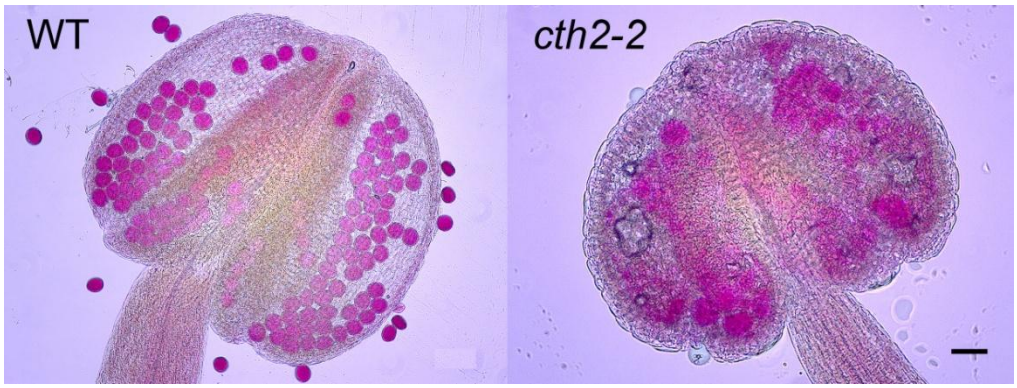

Figure 29: Anthers of *cth2-2* plants do not contain viable pollen.

Shown are representative images of anthers of stage 13 flowers from WT and *cth2-2* plants. Anthers were incubated in Alexander's staining solution for 1 min and destained in water. Images were obtained with a light microscope. Scale bar: 50 µm.

4.20.2 **Toluidine-Blue stain of resin-embedded sections**

The developmental stage at which the pollen development begins to be aberrant in *cth2-2* was determined. For this, resin-embedded three-µm thin sections of WT and *cth2-2* anthers were cut with a microtome and stained with toluidine-blue. Toluidine-blue stains lignins, nucleic acids and proteins, so that histological details can then be observed. During flowering stage 9, tetrads of haploid microspores were found in anthers from both, WT and *cth2-2* (Fig. 30). The

innermost layer of cells in the anther locule, the tapetum, provides nutrients to the developing pollen grains (Ma, 2005). Often a defect in tapetum development causes a disruption of pollen development. However, the tapetum had a similar appearance in WT and *cth2-2* anthers. During pollen development, the microspores are released from the tetrads to develop into mature pollen, as was observed in the WT. In the *cth2-2* mutant no pollen was found post-dehiscence at stage 13. Instead, large cells occupied the space in the locules. These cells were irregular in shape and had a granular appearance. Sometimes only remains of cells were found resulting in almost empty locules. These results showed that the development of pollen is disrupted in *cth2-2* plants after the formation of tetrads of microspores.

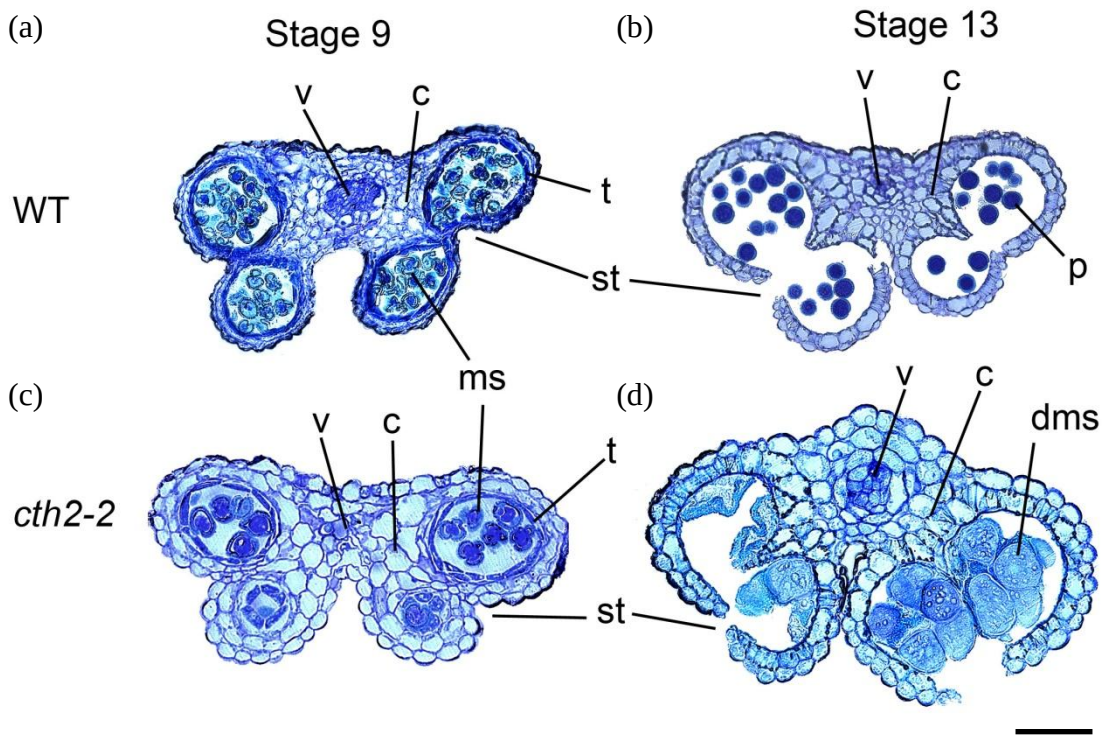

Figure 30: Development of *cth2-2* pollen is disrupted in the transition from microspores to mature pollen.

Images show toluidine-blue stained transverse sections of anthers from (a, b) WT and (c, d) *cth2-2* flowers sampled at the indicated floral stages. Images were obtained using a light microscope. c = connective, dms = degenerated microspores, ms = microspores, p = pollen, st = stomium, t = tapetum, v = vasculature. Scale bar 50 µm.

4.20.3 **Patterns of promoter activity of *CTH2* in floral organs**

To better understand the role of *CTH2* in pollen development, *CTH2* promoter activity was analyzed using transgenic *Arabidopsis thaliana* plants expressing the *uidA* gene under the control of a 1.5-kb fragment of the *CTH2* promoter (see chapter 4.6.1). Histochemical analysis of GUS-activity in floral organs using 5-Bromo-4-chloro-3-indolyl-β-D-glucuronide (X-Gluc) showed a tight spatio-temporal control of *CTH2* promoter activity. Before elongation of the filaments (stage 9) staining was observed in the central part of the anther between the anther lobes (Fig. 31a,b). Staining at this location was not detected at a later stage of development (Fig. 31c,d). Additionally, staining was observed in the vasculature of the petals and also occasionally in the vasculature of the filaments (floral stage 11-12). To localize the domain of *CTH2* promoter activity more exactly, Imagene Green was used. In accordance with the X-Gluc stain, *CTH2* promoter activity was observed in the central part of the connective during floral stage 9 (Fig. 32).

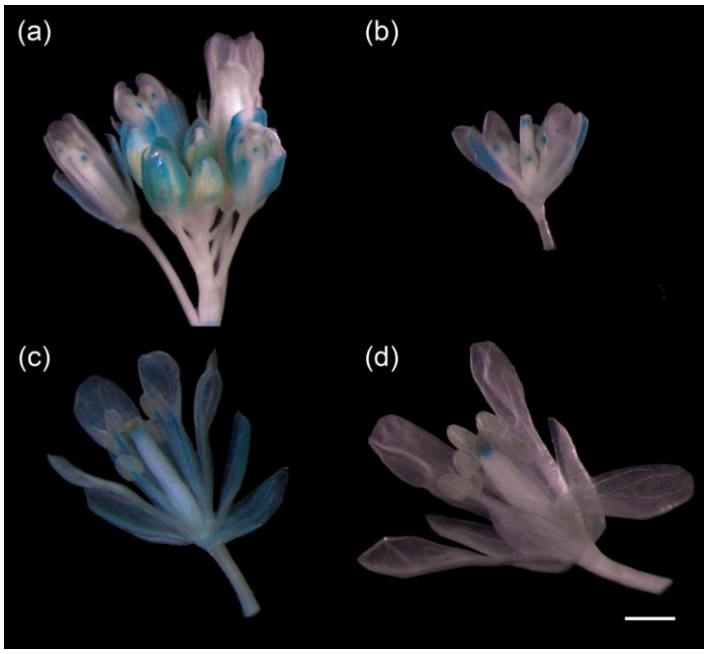

Figure 31: The *CTH2* promoter is transiently active in the central region of anthers during floral stage 9.

Shown are images of an inflorescence and flowers expressing the *uidA* gene under the control of a 1.5-kb *CTH2* promoter fragment. Transformants were generated as described in the main text. Tissues were stained using 5-Bromo-4-chloro-3-indolyl-β-D-glucuronide and destained using ethanol. The panels show: (a) an inflorescence with flowers at different developmental stages (b), a flower at stage 9 during elongation of the filaments (c), a flower at stage 11-12 and (d) a flower at stage 13-14 after dehiscence. Three independent lines were analyzed in the T3 generation after selection on hygromycin, and representative results are shown. Scale bar 1 cm.

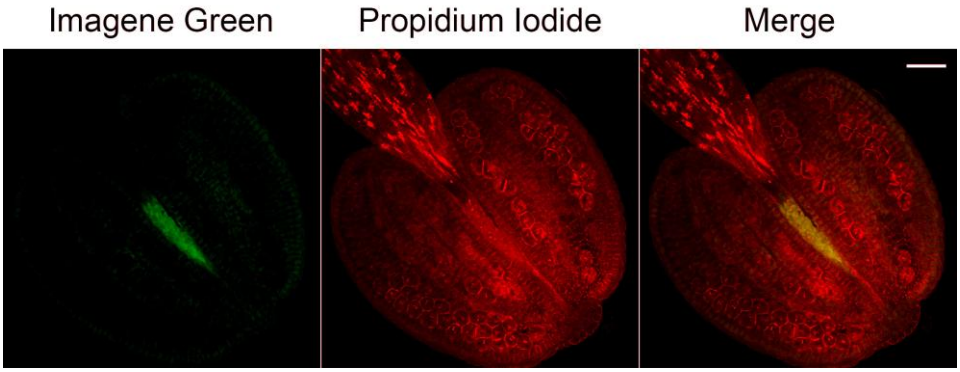

Figure 32: The *CTH2* promoter is active is the connective.

Shown is a single longitudinal, optical section of anthers of flowers at stage 9 from plants expressing the *uidA* gene under the control of a 1.5 kb *CTH2* promoter fragment. Transformants were generated as described in the main text. Anthers were stained for 30 min using Imagene Green. After Imagene Green staining anthers were stained with Propidium Iodide (1 mM) for 1 min, destained with ultrapure H_2O for 1 min, and imaged immediately. Panels show (from left to right): Imagene Green stain, Propidium Iodide stain, overlay of Imagene Green- and Propidium Iodide stains (merge). Three independent lines were analyzed in the T3 generation after selection on hygromycin, and representative results are shown. Images were obtained using a confocal laser-scanning microscope. Scale bar: 50 µm.

4.21 Element concentrations in anthers

Since *CTH2* has a regulatory role in Fe homeostasis (chapter 4.9 ff), elemental concentrations were analyzed in anthers from WT, *cth2-1* and *cth2-2* plants. The sensitivity of the ICP-AES system was sufficient to analyze such small amounts of tissues. However, the biomass of the samples was too small for a reliable quantification. To overcome this, the concentrations of micronutrients (Cu, Fe, Mn, Zn) were related to those of the macronutrients K and Mg. When looking at Fe, both the concentrations relative to K and Mg (Fig. 33a, b) and the absolute concentrations in the sample solution (Fig. 33c, d) were lower in *cth2-2* anthers than in WT or *cth2-1* anthers. For Mn, a reduction in both mutants compared to the WT was found, both absolute and relative. Cu and Zn concentrations seemed to be unaffected. The results for Cu, Fe and Mn could be repeated but Zn concentrations were more variable between experiments. The results indicated a disturbance of Fe homeostasis in *cth2-2* anthers. Since Fe

concentrations were lower in *cth2-2* anthers then in WT anthers, it was tried to rescue the male sterility phenotype by external application of Fe to the anthers.

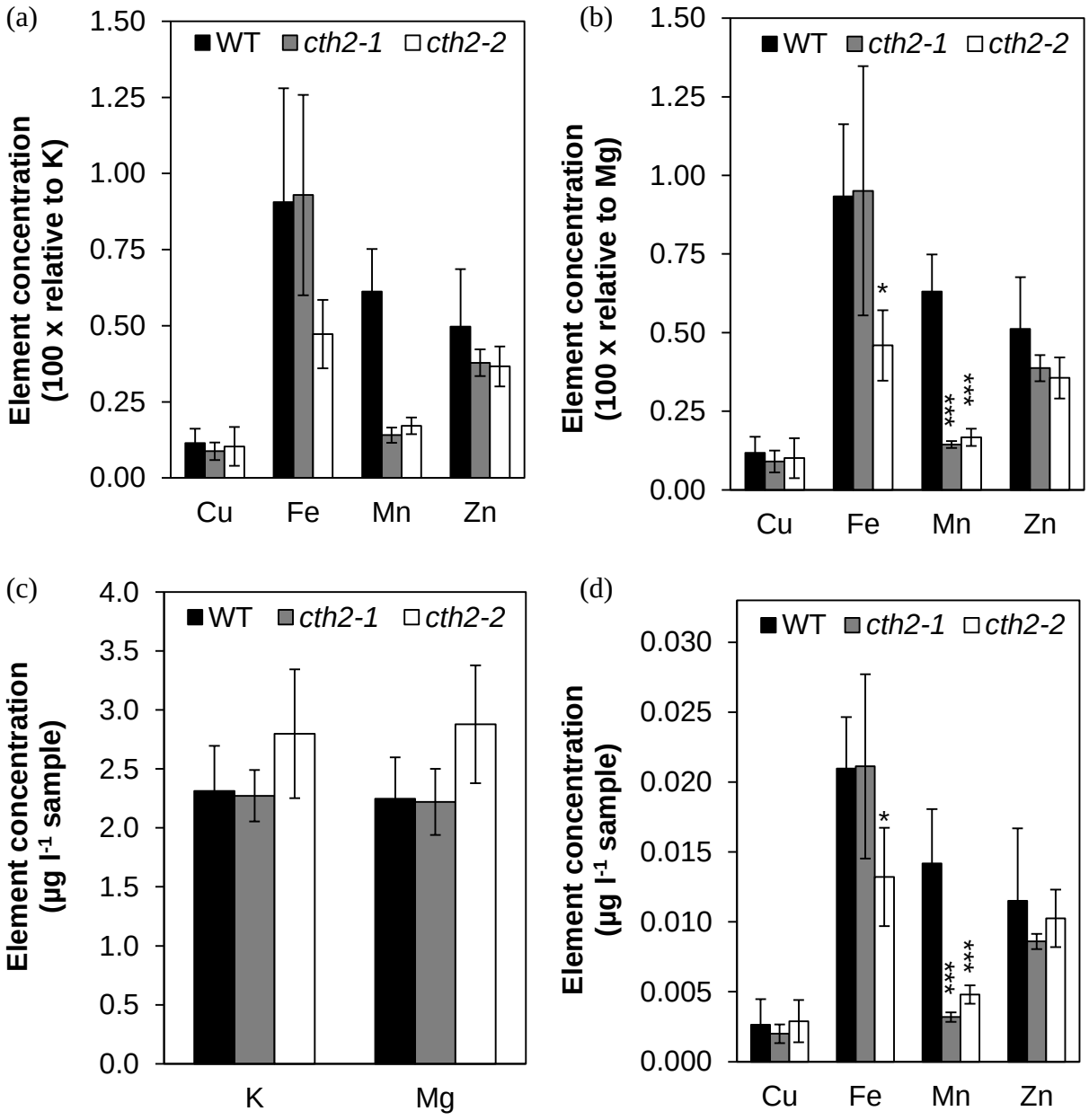

Figure 33: Anthers of *cth2-2* plants contain less Fe then anthers of WT plants.

Shown are (a, b) relative and (c, d) absolute elemental concentrations measured by ICP-AES. For each sample, 60 anthers were harvested from stage 10-11 flowers, pooled and prepared for analysis in a final volume of 3 ml. For each genotype $n = 5$ replicate samples were analyzed. Bars represent arithmetic means ± SD. Data are from one experiment, representative of a total of two independent experiments. Significant differences to WT were detected by Student's *t*-test (* $p < 0.01$; *** $p < 0.001$).

4.22 Chemical rescue of *cth2-2*

To rescue the male sterility phenotype of *cth2-2*, chemicals were applied exogenously to developing flower buds (Table 13). Hormones were sprayed every second day for the duration of five days (3 times in total). Because nicotianamine (NA) stocks were limited, a small volume (2 ml) was used, to completely submerge individual inflorescences for 30 sec every second day for the duration of five days (3 times in total). None of the substances tested here rescued the *cth2-2* mutant by allowing the development of pollen. This result is contradicting the results obtained from the analysis of element concentration in anthers. Still, the inability to rescue *cth2-2* plants by exogenously supplying Fe does not rule out that Fe homeostasis is disturbed. It is possible that exogenously applied Fe does not reach its cellular target sites or that essential Fe-containing proteins require Fe to be supplied in a specific form e.g. chelated with an unidentified molecule.

Table 13: Chemicals applied to *cth2-2* anthers.

All tested substances were applied dissolved in ultrapure H_2O together with 0.025% (v/v) Triton X-100 as a surfactant. Plant hormones were supplied by Sigma-Aldrich (St. Louis, MO, USA). The composition of HG-medium is given in Table 1.

Hormones	50 µM Methyl jasmonate (MeJa)
	10 µM Gibberellic acid (GA_3)
	10 µM Abscisic acid (ABA)
Micronutrient/chelator	3 mM Citrate
	3 mM Citrate + 4 x HG medium
	50 µM Nicotianamine
	50 µM Nicotianamine + 4 x HG medium

4.23 Microarray transcriptome analysis of *cth2-2* anthers

The male sterility of *cth2-2* plants is caused by a lack of CTH2 activity. Since CTH2 is hypothesized to be a regulator of transcript stability, a microarray analysis was performed to identify transcripts, which are deregulated in *cth2-2* anthers compared to WT. This was expected to identify target transcripts as well as to provide information to functionally characterize the developmental defect of *cth2-2.* Anthers were harvested from flowers at stage

10 of WT and *cth2-2* plants. For each sample *ca.* 600 anthers were harvested and pooled. Two replicate samples were collected from each genotype, resulting in $n = 4$ samples in total. RNA was extracted from each sample and analyzed by ATH1 microarrays (see chapter 3.6).

Transcript levels of 1148 genes were significantly (at least two-fold change, $p \leq 0.05$) lower in *cth2-2* anthers than in WT anthers, and those of 897 genes were higher. Out of all transcripts present at higher or lower levels in *cth2-2* than in WT, 28.2% and 35.1% respectively contained at least one ARE (WATTTAW) in their 3'-UTRs.

In a list of the top ten transcripts found at higher levels in *cth2-2* anthers than in WT anthers no obvious gene was found that potentially explains the observed phenotype or potentially is a candidate for *CTH2*-dependent regulation (Table 14 a; see Supplemental Table 7 for the top 100 genes). The same result was obtained with a list of the top ten transcripts found at lower levels in *cth2-2* anthers compared to WT (Table 14 b), with the exception of *PCR11* (*Plant Cadmium Resistance 11*). The *PCR11* transcript showed the highest fold-change in *cth2-2* anthers compared to WT ($\log_2$ fold-change *cth2-2* / WT: -6.85). Different members of the PCR11-family were found to encode a Cd-resistance protein (Song et al., 2004), a Zn-transporter (Song et al., 2010) and a Ca-transporter (Song et al., 2011). Since members of this family have diverse roles in metal homeostasis, it is possible that *PCR11* contributes to Fe homeostasis in anthers.

Table 14: Top 10 de-regulated genes in *cth2-2* anthers compared to WT.

Shown are the top 10 genes with significantly ($p \leq 0.05$) (a) higher (b) lower transcript levels in *cth2-2* anthers compared to WT anthers as determined by microarray analysis.

(a)

AGI code	Tair symbol	Description	$\log_2$ FC *cth2-2* / WT	Adjusted *p*-value	Number of AREs
At1g48940	ENODL6	Early nodulin-like protein 6	4.49	0.0016	-
At4g25920		Protein of unknown function (DUF295)	4.18	0.0011	-
At4g24890	PAP24	Probable inactive purple acid phosphatase 24	4.00	0.0021	-
At1g56360	PAP6	Purple acid phosphatase 6	3.99	0.0013	-
At5g02140		Pathogenesis-related thaumatin superfamily protein	3.80	0.0011	-
At2g21640		Unknown marker for oxidative stress response.	3.63	0.0011	1
At5g08030		PLC-like phosphodiesterases superfamily protein	3.54	0.0014	-
At2g20970		Unknown protein	3.47	0.0013	-
At2g39590		Ribosomal protein S8 family protein	3.45	0.0013	-
At3g50580		Unknown protein	3.44	0.0021	-

(b)

AGI code	Tair symbol	Description	$\log_2$FC *cth2-2* / WT	Adjusted *p*-value	Number of AREs
At1g68610	PCR11	PLANT CADMIUM RESISTANCE 11	-6.85	0.0011	-
At3g62230		F-box protein	-6.8	0.0033	1
At1g01980		FAD-binding berberine family protein	-6.61	0.0038	1
At1g75870		Unknown protein	-6.56	0.0011	-
At1g49290		Unknown protein	-6.49	0.002	-
At2g26850		F-box family protein	-6.29	0.0014	-
At5g20390		Glycosyl hydrolase superfamily protein	-6.28	0.0024	2
At1g14420		Pectate lyase family protein	-6.2	0.0018	-
At1g54070		Dormancy/auxin-associated family protein	-6.11	0.0023	-
At2g05850	SCPLl38	Serine carboxypeptidase-like 38	-6.08	0.0013	-

4.23.1 **Analysis of functional categories**

To examine, how *cth2-2* might cause male sterility, genes with significantly different transcript levels (at least two-fold change, $p \leq 0.05$) in *cth2-2* anthers compared to WT anthers were categorized using the Mapman ontology (Thimm et al., 2004). Transcripts present at significantly higher or lower levels in *cth2-2* than in WT anthers were analyzed separately. Several (sub-)bins were found to be significantly enriched compared to the classification of all transcripts present on the ATH1 array (Table 15).

Table 15: Overrepresented Mapman functional classes (bins) among the genes with different transcript levels in WT compared to *cth2-2*.

Show are significantly overrepresented bins from the Mapman ontology from sets of transcripts found to be (a) more or (b) less abundant in *cth2-2* anthers compared to WT anthers. Overrepresentation is expressed relative to all genes represented on the ATH1 array. *p*-values were calculated by Fisher's exact test and adjusted for multiple comparisons by the Benjamini-Hochberg method.

(a)

Mapman Bin number	Bin name	In set		-fold over-representation	*p*-value
		No. of genes	%		
23.1	nucleotide metabolism.synthesis	7	0.8	5.4	< 0.05
27.4	RNA.RNA binding	18	2.0	2.8	< 0.01
29	protein	256	28.7	2.0	< 0.001
29.2	.synthesis	149	16.7	7.1	< 0.001
29.2.1	.ribosomal protein	136	14.9	8.8	< 0.001
29.2.1.1	.prokaryotic	35	3.9	6.8	< 0.001
29.2.1.1.2	.mitochondrion	5	0.6	7.2	< 0.05
29.2.1.1.3	.unknown organellar	23	2.6	12.8	< 0.001
29.2.1.1.3.2	.50S subunit	18	2.0	15.2	< 0.001
29.2.1.2	.eukaryotic	96	10.8	10.0	< 0.001
29.2.1.2.1	.40S subunit	35	3.9	9.7	< 0.001
29.2.1.2.1.19	.S19	3	0.3	18.4	< 0.05
29.2.1.2.1.515	.S15A	4	0.4	16.3	< 0.05
29.2.1.2.2	.60S subunit	61	6.8	10.1	< 0.001
29.2.1.2.2.7	.L7	3	0.3	18.4	< 0.05
29.2.2	.misc ribosomal protein	6	0.7	11.3	< 0.01
29.2.2.50	.Biosynthesis of ribosomes in *Xenopus* (BRIX)	5	0.6	20.4	< 0.01
29.2.6	.ribosomal RNA	3	0.3	18.4	< 0.05
29.3.2	.targeting.mitochondria	10	1.1	7.4	< 0.001
29.6	.folding	13	1.5	5.1	< 0.001

Table 15, continued.

(b)

Mapman Bin number	Bin name	In set		-fold over representation	*p*-value
		No. of genes	%		
10	cell wall	55	4.9	2.3	< 0.001
10.5.3	.cell wall proteins.LRR	5	0.4	6.1	0.052
10.6	.degradation	16	1.4	2.5	< 0.05
10.6.3	.pectate lyases and polygalacturonases	14	1.3	2.9	< 0.05
10.8.1	.pectin*esterases.PME	10	0.9	4.1	< 0.05
11	lipid metabolism	33	3.0	1.7	0.052
11.8.1	.exotics.sphingolipids	8	0.7	6.5	< 0.01
26.18	misc.pectin methylesterase inhibitor family protein	12	1.1	5.3	< 0.001
29.4	protein.post-ranslational modification	81	7.3	2.4	< 0.001
29.4.1	.kinase	26	2.3	3.5	< 0.001
29.4.1.59	.receptor like cytoplasmatic kinase IX	8	0.7	8.3	< 0.01
30	signalling	99	8.9	1.6	< 0.001
30.2.16	.receptor kinases.Catharanthus roseus-like RLK1	5	0.4	6.1	0.052
30.2.22	.proline extensin like	6	0.5	5.9	< 0.05
30.3	.calcium	29	2.6	2.7	< 0.001
31	cell	59	5.3	1.6	< 0.05
31.1	.organisation	36	3.2	2.0	< 0.01
34	transport	78	7.0	1.6	< 0.01
34.12	.metal	16	1.4	3.5	< 0.01
35.1.21	not assigned.epsin N-terminal homology (ENTH) domain-containing protein	7	0.6	6.9	< 0.01

Out of the 897 genes with higher transcript levels in *cth2-2* anthers than in WT anthers 136 encoded ribosomal proteins. This corresponded to 14.9% of all genes with higher transcript levels in *cth2-2* compared to WT (8.8-fold overrepresented compared to all genes represented on the ATH1 array, $p < 0.001$). On average, the transcript levels of these 136 genes were 2.54 (± 1.28 SD) -fold higher in *cth2-2* anthers compared to WT anthers. Since most of the ribosomal proteins are encoded by multiple genes (Barakat et al., 2001) even small changes in transcript levels may be of biological relevance. Higher transcript levels of genes encoding ribosomal proteins could result in an increased protein synthesis in *cth2-2* anthers compared to WT. In WT plants, the transcript levels of 130 genes out of these 136 were reduced in stamens from stage 15 flowers compared to stamens from stage 12 flowers (Fig. 34). This means that in WT anther development, transcript levels of genes encoding ribosomal proteins

are decreasing with proceeding anther development, while in *cth2-2* anthers this likely happens to a lesser extent. One possibility to explain this is that *cth2-2* anthers are blocked in their development.

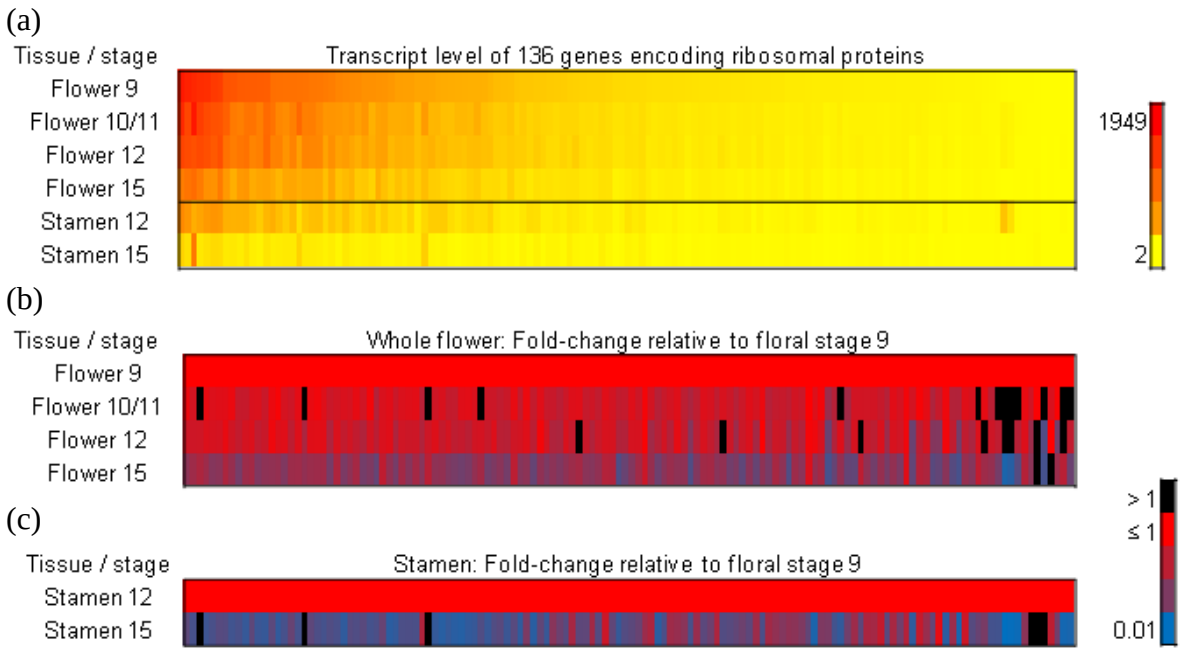

Figure 34: Transcript levels of genes encoding ribosomal proteins decrease with proceeding flower and stamen development.

Shown are heat-map representations of (a) transcript levels and (b, c) fold-changes of transcript levels during WT development relative to the indicated developmental stage. The 136 genes represented here had significantly higher transcript levels (at least two-fold change, $p \leq 0.05$) in *cth2-2* anthers than in WT anthers and belong to the Mapman bin "ribosomal protein". The datasets used consisted of quantile-normalized (gcRMA), linearized signal intensities from the AtGenExpress project (Schmid et al., 2005a). Data was obtained and processed *via* the BAR website using the eNorthern tool (Toufighi et al., 2005). Each column represents one gene and each row represents a developmental stage. Absolute transcript levels (a) are color-coded yellow-to-red. Fold-changes (b, c) of transcript level > 1 are indicated in black, fold-changes ≤ 1 are color-coded red-to-blue.

Transcripts of 18 genes (2.8-fold overrepresented compared to all genes represented on the ATH1 array, $p < 0.001$) encoding proteins with an RNA-binding domain were found to be more abundant in anthers from *cth2-2* plants compared to WT. Loss of CTH2 function in the *cth2-2* mutant may lead to changes in transcript levels of other RNA-binding proteins. For

example, the plants could try to compensate the loss of CTH2 function by increased expression of other genes that are part of a putative CTH2-dependent pathway of transcript degradation. A function of CTH2 in RNA-binding and regulation of transcript stability is in accordance with results from the heterologous expression of *AtCTH2* in yeast (see Figs. 2 and 3) and localization studies in protoplasts (see Figs. 4 and 5).

Transcripts of eight genes (6.5-fold overrepresented compared to all genes represented on the ATH1 array, $p < 0.001$) encoding proteins of the sphingolipid biosynthesis pathway (bin 11.8.1) were found to be less abundant in *cth2-2* anthers then in WT anthers. Disruption of the sphingolipid biosynthesis pathway causes male sterility in *Arabidopsis* (Teng et al., 2008), which makes these genes putative candidates to functionally explain the male sterility phenotype of *cth2-2*. The transcript levels of all 24 genes from the sphingolipid bin were then further analyzed using data from this study and publicly available microarray data. The analysis revealed that the eight genes significantly down-regulated in anthers from *cth2-2* plants compared to WT (data from this study) represented the eight most highly expressed genes in stamens of stage 12 flowers of WT plants among all 24 genes from the sphingolipid bin (publicly available data) (Fig. 35). Thus, it is likely that sphingolipid biosynthesis is impaired in *cth2-2* anthers. Interestingly, six out of these eight significantly regulated genes had at least one ARE in their 3'-UTRs. However, direct target-transcripts of CTH2 are not expected to be found at lower levels in *cth2-2* compared to WT, if CTH2 acts in targeting transcripts for degradation.

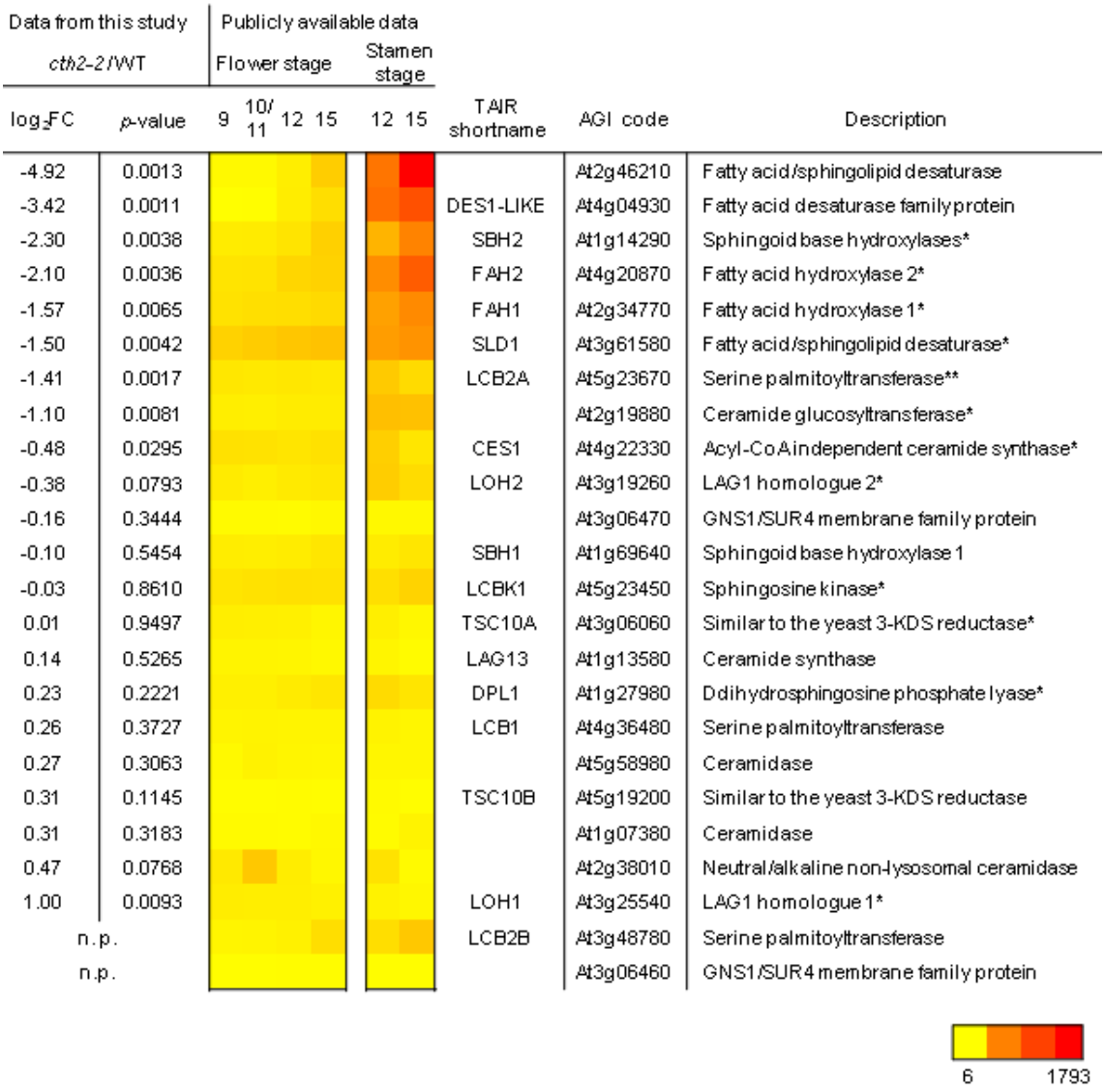

Figure 35: Transcript levels of sphingolipid biosynthesis genes are reduced in *cth2-2* anthers compared to WT anthers.

Shown is a comparison of $\log_2$ fold changes (FC), adjusted *p*-values and transcript levels during development of flowers or stamen of all genes from the Mapman bin "lipid metabolism.exotics.sphingolipids". On the left side, $\log_2$ fold changes of transcript levels in *cth2-2* anthers compared to WT anthers (data from this microarray study) are shown with their respective *p*-values (ebayes function, corrected with the Benjamini-Hochberg method). n.p. (not present) marks genes that were excluded by MAS5 filtering because of too low signal intensity. In the center, a heat map representation of transcript levels in flowers and stamens of Col-0 plants are shown at the indicated stages of floral development. The datasets used consisted of quantile-normalized (gcRMA), linearized signal intensities from the AtGenExpress project (Schmid et al., 2005a). Data was obtained and processed *via* the BAR website using the eNorthern tool (Toufighi et al., 2005). Each row represents one gene and each heat-map column represents a developmental stage. Transcript levels were color-coded yellow-to-red. Rows were sorted from biggest to smallest fold-change between *cth2-2* and WT anthers. Asterisks in the column named "description" represent the number of AUUUA elements in the 3'-UTRs.

4.24 Silencing of *CTH1* and *CTH2* using amiRNA

To analyze the effects of reduced transcript levels of *CTH1* and *CTH2*, WT plants were stably transformed with three different constructs (named *amiRNA A*, *amiRNA B*, *amiRNA C*) using the CaMV 35S promoter to express an artificial microRNA (amiRNA) designed to silence *CTH1* and *CTH2* simultaneously (see chapter 3.3.5). After transformation, T1 plants were screened for the integration of the T-DNA by phosphinothricin (PPT) and resistant plants were allowed to self. For each construct 5 to 12 independent lines were generated and propagated to the T2 generation. Experiments were performed with PPT-selected plants in the T2 generation. First, transcript levels of *CTH1* and *CTH2* were analyzed in 6-week-old plants in the T2 generation grown on soil by qRT-PCR (data not shown). For the *amiRNA A* construct, no lines could be isolated which showed silencing of either *CTH1* or *CTH2*. For each of the constructs *amiRNA B* and *amiRNA C* at least three lines could be isolated that showed either only reduced *CTH1* transcript levels (*amiRNA C*) or reduced *CTH2* and slightly reduced *CTH1* transcript levels (*amiRNA B*). These lines were subsequently grown hydroponically for 45 days alongside WT plants and subjected to Fe deficiency for the final 10 days of cultivation. The silencing of *CTH1* and *CTH2* was then confirmed by qRT-PCR.

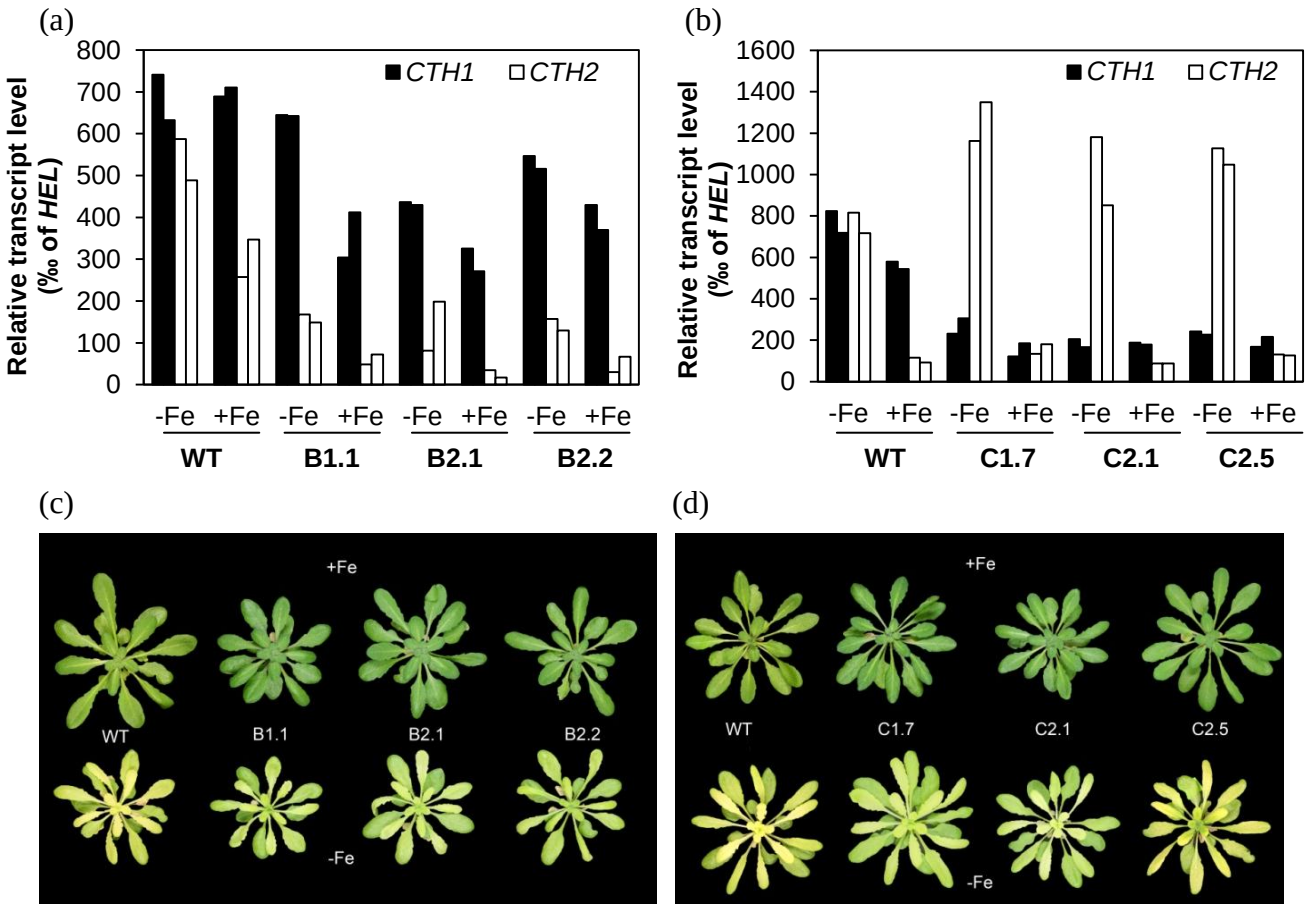

Figure 36: Silencing of either *CTH1* or *CTH2* does not affect the sensitivity of plants to Fe deficiency.

Shown are (a, b) relative transcript levels in shoots of *CTH1* and *CTH2* and (c, d) photographs of shoots of 45-day-old plants grown in hydroponic culture. Plants were grown in the absence of added Fe (-Fe) for the final 10 days of cultivation. Control plants (+Fe) were grown on media containing 5 µM FeHBED throughout. After photographing, tissues were harvested for RNA extraction. RNA was extracted from shoot material pooled from 5 to 10 individual plants and reverse transcribed to cDNA. Relative transcript levels were measured by qPCR with two technical replicates of each reaction. Each bar represents one technical replicate. *Helicase* (*HEL*) is a constitutively expressed control gene used to normalize transcript levels. Data in a) and c) were obtained with the *amiRNA B* construct (lines B1.1, B2.1, B2.2). Data in b) and d) were obtained with the *amiRNA C* construct (lines C1.7, C2.1, C2.5). Both constructs include the CaMV 35S promoter to control expression of the amiRNA and were designed to target both *CTH1* and *CTH2*. Data are from three independent lines in the T2 generation for each construct. Plants carrying the transgene were selected using phosphinothricin. For each of the two construct two replicate experiments were performed and representative results from one experiment for each construct is shown.

In *amiRNA B* plants, relative *CTH2* transcript levels were reduced to between 25% and 29% of WT levels under Fe-deficient conditions and to between 8% and 20% of WT levels under Fe-sufficient conditions (Fig. 36a). Also *CTH1* transcript levels were reduced to a lesser extent (up to 42% of WT levels in Fe-sufficient *amiRNA B 2.1* plants). Although *CTH2* transcript levels were reduced in *amiRNA B* lines, *CTH2* transcript levels still responded to Fe supply. No reduction of fertility was observed in *amiRNA B* plants, different to what was observed in *cth2-2* plants. In *amiRNA C* plants, relative *CTH1* transcript levels were reduced to 25% of WT levels regardless of Fe supply, while *CTH2* transcript levels were increased to between 132% and 163% of WT levels in Fe-deficient conditions (Fig. 36b). In Fe-sufficient conditions, relative *CTH2* transcript levels in *amiRNA C* plants varied between 85% and 151% of WT levels. Plants carrying either the *amiRNA B* or the *amiRNA C* construct showed no obvious phenotype regardless of the Fe status, when compared to WT plants (Fig. 36c, d).

In conclusion, it was possible to reduce transcript levels of *CTH1* or *CTH2* by constitutive expression of amiRNAs directed against the *CTH* transcripts. The reduction of *CTH1* or *CTH2* transcript levels did not influence the sensitivity of plants to Fe deficiency or affect fertility.

5 Discussion

5.1 The *Arabidopsis* CTH2 protein is a functional homologue of *Sc*CTH2

In yeast, *Sc*CTH2 regulates transcript stability under Fe-deficient conditions for metabolic acclimation of the cells to a Fe-poor environment (Puig et al., 2005) (see chapter 1.8.2). In *Arabidopsis thaliana*, two homologous proteins were identified. The most conserved region was the tandem zinc-finger (TZF) domain (Fig. 1a, b). The results from the yeast three-hybrid system (Fig. 2) and the functional complementation of a yeast *cth1Δcth2Δ* mutant by an *AtCTH2* expression construct (Fig. 3) indicated that *Sc*CTH2 and *At*CTH2 are functionally homologous. The fact that *At*CTH2 can functionally complement a *cth1Δcth2Δ* yeast mutant indicates that not only target transcripts, but also components of the transcript degradation machinery may be conserved across organisms. Further evidence for a role of *At*CTH2 in transcript metabolism comes from co-localization analysis (chapter 4.3.2). It was shown that *At*CTH2 localizes to granular structures in the cytosol, which were identified as plants stress granules (Fig. 4b). These are structures in the cytosol where translationally inactive transcripts are stored (Buchan and Parker, 2009).

5.2 *Arabidopsis* CTH2 is localized to hotspots of transcript metabolism in cells

When a CTH2-GFP fusion construct was expressed under the transcriptional control of the CaMV 35S promoter in *Arabidopsis thaliana* mesophyll protoplasts, a strong signal was observed in cytoplasmic foci that partially co-localized with RBP47-tdtomato, a marker for plant stress granules (SGs) (Weber et al., 2008), after a heat-shock (HS) treatment (Fig. 4b). The localization of CTH2 to SGs is a further indication that CTH2 is part of the 5'→3' transcript degradation machinery that regulates gene expression through degradation of transcripts or translation rates.

The aggregation of RBP47 in SGs after HS treatment can be prevented by incubating the cells with the translational inhibitor cycloheximide (Weber et al., 2008), however the localization

of CTH2 in granular structures was not impeded by cycloheximide (Fig. 5). Cycloheximide traps transcripts in polysomes by blocking translational elongation. Since cycloheximide can prevent the localization of RBP47B to SGs it was concluded that SG assembly is, at least partially, dependent on non-ribosome associated mRNAs. Localization of CTH2 to granular structures seems independent from the presence of non-ribosome associated mRNAs. As a conclusion, CTH2 can probably regulate gene expression by initiating degradation or translational inhibition of actively translated mRNAs. CTH2 would thus not be required for bulk degradation of non-ribosome associated mRNAs, but for degradation of a specific set of mRNAs, regardless of their translational status. This result also illustrates that the formation of the granular structures (putative SGs) that form after a HS treatment is partially independent from the presence of untranslated mRNAs.

The human TZF-protein TTP localized to SGs when it is overexpressed in mammalian cells (Kedersha et al., 2005). Further studies revealed that TTP also localized dynamically to processing bodies (PBs) when expressed from its own promoter (Franks and Lykke-Andersen, 2007). In yeast, a GFP-*Sc*CTH2 fusion protein expressed from the endogenous *Sc*CTH2 promoter showed an evenly distributed cytosolic localization (Pedro-Segura et al., 2008). When this construct was transformed into mutants strains defective in mRNA-degrading PB components (*xrn1Δ*, *dcp1Δ*, *dcp2Δ*), localization of GFP-*Sc*CTH2 in PBs was observed, presumably through the accumulation of non-degraded transcripts. A GFP-*Sc*CTH2 fusion construct, using the *ScCTH2* promoter for expression, was localized to the nucleus in mutants defective in nuclear mRNA export and alternatively by translationally fusing it to a nuclear localization sequence, or by abolishing RNA-binding of the TZF domain through mutagenesis (Vergara et al., 2011).

The fact that *At*CTH2 localizes to SGs is in agreement with its hypothesized function of destabilizing transcripts to regulated gene expression. Although *At*CTH2 did not co-localize with the PB component *At*DCP1, in mammalian cells PBs and SGs are often found in close proximity, sometimes even docking with one another, probably to exchange components (Kedersha et al., 2005; Wilczynska et al., 2005). In the current model, mRNAs can shuttle between an active translational state in polysomes and an inactive state in SGs. Once mRNAs are recruited to SGs, they may be transferred to PBs for degradation or reenter the active translational state (Balagopal and Parker, 2009; Buchan and Parker, 2009). TZF proteins, like *Hs*TTP and *Sc*CTH2, show a dynamic localization to the places of transcript processing, so

possibly TZF proteins serve as a link between the different states and localizations that mRNAs undergo throughout the life cycle.

From studies of other TZF proteins it became clear that overexpression or knockout of PB or SG components can influence their subcellular localization as well as the subcellular localization of other PB and SG components. In this study, the CaMV 35S promoter was used, which might bring some limitations. It might be that the overexpression of *AtCTH2* or any of the marker constructs introduces artifacts to the localization analysis. When the constructs were transformed alone, none of the fusion proteins showed different localizations compared to the co-transformations (data not shown). This rules out artifacts from interactions of the co-transformed overexpression constructs. It is likely that *At*CTH2 also has a dynamic localization, but this is most likely obscured by the use of the CaMV 35S promoter.

Since the subcellular localization of CTH2 might have an impact on the stability of CTH2 target transcripts, it would be helpful to determine the subcellular localization of CTH2 in plants grown under Fe-deficient conditions or in the course of anther development. Since plants expressing a *CTH2-GFP* construct under the transcriptional control of a 1.5-kb fragment of the endogenous *CTH2* promoter showed no fluorescence signal, and since the CaMV 35S promoter probably creates artificial localizations, it could be tried to transform *cth2-2* plants with a *pCTH2:CTH2::HA* construct and subsequently localize the fusion protein with immunological methods. A tagged version of the CTH2 protein should be used, since it was not possible to generate a specific anti-CTH2 antibody.

5.3 Two *cth2* alleles have two different phenotypes

In the case of *cth2-1* and *cth2-2*, two different T-DNA insertions in the same locus result in two different phenotypes (Fig. 14). The *cth2-1* allele is dominant and affects growth under Fe-deficient conditions (Fig. 17) The fact that the partial *cth2-1* transcript could be amplified by PCR from oligo(dT)-primed cDNA reaction (Fig. 15) and that it seemed to be spliced correctly suggested that the partial primary transcript is processed into a mature, functional mRNA. Analysis of transcript levels by qRT-PCR showed that the partial transcript in *cth2-1* is not regulated by Fe status unlike the *CTH2* transcript in the WT, but transcript levels were

comparable to the full-length *CTH2* transcript levels in WT plants grown in Fe-sufficient conditions (Fig. 18a). The *cth2-2* allele causes recessive male sterility (Fig. 27). Also in *cth2-2* plants a partial *CTH2* transcript, different from that found in *cth2-1*, could be detected (Fig. 15). The effect of the dominant *cth2-1* allele could be phenocopied by expression of a corresponding partial cDNA in WT plants under the transcriptional control of the CaMV 35S promoter (*35S:CTH2_Cterm*) (compare Figs. 17 and 23). The *cth2-2* mutant was complemented by transformation of a 3.5-kb genomic fragment including the *CTH2* locus (Fig. 28 and Supplemental Fig. 4). For both *cth2-1* and *cth2-2*, this confirms that the T-DNA insertions in the *CTH2* locus are responsible for the observed phenotypes. Since different phenotypes are observed in the two *cth2* lines, it is very likely that the T-DNA insertions have different effects on the presence of putative partial CTH2 proteins. Furthermore, even different consequences for the stability of CTH2 target transcripts can be assumed. However, it cannot be ruled out that a difference between the CTH2-dependent regulation of pollen development and Fe homeostasis exists that allows a dual role of CTH2 in stabilizing and destabilizing transcripts, depending on the tissue or the developmental stage.

Since the two *cth2* alleles result in different phenotypes, it is interesting to understand what the effect on CTH2 target transcripts of each allele is (Fig. 37). From data obtained by heterologous expression of *CTH2* in yeast (Figs. 2 and 3) it was concluded that CTH2 is most likely a negative regulator of transcript stability. This is further supported by existing literature on related proteins from yeast and human (see chapter 1.8). The TZF domain, which was generally shown to mediate interactions with target transcripts (Lai et al., 1999; Puig et al., 2005), is disrupted by the T-DNA insertion in *cth2-2*. If the hypothesis on CTH2 function is correct, then CTH2 target transcripts cannot be degraded in *cth2-2* plants. Apparently this is not critical for Fe homeostasis in rosette leaves, or there might be a functional redundancy with *CTH1*. However, failure to degrade *CTH2* target transcripts leads to a disruption of anther development in the *cth2-2* mutant, probably in the context of a disturbed Fe homeostasis (Figs. 30 and 33). Maybe it is necessary to use a *cth1cth2* double knock-out mutant to observe a phenotype under Fe-deficient conditions also in rosette leaves. Alternatively, Fe homeostasis is too robust, so that no phenotype can be detected in a *CTH2* loss-of-function mutant in the conditions used. In both of these alternative scenarios, the changes in transcript levels of CTH2 target transcripts would be not large enough in *cth2-2* mutant plants to generate a detectable phenotype. In accordance with this, also the Fe supply-dependent changes in transcript levels observed in a *cth1Δcth2Δ* yeast mutant compared to WT cells were quantitatively small (Puig et al., 2005). Since it cannot be ruled out, that CTH2

has a stabilizing effect on target transcripts, it must be considered that the male sterility of *cth2-2* plants is caused by a failure to stabilize CTH2 target transcripts. In this case, direct target transcript of CTH2 in anther development would be found at lower levels in *cth2-2* anthers compared to WT. However, the possibility of CTH2 stabilizing transcripts is unlikely, as it directly contradicts previous results on the molecular function of TZF proteins, as discussed above.

CTH2 function in:

WT	*cth2-1*	*cth2-2*
degradation of target transcripts ↓ target transcript levels reduced	hyperactive degradation of target transcripts ↓ target transcript levels drastically reduced or stabilization of target transcripts ↓ target transcript levels strongly increased	target transcripts not degraded ↓ target transcript levels not reduced
stabilization of target transcripts ↓ target transcript levels increased	hyperactive stabilization of target transcripts ↓ target transcript levels strongly increased or failure to stabilize target transcripts ↓ target transcript levels not increased	target transcripts not stabilized ↓ target transcript levels not increased

Figure 37: Putative molecular consequences of the *cth2-1* and *cth2-2* alleles.

Shown is an overview of alternative putative molecular consequences of the *cth2-1* and *cth2-2* allele on CTH2 target transcripts in plants responding to Fe-deficient conditions. Increases or decreases of target transcript levels are compared to the levels under Fe-sufficient conditions.

Concluding from data obtained with *cth2-1* and *cth2-2*, there is a possibility that a partial protein synthesized in *cth2-1* is binding to transcripts and has a higher degradation activity than full-length CTH2. It is unclear how this functions on a molecular level. It is also unclear

why an overly active CTH2 is disturbing Fe homeostasis but not anther development. Possibly there is a *trans*-acting factor which regulates CTH2 activity, for example according to the tissue type or the Fe status of the plant. A phenotype for *cth2-1* plants is only observed in Fe-deficient, but not in Fe-sufficient conditions. Possibly a signal generated as a part of the Fe-deficiency response in shoots is needed to activate the CTH2-dependent degradation of transcripts and also to activate the putative hyperactive ΔN-CTH2 protein found in *cth2-1* plants. Maybe *CTH2* acts as a fine-tuning system for Fe homeostasis. In the putative gain-of-function mutants *cth2-1* and *35S:CTH2_Cterm* this fine-tuning system would be overly active, which leads to increased degradation of essential transcripts. This in turn could lead to reduced growth and chlorophyll levels, as observed in young leaves of *cth2-1* and *35S:CTH2_Cterm* plants. This is in agreement with the adequate Fe contents found in these leaves (Fig. 24d), which indicates that lack of Fe in the leaves is not directly responsible for the observed phenotypes.

If a transcript-stabilizing function of CTH2 is assumed, target transcripts of CTH2 could be hyper-stabilized in *cth2-1* plants, when compared to WT plants. Alternatively, a dominant-negative effect in *cth2-1* could lead to decreased stability of CTH2 target transcripts. A transcript stabilizing activity of wild-type CTH2 implies that CTH2 target transcripts encode essential Fe-dependent proteins opposed to non-essential Fe-dependent protein, as is the case in yeast. In WT plants under Fe-deficient conditions, CTH2 activity would cause preferential expression of these essential genes prior to genes encoding non-essential Fe-dependent proteins. It is unclear how hyper-stabilization of transcripts encoding essential Fe-dependent proteins could lead to impaired growth or chlorosis, as observed in *cth2-1* and *35S:CTH2_Cterm* plants. Decreased stability of transcripts (implying a dominant-negative effect) encoding essential Fe-dependent proteins could provide an explanation for the observed phenotypes. But as discussed for the *cth2-2* mutant, a transcript stabilizing role contradicts data obtained from heterologous expression of *CTH2* in yeast and literature on yeast and human homologues of CTH2.

Another interesting observation was that relative transcript levels of the partial *CTH2* transcript in *cth2-1* were comparable to WT *CTH2* transcript levels in shoots, but near the detection limit of qRT-PCR in roots (Fig. 18). Expression of this partial transcript is not controlled by a defined promoter region. However, there is a CaMV 35S promoter in the T-DNA at *ca.* 1 kb distance from the LB region. Probably transcriptional activity from this promoter is enough to achieve low transcript levels of the partial *CTH2* transcripts. If this is

the only factor that contributes to expression, then expression levels are expected to be equal in roots and shoots. The differences in expression levels indicate that there might be additional factors other than transcription that contribute to expression level, for example transcript stability. In mammals, the CTH2 homologue TTP regulates the stability of its own transcript in a negative feedback loop (Tchen, 2004). If a similar situation is found in plants, different mechanisms controlling *CTH2* transcript levels might be acting in shoots and roots.

5.4 A partial *CTH2* transcript may influence the stability of target transcripts

From the literature on yeast and mammalian TZF proteins it is likely that the putative N-terminally truncated protein in *cth2-1* (and in *35S:CTH2_Cterm* lines) retains the ability to bind RNA since the region of the transcript encoding the TZF domain is intact (Fig. 14a). Accordingly, in *cth2-2* any C-terminally truncated protein that might be synthesized from the *CTH2* locus is very unlikely to have RNA-binding activity since the T-DNA insertion is in the region encoding the first zinc finger of the TZF domain (Fig. 14b).

Translation could be initiated at Met_{140}, for which the codon is located 13 bp downstream of the T-DNA in *cth2-1*, so that a ΔN-CTH2 protein could be made. This partial protein would also contain the conserved region 2, but not the conserved region 1, described in Fig. 1c. While the TZF regions of *Sc*CTH2 and *Hs*TTP are quite well studied, less is known about the function of other regions of the proteins. The amino acids found N-terminally of the TZF domain of CTH2 contained no known sequence motif. Except for two regions conserved among plant TZF proteins, the amino acid sequence of the N-terminus is not well conserved between organisms. Even the two conserved regions in the N-terminus of plant TZF proteins seemed to be plant specific, as there were no corresponding sequences found in human or yeast TZF proteins.

In yeast, it was shown that the lack of a conserved region within the first 57 amino acids of the *Sc*CTH2 protein sequence is sufficient to suppress degradation of the *SDH4* transcript, which is a target of *Sc*CTH2 (Prouteau et al., 2008). This ΔN-CTH2 protein from yeast was still able to bind to RNA. It was also speculated that the N-terminus is necessary for the interaction of *Sc*CTH2 with components of the cellular RNA degradation machinery. Proteins from the 5'- to 3'- degradation pathway (DHH1, XRN1, DCP1, DCP2) were shown to be

involved in *Sc*CTH2-mediated degradation of transcripts (Pedro-Segura et al., 2008). In Vergara et al., 2011 it was shown that a ΔN_{89}-CTH2 protein had the same dynamic localization as full-length CTH2 but failed to facilitate RNA degradation. A very similar situation was observed for the human TTP. The N-terminal domain of TTP interacted with mRNA decay enzymes, and deletion of the N-terminal domain resulted in decreased transcript degradation activity (Lykke-Andersen and Wagner, 2005).

It is possible that the putative ΔN-CTH2 protein in *cth2-1* has decreased transcript degradation activity compared to WT CTH2 protein. But to explain the dominance of the *cth2-1* allele and the *35S:CTH2_Cterm* transgene in WT plants one has to assume that a ΔN-CTH2 protein is outcompeting the WT CTH2 protein for binding to target transcripts. This could lead to strong stabilization of transcripts. Since this is essentially the same direction of the expected effect of the *cth2-2* allele, the effect of a putative ΔN-CTH2 protein must be stronger because *cth2-1* and *35S:CTH2_Cterm* plants are hypersensitive to Fe deficiency, while *cth2-2* plants are not. Thus *cth2-1* would be a stronger allele than *cth2-2*.

For the mammalian ZFP36L2 (a *Hs*TTP homologue) it was shown that ovules from homozygous ΔN_{29}-ZFP36L2 mutant led to the arrest of embryo development at the two-cell stage (Ramos et al., 2004). The ΔN_{29}-ZFP36L2 protein had a destabilizing effect on transcripts, comparable to full-length ZFP36L2. However, the ΔN_{29}-ZFP36L2 protein proved to be more resistant to stimulus induced down-regulation, so it accumulated at much higher levels than the WT protein (Ramos, 2012). This scenario could explain the dominant phenotype of the *cth2-1* mutant by accumulation of a partial, ΔN-CTH2 protein which still has a transcript degradation activity.

From the literature it seems that deletion of the N-terminal domain of TZF proteins sometimes leads to impaired transcript degradation activity and sometimes does not influence this activity, and thus, this is not consistent between TZF proteins. To further analyze this it would be important to measure protein levels of WT CTH2 and the putative partial protein found in *cth2-1*. A time course experiment could be done, analyzing (partial) CTH2 protein levels during the Fe-deficiency response. This could give information about the kinetics of accumulation of (partial) CTH2 proteins in response to Fe deficiency. Additionally, heterologous expression of partial *AtCTH2* cDNAs in yeast and subsequent analysis of transcript levels of *Sc*CTH2 target transcripts (as shown in Fig. 3 for the full-length *AtCTH2* coding sequence) could clarify the effect of a ΔN-CTH2 protein on transcript stability. To ultimately decide what the effect of a partial ΔN-CTH2 protein on transcript stability is

transcript levels of CTH2 target transcripts have to be analyzed *in planta*. However, in this study, no target transcripts could be identified.

5.5 The role of *CTH2* in Fe homeostasis

Relative *CTH2* transcript levels increased *ca.* four-fold in shoots under Fe-deficient conditions compared to Fe-sufficient conditions (Fig. 8). In roots, no Fe-status dependent changes in *CTH2* transcript levels were observed. An increase of *CTH2* transcript levels under Fe-deficient conditions is in agreement with a potential role for *CTH2* in the physiological acclimation to Fe deficiency. The Fe deficiency-dependent increase of *CTH2* transcripts levels was only found in shoots of 45-day-old, short-day grown plants, but not in roots or in 28-day-old plants (compare Figs. 7 and 8). The Fe-dependent regulation of *CTH2* transcript levels in shoots was thus age-dependent. It seems that *CTH2* might have a role in Fe homeostasis only in plants that have reached a certain age (here: 45 days). Consistently, a hypersensitivity to Fe-deficiency of *cth2-1* plants (chapter 4.10) was not found in 28-days-old plants (data not shown).

Both, mature, *cth2-1* and 45-day-old *35S:CTH2_Cterm* plants were more sensitive to Fe deficiency, indicated by decreased chlorophyll concentrations and lower biomass of young leaves compared to WT plants (Figs. 17, 23 and 24). Chlorophyll concentrations of the young leaves of mutant plants grown under Fe-deficient conditions reached nearly zero, while older leaves were able to maintain WT-like chlorophyll concentrations. This indicated that correct regulation of *CTH2* activity is most critical for the development of newly formed leaves.

Through analysis of hemizygous CTH2/*cth2-1* plants it was shown that the T-DNA insertion in *cth2-1* causes a dominant sensitivity to Fe deficiency (Figs.16 and 17). Since the presence of one *cth2-1* (and one wild-type) allele is sufficient to cause a phenotype, the activity of the *cth2-1* gene product dominates over the activity of the WT gene product. This activity could result in a gain-of-function or in a dominant-negative effect. Hypersensitivity to Fe-deficiency was not found in a knockout of *CTH2* (*cth2-2*) or in plants with reduced *CTH2* transcript levels (*amiRNA B*). Possibly a double knockout of both *CTH* genes is necessary to observe a growth defect under Fe-deficient conditions as discussed above. The phenotype of *35S:CTH2_Cterm* lines, which was very similar to that of *cth2-1* plants, confirmed that the phenotype observed in *cth2-1* is due to a partial *CTH2* transcript (compare Figs. 17 and 23).

Moreover, both full-length CTH2 and N-terminus did not cause a hypersensitivity to Fe deficiency, suggesting that this is specific for expression or overexpression of a partial *CTH2* sequence encoding the C-terminal TZF domain.

Fe content of individual leaves of *cth2-1* and *35S:CTH2_Cterm* plants (Fig. 24d) and Fe concentrations in bulk shoot and root tissues of *cth2-1* plants (Fig. 19) were comparable to WT. Also, Fe-dependent regulation of transcript levels of *FRO3*, *FER1*, *YSL1* and *YSL2* in shoots (Figs. 20 and 25) was present in *cth2-1* and *35S:CTH2_Cterm* plants, although the extent of regulation of *FER1* and *YSL1* differed from those observed in WT plants. From these data it was concluded that *cth2-1* and *35S:CTH2_Cterm* plants are not affected in the uptake and distribution of Fe or in the activation of the Fe-deficiency response. This is in contrast to other published mutants impaired in Fe homeostasis. There are mutants that are defective in the uptake of Fe, like *irt1* (Vert, 2002) or *frd1* (Robinson et al., 1999). In addition, mutants defective in signaling of Fe-status (Bauer et al., 2007; García et al., 2011) or Fe mobility (Haydon et al., 2012; Curie et al., 2009; Green, 2004) are known.

The reduction of Fe concentrations in all leaves of WT plants grown under Fe-deficient conditions compared to Fe-sufficient conditions suggested that WT plants remobilize part of their leaf Fe pool from the older to the younger, developing leaves, when they are challenged with Fe-deficient growth conditions (Fig. 24a). Older leaves of WT plants developed in the preceding cultivation period on soil, where available Fe was supposedly not limiting. When the plants were transferred to medium without Fe, the Fe concentrations in all leaves, regardless of their age, were reduced. This suggested that a fraction of the Fe from older leaves was transferred to younger leaves. This transfer likely occurs *via* the phloem, since young leaves are a sink tissue until they become net exporters of photosynthates at 40% of the final leaf size (Taiz and Zeiger, 2010). This process seemed to be unaffected in *cth2-1* and *35S:CTH2_Cterm* plants. Young leaves of mutant plants grown under Fe-deficient conditions contained the same total amount of Fe as leaves from WT plants (Fig. 24d). Also the analysis of Fe concentrations in bulk tissues from *cth2-1* plants showed no significant differences to WT plants (Fig. 19). Still, young leaves of mutant plants were chlorotic and of smaller size than WT leaves of comparable relative age. This suggests that the Fe contained in the young leaves might be unable to reach its cellular target sites, like the chloroplasts. For example, Fe export from phloem or import into mesophyll cells could be impaired. A similar situation is found in *frd3* mutant plants (Durrett et al., 2007) in which xylem and leaf apoplastic mobility of Fe is impaired. It is also possible that Fe import into chloroplasts or mitochondria is

impaired. To test this, Perl's stain could visualize accumulations of Fe at the tissue level (Roschzttardtz et al., 2010). A modified Perl's stain was recently proposed for the visualization of Fe accumulations at the cellular level (Roschzttardtz et al., 2011).

In agreement with metal contents, analyses of relative transcript levels support that *cth2-1* and *35S:CTH2_Cterm* plants are not impaired in the uptake and distribution of Fe at the level of the whole plant. This is indicated by unaltered expression of the Fe-deficiency marker genes *IRT1, FRO2, FRO3* and *YSL2* (Figs. 20 and 25). Relative transcript levels of *FER1*, an Fe storage protein, were elevated in *35S:CTH2_Cterm* plants in younger (5-fold) and older (3-fold) leaves grown in Fe deficiency compared to the respective WT controls (Fig. 25). This could reflect the increased Fe concentrations found in these leaves, but could alternatively provide the explanation for a lack of available Fe for Fe-dependent protein activity. In fact, *FER1* itself could be a target for CTH2-dependent regulation, if the partial ΔN-CTH2 protein had a stabilizing effect on the *FER1* transcript. This interpretation implies a gain-of-function of the partial ΔN-CTH2 protein, whereas the full-length CTH2 protein, when active, may act to destabilize the *FER1* transcript. As a consequence, overly abundant FER1 protein could scavenge all available Fe, leading to physiological Fe deficiency despite adequate tissue Fe content The stability of the *FER1* transcript is negatively regulated *via* a downstream *cis*-acting (DST) motif in its 3'-UTR. In two *trans*-acting *Arabidopsis* mutants (*dst1*, *dst2*) this regulation is abolished, *FER1* transcript is stabilized and FER1 protein levels are increased (Arnaud et al., 2006; Ravet et al., 2011). However, the DST motif found in the *FER1* transcript ($CGAN_{15}TTAGATTN_{23}TGTAG$) is different from the consensus binding motif for TZF proteins (WATTTAW). *FER1* transcript levels were reduced in both, older and younger leaves from *35S:CTH2_Cterm* lines grown under Fe-deficient conditions, when compared to WT. However, only the young leaves of *35S:CTH2_Cterm* lines, but not the old leaves were more chlorotic and of smaller size compared to WT. This possibly contradicts the hypothesis that misregulation of *FER1* transcript stability is responsible for the observed phenotype. Since *FER1* is regulated posttranscriptionally, also protein levels of FER1 could be analyzed by immuno-blot to investigate whether increased FER1 protein levels in young leaves contribute to slow growth and chlorosis observed in *cth2-1* and *35S:CTH2_Cterm* plants. When *FER1* transcript levels were analyzed in whole rosettes from WT and *cth2-1* plants by qRT-PCR and microarray analysis, it was found that transcript levels were reduced 1.45 fold in *cth2-1* compared to WT in Fe deficient conditions. It is unclear why a different direction of regulation was observed in bulk tissues compared to pools of the five youngest or oldest leaves. It is likely that this reflects differences in the experimental setup or differences in

sampling. Also, in all experiments with bulk shoot tissues, the differences in relative expression levels between WT and *cth2-1* (1.45 fold) were smaller compared to the differences between Fe-deficiency and sufficiency (14 fold) (

Table 9), which makes comparison between WT and *cth2-1* more prone to artifacts.

The expression of *YSL1* was reduced to *ca*. 50% of WT levels in young leaves from *35S:CTH2_Cterm* plants grown under Fe-deficient conditions (Fig. 25a). Since the *YSL1* transcript has two AREs in its 3'-UTR, it is a possible candidate gene for *CTH2*-dependent regulation. In the literature it is suggested that *YSL1* moves Fe from the apoplast to the symplast during xylem unloading (Conte and Walker, 2011). Reduced expression of *YSL1* in senescent leaves might contribute to the remobilization of Fe to the younger leaves (Waters et al., 2006). This is in accordance with the much higher expression levels of *YSL1* in older leaves compared to younger leaves. If *YSL1* function is impaired, Fe allocation to mesophyll cells of young leaves would be disturbed. However, since Fe content in leaves of *35S:CTH2_Cterm* plant, regardless of their relative age, is comparable to WT, leaf-to-leaf Fe transport seems unaffected (Fig. 24d). It would be useful to analyze the 3'-UTR of *YSL1* in the Y3H-system to show a possible interaction of *At*CTH2 with putative target transcripts from *Arabidopsis*.

The observed chlorosis of young leaves might be a symptom of physiological Fe deficiency. However, Fe concentrations in the young leaves of *cth2-1* and *35S:CTH2_Cterm* plants grown under Fe-deficient conditions were higher when compared to WT plants (Fig. 24b), and not lower as one would expect from the chlorosis. The regulation of three Fe-deficiency marker genes (*YSL1*, *YSL2*, *FRO3*) in young leaves of *35S:CTH2_Cterm* plants was comparable to WT plants, which shows that these leaves were physiologically Fe-deficient (Figure 25a to c). There is the possibility that although these leaves were physiologically Fe-deficient, the true reason for the enhanced chlorosis compared to WT leaves was, at least in part, that Fe deficiency triggers or enhances the activity of the partial CTH2 protein present in *cth2-1* and *35S:CTH2_Cterm* mutants. For this possibility CTH2 itself does not necessarily act in Fe homoestasis. A hyperactive partial CTH2 protein could affect gene expression, presumably by degrading transcripts of essential genes, and cause the observed reduction in biomass and chlorophyll. Thus, the phenotype of *cth2-1* and *35S:CTH2_Cterm* plants is not directly caused

by Fe deficiency. In fact, the Fe content of young leaves of *cth2-1* and *35S:CTH2_Cterm* plants grown under Fe-deficient conditions was comparable to WT (Fig. 24d). However, since a phenotype for both mutants was only observed under Fe-deficient conditions, it seems likely that decreased Fe availability is, at least partially, the reason for the observed phenotypes.

Cellular metabolism changes during Fe deficiency, so it is likely that some of these changes are critical for growth under Fe-deficient conditions. Misregulation of such changes could cause the phenotype observed in *cth2-1* and *35S:CTH2_Cterm* plants. By analogy with yeast, *AtCTH2*-dependent remodeling of metabolism under Fe-deficient conditions might allow plants to change gene expression, so that Fe is dedicated to essential proteins. The hypothesis of inefficient Fe use under Fe-deficient conditions of *cth2-1* and *35S:CTH2_Cterm* plants is in general agreement with the known function of *ScCTH2* (Puig et al., 2008; Puig et al., 2005). In *cth2-1* and *35S:CTH2_Cterm* plants, Fe might be wastefully allocated to non-essential proteins, thus causing a disruption of the functions of essential Fe-dependent proteins. This is probably due to the presence of a partial ΔN-CTH2 protein. When plants respond to Fe deficiency, they increase *CTH2* transcript levels, and supposedly also CTH2 protein levels, to adapt to growth under Fe-deficient conditions. In the *cth2-1* mutant, the partial ΔN-CTH2 protein is probably hyperactive or accumulates to higher levels compared to WT CTH2 protein, in analogy to the mouse ΔN-Zfp36l2 TZF protein (Ramos, 2012). The effect could be that the stability of CTH2 target transcripts is reduced more strongly in *cth2-1* plants compared to WT. Since CTH2 might target transcripts encoding Fe-containing proteins that are essential for processes like photosynthesis or oxidative phosphorylation (chapter 1.4), this may be detrimental for growth and cause chlorosis.

The challenge is now to identify the changes in gene expression in leaves that cause the observed hypersensitivity to Fe deficiency. A new transcriptomics approach should be pursued to find target transcripts of CTH2. Since the microarray experiment comparing WT and *cth2-1* plants (chapter 4.17) was not successful in finding candidate genes, a new approach could be pursued. The experiment could be repeated using only young leaves from WT and *cth2*-1 or *35S:CTH2_Cterm* plants growing under Fe-deficient and sufficient conditions. Hopefully this will identify targets of *CTH2* dependent regulation of transcript stability more clearly.

5.6 The role of *CTH2* in pollen development

In the *cth2-2* mutant, the T-DNA insertion causes recessive, sporophytic male sterility through the disruption of pollen development, which was complemented using a genomic construct (Fig. 28). No viable pollen was ever observed in anthers from *cth2-2* plants, so the *cth2-2* allele is most likely a complete null allele. Heterozygous CTH2/*cth2-2* plants showed normal fertility, so *CTH2* is a haplosufficient gene. Because of the T-DNA insertion in the region encoding the TZF domain, no protein containing an intact TZF domain originates from the *CTH2* locus in *cth2-2* (Fig. 14b). Therefore, it is likely that the transcript-binding activity of CTH2 is not present in *cth2-2* plants. Thus, *cth2-2* is likely to be a loss-of-function allele. This is in contrast with the *cth2-1* mutant, in which a transcript encoding the TZF domain is still present (Fig. 15b), consistent with different phenotypes observed in *cth2-1*, when compared to *cth2-2* (Fig. 16). Assuming that CTH2 has the same biochemical function in plants as known in yeast or mammals, male sterility is a consequence of the failure to down-regulate one or more transcripts. Additionally, it seems that *CTH1* and *CTH2* are not functionally redundant during pollen development.

Development of anthers seemed not to be interrupted until flower stage 9. In both WT and *cth2-2*, tetrads of microspores could be observed (Fig. 30). This means that meiosis occurred in *cth2-2* plants. During meiosis the microspores are held together by callose. The developmental defect in *cth2-2* anthers most likely occurs during or after release of the microspores from the tetrads.

In *Arabidopsis thaliana*, a number of mutations are known that affect anther development (Sanders et al., 1999). One class of mutations interferes with floral organ identity. In these mutants, typically a transcription factor is affected and the development of the whole stamen whorl is disturbed (Sablowski, 2007). Since *cth2-2* flowers show WT-like whorl development and numbers of organs, *cth2-2* does not belong to this class of mutants. Another type of male sterile mutants is defective in anther dehiscence or in the timing of dehiscence. These mutants often fail to synthesize or sense jasmonic acid (JA) (Ishiguro, 2001; Mandaokar and Browse, 2009; Wasternack, 2007). When anthers from these mutants are opened manually and used for pollination, the pollen is usually viable. This is not the case for *cth2-2*, since no viable pollen was found inside the anthers (Fig. 29). JA-synthesis mutants can be rescued by the application

of exogenous JA. However, *cth2-2* could not be rescued by spraying the inflorescence with 50 µM methyl-JA. This shows that *cth2-2* is not a JA-synthesis mutant, but does not rule out the possibility that there is a defect in JA perception. There are a number of known male sterile mutants in which biosynthetic pathways or transport mechanisms are disrupted (Dietrich et al., 2008; Chen et al., 2011; Jessen et al., 2011; Munoz-Bertomeu et al., 2010; Dobritsa et al., 2009; Tang et al., 2009; Teng et al., 2008). From phenotypic analysis, *cth2-2* is similar to these mutants, although *CTH2* does not encode an enzyme or a transporter, but a regulatory protein.

Analysis of promoter activity using a *pCTH2:GUS* construct showed the region and the time-point of *CTH2* promoter activity (Figs. 31 and 32). The promoter of *CTH2* is active in the central part of the connective tissue; in the part closest to the vasculature. No promoter activity was found in other parts of the anther or in pollen. All nutrients that are transported to the developing pollen pass through the vasculature and the adjacent parts of the connective. It is possible that the connective has a role in unloading nutrients from the filament into the developing anther. In addition, it seems that the timing of *CTH2* promoter activity is highly regulated. The promoter of *CTH2* was found to be active in the connective at flowering stage 9 (Fig. 31b). In this case, the promoter activity is in accordance with the transcript levels. In unopened flower buds (stage 8-10) *CTH2* transcript levels were *ca.*10-fold higher than in opened flowers (stage 12-13) (Fig. 6). This is in agreement with publicly available microarray data from the AtGenExpress project (Schmid et al., 2005b). With the beginning of stage 10, the anther filaments begin to elongate, and the transition from microspores to pollen grains begins. This is another indication making it plausible that meiosis is unaffected in *cth2-2*, since meiosis occurs at stage 9, before the filament elongates and before *CTH2* promoter activity and transcript levels reached their maximum.

Other examples for genes which are critical for fertility and which are expressed in the connective are *MYB24* and *MYB108* (Mandaokar and Browse, 2009). *Arabidopsis myb108* mutants exhibited reduced male fertility that was associated with delayed anther dehiscence and reduced pollen viability. The promoter activity of *MYB108* was localized to the connective and the vascular region of the anther and strongest during flower stage 15. The tapetum is well characterized as a nutritive tissue for the developing pollen and undergoes characteristic morphological changes during anther development (Ariizumi and Toriyama, 2011; Pacini et al., 1985; Piffanelli et al., 1998). In sections of *cth2-2* anthers no apparent

difference was found in tapetum morphology compared to WT (Fig. 30), which indicates normal function of the tapetum.

The defect in male gametophyte development of *cth2-2* plants was located in the anther locules, distant from the location of *CTH2* promoter activity in the connective (compare Figs. 30 and 32). It thus appears that the localization of *CTH2* promoter activity is different from the localization, where the lack CTH2 activity caused a disruption of development. The processes that are regulated in a CTH2-dependent way in the connective tissue are thus critical for pollen development, but it is unclear which processes these are. Alternatively, this could mean that either the *CTH2* transcript or the CTH2 protein are translocated within the anther.

5.6.1 Search for candidate genes and mechanisms that explain the male sterile phenotype of *cth2-2* plants

Genes that encode ribosomal proteins represent *ca.* 15% (8.8-fold overrepresentation compared to all genes represented on the ATH1 array) of all genes expressed at higher levels in *cth2-2* anthers compared to WT anthers. Since protein synthesis is the main function of ribosomes it can be concluded from the microarray data that global protein synthesis might be increased in *cth2-2* anthers from stage 9 flowers compared to anthers from WT plants. Alternatively, protein synthesis might be negatively affected in *cth2-2* anthers and the observed increase in transcript levels is due to a compensation effect.

Transcript levels of genes that encode ribosomal proteins were higher in *cth2-2* anthers then in WT anthers. If the transcripts of these genes represent direct targets for CTH2-dependent regulation, this supports the hypothesis that CTH2 is destabilizing transcripts and that *cth2-2* is a loss-of-function mutant. However, it not likely that all of them are direct targets for CTH2-dependent regulation, because only 40% have at least one ARE in their 3'-UTR. However, only 15% out of all *Arabidopsis* transcripts have at least one ARE in their 3'-UTR, but at this stage it is unclear if this overrepresentation of AREs is biologically relevant. It is also possible that the increased transcript levels of genes encoding ribosomal proteins observed in *cth2-2* anthers are a secondary consequence of a developmental block. Transcript levels of genes encoding ribosomal proteins decrease in the course of anther development in WT. Since development in *cth2-2* is disrupted after stage 9, increased transcript levels of

genes encoding ribosomal proteins may be a consequence of this. To find out if CTH2 directly regulates the stability of transcripts encoding ribosomal proteins, the 3'-UTRs of these transcripts could be analyzed in the Y3H system and in a *cth1Δcth2Δ* mutant as described in chapter 4.2.

Another bin that was enriched significantly among the genes with higher transcript levels in *cth2-2* anthers compared to WT was "RNA.RNA binding". This bin was only slightly, but significantly, enriched (2.8-fold overrepresentation compared to all genes represented on the ATH1 array, $p < 0.01$). A misregulation of RNA-binding proteins may be related to the hypothesized role of CTH2 in post-transcriptional regulation of gene expression, and could indicate an alternative cause for the developmental defect observed in *cth2-2* anthers. However, further experiments are needed to determine the precise roles of *CTH2* in post-transcriptional regulation of gene expression anther development. For example, it could be checked whether available mutants of misregulated genes encoding RNA-binding proteins show aberrations in anther or pollen development. Anthers of *cth2-2* seem to have a block in development. Possibly, the genes encoding RNA-binding proteins found in this analysis represent other components of a CTH2-dependent regulatory pathway in anther development, which are up-regulated in an attempt to compensate the lack of CTH2. The highest expressed genes from WT anthers from stage 12 flowers found in this analysis could be candidate genes to dissect this putative pathway.

Eight genes out of 24, annotated as belonging the sphingolipid (SL) biosynthesis pathway, showed lower transcript levels in *cth2-2* anthers compared to WT anthers (Fig. 35). This is only 0.7% of the total number of transcripts present at lower levels, but enrichment of the sub-bin was found to be significant (6.5-fold overrepresentation compared to all genes represented on the ATH1 array, $p < 0.01$). Interestingly, the eight genes identified by the microarray analysis correspond to the eight most highly expressed genes among all genes from the SL biosynthesis pathway in stamens from stage-12 flowers in WT plants (Fig. 35). However, it is unlikely that they are direct targets for *cth2-2* dependent regulation, since they are expressed at lower, and not higher levels in the *cth2-2* mutant compared to WT. Since *cth2-2* is a loss-of-function allele, direct target transcripts are expected to be more abundant in *cth2-2* plants than in WT plants.

The SL biosynthesis pathway seems to be essential for pollen development. A mutant of *Long-Chain Base 1* (*LCB1*), encoding a subunit of the serine-palmitoyltransferase enzyme complex, which catalyzes the first step in SL biosynthesis, initiates apoptotic cell death in

binucleate microspores and is thus gametophytic male sterile (Teng et al., 2008). Also, mutants in either of the two *LCB2* genes fail to transmit the mutant allele *via* haploid pollen (Dietrich et al., 2008). A *tsc10A* (*3-keto-dihydropshingosin recutase*) mutant was reported to show an altered leaf ionome and contained *ca.* 20% less Fe in the shoots then WT plants. A double knock-out of *TSC10A* and *TSC10B* could not be recovered from crosses of the single knock-outs (Chao et al., 2011). In yeast, the SL biosynthesis pathway was impaired when cells were grown under Fe-deficient conditions (Shakoury-Elizeh et al., 2010). More specifically, the pathway was blocked because SCS7, a heme-containing ceramide hydroxylase and SUR2, a di-iron-sphingosine hydroxylase, lost their Fe cofactors under Fe-deficient conditions. These findings suggest that Fe homeostasis and SL biosynthesis may be linked in *Arabidopsis* and that sphingolipid biosynthesis is important for pollen development.

Out of the eight genes with lower transcript levels in *cth2-2* compared to WT from the SL biosynthesis pathway, five were found to encode heme- or Fe-containing proteins according to the Interpro database (Hunter et al., 2011). These five genes are candidates for further investigation of the male sterile phenotype of *cth2-2*. It would be insightful to measure the concentrations of all metabolites from the SL pathways in anthers from *cth2-2* plants to check if the reduction in transcript levels correlates with the concentrations of metabolites. Furthermore, since *lcb1* and *lcb2* mutants also show a male-sterile phenotype they could be crossed with *cth2-2* to see if *CTH2* and *LCB1/2* interact genetically. It could also be tried to rescue *cth2-2* plants by supplying SLs directly to developing anthers by spraying.

5.6.2 **The defect in *cth2-2* anthers might be related to a disturbed Fe homeostasis.**

In the supply of nutrients to the developing pollen grain, the connective likely has an important role in translocating nutrients to the anther lobes. Since a role for *CTH2* in Fe homeostasis is probable, the defect in pollen development in the *cth2-2* mutant might be caused by a defect in Fe homoeostasis. The simplest hypothesis would be a lack of Fe during pollen development. A reduced Fe content relative to K and Mg was indeed found in *cth2-2* anthers, when compared to WT (Fig. 33). It is reasonable to conclude that insufficient Fe supply might be the cause of the defect in pollen development, although the inability to rescue the *cth2-2* mutant by applying Fe directly to the developing flowers argues against this.

A disturbance in metal homeostasis can lead to decreased fertility of plants. An analysis of *frd3* mutants showed a direct connection of pollen development and Fe homeostasis. *FRD3* encodes a citrate transporter (Durrett et al., 2007) that is important for root-to-shoot translocation of Fe (Rogers, 2002),Green 2004 #204}. In Roschzttardtz et al., 2011b it was shown that *FRD3* is also critical for Fe mobility in the anther locules during pollen development. Lack of FRD3 activity led to apoplastic deposits of Fe in the anther locule. Interestingly, *FRD3* activity is important in the developing pollen grains (the gametophyte), as opposed to *CTH2*, which acts through the sporophyte.

Another mutant exhibiting disturbed pollen development is the *ysl1ysl3* double mutant (Waters et al., 2006). It was shown that the *ysl1ysl3* double mutant produces less viable pollen, but this phenotype is poorly characterized. Also, the authors provide indirect evidence for long-distance transport of Fe dependent on YSL1 and YSL3 (Le Jean et al., 2005; Waters et al., 2006). Another example, in which a disturbance of ion homeostasis disrupts pollen development is *MIA1* (Jakobsen et al., 2005). It was shown that *mia1* plants have a severe reduction in fertility. *MIA1* encodes a subfamily V P-type ATPase cation pump. Although the authors show an imbalance of Cu, Fe, Mn, Mo and Zn only in leaves, it is concluded that an imbalance in the anthers is responsible for the reduced fertility. These examples show the necessity for proper nutrient supply to developing pollen grains.

FRD3, *YSL1*, *YSL2* and *MIA1* encode membrane transport-proteins, and mutants affected in their functions also show pleiotropic phenotypes in vegetative parts of the plant. *CTH2* is the first reported gene that might have regulatory role in Fe homeostasis and is essential for pollen development. Unfortunately, direct evidence for a role of *CTH2* in Fe homeostasis of anthers could not be provided, as the *cth2-2* mutant phenotype could not be rescued through supply of exogenous Fe or Fe chelators (Table 13). By contrast, the *frd3* mutant was rescued by watering with a Fe-chelator solution (Roschzttardtz et al., 2011b). But even in this case, the degree of rescue of the fertility defect was only marginal. It would be interesting to see how *frd3* reacts to spraying with Fe-containing solutions. Maybe external application does not allow the Fe to get into the appropriate tissues. Alternatively, Fe has to be supplied together with a ligand. Two known chelators of Fe in plants (citrate and NA) have been used unsuccessfully in attempts to rescue the male sterility defect of *cth2-2* in this thesis. It is also possible that a secondary effect leads to lower relative micronutrient contents. There are differences in morphology between WT and *cth2-2* anthers. The observed decrease in Fe

concentrations could thus be a consequence of the defect in pollen development and not the cause.

5.7 The activity of the *CTH2* promoter in vegetative tissues does not correlate with steady-state transcript levels

There were some discrepancies between *CTH2* promoter activity, as detected by GUS activity in seedlings of *pCTH2:GUS* plants, and relative transcript levels of *CTH2* analyzed by qRT-PCR (compare Figs. 7a and 10a to d). It was striking how strongly the *CTH2* promoter was able to activate *uidA* expression in seedlings. Seedlings of *pCTH2:GUS* plants were stained for 1 to 4 h, whereas for other constructs, staining is usually done overnight. This was in contrast to the detected *CTH2* transcript levels, which were rather low.

In shoots, GUS staining, and thus promoter activity, changed drastically dependent on the developmental stage. This was not reflected at the transcript level of *CTH2*, which was approximately constant and low at all analyzed stages of development (Figs. 6, 7 and 8). Transcript levels measured by qRT-PCR were increased when plants were grown under Fe-deficient conditions, when compared with Fe-sufficient conditions (Fig. 8). Instead, when transgenic *pCTH2:GUS* plants were subjected to Fe deprivation, no change in GUS staining was observed (Fig. 11).

The described discrepancies suggest that *CTH2* transcript levels might be regulated post-transcriptionally, possibly at the level of transcript stability. Since *CTH2* encodes a regulator of transcript stability, it might even regulate the stability of its own transcript *via* a negative feedback loop, as described for the human TTP transcript (Tchen, 2004).

Another apparent discrepancy between promoter activity and transcript levels of *CTH2* was found when plants were wounded. Activity of the *CTH2* promoter was strongest 5 min after wounding (Fig. 12). However, at this time point no changes in transcript levels could be observed (Fig. 13). Only 24 hours after wounding, a moderate (two-fold) increase of *CTH2* transcript levels was observed. Although in this work no role for *CTH2* in the response to wounding is shown, the possibility is intriguing. To reproduce successfully, all pathogens have to acquire Fe from its host body fluids. So mechanisms have evolved in humans that allow the withholding of Fe in the case of an infection (Weinberg, 1999). From plant studies

with fungal pathogens it was shown that Fe and Fe-siderophores can be a key factor in virulence (Expert et al., 1996; Smits and Duffy, 2011). A specific Fe-withholding mechanism was proposed but has not yet been demonstrated (Djennane et al., 2011). An effect of *CTH2* on Fe homeostasis is shown in this thesis. At this point, a possible function of *CTH2* as a link between Fe homeostasis and the response to wounding in plants is highly speculative.

5.8 Silencing of *CTH1* and *CTH2* using amiRNA

In an effort to silence *CTH1* and *CTH2* the amiRNA technology (Schwab et al., 2006) was employed (chapter 4.24). One construct (*amiRNA* A) did not lead to target gene silencing for unknown reasons. However, in several independent lines, a reduction in either *CTH2* (*amiRNA B)* or *CTH1* (*amiRNA C*) transcript level was observed (Fig. 36a, b). Since transcript levels were lower in the respective amiRNA lines than in WT, it is likely that also CTH1 and CTH2 protein levels were lower in these lines.

Both amiRNA lines were grown under Fe-sufficient and Fe-deficient conditions, but no evident phenotype was observed in either condition (Fig. 36c, d). This is in accordance with the results obtained with the *cth2-2* mutant. In this mutant, no functional CTH2 protein can be made, and these plants also showed no visible phenotype at the vegetative stage when grown under Fe-deficient conditions. In the *cth2-2* mutant, loss of *CTH2* function led to male sterility. Since no defect in anther development was observed in the *amiRNA B* lines, this might indicate that even minute amounts of *CTH2* transcript are sufficient to maintain normal fertility.

There is the possibility of compensatory effects in the *amiRNA* lines. In the *amiRNA C* lines 1.7 and 2.5 *CTH1* transcript levels were reduced, but *CTH2* transcript levels seemed to be increased to higher levels when compared to WT plants, under Fe deficiency. This indicates that both CTH proteins might exhibit some degree of functional redundancy. It is very likely that both CTH proteins have overlapping functions, comparable to the two homologues in yeast (Puig et al., 2008). However, compensation effects have to be interpreted with caution, since it is very likely that *CTH* genes are also regulated posttranscriptionally, so steady-state transcript levels are likely to be of limited value as a proxy of *in vivo* protein levels.

5.9 Outlook

In this thesis a role for *CTH2* in Fe homeostasis and anther development was identified. However, a number of open questions remain. Although the effects of a *CTH2* gain-of-function and loss-of-function could be described, it remains unclear which precise regulatory and biochemical functions CTH2 has, and which genes are direct targets of regulation by CTH2. Further research needs to concentrate on finding target RNAs and protein-binding partners of CTH2 and on uncovering the biochemical mechanisms that lead to the observed phenotypes.

It would be most important to identify direct target transcripts for CTH2-dependent regulation. This was attempted in this thesis, but was it not successful. As discussed in chapter 5.5, an improved transcriptomics approach might be more promising. It would also help to understand *CTH2* function, if protein interaction partners were identified. For this, a yeast two-hybrid approach seems feasible. Finding protein interaction partners of CTH2 might also contribute insights on plant RNA-binding proteins and their role in responses to the environment and in development.

The increased Fe-deficiency induced chlorosis in young leaves of *cth2-1* and *35S:CTH2_Cterm* plants deserves further attention. For example, the activities of Fe-dependent enzymes, like catalase or Fe superoxide-dismutase, could be analyzed as markers of physiological Fe status. Alternatively or additionally, protein levels of Fe-containing components of the photosynthetic apparatus could be determined using specific antibodies.

The results in this thesis implicate a regulatory role for the N-terminus of CTH2 in CTH2-activity. Therefore the N-terminus of CTH2 should be analyzed in detail. Since *AtCTH2* can complement the *cth1Δcth2Δ* yeast mutant, different partial *AtCTH2* cDNAs could be functionally tested in the yeast mutant and analyzed for transcript degradation activity and sub-cellular localization. Maybe functions for the conserved regions CR1 and CR2 (Fig. 1c) can be found using a mutagenesis approach. Also the localization of other components of PBs and SGs could be analyzed in *cth2-1* and *cth2-2* mutants to clarify the impact of these mutations on global transcript turnover.

Other unanswered questions are related to the defect in anther development. It was found here based on transcriptomics that SL metabolism might be disturbed in anthers of *cth2-2*. Since there are *Arabidopsis* mutants available in which SL metabolism is disturbed and these mutants show also a defect in pollen development, it is an obvious experiment to cross these mutants to *cth2-2* to see if they complement each other. It could be attempted to rescue the *cth2-2* mutant be supplying intermediates of the SL biosynthesis pathway directly to the inflorescence.

6 Literature

Addepalli, B., and Hunt, A.G. (2007). A novel endonuclease activity associated with the Arabidopsis ortholog of the 30-kDa subunit of cleavage and polyadenylation specificity factor. Nucl. Acids Res. **35** (13): 4453–4463.

Addepalli, B., and Hunt, A.G. (2008). Ribonuclease activity is a common property of Arabidopsis CCCH-containing zinc-finger proteins. FEBS Lett. **582** (17): 2577–2582.

Alexander, M.P. (1969). Differential staining of aborted and nonaborted pollen. Stain Technol. **44** (3): 117–122.

Allmang, C., Mitchell, P., Petfalski, E., and Tollervey, D. (2000). Degradation of ribosomal RNA precursors by the exosome. Nucl. Acids Res. **28** (8): 1684–1691.

Alonso, J.M. (2003). Genome-Wide Insertional Mutagenesis of Arabidopsis thaliana. Science **301** (5633): 653–657.

Altschul, S.F., Gish, W., Miller, W., Myers, E.W., and Lipman, D.J. (1990). Basic local alignment search tool. J. Mol. Biol. **215** (3): 403–410.

Anderson, G.J., and Vulpe, C.D. (2009). Mammalian iron transport. Cell. Mol. Life Sci. **66** (20): 3241–3261.

Anderson, P., and Kedersha, N. (2006). RNA granules. J. Cell Biol. **172** (6): 803–808.

Ariizumi, T., and Toriyama, K. (2011). Genetic Regulation of Sporopollenin Synthesis and Pollen Exine Development. Annu Rev Plant Biol **62** (1): 437–460.

Arnaud, N., Murgia, I., Boucherez, J., Briat, J.-F., Cellier, F., and Gaymard, F. (2006). An iron-induced nitric oxide burst precedes ubiquitin-dependent protein degradation for Arabidopsis AtFer1 ferritin gene expression. J. Biol. Chem. **281** (33): 23579–23588.

Atkins, C. (2000). Biochemical aspects of assimilate transfers along the phloem path: N-solutes in lupins. Func. Plant Biol. **27** (6): 531.

Bailey, T.L., Boden, M., Buske, F.A., Frith, M., Grant, C.E., Clementi, L., Ren, J., Li, W.W., and Noble, W.S. (2009). MEME SUITE: tools for motif discovery and searching. Nucl. Acids Res. **37** (Web Server): W202.

Balagopal, V., and Parker, R. (2009). Polysomes, P bodies and stress granules: states and fates of eukaryotic mRNAs: Nucleus and gene expression. Curr. Opin. Cell Biol. **21** (3): 403–408.

Baou, M., Jewell, A., and Murphy, J. (2009). TIS11 family proteins and their roles in posttranscriptional gene regulation. J. Biomed. Biotechnol. **2009**: 634520.

Barakat, A., Szick-Miranda, K., Chang, I.F., Guyot, R., Blanc, G., Cooke, R., Delseny, M., and Bailey-Serres, J. (2001). The organization of cytoplasmic ribosomal protein genes in the Arabidopsis genome. Plant Physiol **127** (2): 398–415.

Barberon, M., Zelazny, E., Robert, S., Conéjéro, G., Curie, C., Friml, J., and Vert, G. (2011). Monoubiquitin-dependent endocytosis of the IRON-REGULATED TRANSPORTER 1 (IRT1) transporter controls iron uptake in plants. Proc Natl Acad Sci U S A **108** (32): E450-E458.

Barreau, C., Paillard, L., and Osborne, H.B. (2005). AU-rich elements and associated factors: are there unifying principles? Nucl. Acids Res. **33** (22): 7138–7150.

Bauer, P., Ling, H.-Q., and Guerinot, M.L. (2007). FIT, the FER-LIKE IRON DEFICIENCY INDUCED TRANSCRIPTION FACTOR in Arabidopsis. Plant Physiol. Biochem. **45** (5): 260–261.

Baulcombe, D. (2004). RNA silencing in plants. Nature **431** (7006): 356–363.

Benoist, B. de (2008). Worldwide prevalence of anaemia 1993-2005 of: WHO Global Database of anaemia (Geneva: World Health Organization).

Berg, J.M., Stryer, L., and Tymoczko, J.L. (2007). Biochemie (Heidelberg [u.a.]: Elsevier, Spektrum, Akad. Verl.).

Bernal, M., Casero, D., Singh, V., Wilson, G.T., Grande, A., Yang, H., Dodani, S.C., Pellegrini, M., Huijser, P., Connolly, E.L., Merchant, S.S., and Krämer, U. (2012). Transcriptome Sequencing Identifies SPL7-Regulated Copper Acquisition Genes FRO4/FRO5 and the Copper Dependence of Iron Homeostasis in Arabidopsis. Plant Cell.

Bertani, G. (1951). Studies on lysogenesis. I. The mode of phage liberation by lysogenic Escherichia coli. J. Bacteriol. **62** (3): 293–300.

Bertini, I., Cavallaro, G., and Rosato, A. (2006). Cytochrome c: occurrence and functions. Chem Rev **106** (1): 90–115.

Bowman, J. (1994). Arabidopsis: An atlas of morphology and development / John Bowman, editor (New York ; London: Springer-Verlag).

Brandt, U. (2006). Energy converting NADH:quinone oxidoreductase (complex I). Annu. Rev. Biochem. **75**: 69–92.

Briat, J.-F., Duc, C., Ravet, K., and Gaymard, F. (2010). Ferritins and iron storage in plants. Biochim. Biophys. Acta. **1800** (8): 806–814.

Brown, J.C., and Tiffin, L.O. (1965). Iron Stress as Related to the Iron and Citrate Occurring in Stem Exudate. Plant Physiol. **40** (2): 395–400.

Buchan, J.R., and Parker, R. (2009). Eukaryotic stress granules: the ins and outs of translation. Mol. Cell **36** (6): 932–941.

Burbidge, E. (1957). Synthesis of the Elements in Stars. Rev. Mod. Physics **29** (4): 547–650.

Busi, M., Maliandi, M., Valdez, H., Clemente, M., Zabaleta, E., Araya, A., and Gomez-Casati, D. (2006). Deficiency of Arabidopsis thaliana frataxin alters activity of mitochondrial Fe-S proteins and induces oxidative stress. Plant J. **48** (6): 873–882.

Campanella, J.J., Bitincka, L., and Smalley, J. (2003). MatGAT: An application that generates similarity/identity matrices using protein or DNA sequences. BMC Bioinformatics **4** (1): 29.

Carballo, E., Gilkeson, G.S., and Blackshear, P.J. (1997). Bone marrow transplantation reproduces the tristetraprolin-deficiency syndrome in recombination activating gene-2 (-/-) mice. Evidence that monocyte/macrophage progenitors may be responsible for TNFα overproduction. J. Clin. Invest. **100** (5): 986–995.

Carballo, E., Lai, W.S., and Blackshear, P.J. (1998). Feedback Inhibition of Macrophage Tumor Necrosis Factor-{alpha} Production by Tristetraprolin. Science **281** (5379): 1001–1005.

Carballo, E., Lai, W.S., and Blackshear, P.J. (2000). Evidence that tristetraprolin is a physiological regulator of granulocyte-macrophage colony-stimulating factor messenger RNA deadenylation and stability. Blood **95** (6): 1891–1899.

Chaney, R.L. (1988). Plants can utilize iron from Fe-N,N'-di-(2-hydroxybenzoyl)-ethylene diamine-N,N'-diacetic acid, a ferric chelate with 10 6 greater formation constant than Fe-EDDHA. J. Plant Nutr. **11** (6-11): 1033–1050.

Chao, D.-Y., Gable, K., Chen, M., Baxter, I., Dietrich, C.R., Cahoon, E.B., Guerinot, M.L., Lahner, B., Lu, S., Markham, J.E., Morrissey, J., Han, G., Gupta, S.D., Harmon, J.M., Jaworski, J.G., Dunn, T.M., and Salt, D.E. (2011). Sphingolipids in the Root Play an Important Role in Regulating the Leaf Ionome in Arabidopsis thaliana. Plant Cell **23** (3): 1061–1081.

Chekanova, J.A., Gregory, B.D., Reverdatto, S.V., Chen, H., Kumar, R., Hooker, T., Yazaki, J., Li, P., Skiba, N., Peng, Q., Alonso, J., Brukhin, V., Grossniklaus, U., Ecker, J.R., and Belostotsky, D.A. (2007). Genome-wide high-resolution mapping of exosome substrates reveals hidden features in the Arabidopsis transcriptome. Cell **131** (7): 1340–1353.

Chen, C., and Paw, B.H. (2012). Cellular and mitochondrial iron homeostasis in vertebrates. Biochim. Biophys. Acta.

Chen, C.Y., and Shyu, A.B. (1995). AU-rich elements: characterization and importance in mRNA degradation. Trends Biochem. Sci. **20** (11): 465–470.

Chen, W., Yu, X.-H., Zhang, K., Shi, J., Oliveira, S. de, Schreiber, L., Shanklin, J., and Zhang, D. (2011). Male Sterile2 Encodes a Plastid-Localized Fatty Acyl Carrier Protein Reductase Required for Pollen Exine Development in Arabidopsis. Plant Physiol. **157** (2): 842–853.

Chen, W.W., Yang, J.L., Qin, C., Jin, C.W., Mo, J.H., Ye, T., and Zheng, S.J. (2010). Nitric oxide acts downstream of auxin to trigger root ferric-chelate reductase activity in response to iron deficiency in Arabidopsis. Plant Physiol. **154** (2): 810–819.

Cheng, Y., Kato, N., Wang, W., Li, J., and Chen, X. (2003). Two RNA binding proteins, HEN4 and HUA1, act in the processing of AGAMOUS pre-mRNA in Arabidopsis thaliana. Dev. Cell. **4** (1): 53–66.

Chiba, Y., Johnson, M.A., Lidder, P., Vogel, J.T., van Erp, H., and Green, P.J. (2004). AtPARN is an essential poly(A) ribonuclease in Arabidopsis. Gene **328**: 95–102.

Chiu, W., Niwa, Y., Zeng, W., Hirano, T., Kobayashi, H., and Sheen, J. (1996). Engineered GFP as a vital reporter in plants. Curr. Biol. **6** (3): 325–330.

Chu, H.-H., Chiecko, J., Punshon, T., Lanzirotti, A., Lahner, B., Salt, D.E., and Walker, E.L. (2010). Successful Reproduction Requires the Function of Arabidopsis YELLOW STRIPE-LIKE1 and YELLOW STRIPE-LIKE3 Metal-Nicotianamine Transporters in Both Vegetative and Reproductive Structures. Plant Physiol. **154** (1): 197–210.

Clemens, S., Palmgren, M.G., and Kramer, U. (2002). A long way ahead: understanding and engineering plant metal accumulation. Trends Plant Sci. **7** (7): 309–315.

Clough, S.J., and Bent, A.F. (1998). Floral dip: a simplified method for Agrobacterium-mediated transformation of Arabidopsis thaliana. Plant J. **16** (6): 735–743.

Colangelo, E.P., and Guerinot, M.L. (2004). The essential basic helix-loop-helix protein FIT1 is required for the iron deficiency response. Plant Cell **16** (12): 3400–3412.

Connolly, E.L., Fett, J.P., and Guerinot, M.L. (2002). Expression of the IRT1 metal transporter is controlled by metals at the levels of transcript and protein accumulation. Plant Cell **14** (6): 1347–1357.

Conte, S.S., and Walker, E.L. (2011). Transporters Contributing to Iron Trafficking in Plants. Mol Plant **4** (3): 464–476.

Cornell, R., and Schwertmann, U. (2003). The iron oxides: structure, properties, reactions, occurrences, and uses (Wiley-VCH).

Cougot, N., Babajko, S., and Seraphin, B. (2004). Cytoplasmic foci are sites of mRNA decay in human cells. J. Cell Biol. **165** (1): 31–40.

Curie, C., Cassin, G., Couch, D., Divol, F., Higuchi, K., Le Jean, M., Misson, J., Schikora, A., Czernic, P., and Mari, S. (2009). Metal movement within the plant: contribution of nicotianamine and yellow stripe 1-like transporters. Ann. Bot. **103** (1): 1–11.

Curie, C., Panaviene, Z., Loulergue, C., Dellaporta, S.L., Briat, J.-F., and Walker, E.L. (2001). Maize yellow stripe1 encodes a membrane protein directly involved in Fe(III) uptake. Nature **409** (6818): 346–349.

Curtis, M.D., and Grossniklaus, U. (2003). A gateway cloning vector set for high-throughput functional analysis of genes in planta. Plant Physiol. **133** (2): 462–469.

Czechowski, T., Stitt, M., Altmann, T., Udvardi, M.K., and Scheible, W.-R. (2005). Genome-wide identification and testing of superior reference genes for transcript normalization in Arabidopsis. Plant Physiol. **139** (1): 5–17.

Delaney, K.J., Xu, R., Zhang, J., Li, Q.Q., Yun, K.Y., Falcone, D.L., and Hunt, A.G. (2006). Calmodulin interacts with and regulates the RNA-binding activity of an Arabidopsis polyadenylation factor subunit. Plant Physiol. **140** (4): 1507–1521.

Delhaize, E. (1996). A metal-accumulator mutant of Arabidopsis thaliana. Plant Physiol. **111** (3): 849–855.

DeMaeyer, E., and Adiels-Tegman, M. (1985). The prevalence of anaemia in the world. World Health Stat Q **38** (3): 302–316.

DiDonato, R.J., Roberts, L.A., Sanderson, T., Eisley, R.B., and Walker, E.L. (2004). Arabidopsis Yellow Stripe-Like2 (YSL2). Plant J. **39** (3): 403–414.

Dietrich, C., Han, G., Chen, M., Berg, R., Dunn, T., and Cahoon, E. (2008). Loss-of-function mutations and inducible RNAi suppression of Arabidopsis LCB2 genes reveal the critical role of sphingolipids in gametophytic and sporophytic cell viability. Plant J. **54** (2): 284–298.

Di Targiani, R., Lee, S., Wassink, S., and Michel, S. (2006). Functional characterization of iron-substituted tristetraprolin-2D (TTP-2D, NUP475-2D): RNA binding affinity and selectivity. Biochemistry **45** (45): 13641–13649.

Djennane, S., Cesbron, C., Sourice, S., Cournol, R., Dupuis, F., Eychenne, M., Loridon, K., and Chevreau, E. (2011). Iron homeostasis and fire blight susceptibility in transgenic pear plants overexpressing a pea ferritin gene. Plant Sci. **180** (5): 694–701.

Dobritsa, A.A., Shrestha, J., Morant, M., Pinot, F., Matsuno, M., Swanson, R., Moller, B.L., and Preuss, D. (2009). CYP704B1 Is a Long-Chain Fatty Acid -Hydroxylase Essential for Sporopollenin Synthesis in Pollen of Arabidopsis. Plant Physiol. **151** (2): 574–589.

Durrett, T.P., Gassmann, W., and Rogers, E.E. (2007). The FRD3-Mediated Efflux of Citrate into the Root Vasculature Is Necessary for Efficient Iron Translocation. Plant Physiol. **144** (1): 197–205.

Duy, D., Stube, R., Wanner, G., and Philippar, K. (2011). The Chloroplast Permease PIC1 Regulates Plant Growth and Development by Directing Homeostasis and Transport of Iron. Plant Physiol. **155** (4): 1709–1722.

Duy, D., Wanner, G., Meda, A.R., Wiren, N. von, Soll, J., and Philippar, K. (2007). PIC1, an Ancient Permease in Arabidopsis Chloroplasts, Mediates Iron Transport. Plant Cell **19** (3): 986–1006.

Dybczyński, R., Polkowska-Motrenko, H., Samczyński, Z., and Szopa, Z. (1998). Virginia Tobacco Leaves (CTA-VTL-2) – new Polish CRM for inorganic trace analysis including microanalysis. Fresenius J. Anal. Chem. **360** (3-4): 384–387.

Edwards, K., Johnstone, C., and Thompson, C. (1991). A simple and rapid method for the preparation of plant genomic DNA for PCR analysis. Nucl. Acids Res. **19** (6): 1349.

Eide, D., Broderius, M., Fett, J., and Guerinot, M.L. (1996). A novel iron-regulated metal transporter from plants identified by functional expression in yeast. Proc Natl Acad Sci U S A **93** (11): 5624–5628.

Eisenstein, R.S. (2000). IRON REGULATORY PROTEINS AND THE MOLECULAR CONTROL OF MAMMALIAN IRON METABOLISM. Annu. Rev. Nutr. **20** (1): 627–662.

Eulalio, A., Behm-Ansmant, I., and Izaurralde, E. (2007). P bodies: at the crossroads of post-transcriptional pathways. Nat. Rev. Mol. Cell Biol. **8** (1): 9–22.

Expert, D., Enard, C., and Masclaux, C. (1996). The role of iron in plant host-pathogen interactions. Trends Microbiol. **4** (6): 232–237.

Fischer, N., and Weis, K. (2002). The DEAD box protein Dhh1 stimulates the decapping enzyme Dcp1. EMBO J. **21** (11): 2788–2797.

Franks, T.M., and Lykke-Andersen, J. (2007). TTP and BRF proteins nucleate processing body formation to silence mRNAs with AU-rich elements. Genes Dev. **21** (6): 719–735.

Fukuyama, K. (2004). Structure and function of plant-type ferredoxins. Photosynth. Res. **81** (3): 289–301.

Garcia, M., Lucena, C., Romera, F., Alcántara, E., and Perez-Vicente, R. (2010). Ethylene and nitric oxide involvement in the up-regulation of key genes related to iron acquisition and homeostasis in Arabidopsis. J. Exp. Bot. **61** (14): 3885–3899.

García, M.J., Suárez, V., Romera, F.J., Alcántara, E., and Pérez-Vicente, R. (2011). A new model involving ethylene, nitric oxide and Fe to explain the regulation of Fe-acquisition genes in Strategy I plants. Plant Physiol Biochem **49** (5): 537–544.

Garneau, N.L., Wilusz, J., and Wilusz, C.J. (2007). The highways and byways of mRNA decay. Nat. Rev. Mol. Cell Biol. **8** (2): 113–126.

Gautier, L., Cope, L., Bolstad, B.M., and Irizarry, R.A. (2004). affy--analysis of Affymetrix GeneChip data at the probe level. Bioinformatics **20** (3): 307–315.

Gentleman, R.C., Carey, V.J., Bates, D.M., Bolstad, B., Dettling, M., Dudoit, S., Ellis, B., Gautier, L., Ge, Y., Gentry, J., Hornik, K., Hothorn, T., Huber, W., Iacus, S., Irizarry, R., Leisch, F., Li, C., Maechler, M., Rossini, A.J., Sawitzki, G., Smith, C., Smyth, G., Tierney, L., Yang, J.Y.H., and Zhang, J. (2004). Bioconductor: open software development for computational biology and bioinformatics. Genome Biol **5** (10): R80.

Gilks, N., Kedersha, N., Ayodele, M., Shen, L., Stoecklin, G., Dember, L., and Anderson, P. (2004). Stress granule assembly is mediated by prion-like aggregation of TIA-1. Mol. Biol. Cell **15** (12): 5383–5398.

Goeres, D., Van, N., Zhang, W., Fauver, N., Spencer, M., and Sieburth, L. (2007). Components of the Arabidopsis mRNA decapping complex are required for early seedling development. Plant Cell **19** (5): 1549–1564.

Goodstein, D.M., Shu, S., Howson, R., Neupane, R., Hayes, R.D., Fazo, J., Mitros, T., Dirks, W., Hellsten, U., Putnam, N., and Rokhsar, D.S. (2011). Phytozome: a comparative platform for green plant genomics. Nucleic Acids Research **40** (D1): D1178.

Graziano, M., and Lamattina, L. (2007). Nitric oxide accumulation is required for molecular and physiological responses to iron deficiency in tomato roots. Plant J. **52** (5): 949–960.

Graziano, M., Beligni, M.V., and Lamattina, L. (2002). Nitric oxide improves internal iron availability in plants. Plant Physiol. **130** (4): 1852–1859.

Green, L.S. (2004). FRD3 Controls Iron Localization in Arabidopsis. Plant Physiol. **136** (1): 2523–2531.

Hanahan, D. (1983). Studies on transformation of Escherichia coli with plasmids. J. Mol. Biol. **166** (4): 557–580.

Hartley, J.L. (2000). DNA Cloning Using In Vitro Site-Specific Recombination. Genome Res. **10** (11): 1788–1795.

Haydon, M.J., Kawachi, M., Wirtz, M., Hillmer, S., Hell, R., and Krämer, U. (2012). Vacuolar Nicotianamine Has Critical and Distinct Roles under Iron Deficiency and for Zinc Sequestration in Arabidopsis. Plant Cell.

Hellens, R.P., Edwards, E.A., Leyland, N.R., Bean, S., and Mullineaux, P.M. (2000). pGreen: a versatile and flexible binary Ti vector for Agrobacterium-mediated plant transformation. Plant Mol. Biol. **42** (6): 819–832.

Hoagland, D.R., and Arnon, D.I. (1938). The water-culture method for growing plants without soil (Berkeley, Calif: University of California, College of Agriculture, Agricultural Experiment Station).

Houseley, J., LaCava, J., and Tollervey, D. (2006). RNA-quality control by the exosome. Nat. Rev. Mol. Cell Biol. **7** (7): 529–539.

Hudson, B.P., Martinez-Yamout, M.A., Dyson, H.J., and Wright, P.E. (2004). Recognition of the mRNA AU-rich element by the zinc finger domain of TIS11d. Nat. Struct. Mol. Biol. **11** (3): 257–264.

Hunter, S., Jones, P., Mitchell, A., Apweiler, R., Attwood, T.K., Bateman, A., Bernard, T., Binns, D., Bork, P., Burge, S., Castro, E. de, Coggill, P., Corbett, M., Das, U., Daugherty, L., Duquenne, L., Finn, R.D., Fraser, M., Gough, J., Haft, D., Hulo, N., Kahn, D., Kelly, E., Letunic, I., Lonsdale, D., Lopez, R., Madera, M., Maslen, J., McAnulla, C., McDowall, J., McMenamin, C., Mi, H., Mutowo-Muellenet, P., Mulder, N., Natale, D., Orengo, C., Pesseat, S., Punta, M., Quinn, A.F., Rivoire, C., Sangrador-Vegas, A., Selengut, J.D., Sigrist, C.J.A., Scheremetjew, M., Tate, J., Thimmajanarthanan, M., Thomas, P.D., Wu, C.H., Yeats, C., and Yong, S.-Y. (2011). InterPro in 2011: new developments in the family and domain prediction database. Nucleic Acids Research **40** (D1): D306.

Ishiguro, S. (2001). The DEFECTIVE IN ANTHER DEHISCENCE1 Gene Encodes a Novel Phospholipase A1 Catalyzing the Initial Step of Jasmonic Acid Biosynthesis, Which Synchronizes Pollen Maturation, Anther Dehiscence, and Flower Opening in Arabidopsis. Plant Cell **13** (10): 2191–2209.

Iwasaki, S., Takeda, A., Motose, H., and Watanabe, Y. (2007). Characterization of Arabidopsis decapping proteins AtDCP1 and AtDCP2, which are essential for post-embryonic development. FEBS Lett. **581** (13): 2455–2459.

Jakobsen, M.K., Poulsen, L.R., Schulz, A., Fleurat-Lessard, P., Moller, A., Husted, S., Schiott, M., Amtmann, A., and Palmgren, M.G. (2005). Pollen development and fertilization in Arabidopsis is dependent on the MALE GAMETOGENESIS IMPAIRED ANTHERS gene encoding a Type V P-type ATPase. Genes Dev. **19** (22): 2757–2769

Jakoby, M., Wang, H.-Y., Reidt, W., Weisshaar, B., and Bauer, P. (2004). FRU (BHLH029) is required for induction of iron mobilization genes in Arabidopsis thaliana. FEBS Lett. **577** (3): 528–534.

Jefferson, R.A., Kavanagh, T.A., and Bevan, M.W. (1987). GUS fusions: beta-glucuronidase as a sensitive and versatile gene fusion marker in higher plants. EMBO J. **6** (13): 3901–3907.

Jeong, J., Cohu, C., Kerkeb, L., Pilon, M., Connolly, E., and Guerinot, M. (2008). Chloroplast Fe(III) chelate reductase activity is essential for seedling viability under iron limiting conditions. Proc Natl Acad Sci U S A **105** (30): 10619–10624.

Jessen, D., Olbrich, A., Knüfer, J., Krüger, A., Hoppert, M., Polle, A., and Fulda, M. (2011). Combined activity of LACS1 and LACS4 is required for proper pollen coat formation in Arabidopsis. Plant J. **68** (4): 715–726.

Jiao, Y., Riechmann, J.L., and Meyerowitz, E.M. (2008). Transcriptome-Wide Analysis of Uncapped mRNAs in Arabidopsis Reveals Regulation of mRNA Degradation. Plant Cell **20** (10): 2571–2585.

Johnson, D., Dean, D., Smith, A., and Johnson, M. (2005). Structure, function, and formation of biological iron-sulfur clusters. Annu. Rev. Biochem. **74**: 247–281.

Johnson, M.A., Perez-Amador, M.A., Lidder, P., and Green, P.J. (2000). Mutants of Arabidopsis defective in a sequence-specific mRNA degradation pathway. Proc Natl Acad Sci U S A **97** (25): 13991–13996.

Jones-Rhoades, M.W., Bartel, D.P., and Bartel, B. (2006). MicroRNAs and their regulatory roles in plants. Annu Rev Plant Biol **57** (1): 19–53.

Joshua-Tor, L. (2006). The Argonautes. Cold Spring Harbor Symposia on Quantitative Biology **71** (0): 67–72.

Kastenmayer, J.P., and Green, P.J. (2000). Novel features of the XRN-family in Arabidopsis: Evidence that AtXRN4, one of several orthologs of nuclear Xrn2p/Rat1p, functions in the cytoplasm. Proc Natl Acad Sci U S A **97** (25): 13985–13990.

Kedersha, N., Cho, M.R., Li, W., Yacono, P.W., Chen, S., Gilks, N., Golan, D.E., and Anderson, P. (2000). Dynamic Shuttling of Tia-1 Accompanies the Recruitment of mRNA to Mammalian Stress Granules. J. Cell Biol. **151** (6): 1257–1268.

Kedersha, N., Stoecklin, G., Ayodele, M., Yacono, P., Lykke-Andersen, J., Fritzler, M.J., Scheuner, D., Kaufman, R.J., Golan, D.E., and Anderson, P. (2005). Stress granules and processing bodies are dynamically linked sites of mRNP remodeling. J. Cell Biol. **169** (6): 871–884.

Kerkeb, L., Mukherjee, I., Chatterjee, I., Lahner, B., Salt, D.E., and Connolly, E.L. (2008). Iron-Induced Turnover of the Arabidopsis IRON-REGULATED TRANSPORTER1 Metal Transporter Requires Lysine Residues. Plant Physiol. **146** (4): 1964–1973.

Kim, D.H., Yamaguchi, S., Lim, S., Oh, E., Park, J., Hanada, A., Kamiya, Y., and Choi, G. (2008). SOMNUS, a CCCH-type zinc finger protein in Arabidopsis, negatively regulates light-dependent seed germination downstream of PIL5. Plant Cell **20** (5): 1260–1277.

Kim, S.A., Punshon, T., Lanzirotti, A., Li, L., Alonso, J.M., Ecker, J.R., Kaplan, J., and Guerinot, M.L. (2006). Localization of Iron in Arabidopsis Seed Requires the Vacuolar Membrane Transporter VIT1. Science **314** (5803): 1295–1298.

Kirkman, H.N., and Gaetani, G.F. (1984). Catalase: a tetrameric enzyme with four tightly bound molecules of NADPH. Proc Natl Acad Sci U S A **81** (14): 4343–4347.

Klatte, M., Schuler, M., Wirtz, M., Fink-Straube, C., Hell, R., and Bauer, P. (2009). The Analysis of Arabidopsis Nicotianamine Synthase Mutants Reveals Functions for Nicotianamine in Seed Iron Loading and Iron Deficiency Responses. Plant Physiol. **150** (1): 257–271.

Koncz, C., and Schell, J. (1986). The promoter of TL-DNA gene 5 controls the tissue-specific expression of chimaeric genes carried by a novel type of Agrobacterium binary vector. Molec. Gen. Genet. **204** (3): 383–396.

Kong, Z., Li, M., Yang, W., Xu, W., and Xue, Y. (2006). A novel nuclear-localized CCCH-type zinc finger protein, OsDOS, is involved in delaying leaf senescence in rice. Plant Physiol. **141** (4): 1376–1388.

Krüger, C., Berkowitz, O., Stephan, U., and Hell, R. (2002). A metal-binding member of the late embryogenesis abundant protein family transports iron in the phloem of Ricinus communis L. J. Biol. Chem. **277** (28): 25062–25069.

Lai, W.S., Carballo, E., Strum, J.R., Kennington, E.A., Phillips, R.S., and Blackshear, P.J. (1999). Evidence that tristetraprolin binds to AU-rich elements and promotes the deadenylation and destabilization of tumor necrosis factor alpha mRNA. Mol. Cell. Biol. **19** (6): 4311–4323.

Lai, W.S., Parker, J.S., Grissom, S.F., Stumpo, D.J., and Blackshear, P.J. (2006). Novel mRNA targets for tristetraprolin (TTP) identified by global analysis of stabilized transcripts in TTP-deficient fibroblasts. Mol. Cell. Biol. **26** (24): 9196–9208.

Lanquar, V., Lelievre, F., Bolte, S., Hames, C., Alcon, C., Neumann, D., Vansuyt, G., Curie, C., Schroder, A., Kramer, U., Barbier-Brygoo, H., and Thomine, S. (2005). Mobilization of vacuolar iron by AtNRAMP3 and AtNRAMP4 is essential for seed germination on low iron. EMBO J. **24** (23): 4041–4051.

Lanquar, V., Ramos, M., Lelievre, F., Barbier-Brygoo, H., Krieger-Liszkay, A., Kramer, U., and Thomine, S. (2010). Export of vacuolar manganese by AtNRAMP3 and AtNRAMP4 is required for optimal photosynthesis and growth under manganese deficiency. Plant Physiol. **152** (4): 1986–1999.

Le Jean, M., Schikora, A., Mari, S., Briat, J.-F., and Curie, C. (2005). A loss-of-function mutation in AtYSL1 reveals its role in iron and nicotianamine seed loading. Plant J. **44** (5): 769–782.

Lee, S., and Michel, S. (2010). Cysteine oxidation enhanced by iron in tristetraprolin, a zinc finger peptide. Inorg. Chem. **49** (3): 1211–1219.

Li, C., Pontes, O., El-Shami, M., Henderson, I., Bernatavichute, Y., Chan, S.-L., Lagrange, T., Pikaard, C., and Jacobsen, S. (2006). An ARGONAUTE4-containing nuclear processing center colocalized with Cajal bodies in Arabidopsis thaliana. Cell **126** (1): 93–106.

Li, Z., and Thomas, T.L. (1998). PEI1, an embryo-specific zinc finger protein gene required for heart-stage embryo formation in Arabidopsis. Plant Cell **10** (3): 383–398.

Liang, W., Li, C., Liu, F., Jiang, H., Li, S., Sun, J., Wu, X., and Li, C. (2009). The Arabidopsis homologs of CCR4-associated factor 1 show mRNA deadenylation activity and play a role in plant defence responses. Cell Res. **19** (3): 307–316.

Lill, R. (2009). Function and biogenesis of iron–sulphur proteins. Nature **460** (7257): 831–838.

Lin, P.-C., Pomeranz, M.C., Jikumaru, Y., Kang, S.G., Hah, C., Fujioka, S., Kamiya, Y., and Jang, J.-C. (2010). The Arabidopsis tandem zinc finger protein AtTZF1 affects ABA- and GA-mediated growth, stress and gene expression responses. Plant J. **65** (2): 253–268.

Ling, H.Q., Koch, G., Baumlein, H., and Ganal, M.W. (1999). Map-based cloning of chloronerva, a gene involved in iron uptake of higher plants encoding nicotianamine synthase. Proc Natl Acad Sci U S A **96** (12): 7098–7103.

Ling, H.Q., Pich, A., Scholz, G., and Ganal, M.W. (1996). Genetic analysis of two tomato mutants affected in the regulation of iron metabolism. Mol Gen Genet **252** (1-2): 87–92.

Lingam, S., Mohrbacher, J., Brumbarova, T., Potuschak, T., Fink-Straube, C., Blondet, E., Genschik, P., and Bauer, P. (2011). Interaction between the bHLH transcription factor FIT and ETHYLENE INSENSITIVE3/ETHYLENE INSENSITIVE3-LIKE1 reveals molecular linkage between the regulation of iron acquisition and ethylene signaling in Arabidopsis. Plant Cell **23** (5): 1815–1829.

Liu, H., Rodgers, N.D., Jiao, X., and Kiledjian, M. (2002). The scavenger mRNA decapping enzyme DcpS is a member of the HIT family of pyrophosphatases. EMBO J. **21** (17): 4699–4708.

Liu, J., Carmell, M., Rivas, F., Marsden, C., Thomson, J., Song, J.-J., Hammond, S., Joshua-Tor, L., and Hannon, G. (2004). Argonaute2 is the catalytic engine of mammalian RNAi. Science **305** (5689): 1437–1441.

Liu, J., Valencia-Sanchez, M.A., Hannon, G.J., and Parker, R. (2005). MicroRNA-dependent localization of targeted mRNAs to mammalian P-bodies. Nat. Cell Biol. **7** (7): 719–723.

Lorkovic, Z., and Barta, A. (2002). Genome analysis: RNA recognition motif (RRM) and K homology (KH) domain RNA-binding proteins from the flowering plant Arabidopsis thaliana. Nucl. Acids Res. **30** (3): 623–635.

Lorkovic, Z.J., Wieczorek, K., Klahre, U., Hemmings-Mieszczak, M., and Filipowicz, W. (2000). RBP45 and RBP47, two oligouridylate-specific hnRNP-like proteins interacting with poly(A)+ RNA in nuclei of plant cells. RNA **6** (11): 1610–1624.

Lucena, C., Waters, B.M., Romera, F.J., García, M.J., Morales, M., Alcántara, E., and Pérez-Vicente, R. (2006). Ethylene could influence ferric reductase, iron transporter, and H+-ATPase gene expression by affecting FER (or FER-like) gene activity. J. Exp. Bot. **57** (15): 4145–4154.

Lykke-Andersen, J., and Wagner, E. (2005). Recruitment and activation of mRNA decay enzymes by two ARE-mediated decay activation domains in the proteins TTP and BRF-1. Genes Dev. **19** (3): 351–361.

Ma, H. (2005). MOLECULAR GENETIC ANALYSES OF MICROSPOROGENESIS AND MICROGAMETOGENESIS IN FLOWERING PLANTS. Annu Rev Plant Biol **56** (1): 393–434.

Maliandi, M., Busi, M., Turowski, V., Leaden, L., Araya, A., and Gomez-Casati, D. (2011). The mitochondrial protein frataxin is essential for heme biosynthesis in plants. FEBS J. **278** (3): 470–481.

Mandaokar, A., and Browse, J. (2009). MYB108 Acts Together with MYB24 to Regulate Jasmonate-Mediated Stamen Maturation in Arabidopsis. Plant Physiol. **149** (2): 851–862.

Mangus, D., Evans, M., and Jacobson, A. (2003). Poly(A)-binding proteins: multifunctional scaffolds for the post-transcriptional control of gene expression. Genome Biol. **4** (7): 223.

McClure, B.A., Hagen, G., Brown, C.S., Gee, M.A., and Guilfoyle, T.J. (1989). Transcription, organization, and sequence of an auxin-regulated gene cluster in soybean. Plant Cell **1** (2): 229–239.

Meiser, J., Lingam, S., and Bauer, P. (2011). Post-translational regulation of the Fe deficiency bHLH transcription factor FIT is affected by iron and nitric oxide. Plant Physiol. **157** (4): 2154–2166.

Mlotshwa, S., Pruss, G.J., Gao, Z., Mgutshini, N.L., Li, J., Chen, X., Bowman, L.H., and Vance, V. (2010). Transcriptional silencing induced by Arabidopsis T-DNA mutants is associated with 35S promoter siRNAs and requires genes involved in siRNA-mediated chromatin silencing. Plant J. **64** (4): 699–704.

Mori, S. (1999). Iron acquisition by plants. Curr Opin Plant Biol **2** (3): 250–253.

Mukherjee, I., Campbell, N.H., Ash, J.S., and Connolly, E.L. (2006). Expression profiling of the Arabidopsis ferric chelate reductase (FRO) gene family reveals differential regulation by iron and copper. Planta **223** (6): 1178–1190.

Munoz-Bertomeu, J., Cascales-Minana, B., Irles-Segura, A., Mateu, I., Nunes-Nesi, A., Fernie, A.R., Segura, J., and Ros, R. (2010). The Plastidial Glyceraldehyde-3-Phosphate Dehydrogenase Is Critical for Viable Pollen Development in Arabidopsis. Plant Physiol. **152** (4): 1830–1841.

Murashige, T., and Skoog, F. (1962). A Revised Medium for Rapid Growth and Bio Assays with Tobacco Tissue Cultures. Physiol. Plant. **15** (3): 473–497.

Nakagawa, T., Suzuki, T., Murata, S., Nakamura, S., Hino, T., Maeo, K., Tabata, R., Kawai, T., Tanaka, K., Niwa, Y., Watanabe, Y., Nakamura, K., Kimura, T., and Ishiguro, S. (2007). Improved Gateway binary vectors: high-performance vectors for creation of fusion constructs in transgenic analysis of plants. Biosci. Biotechnol. Biochem. **71** (8): 2095–2100.

Nemeth, E., and Ganz, T. (2006). Regulation of iron metabolism by hepcidin. Annu. Rev. Nutr. **26**: 323–342.

Newman, T.C., Ohme-Takagi, M., Taylor, C.B., and Green, P.J. (1993). DST sequences, highly conserved among plant SAUR genes, target reporter transcripts for rapid decay in tobacco. Plant Cell **5** (6): 701–714.

Nishimura, N., Kitahata, N., Seki, M., Narusaka, Y., Narusaka, M., Kuromori, T., Asami, T., Shinozaki, K., and Hirayama, T. (2005). Analysis of ABA hypersensitive germination2 revealed the pivotal functions of PARN in stress response in Arabidopsis. Plant J. **44** (6): 972–984.

Nouet, C., Motte, P., and Hanikenne, M. (2011). Chloroplastic and mitochondrial metal homeostasis. Trends Plant Sci. **16** (7): 395–404.

Ogilvie, R.L., Abelson, M., Hau, H.H., Vlasova, I., Blackshear, P., and Bohjanen, P.R. (2005). Tristetraprolin Down-Regulates IL-2 Gene Expression through AU-Rich Element-Mediated mRNA Decay **174** (2): 953–961.

Pacini, E., Franchi, G.G., and Hesse, M. (1985). The tapetum: Its form, function, and possible phylogeny inEmbryophyta. Plant Syst. Evol. **149** (3-4): 155–185.

Parker, R., and Sheth, U. (2007). P bodies and the control of mRNA translation and degradation. Mol. Cell **25** (5): 635–646.

Patel, S., and Bellini, M. (2008). The assembly of a spliceosomal small nuclear ribonucleoprotein particle. Nucl. Acids Res. **36** (20): 6482–6493.

Pedro-Segura, E., Vergara, S.V., Rodriguez-Navarro, S., Parker, R., Thiele, D.J., and Puig, S. (2008). The Cth2 ARE-binding protein recruits the Dhh1 helicase to promote the decay of succinate dehydrogenase SDH4 mRNA in response to iron deficiency. J. Biol. Chem. **283** (42): 28527–28535.

Piffanelli, P., Ross, J.H.E., and Murphy, D.J. (1998). Biogenesis and function of the lipidic structures of pollen grains. Sex. Plant Reprod. **11** (2): 65–80.

Pomeranz M., Hah C., Lin P., Kang S., Finer J., Blackshear P., and Jang J. (2010a). The Arabidopsis tandem zinc finger protein AtTZF1 traffics between the nucleus and cytoplasmic foci and binds both DNA and RNA. Plant Physiol. **152** (1): 151–165.

Pomeranz, M., Lin, P., Finer, J., and Jang, J. (2010b). AtTZF gene family localizes to cytoplasmic foci. Plant Signal. Behav. **5** (2): 190–192.

Porra, R.J., Thompson, W.A., and Kriedemann, P.E. (1989). Determination of accurate extinction coefficients and simultaneous equations for assaying chlorophylls a and b extracted with four different solvents: verification of the concentration of chlorophyll standards by atomic absorption spectroscopy. Biochim. Biophys. Acta. **975** (3): 384–394.

Prouteau, M., Daugeron, M.C., and Seraphin, B. (2008). Regulation of ARE transcript 3' end processing by the yeast Cth2 mRNA decay factor. EMBO J. **27** (22): 2966–2976.

Puig, S., Askeland, E., and Thiele, D.J. (2005). Coordinated remodeling of cellular metabolism during iron deficiency through targeted mRNA degradation. Cell **120** (1): 99–110.

Puig, S., Vergara, S.V., and Thiele, D.J. (2008). Cooperation of two mRNA-binding proteins drives metabolic adaptation to iron deficiency. Cell Metab. **7** (6): 555–564.

Punta, M., Coggill, P.C., Eberhardt, R.Y., Mistry, J., Tate, J., Boursnell, C., Pang, N., Forslund, K., Ceric, G., Clements, J., Heger, A., Holm, L., Sonnhammer, E.L.L., Eddy, S.R., Bateman, A., and Finn, R.D. (2011). The Pfam protein families database. Nucleic Acids Research **40** (D1): D290.

Ramakers, C., Ruijter, J., Deprez, R., and Moorman, A. (2003). Assumption-free analysis of quantitative real-time polymerase chain reaction (PCR) data. Neurosci. Lett. **339** (1): 62–66.

Ramos, S.B.V. (2012). Characterization of N-Zfp36l2 Mutant Associated with Arrest of Early Embryonic Development and Female Infertility. J. Biol. Chem. **287** (16): 13116–13127.

Ramos, S.B.V., Stumpo, D.J., Kennington, E.A., Phillips, R.S., Bock, C.B., Ribeiro-Neto, F., and Blackshear, P.J. (2004). The CCCH tandem zinc-finger protein Zfp36l2 is crucial for female fertility and early embryonic development. Development **131** (19): 4883–4893.

Ravet, K., Reyt, G., Arnaud, N., Krouk, G., Djouani, E.B., Boucherez, J., Briat, J.F., and Gaymard, F. (2011). Iron and ROS control of the DownSTream mRNA decay pathway is essential for plant fitness. EMBO J. **31** (1): 175–185.

Ravet, K., Touraine, B., Boucherez, J., Briat, J.-F., Gaymard, F., and Cellier, F. (2009). Ferritins control interaction between iron homeostasis and oxidative stress in Arabidopsis. Plant J. **57** (3): 400–412.

Reichel, C., Mathur, J., Eckes, P., Langenkemper, K., Koncz, C., Schell, J., Reiss, B., and Maas, C. (1996). Enhanced green fluorescence by the expression of an Aequorea victoria green fluorescent protein mutant in mono- and dicotyledonous plant cells. Proc Natl Acad Sci U S A **93** (12): 5888–5893.

Reilly, C. (2004). The nutritional trace metals (Oxford, OX, UK ;, Ames, IA, USA: Blackwell Pub.).

Rellan-Alvarez, R., Giner-Martinez-Sierra, J., Orduna, J., Orera, I., Rodriguez-Castrillon, J., Garcia-Alonso, J., Abadia, J., and Alvarez-Fernandez, A. (2010). Identification of a tri-iron(III), tri-citrate complex in the xylem sap of iron-deficient tomato resupplied with iron: new insights into plant iron long-distance transport. Plant Cell Physiol. **51** (1): 91–102.

Reverdatto, S.V., Dutko, J.A., Chekanova, J.A., Hamilton, D.A., and Belostotsky, D.A. (2004). mRNA deadenylation by PARN is essential for embryogenesis in higher plants. RNA **10** (8): 1200–1214.

Ribot, C., Zimmerli, C., Farmer, E.E., Reymond, P., and Poirier, Y. (2008). Induction of the Arabidopsis PHO1;H10 Gene by 12-Oxo-Phytodienoic Acid But Not Jasmonic Acid via a CORONATINE INSENSITIVE1-Dependent Pathway. Plant Physiol. **147** (2): 696–706.

Robinson, N.J., Procter, C.M., Connolly, E.L., and Guerinot, M.L. (1999). A ferric-chelate reductase for iron uptake from soils. Nature **397** (6721): 694–697.

Rodriguez-Rosales, M., Galvez, F., Huertas, R., Aranda, M., Baghour, M., Cagnac, O., and Venema, K. (2009). Plant NHX cation/proton antiporters. Plant Signal. Behav. **4** (4): 265–276.

Rogers, E.E. (2002). FRD3, a Member of the Multidrug and Toxin Efflux Family, Controls Iron Deficiency Responses in Arabidopsis. Plant Cell **14** (8): 1787–1799.

Römheld, V., and Marschner, H. (1986). Evidence for a Specific Uptake System for Iron Phytosiderophores in Roots of Grasses. Plant Physiol. **80** (1): 175–180.

Roschzttardtz, H., Grillet, L., Isaure, M.-P., Conejero, G., Ortega, R., Curie, C., and Mari, S. (2011a). Plant Cell Nucleolus as a Hot Spot for Iron. J. Biol. Chem. **286** (32): 27863–27866.

Roschzttardtz, H., Seguela-Arnaud, M., Briat, J.-F., Vert, G., and Curie, C. (2011b). The FRD3 Citrate Effluxer Promotes Iron Nutrition between Symplastically Disconnected Tissues throughout Arabidopsis Development. Plant Cell **23** (7): 2725–2737.

Rouault, T. (2006). The role of iron regulatory proteins in mammalian iron homeostasis and disease. Nat. Chem. Biol. **2** (8): 406–414.

Rutherford, J.C., Jaron, S., Ray, E., Brown, P.O., and Winge, D.R. (2001). A second iron-regulatory system in yeast independent of Aft1p **98** (25): 14322–14327.

Sablowski, R. (2007). Flowering and determinacy in Arabidopsis. J. Exp. Bot. **58** (5): 899–907.

Sambrook, J., Fritsch, E.F., and Maniatis, T. (2001). Molecular cloning: A laboratory manual (Cold Spring Harbor, NY: Cold Spring Harbor Laboratory Press).

Sanders, P.M., Bui, A.Q., Weterings, K., McIntire, K.N., Hsu, Y.-C., Lee, P.Y., Truong, M.T., Beals, T.P., and Goldberg, R.B. (1999). Anther developmental defects in Arabidopsis thaliana male-sterile mutants. Sex. Plant Reprod. **11** (6): 297–322.

Sanduja, S., Blanco, F., and Dixon, D. (2011). The roles of TTP and BRF proteins in regulated mRNA decay. Wiley Interdiscip Rev RNA **2** (1): 42–57.

Sanger, F., Nicklen, S., and Coulson, A.R. (1977). DNA sequencing with chain-terminating inhibitors. Proc Natl Acad Sci U S A **74** (12): 5463–5467.

Santi, S., and Schmidt, W. (2009). Dissecting iron deficiency-induced proton extrusion in Arabidopsis roots. New. Phytol. **183** (4): 1072–1084.

Schaaf, G., Schikora, A., Haberle, J., Vert, G., Ludewig, U., Briat, J.-F., Curie, C., and Wiren, N. von (2005). A Putative Function for the Arabidopsis Fe-Phytosiderophore Transporter Homolog AtYSL2 in Fe and Zn Homeostasis. Plant Cell Physiol. **46** (5): 762–774.

Scheffer, F., Schachtschabel, P., and Blume, H.-P. (2002). Lehrbuch der Bodenkunde (Heidelberg [u.a.]: Spektrum, Akad. Verl.).

Schmid, M., Davison, T., Henz, S., Pape, U., Demar, M., Vingron, M., Scholkopf, B., Weigel, D., and Lohmann, J. (2005a). A gene expression map of Arabidopsis thaliana development. Nat. Genet. **37** (5): 501–506.

Schmid, M., Davison, T.S., Henz, S.R., Pape, U.J., Demar, M., Vingron, M., Schölkopf, B., Weigel, D., and Lohmann, J.U. (2005b). A gene expression map of Arabidopsis thaliana development. Nat. Genet. **37** (5): 501–506.

Schmitz, R.J., Hong, L., Michaels, S., and Amasino, R.M. (2005). FRIGIDA-ESSENTIAL 1 interacts genetically with FRIGIDA and FRIGIDA-LIKE 1 to promote the winter-annual habit of Arabidopsis thaliana. Development **132** (24): 5471–5478.

Schwab, R., Ossowski, S., Riester, M., Warthmann, N., and Weigel, D. (2006). Highly specific gene silencing by artificial microRNAs in Arabidopsis. Plant Cell **18** (5): 1121–1133.

Sen, G.L., and Blau, H.M. (2005). Argonaute 2/RISC resides in sites of mammalian mRNA decay known as cytoplasmic bodies. Nat. Cell Biol. **7** (6): 633–636.

SenGupta, D.J., Zhang, B., Kraemer, B., Pochart, P., Fields, S., and Wickens, M. (1996). A three-hybrid system to detect RNA-protein interactions in vivo. Proc Natl Acad Sci U S A **93** (16): 8496–8501.

Shakoury-Elizeh, M., Protchenko, O., Berger, A., Cox, J., Gable, K., Dunn, T.M., Prinz, W.A., Bard, M., and Philpott, C.C. (2010). Metabolic Response to Iron Deficiency in Saccharomyces cerevisiae. J. Biol. Chem. **285** (19): 14823–14833.

Shakoury-Elizeh, M., Tiedeman, J., Rashford, J., Ferea, T., Demeter, J., Garcia, E., Rolfes, R., Brown, P.O., Botstein, D., and Philpott, C.C. (2004). Transcriptional remodeling in response to iron deprivation in Saccharomyces cerevisiae. Mol. Biol. Cell **15** (3): 1233–1243.

Shenker, M., and Chen, Y. (2005). Increasing Iron Availability to Crops: Fertilizers, Organo-Fertilizers, and Biological Approaches. Soil Sci. Plant Nutri. **51** (1): 1–17.

Sheth, U., and Parker, R. (2003). Decapping and Decay of Messenger RNA Occur in Cytoplasmic Processing Bodies **300** (5620): 805–808.

Shimoni-Shor, E., Hassidim, M., Yuval-Naeh, N., and Keren, N. (2010). Disruption of Nap14, a plastid-localized non-intrinsic ABC protein in Arabidopsis thaliana results in the over-accumulation of transition metals and in aberrant chloroplast structures. Plant Cell Environ. **33** (6): 1029–1038.

Sivitz, A., Grinvalds, C., Barberon, M., Curie, C., and Vert, G. (2011). Proteasome-mediated turnover of the transcriptional activator FIT is required for plant iron-deficiency responses. Plant J. **66** (6): 1044–1052.

Smits, T.H.M., and Duffy, B. (2011). Genomics of iron acquisition in the plant pathogen Erwinia amylovora: insights in the biosynthetic pathway of the siderophore desferrioxamine E. Arch. Microbiol. **193** (10): 693–699.

Smyth, D.R., Bowman, J.L., and Meyerowitz, E.M. (1990). Early flower development in Arabidopsis. Plant Cell **2** (8): 755–767.

Smyth, G. (2005). Limma: linear models for microarray data. In Bioinformatics and Computational Biology Solutions using R and Bioconductor, R. Gentleman, V. Carey, S. Dudoit, R. Irizarry, and W. Huber, eds (New York, NY: Springer New York), pp. 397–420.

Song, W.-Y., Choi, K.-S., Alexis, D.A., Martinoia, E., and Lee, Y. (2011). Brassica juncea plant cadmium resistance 1 protein (BjPCR1) facilitates the radial transport of calcium in the root. Proceedings of the National Academy of Sciences **108** (49): 19808–19813.

Song, W.-Y., Choi, K.S., Kim, D.Y., Geisler, M., Park, J., Vincenzetti, V., Schellenberg, M., Kim, S.H., Lim, Y.P., Noh, E.W., Lee, Y., and Martinoia, E. (2010). Arabidopsis PCR2 is a zinc exporter involved in both zinc extrusion and long-distance zinc transport. Plant Cell **22** (7): 2237–2252.

Song, W.-Y., Martinoia, E., Lee, J., Kim, D., Kim, D.-Y., Vogt, E., Shim, D., Choi, K.S., Hwang, I., and Lee, Y. (2004). A novel family of cys-rich membrane proteins mediates cadmium resistance in Arabidopsis. Plant Physiol **135** (2): 1027–1039.

Souret, F.F., Kastenmayer, J.P., and Green, P.J. (2004). AtXRN4 degrades mRNA in Arabidopsis and its substrates include selected miRNA targets. Mol. Cell **15** (2): 173–183.

Stanek, D., and Neugebauer, K. (2006). The Cajal body: a meeting place for spliceosomal snRNPs in the nuclear maze. Chromosoma **115** (5): 343–354.

Stevenson, F.J. (1994). Humus chemistry: Genesis, composition, reactions (New York: Wiley).

Strassner, J., Schaller, F., Frick, U., Howe, G., Weiler, E., Amrhein, N., Macheroux, P., and Schaller, A. (2002). Characterization and cDNA-microarray expression analysis of 12-oxophytodienoate reductases reveals differential roles for octadecanoid biosynthesis in the local versus the systemic wound response. Plant J. **32** (4): 585–601.

Sun, J., Jiang, H., Xu, Y., Li, H., Wu, X., Xie, Q., and Li, C. (2007). The CCCH-type zinc finger proteins AtSZF1 and AtSZF2 regulate salt stress responses in Arabidopsis. Plant Cell Physiol. **48** (8): 1148–1158.

Taiz, L., and Zeiger, E. (2010). Plant physiology (Sunderland, MA: Sinauer Associates).

Takahashi, M., Terada, Y., Nakai, I., Nakanishi, H., Yoshimura, E., Mori, S., and Nishizawa, N.K. (2003). Role of nicotianamine in the intracellular delivery of metals and plant reproductive development. Plant Cell **15** (6): 1263–1280.

Tan, Y.-F., O'Toole, N., Taylor, N., and Millar, A. (2010). Divalent metal ions in plant mitochondria and their role in interactions with proteins and oxidative stress-induced damage to respiratory function. Plant Physiol. **152** (2): 747–761.

Tang, L.K., Chu, H., Yip, W.K., Yeung, E.C., and Lo, C. (2009). An anther-specific dihydroflavonol 4-reductase-like gene (DRL1) is essential for male fertility in Arabidopsis. New. Phytol. **181** (3): 576–587.

Tchen, C.R. (2004). The Stability of Tristetraprolin mRNA Is Regulated by Mitogen-activated Protein Kinase p38 and by Tristetraprolin Itself. J. Biol. Chem. **279** (31): 32393–32400.

Teixeira, D., Sheth, U., Valencia-Sanchez, M.A., Brengues, M., and Parker, R. (2005). Processing bodies require RNA for assembly and contain nontranslating mRNAs. RNA **11** (4): 371–382.

Teng, C., Dong, H., Shi, L., Deng, Y., Mu, J., Zhang, J., Yang, X., and Zuo, J. (2008). Serine Palmitoyltransferase, a Key Enzyme for de Novo Synthesis of Sphingolipids, Is Essential for Male Gametophyte Development in Arabidopsis. Plant Physiol. **146** (3): 1322–1332.

Terry, N., and Abadia, J. (1986). Function of iron in chloroplasts. J. of Plant Nutrition **9** (3): 609–646.

Thimm, O., Blasing, O., Gibon, Y., Nagel, A., Meyer, S., Kruger, P., Selbig, J., Muller, L., Rhee, S., and Stitt, M. (2004). MAPMAN: a user-driven tool to display genomics data sets onto diagrams of metabolic pathways and other biological processes. Plant J. **37** (6): 914–939.

Thomine, S., Lelievre, F., Debarbieux, E., Schroeder, J., and Barbier-Brygoo, H. (2003). AtNRAMP3, a multispecific vacuolar metal transporter involved in plant responses to iron deficiency. Plant J. **34** (5): 685–695.

Toufighi, K., Brady, S.M., Austin, R., Ly, E., and Provart, N.J. (2005). The Botany Array Resource: e-Northerns, Expression Angling, and promoter analyses. Plant J. **43** (1): 153–163.

Tsukamoto, T., Nakanishi, H., Uchida, H., Watanabe, S., Matsuhashi, S., Mori, S., and Nishizawa, N. (2009). (52)Fe translocation in barley as monitored by a positron-emitting

tracer imaging system (PETIS): evidence for the direct translocation of Fe from roots to young leaves via phloem. Plant Cell Physiol. **50** (1): 48–57.

Tyree, M.T., and Zimmermann, M.H. (2002). Xylem structure and the ascent of sap ([S.l.]: Springer).

Valko, M., Morris, H., and Cronin, M.T. (2005). Metals, toxicity and oxidative stress. Curr. Med. Chem. **12** (10): 1161–1208.

Vanacova, S., and Stefl, R. (2007). The exosome and RNA quality control in the nucleus. EMBO Rep. **8** (7): 651–657.

Vergara, S., Puig, S., and Thiele, D. (2011). Early recruitment of AU-rich element-containing mRNAs determines their cytosolic fate during iron deficiency. Mol. Cell. Biol. **31** (3): 417–429.

Vert, G. (2002). IRT1, an Arabidopsis Transporter Essential for Iron Uptake from the Soil and for Plant Growth. Plant Cell **14** (6): 1223–1233.

Wallace, A. (1991). Rational approaches to control of iron deficiency other than plant breeding and choice of resistant cultivars. In Iron Nutrition and Interactions in Plants: Proceedings of the Fifth International Symposium on Iron Nutrition and Interactions in Plants, 11-17 June 1989, Jerusalem, Israel, 1989, Y. Chen and Y. Hadar, eds (Kluwer Academic), pp. 332-330.

Wallace, A., and Wallace, G.A. (1992). Some of the problems concerning iron nutrition of plants after four decades of synthetic chelating agents. Journal of Plant Nutrition **15** (10): 1487–1508.

Wang, D., Guo, Y., Wu, C., Yang, G., Li, Y., and Zheng, C. (2008a). Genome-wide analysis of CCCH zinc finger family in Arabidopsis and rice. BMC Genomics **9**: 44.

Wang, L., Xu, Y., Zhang, C., Ma, Q., Joo, S.H., Kim, S.K., Xu, Z., and Chong, K. (2008b). OsLIC, a Novel CCCH-Type Zinc Finger Protein with Transcription Activation, Mediates Rice Architecture via Brassinosteroids Signaling. PLoS ONE **3** (10): e3521.

Wasternack, C. (2007). Jasmonates: An Update on Biosynthesis, Signal Transduction and Action in Plant Stress Response, Growth and Development. Ann. Bot. **100** (4): 681–697.

Waterhouse, A.M., Procter, J.B., Martin, D.M.A., Clamp, M., and Barton, G.J. (2009). Jalview Version 2--a multiple sequence alignment editor and analysis workbench. Bioinformatics **25** (9): 1189–1191.

Waters, B.M., and Grusak, M.A. (2007). Whole-plant mineral partitioning throughout the life cycle in Arabidopsis thaliana ecotypes Columbia, Landsberg erecta, Cape Verde Islands, and the mutant line ysl1ysl3. New. Phytol. **177** (20): 389–405.

Waters, B.M., Chu, H.-H., DiDonato, R.J., Roberts, L.A., Eisley, R.B., Lahner, B., Salt, D.E., and Walker, E.L. (2006). Mutations in Arabidopsis Yellow Stripe-Like1 and Yellow Stripe-Like3 Reveal Their Roles in Metal Ion Homeostasis and Loading of Metal Ions in Seeds. Plant Physiol. **141** (4): 1446–1458.

Weber, C., Nover, L., and Fauth, M. (2008). Plant stress granules and mRNA processing bodies are distinct from heat stress granules. Plant J. **56** (4): 517–530.

Weinberg, E.D. (1999). The Role of Iron In Protozoan and Fungal Infectious Diseases. J. Eukary. Microbiol. **46** (3): 231–238.

Wilczynska, A., Aigueperse, C., Kress, M., Dautry, F., and Weil, D. (2005). The translational regulator CPEB1 provides a link between dcp1 bodies and stress granules. J. Cell Sci. **118** (Pt 5): 981–992.

Wiren, N. von, Klair, S., Bansal, S., Briat, J.F., Khodr, H., Shioiri, T., Leigh, R.A., and Hider, R.C. (1999). Nicotianamine chelates both FeIII and FeII. Implications for metal transport in plants. Plant Physiol. **119** (3): 1107–1114.

Worthington, M.T., Amann, B.T., Nathans, D., and Berg, J.M. (1996). Metal binding properties and secondary structure of the zinc-binding domain of Nup475 **93** (24): 13754–13759.

Worthington, M.T., Pelo, J.W., Sachedina, M.A., Applegate, J.L., Arseneau, K.O., and Pizarro, T.T. (2002). RNA binding properties of the AU-rich element-binding recombinant Nup475/TIS11/tristetraprolin protein. J. Biol. Chem. **277** (50): 48558–48564.

Xu, J., Yang, J.Y., Niu, Q.W., and Chua, N.H. (2006). Arabidopsis DCP2, DCP1, and VARICOSE form a decapping complex required for postembryonic development. Plant Cell **18** (12): 3386–3398.

Yamaguchi-Iwai, Y., Dancis, A., and Klausner, R.D. (1995). AFT1: a mediator of iron regulated transcriptional control in Saccharomyces cerevisiae. EMBO J. **14** (6): 1231–1239.

Ye, H., Pilon, M., and Pilon-Smits, E. (2006). CpNifS-dependent iron-sulfur cluster biogenesis in chloroplasts. New Phytol **171** (2): 285–292.

Yoo, S.-D., Cho, Y.-H., and Sheen, J. (2007). Arabidopsis mesophyll protoplasts: a versatile cell system for transient gene expression analysis. Nat. Protoc. **2** (7): 1565–1572.

Yuan, Y., Wu, H., Wang, N., Li, J., Zhao, W., Du, J., Wang, D., and Ling, H.-Q. (2008). FIT interacts with AtbHLH38 and AtbHLH39 in regulating iron uptake gene expression for iron homeostasis in Arabidopsis. Cell Res. **18** (3): 385–397.

Yuan, Y.X., Zhang, J., Wang, D.W., and Ling, H.Q. (2005). AtbHLH29 of Arabidopsis thaliana is a functional ortholog of tomato FER involved in controlling iron acquisition in strategy I plants. Cell Res. **15** (8): 613–621.

Zhu, J., Fu, X., Koo, Y., Zhu, J.-K., Jenney, F., Adams, M., Zhu, Y., Shi, H., Yun, D.-J., Hasegawa, P., and Bressan, R. (2007). An enhancer mutant of Arabidopsis salt overly sensitive 3 mediates both ion homeostasis and the oxidative stress response. Mol. Cell. Biol. **27** (14): 5214–5224.

7 Supplemental data

7.1 Supplemental tables

Supplemental Table 1: Concentrations of nutrients and vitamins in 0.5 x MS medium.

Nutrient	Concentration (mg l^{-1})
NH_4NO_3	1650
H_3BO_3	6.2
$CaCl_2$, anhydrous	332.2
$CoCl_2 \cdot 6\ H_2O$	0.025
$CuSO_4 \cdot 5\ H_2O$	0.025
$Na_2EDTA \cdot 2\ H_2O$	37.26
$Fe_2(SO_4)_3 \cdot 7\ H_2O$	27.28
$MgSO_4$, anhydrous	180.7
$MnSO_4 \cdot H_2O$	16.9
$Na_2MoO_4 \cdot 2$ H2O	0.25
KI	0.83
KNO_3	1900
KH_2PO_4	170
$ZnSO_4 \cdot 7$ H2O	8.6
Glycine (free base)	2
Myo-inositol	100
Nicotinic acid (free acid)	0.5
Pyridoxine HCl	0.5
Thiamine HCl	0.1

Supplemental Table 2: Composition of calibration standards for ICP-AES.

	Concentration (µg ml^{-1})				
Element	Standard 1	Standard 2	Standard 3	Standard 4	Standard 5
B	0.05	0.1	0.2	0.6	/
Ca	40	350	250	20	10
Cd	0.01	0.05	0.1	0.2	1
Co	0.005	0.01	0.02	0.05	0.1
Cr	0.005	0.01	0.02	0.05	0.1
Cu	0.005	0.02	0.1	0.2	0.5
Fe	0.05	0.125	0.5	2	10
K	10	50	100	150	250
Mg	2.5	5	10	50	100
Mn	0.05	0.1	0.2	1	4
Mo	0.005	0.01	0.02	0.1	0.5
Na	80	40	20	4	1
Ni	0.025	0.1	0.4	2	8
P	1	5	10	20	40
S	1	5	10	20	40
Se	0.05	0.1	0.2	0.5	1
Zn	0.05	0.1	0.4	1	2

Supplemental Table 3: Wavelengths used to detect fluorophores in Confocal laser-scanning microscopy.

Fluorophor	Excitation wavelength (nm)	Recorded emission wavelength (nm)
eGFP	488	515 – 535
mCherry	563	595 – 625
Tdtomato	563	580 – 620
Imagene Green	488	515 – 535

Supplemental Table 4: Stages of pollen and stamen development (Bowman, 1994).

approximate floral stage	Pollen development stage	Stamen morphology
7	Archesporial cell divided to give rise to primary parietal and sporogenous cells	Filament and anther regions distinct
8	Microsporocytes conspicuous	Anther region becomes lobed on adaxial side
9	Pollen mother cells (PMCs) become separated from each other and from tapetum by a callose wall PMCs undergo meiosis to form tetrads (isobilateral and tetrahedral) of microspores	The three anther wall layers (endthecium, middle, tapetum) are evident
10	Microspores separate from each other after breakdown of the callose wall, and lie freely in pollen sac Microspores round up, walls thicken due to formation of the exine; bacula of exine visible	Filaments begin to elongate
11-12	First mitotic division of microspores follows resorption of prominent vacuole Second mitotic division of microspores; storage bodies visible in microspores Dessication of pollen grains	Tapetum degenerating
13		Dehiscence
14		Fertilization

Supplemental Table 5: Oligonucleotide pairs used for qPCR.

Target gene	Sequence 5'- to 3'-	comment
CTH2	CTACGCAGAAGGTGTATGTGCG	
	CCTCCTGATCTTCTTTCTTCCCTC	
CTH1	ACTGGAGCTTGTTGTTACGGC	
	GTGGATGCCTAATCACAGGAC	
EF1α	TGAGCACGCTCTTCTTGCTTTCA	Constitutively expressed gene used for target gene normalization
	GGTGGTGGCATCCATCTTGTTACA	
HEL	CCATTCTACTTTTTGGCGGCT	
	TCAATGGTAACTGATCCACTCTGATG	
IRT1	CCCCGCAAATGATGTTACCTT	Fe deficiency marker genes
	GGTATCGCAAGAGCTGTGCAT	
FRO2	ATTTACCCGATCGACCACAACA	
	TGCTCACGGAGATGACCAAGA	
FER1	TGGACACAAACAACATGCCG	
	ATTGGAATGGCCAGATCGG	
FRO3	GATTCTACTGGCTTCTCTTGG	
	CTAATCCGGCCTTCACTAAC	
YSL1	CAATGGCTTCCACACACAAGG	
	ACCACTGGAAGAAACCCCACA	
YSL2	GATTCTTTGCCTTTGCGGTTG	
	GAACGGTACAGCCATTGCCAT	
OPR3	TCGCTACCACGCCTACGG	Wounding response marker genes
	TCATCACTCCCTTGCCTTCC	
PHO1;10	TACTGGTCCCTCACAAAAGCG	
	TCACATTCACTACCATGGCTGC	
CTH2_Cterm	GGCAAGAGACAGGGACATGC	Used to quantify expression from *35S:CTH2_Cterm*
	CGTGAGCGAACTGGCAATG	
At1g62930	GAGTTGCGGGTTTGTTGGAG	Putative candidate genes for *CTH2* dependent regulation
	CAAGACAGCATTTCCAGATAGCAT	
At4g38070	GAAAGCAAAGGCGGTGAGAG	
	CAAGGCACACTTGGTTCTTCC	
At5g55840	AAGACAGTGAAGGTGCAACCTTACT	
	AGTTTTTGAGTTGTATTTGTCAGAGAAAG	
At1g07135	AGATCAAGCGGCAGCATGAA	
	AGATCAAGCGGCAGCATGAA	
At1g08940	ACGGTGGCAGAGTTCGAGC	
	TCTGAACTCGCAGTTCCCAAAG	

Oligonucleotides for qPCR, continued

Target gene	Sequence 5‘-3‘	Comment
At4g24120	TCAGGGCTAATCTGTGGCGA	Putative candidate genes for *CTH2* dependent regulation
	AAGCACCGCCGCAGGTA	
At5g10770	TCTGGCGTTTGCAGGGAATA	
	TTTCCAAAGATGGCAGCGTT	
At5g54490	AAACGCATCGACGGTTCTTG	
	CGAACATCGTCGTCCGTTAGAT	
At3g49620	TCAGGTGAAAAACGTGGACGGTGA	
	TGATCCAGGGATCGGAATAGCTGGT	
At3g55970	ACAGTCGAACCAGCTCCTCATGC	
	GCTCAGCATCTGAATTTGGTCACCC	
At4g15160	GGAGCTGGACATACAGTGCCTAGC	
	CCCTCGATGACGACAGAGGAACAC	
At5g13220	AGGAGATCTTCCCATCGCAAGGAGA	
	GAGATCGTTTAGGCCGATGTCGGA	
At5g52760	TGGAGTAGTTTCTCGAGCCATGACC	
	TCAATTGCAACACAGCGTTCTTTGC	
At5g59540	ACGGACCGATGAAAGAGCTTGTGT	
	TGCGACGTTCCATCGAGACCTT	
At1g72260	TCAGCTGATGCTACCAATGAGCACT	
	GCACATTGTTCCGACGCTCCA	
At2g44790	GAGCCAGGGTGGAGTCAGTGC	
	CTGACGTGGCACACAAACCCAA	
At5g02780	CCCGGTTAAAGAAACAGCATCAGCC	
	TAAGCTCGCCAAGGAAGAAAGGACC	
At5g47220	TTAGGATGCGTGGTTCCCGCG	
	CGAACCGGGTCAGGTTCACCG	
At4g17500	AGAAGAGGAGAACGGTGGCC	
	CCGTCAATCCCTTATCCATTCC	

Supplemental Table 6: Accession numbers of amino acid sequences used to find regions that are conserved between species in plant TZF proteins.

Species	Accession no. (Joint Genome Institute database)
Aquilegia coerulea	AcoGoldSmith_v1.017613m.aco.18143960
Arabidopsis lyrata	fgenesh2_kg.2__1068__aly.475938
	fgenesh2_kg.2__907__aly..475777
Arabidopsis thaliana	AT1G66810.1.ath.19651282
	AT1G68200.1.ath.19649512
Brachyopodium distachyon	Bradi1g64800.1.bdi.16479122
	Bradi2g15670.1.bdi.16482713
	Bradi2g45090.1.bdi.16485898
Carica papaya	evm.model.supercontig_170.22.cpa.16410841
Citrus clementine	clementine0.9_015609m.ccl.19253494
	clementine0.9_031938m.ccl.19268777
Citrus sinensis	orange1.1g020338m.csi.18138922
	orange1.1g022289m.csi.18131094
Cucumis sativus	Cucsa.087930.1.csa.16956924
	Cucsa.280660.1.csa.16974246
Eucalyptus grandis	Eucgr.F02796.1.egr.18760010
Glycine max	Glyma10g41530.1.gma.16281765
	Glyma20g25710.1.gma.16316827
Manihot esculenta	cassava4.1_022862m.mes.17991169
	cassava4.1_030852m.mes.17989575
	cassava4.1_032507m.mes.17987534
Mimulus guttatus	mgv1a021661m.mgu.17685549
	mgv1a024953m.mgu.17673752
	mgv1a026739m.mgu.17685692
Oryza sativa	LOC_Os01g45730.1.osa.16833923
	LOC_Os05g50080.1.osa.16863029
Populus trichocarpa	POPTR_0005s15100.1.ptr.18206865
	POPTR_0010s12860.1.ptr.18240251
Prunus persica	ppa017322m.ppe.17657913
	ppa018479m.ppe.17650619
Ricinus communis	29586.m000617.rco.16803197
	29660.m000770.rco.16805019
Setaria italica	Si002050m.sit.19677948
	Si022648m.sit.19700258
	Si039512m.sit.19684629
Sorghum bicolor	Sb01g037830.1.sbi.1953669
	Sb09g029330.1.sbi.1981948
Vitis vinifera	GSVIVT01011819001.vvi.17823589
	GSVIVT01030969001.vvi.17837284
Zea mays	GRMZM2G149347_T02.zma.19508089
	GRMZM2G157927_T02.zma.19521485
	GRMZM2G427438_T01.zma.19610364
	GRMZM5G830949_T01.zma.19576822

Supplemental Table 7: Genes with significantly different transcript levels in *cth2-2 vs.* WT anthers.

(a) Top 100 up-regulated genes in *cth2-2* anthers compared to WT anthers.

AGI	Tair symbol	Description	log_2FC *cth2-2* / WT	Adjusted *p* value	Contains ARE in 3'-UTR
At1g48940	ENODL6	Early nodulin-like protein 6	4.49	0.0016	-
At4g25920		Protein of unknown function (DUF295)	4.18	0.0011	-
At4g24890	PAP24	Probable inactive purple acid phosphatase 24	4.00	0.0021	-
At1g56360	PAP6	Purple acid phosphatase 6	3.99	0.0013	-
At5g02140		Pathogenesis-related thaumatin superfamily protein	3.80	0.0011	-
At2g21640		Unknown marker for oxidative stress response.	3.63	0.0011	yes
At5g08030		PLC-like phosphodiesterases superfamily protein	3.54	0.0014	-
At2g20970		Unknown protein	3.47	0.0013	-
At2g39590		Ribosomal protein S8 family protein	3.45	0.0013	-
At3g50580		Unknown protein	3.44	0.0021	-
At2g46880	PAP14	Purple acid phosphatase 14	3.43	0.0023	-
At5g17340		Putative membrane lipoprotein	3.43	0.0011	-
At2g16520			3.42	0.0019	-
At4g36350	PAP25	Purple acid phosphatase 25	3.39	0.0015	-
At3g30730		unknown protein	3.36	0.0011	-
At1g74990		RING/U-box superfamily protein	3.33	0.0011	-
At3g45320		Unknown protein	3.30	0.0021	-
At3g18610	PARLL1	Nucleolin like 2	3.21	0.0011	yes
At1g22010		Unknown protein	3.17	0.0034	-
At1g29090		Cysteine proteinases superfamily protein	3.14	0.0013	-
At3g03510		Phototropic-responsive NPH3 family protein	3.14	0.0011	-
At2g03170	ASK14	SKP1-like 14	3.13	0.0026	-
At1g64220	TOM7-2	Translocase of outer membrane 7 kDa subunit 2	3.12	0.0016	-
At5g53510	OPT9	Oligopeptide transporter 9	3.09	0.0011	-
At1g61800	GPT2	Glucose-6-phosphate/phosphate translocator 2	3.08	0.0011	-
At1g61630	ENT7	Equilibrative nucleoside transporter 7	3.05	0.0013	-
At1g36150		Bifunctional inhibitor/lipid-transfer protein/seed storage 2S albumin superfamily protein	3.00	0.0066	-
At5g59240		40S ribosomal protein S8-2	2.99	0.0015	-
At3g58290		TRAF-like superfamily protein	2.96	0.0016	-
At3g15440		Unknown protein	2.96	0.0011	-
At5g63690		Nucleic acid-binding, OB-fold-like protein	2.90	0.0011	-
At5g57980	RPB5C	RNA polymerase II fifth largest subunit, C	2.88	0.0013	-
At5g61940		Ubiquitin carboxyl-terminal hydrolase-related protein	2.86	0.0018	-
At3g09380		Protein of unknown function (DUF59)	2.86	0.0014	-
At5g53960		ATP binding;DNA binding;DNA topoisomerase (ATP-hydrolyzing)s	2.81	0.0016	yes
At5g43340	PHT6	Phosphate transporter 1;6	2.80	0.0025	-

AGI	Tair symbol	Description	log_2FC *cth2-2* / WT	Adjusted *p* value	Contains ARE in 3'-UTR
At5g59810	SBT5.4	Subtilase family protein	2.80	0.0018	-
At3g28540		P-loop containing nucleoside triphosphate hydrolases superfamily protein	2.79	0.0063	yes
At5g51440		HSP20-like chaperones superfamily protein	2.79	0.0011	-
At3g15357		Unknown protein	2.77	0.0017	-
At3g28230		Unknown protein	2.75	0.0011	-
At2g28680		RmlC-like cupins superfamily protein	2.75	0.0018	yes
At1g21290		Transposable element gene	2.71	0.0017	-
At2g20800	NDB4	NAD(P)H dehydrogenase B4	2.7	0.0011	-
At3g01070	ENODL16	Early nodulin-like protein 16	2.67	0.0015	-
At1g07340	STP2	Sugar transporter 2	2.62	0.0042	-
At1g07180	NDI1	Alternative NAD(P)H dehydrogenase 1	2.61	0.0011	-
At5g13600		Phototropic-responsive NPH3 family protein	2.58	0.0036	-
At3g51920	CAM9	Calmodulin 9	2.58	0.0013	-
At1g17960		Threonyl-tRNA synthetase	2.57	0.0034	-
At2g41730		Unknown protein	2.56	0.0049	yes
At1g79800	ENODL7	Early nodulin-like protein 7	2.54	0.0013	-
At4g13700	PAP23	purple acid phosphatase 23	2.54	0.0022	-
At1g68200	CTH2	Zinc finger C-x8-C-x5-C-x3-H type family protein	2.53	0.0011	-
At2g42480		TRAF-like family protein	2.52	0.0012	-
At1g22090		Protein of unknown function (DUF626)	2.49	0.003	-
At4g05230		Ubiquitin-like superfamily protein	2.48	0.0029	-
At4g29650		Cytidine/deoxycytidylate deaminase family protein	2.43	0.0034	-
At1g70400		Unknown protein	2.43	0.0011	yes
At5g06520		SWAP (Suppressor-of-White-APricot)/surp domain-containing protein	2.43	0.0011	-
At4g24950		Unknown protein	2.41	0.0069	-
At5g63750	ARI13	RING/U-box superfamily protein	2.40	0.0016	-
At5g41090	NAC95	NAC domain containing protein 95	2.40	0.0049	-
At2g04025	RGF3	Encodes a root meristem growth factor (RGF)	2.38	0.0011	-
At2g29880		Unknown protein	2.38	0.0036	yes
At4g10260		pfkB-like carbohydrate kinase family protein	2.37	0.0065	yes
At1g36240		Ribosomal protein L7Ae/L30e/S12e/Gadd45 family protein	2.36	0.0013	-
At2g16360		Ribosomal protein S25 family protein	2.34	0.0046	-
At5g43590		Acyl transferase/acyl hydrolase/lysophospholipase superfamily protein	2.29	0.0017	-
At5g64870		SPFH/Band 7/PHB domain-containing membrane-associated protein family	2.29	0.0043	yes
At4g35120		Galactose oxidase/kelch repeat superfamily protein	2.28	0.002	-
At2g36180		EF hand calcium-binding protein family	2.27	0.0069	-
At2g48130		Bifunctional inhibitor/lipid-transfer protein/seed storage 2S albumin superfamily protein	2.27	0.0021	yes
At1g08670		ENTH/VHS family protein	2.24	0.0042	-
At1g80740	CMT1	Chromomethylase 1	2.24	0.0031	-

AGI	Tair symbol	Description	log_2FC *cth2-2* / WT	Adjusted *p* value	Contains ARE in 3'-UTR
At3g59480		pfkB-like carbohydrate kinase family protein	2.24	0.0017	-
At1g23410		Ribosomal protein S27a / Ubiquitin family protein	2.21	0.0038	-
At1g01640		BTB/POZ domain-containing protein	2.20	0.0018	yes
At2g11810	MGDC	monogalactosyldiacylglycerol synthase type C	2.20	0.0027	-
At5g48550		F-box associated ubiquitination effector family protein	2.19	0.0056	-
At4g15210	BETA-AMY	β-amylase 5	2.19	0.0024	yes
At1g50400		Eukaryotic porin family protein	2.17	0.0105	-
At5g09380		DNA-directed RNA polymerase III RPC4 family protein	2.16	0.0018	-
At3g16580		F-box/kelch-repeat protein At3g16580	2.15	0.002	yes
At3g52450	PUB22	Plant U-box 22	2.14	0.0078	yes
At3g24130		Pectin lyase-like superfamily protein	2.13	0.0013	-
At5g40260	SWEET8	Nodulin MtN3 family protein	2.13	0.002	-
At5g48710		Ubiquitin-like superfamily protein	2.11	0.0034	-
At2g31770	ARI9	RING/U-box superfamily protein	2.10	0.0021	-
At5g63070		Ribosomal protein S19 family protein	2.09	0.0091	-
At4g00390		DNA-binding storekeeper protein-related transcriptional regulator	2.09	0.0046	-
At2g18190		P-loop containing nucleoside triphosphate hydrolases superfamily protein	2.09	0.0013	-
At1g69480		EXS (ERD1/XPR1/SYG1) family protein	2.08	0.0013	-
At3g61610		Galactose mutarotase-like superfamily protein	2.07	0.0043	-
At5g02050		Mitochondrial glycoprotein family protein	2.07	0.0027	-
At4g28460		Unknown protein	2.07	0.0013	-
At1g05290		CCT motif family protein	2.06	0.0013	-
At5g08600		U3 ribonucleoprotein (Utp) family protein	2.05	0.0021	-
At2g47010		Unknown protein	2.03	0.0018	-
At5g17470		EF hand calcium-binding protein family	2.03	0.0051	-

(b) Top 100 down-regulated genes in *cth2-2* anthers compared to WT anthers

AGI	Tair symbol	Description	log_2FC *cth2-2* / WT	Adjusted *p* value	Contains ARE in 3'-UTR
At1g68610	PCR11	PLANT CADMIUM RESISTANCE 11	-6.85	0.0011	-
At3g62230		F-box protein	-6.8	0.0033	yes
At1g01980		FAD-binding Berberine family protein	-6.61	0.0038	yes
At1g75870		Unknown protein	-6.56	0.0011	-
At1g49290		Unknown protein	-6.49	0.002	-
At2g26850		F-box family protein	-6.29	0.0014	-
At5g20390		Glycosyl hydrolase superfamily protein	-6.28	0.0024	yes
At1g14420		Pectate lyase family protein	-6.2	0.0018	-

AGI	Tair symbol	Description	log_2FC *cth2-2* / WT	Adjusted *p* value	Contains ARE in 3'-UTR
At1g54070		Dormancy/auxin associated family protein	-6.11	0.0023	-
At2g05850	SCPLl38	Serine carboxypeptidase-like 38	-6.08	0.0013	-
At5g27870		Plant invertase/pectin methylesterase inhibitor superfamily	-6.08	0.0016	-
At4g39610		Protein of unknown function, DUF617	-6.04	0.0025	yes
At3g06830		Plant invertase/pectin methylesterase inhibitor superfamily	-6.03	0.0016	yes
At1g66210		Subtilisin-like serine endopeptidase family protein	-6.02	0.0028	yes
At1g23350		Plant invertase/pectin methylesterase inhibitor superfamily protein	-5.99	0.0035	-
At3g20530		Protein kinase superfamily protein	-5.99	0.0015	yes
At5g39400	PTEN1	PTEN1; phosphatase	-5.98	0.0027	yes
At2g02720		Pectate lyase family protein	-5.9	0.0027	-
At2g44560	GH9B11	Glycosyl hydrolase 9B11	-5.88	0.0016	yes
At2g31500	CPK24	Calcium-dependent protein kinase 24	-5.87	0.0016	-
At5g65530		Protein kinase superfamily protein	-5.83	0.0013	-
At5g23270	STP11	Sugar transporter 11	-5.8	0.0024	-
At3g02970	EXL6	EXORDIUM like 6	-5.78	0.0027	-
At1g25240		ENTH/VHS/GAT family protein	-5.77	0.0029	-
At1g30710		FAD-binding Berberine family protein	-5.77	0.0018	yes
At4g35700		Zzinc finger (C2H2 type) family protein	-5.77	0.0011	-
At5g61710		Unknown protein	-5.75	0.0013	-
At3g06260	GATL4	Galacturonosyltransferase-like 4	-5.75	0.0016	yes
At3g20580	COBL10	COBRA-like protein 10 precursor	-5.73	0.0016	-
At3g43860	GH9A4	Glycosyl hydrolase 9A4	-5.72	0.0024	-
At4g27580		Unknown protein	-5.69	0.0023	yes
At2g41860	CPK14	Calcium-dependent protein kinase 14	-5.68	0.0013	yes
At2g18180		Sec14p-like phosphatidylinositol transfer family protein	-5.67	0.0012	-
At3g19020		Leucine-rich repeat (LRR) family protein	-5.66	0.0027	yes
At3g25170	RALFL26	RALF-like 26	-5.64	0.0033	yes
At1g18990		Protein of unknown function, DUF593	-5.64	0.0017	-
At5g15140		Aldose-1 epimerase family protein	-5.64	0.0016	yes
At5g12000		Protein kinase protein with adenine nucleotide alpha hydrolases-like domain	-5.63	0.0018	yes
At2g26450		Plant invertase/pectin methylesterase inhibitor superfamily	-5.62	0.0028	-
At3g54800		Pleckstrin homology (PH) and lipid-binding START domains-containing protein	-5.6	0.0026	yes
At2g33420		Protein of unknown function (DUF810)	-5.59	0.0016	yes
At3g62710		Glycosyl hydrolase family protein	-5.59	0.0027	yes
At2g15880		Leucine-rich repeat (LRR) family protein	-5.59	0.0013	-
At1g01460	PIPK11	Phosphatidylinositol-4-phosphate 5-kinase, core	-5.58	0.0011	-
At5g04180	ACA3	ACA3 (ALPHA CARBONIC ANHYDRASE 3); carbonate dehydratase/ zinc ion binding	-5.58	0.0028	-

AGI	Tair symbol	Description	log_2FC *cth2-2* / WT	Adjusted *p* value	Contains ARE in 3'-UTR
At1g76370		Protein kinase superfamily protein	-5.54	0.0018	yes
At2g47340		Plant invertase/pectin methylesterase inhibitor superfamily protein	-5.53	0.0016	-
At1g04540		Calcium-dependent lipid-binding (CaLB domain) family protein	-5.53	0.0013	-
At2g24450	FLA3	FASCICLIN-like arabinogalactan protein 3 precursor	-5.52	0.0018	yes
At1g11770		FAD-binding Berberine family protein	-5.51	0.0036	-
At3g25165	RALFL25	RALF-like 25	-5.5	0.0031	yes
At2g46360		Unknown protein	-5.5	0.0012	yes
At3g17980		C2 domain-containing protein	-5.49	0.0025	yes
At4g03290		EF hand calcium-binding protein family	-5.49	0.0036	yes
At1g49490		Leucine-rich repeat (LRR) family protein	-5.48	0.0013	-
At4g24640	APPB1	Plant invertase/pectin methylesterase inhibitor superfamily protein	-5.48	0.0021	yes
At3g17060		Pectin lyase-like superfamily protein	-5.48	0.0034	yes
At5g39420	CDC2c	ATP binding / kinase/ protein kinase/ protein serine/threonine kinase.	-5.46	0.0013	yes
At5g41780		Myosin heavy chain-related	-5.46	0.0016	-
At1g03050		ENTH/ANTH/VHS superfamily protein	-5.45	0.0012	-
At1g44160		HSP40/DnaJ peptide-binding protein	-5.45	0.0015	-
At3g20220		SAUR-like auxin-responsive protein family	-5.44	0.0039	-
At4g04980		Unknown protein	-5.44	0.0011	-
At3g05610		Plant invertase/pectin methylesterase inhibitor superfamily	-5.44	0.0025	yes
At3g50310	MAPKKK20	Mitogen-activated protein kinase kinase kinase 20	-5.44	0.0013	-
At5g16100		Unknown protein	-5.43	0.0011	-
At3g21570		Unknown protein	-5.41	0.0023	yes
At2g23900		Pectin lyase-like superfamily protein	-5.4	0.0013	yes
At1g78460		SOUL heme-binding family protein	-5.38	0.0019	yes
At1g60240		NAC domain transcriptional regulator superfamily protein	-5.37	0.0013	-
At1g01310		CAP (Cysteine-rich secretory proteins, Antigen 5, and Pathogenesis-related 1 protein) superfamily protein	-5.37	0.0013	-
At1g68110		ENTH/ANTH/VHS superfamily protein	-5.36	0.002	yes
At3g52600	INV2	Cell wall invertase 2	-5.36	0.0041	-
At4g25780		CAP (Cysteine-rich secretory proteins, Antigen 5, and Pathogenesis-related 1 protein) superfamily protein	-5.35	0.0019	-
At3g02810		Protein kinase superfamily protein	-5.35	0.002	-
At5g28680	ANX2	Malectin/receptor-like protein kinase family protein	-5.34	0.0026	-
At5g12180	CPK17	Calcium-dependent protein kinase 17	-5.34	0.0011	-
At2g16730	BGAL13	Glycosyl hydrolase family 35 protein	-5.3	0.0035	-
At5g27980		Seed maturation protein	-5.3	0.0027	-
At2g45800		GATA type zinc finger transcription factor family protein	-5.3	0.0023	yes
At1g70540	EDA24	Plant invertase/pectin methylesterase inhibitor superfamily protein	-5.29	0.0025	-
At3g18810		Protein kinase superfamily protein	-5.29	0.0012	-

AGI	Tair symbol	Description	log_2FC *cth2-2* / WT	Adjusted *p* value	Contains ARE in 3'-UTR
At2g33870	RABA1h	RABA1h (Arabidopsis Rab GTPase homolog A1h); GTP binding	-5.27	0.0011	-
At3g11740		Protein of unknown function (DUF567)	-5.25	0.0015	yes
At1g79860	ATROPGEF12	RHO guanyl-nucleotide exchange factor 12	-5.23	0.0011	-
At5g46770		Unknown protein	-5.22	0.0011	yes
At3g01620		beta-1,4-N-acetylglucosaminyltransferase family protein	-5.17	0.0012	yes
At2g19010		GDSL-like Lipase/Acylhydrolase superfamily protein	-5.16	0.0016	-
At4g15980		Plant invertase/pectin methylesterase inhibitor superfamily	-5.16	0.0013	-
At4g18395		Unknown protein	-5.16	0.0013	yes
At5g39310	ATEXPA24	Expansin A24	-5.15	0.0027	-
At3g55180		α/β-Hydrolases superfamily protein	-5.14	0.0013	-
At3g10460		Plant self-incompatibility protein S1 family	-5.13	0.0037	yes
At5g45840		Leucine-rich repeat protein kinase family protein	-5.13	0.0013	-
At3g04630	WDL1	WVD2-like 1	-5.12	0.0012	yes
At3g26110		Anther-specific protein agp1-like	-5.12	0.0027	-
At3g28770		Protein of unknown function (DUF1216)	-5.12	0.0013	-
At1g10620		Protein kinase superfamily protein	-5.12	0.0013	-
At1g61860		Protein kinase superfamily protein	-5.09	0.0011	yes
At5g42340	PUB15	Plant U-Box 15	-5.09	0.0013	-

7.2 Supplemental Figures

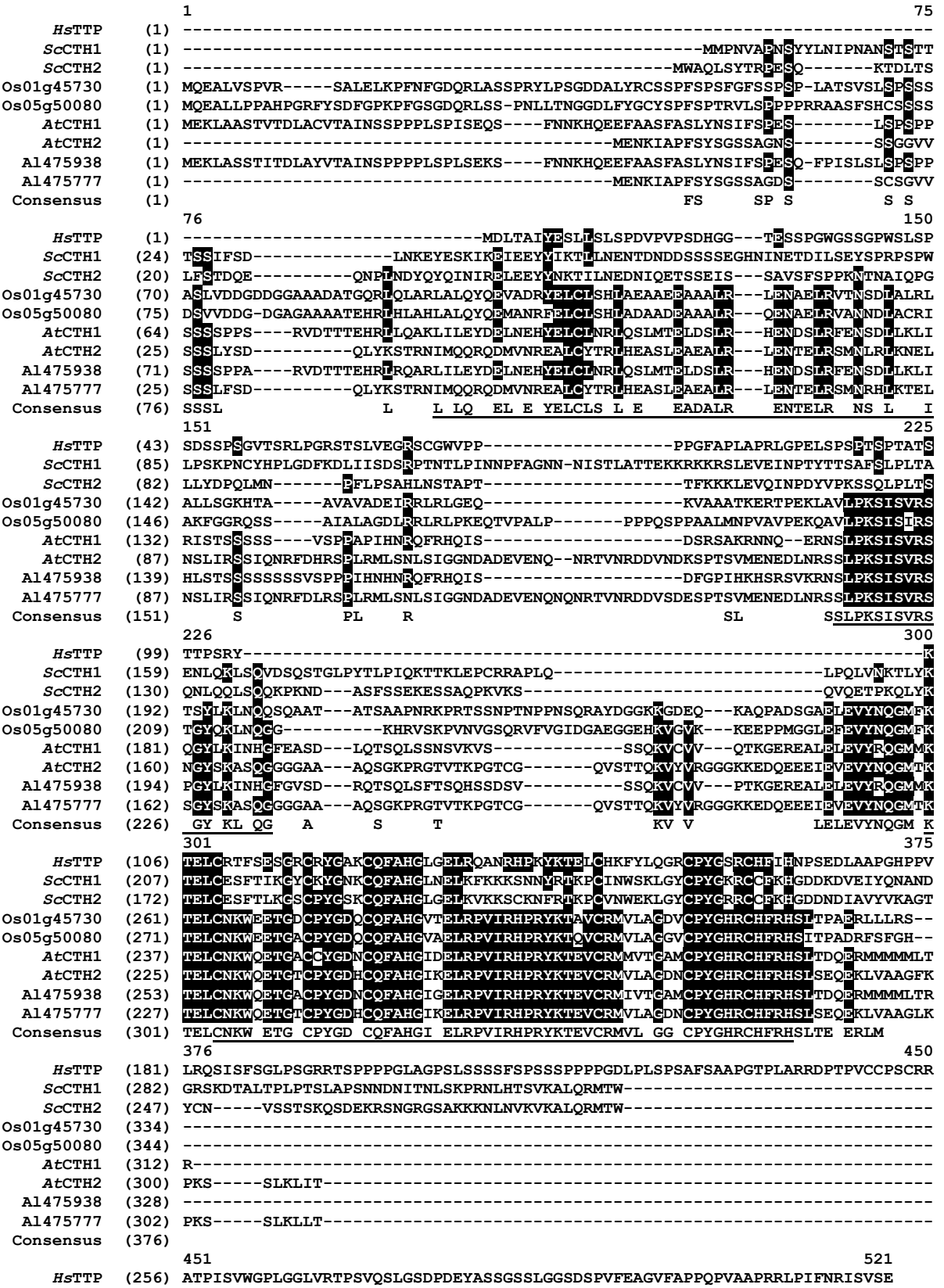

Supplemental Figure 1: Alignment of amino acid sequences of nine TZF-proteins.

Shown is an alignment of amino acid sequences of nine TZF-proteins using the CLUSTALX algorithm. White-on-black characters show residues conserved in at least five of the sequences. *Hs*TTP, *Sc*CTH1/2 and *At*CTH1/2

are described in the main text (chapters 1.8.1, 1.10 and 4.1). Os01g45730 and Os05g50080 are two rice loci encoding the proteins most similar to *At*CTH2. Al475938 and Al475777 are two *Arabidopsis lyrata* loci encoding the proteins most similar to *At*CTH2. The underlined parts of the consensus sequence represent the conserved regions 1 and 2 and the TZF domain (see Fig. 1c).

```
           1                                                                    75
WT CTH2    (1)ATGGAAAACAAAATCGCGCCGTTTAGTTACAGCGGAAGCTCCGCCGGAAATTCATCCAGTGGCGGCGTCGTTTCG
cth2-1     (1)-------------------------------------------------------------------------
cth2-2     (1)ATGGAAAACAAAATCGCGCCGTTTAGTTACAGCGGAAGCTCCGCCGGAAATTCATCCAGTGGCGGCGTCGTTTCG
           76                                                                  150
WT CTH2   (76)TCGTCTCTCTACTCTGATCAACTCTACAAGTCGACTCGCAACATAATGCAACAGCGTCAAGATATGGTGAATCGC
cth2-1     (1)-------------------------------------------------------------------------
cth2-2    (76)TCGTCTCTCTACTCTGATCAACTCTACAAGTCGACTCGCAACATAATGCAACAGCGTCAAGATATGGTGAATCGC
          151                                                                  225
WT CTH2 (151)GAGGCGTTGTGTTACACGCGTCTCCATGAGGCTTCGCTTGAAGCAGAAGCGCTTCGTCTAGAGAACACTGAACTC
cth2-1     (1)-------------------------------------------------------------------------
cth2-2  (151)GAGGCGTTGTGTTACACGCGTCTCCATGAGGCTTCGCTTGAAGCAGAAGCGCTTCGTCTAGAGAACACTGAACTC
          226                                                                  300
WT CTH2 (226)CGATCGATGAATCTTCGTCTCAAGAATGAGCTCAACAGTCTCATCAGATCTTCGATCCAGAACCGATTTGATCAT
cth2-1     (1)-------------------------------------------------------------------------
cth2-2  (226)CGATCGATGAATCTTCGTCTCAAGAATGAGCTCAACAGTCTCATCAGATCTTCGATCCAGAACCGATTTGATCAT
          301                                                                  375
WT CTH2 (301)CGATCTCCGCTTCGGATGCTTAGCAATCTTTCGATCGGAGGTAATGACGCCGACGAAGTGGAGAATCAGAACCGT
cth2-1     (1)-------------------------------------------------------------------------
cth2-2  (301)CGATCTCCGCTTCGGATGCTTAGCAATCTTTCGATCGGAGGTAATGACGCCGACGAAGTGGAGAATCAGAACCGT
          376                                                                  450
WT CTH2 (376)ACGGTTAATCGCGATGACGTCAATGATAAGAGTCCGACGAGTGTTATGGAGAATGAGGATCTGAATCGCTCTTCG
cth2-1     (1)-------------------------------GTCCGACGAGTGTTATGGAGAATGAGGATCTGAATCGCTCTTCG
cth2-2  (376)ACGGTTAATCGCGATGACGTCAATGATAAGAGTCCGACGAGTGTTATGGAGAATGAGGATCTGAATCGCTCTTCG
          451                                                                  525
WT CTH2 (451)CTTCCAAAGAGCATCTCTGTGAGATCTAATGGCTACTCTAAGGCAAGTCAGGGAGGTGGTGGTGCGGCTGCTCAA
cth2-1    (45)CTTCCAAAGAGCATCTCTGTGAGATCTAATGGCTACTCTAAGGCAAGTCAGGGAGGTGGTGGTGCGGCTGCTCAA
cth2-2  (451)CTTCCAAAGAGCATCTCTGTGAGATCTAATGGCTACTCTAAGGCAAGTCAGGGAGGTGGTGGTGCGGCTGCTCAA
          526                                                                  600
WT CTH2 (526)AGTGGAAAACCTCGTGGAACCGTCACTAAGCCTGGGACTTGTGGTCAAGTCAGTACTACGCAGAAGGTGTATGTG
cth2-1  (120)AGTGGAAAACCTCGTGGAACCGTCACTAAGCCTGGGACTTGTGGTCAAGTCAGTACTACGCAGAAGGTGTATGTG
cth2-2  (526)AGTGGAAAACCTCGTGGAACCGTCACTAAGCCTGGGACTTGTGGTCAAGTCAGTACTACGCAGAAGGTGTATGTG
          601                                                                  675
WT CTH2 (601)CGAGGAGGAGGGAAGAAAGAAGATCAGGAGGAAGAGATAGAAGTGGAGGTGTACAATCAAGGGATGACAAAGACA
cth2-1  (195)CGAGGAGGAGGGAAGAAAGAAGATCAGGAGGAAGAGATAGAAGTGGAGGTGTACAATCAAGGGATGACAAAGACA
cth2-2  (601)CGAGGAGGAGGGAAGAAAGAAGATCAGGAGGAAGAGATAGAAGTGGAGGTGTACAATCAAGGGATGACAAAGACA
          676                                                                  750
WT CTH2 (676)GAGCTGTGCAACAAATGGCAAGAGACAGGGACATGCCCATATGGTGACCATTGCCAGTTCGCTCACGGCATTAAG
cth2-1  (270)GAGCTGTGCAACAAATGGCAAGAGACAGGGACATGCCCATATGGTGACCATTGCCAGTTCGCTCACGGCATTAAG
cth2-2  (676)GAGCTGTGCAACAAATGGCAAGAGACAGGGACATGCCCATATGGTGACCATTGCCAGTTCGCTCACGGCA-----
          751                                                                  825
WT CTH2 (751)GAACTCCGTCCAGTGATCCGCCATCCCCGTTACAAGACTGAGGTTTGCAGAATGGTTCTTGCTGGTGATAACTGT
cth2-1  (345)GAACTCCGTCCAGTGATCCGCCATCCCCGTTACAAGACTGAGGTTTGCAGAATGGTTCTTGCTGGTGATAACTGT
cth2-2  (746)-------------------------------------------------------------------------
          826                                                                  900
WT CTH2 (826)CCTTATGGTCACCGTTGCCACTTCCGCCACTCACTATCTGAGCAGGAGAAGCTCGTTGCTGCTGGTTTCAAACCC
cth2-1  (420)CCTTATGGTCACCGTTGCCACTTCCGCCACTCACTATCTGAGCAGGAGAAGCTCGTTGCTGCTGGTTTCAAACCC
cth2-2  (746)-------------------------------------------------------------------------
          901                          927
WT CTH2 (901)AAGTCATCCCTCAAGCTGATCACATGA
cth2-1  (495)AAGTCATCCCTCAAGCTGATCACATGA
cth2-2  (746)---------------------------
```

Supplemental Figure 2: Alignment of full-length and partial *CTH2* cDNA sequences.

Shown is an alignment of the full-length *CTH2* cDNA with the sequences obtained from sequencing of the partial transcripts found in *cth2-1* and in *cth2-2*. The full-length *CTH2* cDNA sequence was obtained from TAIR. Partial *CTH2* transcripts were amplified by PCR as described in the main text, cloned into pGEM-T and sequenced using vector-specific primers. The 5'- and 3'- ends of the sequencing results were trimmed to remove vector sequences, and in the case of *cth2-1* T-DNA sequences.

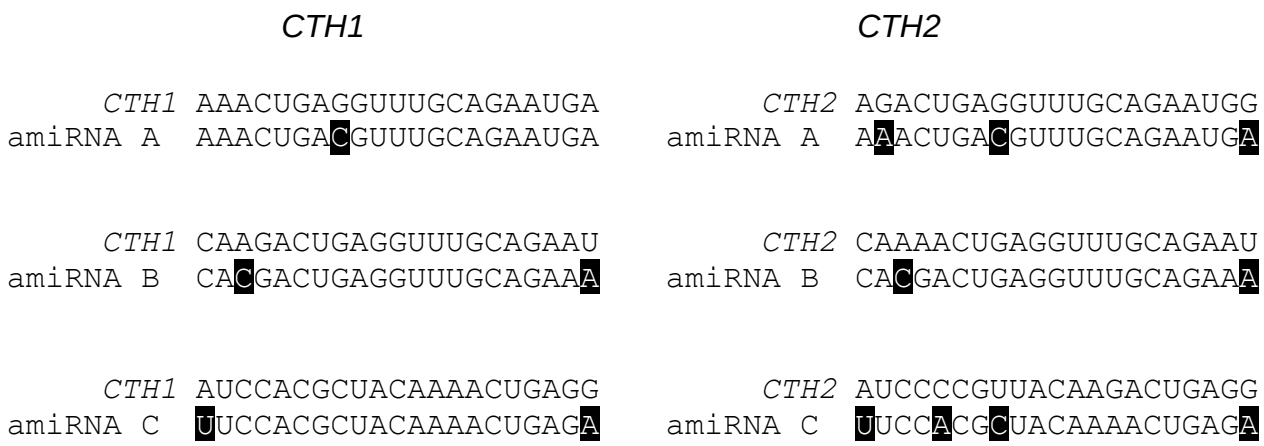

Supplemental Figure 3: Alignment of amiRNA targeting portions with their transcript target sequences.

Shown are RNA sequence alignments of three amiRNAs (amiRNA A, amiRNA B, amiRNA C), all designed to silence *CTH1* and *CTH2*. The amiRNA sequences show the portion of the mature amiRNA that gives target specificity. *CTH* sequences are from the respective transcript. White-on-black characters show mismatches between the amiRNA and the target sequences.

(a)

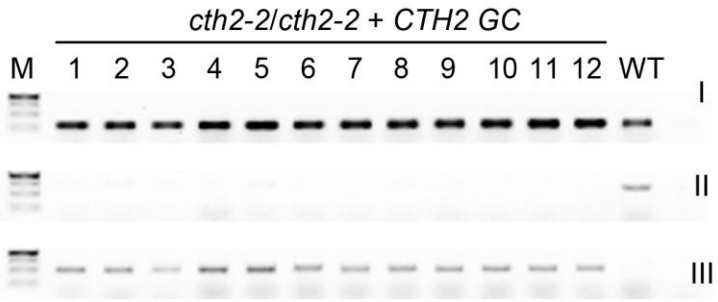

(b)

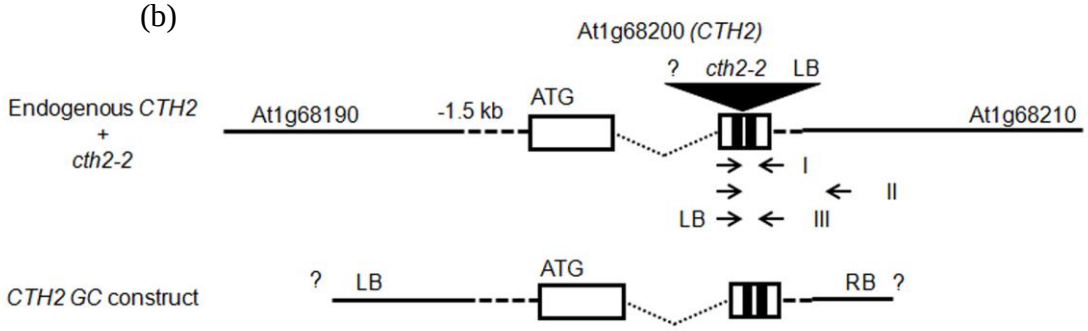

(c)

	I	II	III
endogenous *CTH2*	309 bp	725 bp	-
CTH2 GC	309 bp	-	-
cth2-2 T-DNA	-	-	542 bp

Supplemental Figure 4: Genotyping strategy for genetically complemented *cth2-2* plants.

Shown is (a) an agarose gel with PCR products from genotyping reactions for 12 homozygous *cth2-2* plants, carrying the *CTH2 GC* constructs, (b) a schematic representation of the *CTH2* locus showing the position of the *cth2-2* insertion in comparison to the *CTH2* genomic complementation construct (*CTH2 GC*) and (c) a table with expected amplicon sizes for each primer combination. To generate *cth2-2 GC* plants *CTH2/cth2-2* plants were transformed with the GC construct. T1 plants were screened using hygromycin to select for the presence of the *CTH2* GC construct. Hygromycin resistant plants were genotyped by PCR (data not shown) and homozygous *cth2-2* plants were propagated to the T2 generation. Plant in the T2 generation were selected by hygromycin for the presence of the *CTH2 GC* construct and genotyped by PCR. In (a) three different primer combinations are used to amplify a product from (I) the endogenous and the transgenic *CTH2*, (II) only the endogenous *CTH2* or (III) the T-DNA insertion found in *cth2-2*. Lanes were loaded with a size standard (M; band sizes are, from top to bottom 1000 bp, 750 bp, 500 bp, 250 bp) or PCR reactions using genomic DNA from *cth2-2*/*cth2-2 + CTH2 GC* plant or WT plants as a template. In (b) dashed lines represent promoter and UTRs, white boxes represent exons, dashed angled lines represent the intron, black boxes represent the sequences encoding the CCCH-type zinc fingers, LB and RB are T-DNA border sequences, ATG is the translational start, ? is an unidentified T-DNA border or unknown genomic sequences adjacent to the insertion site of the *CTH2* GC construct and arrows represent annealing sites of primers used for reaction I-III. Note that the reverse primer for reaction II anneals in the intergenic region which is not found in the *CTH2* genomic complementation construct. The gene representation is not drawn to scale. In (c), expected product sizes for each primer pair (I-III) are given. – indicates that no product is expected.

7.3 Vector maps

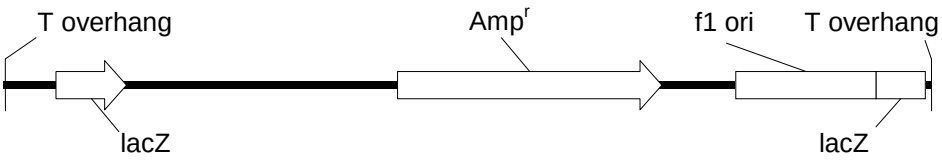

pGEM-T easy
3017 bp

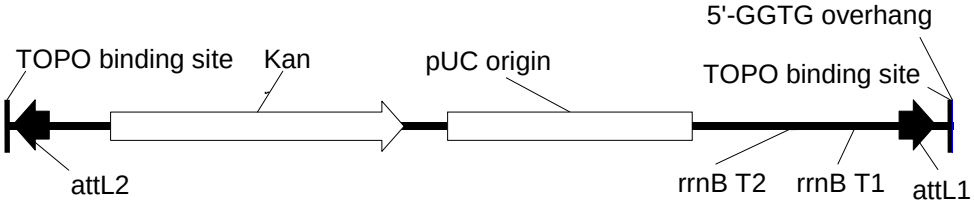

pENTR/D-TOPO
2610 bp

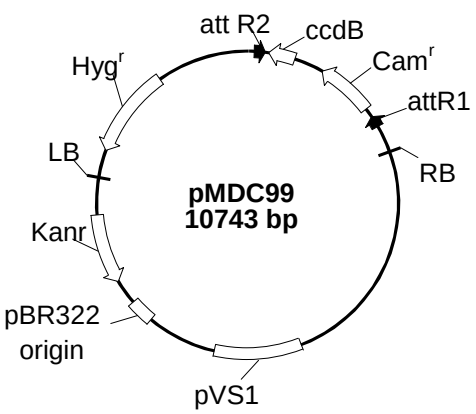

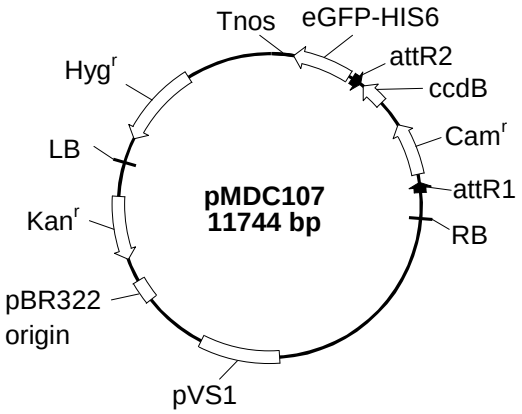

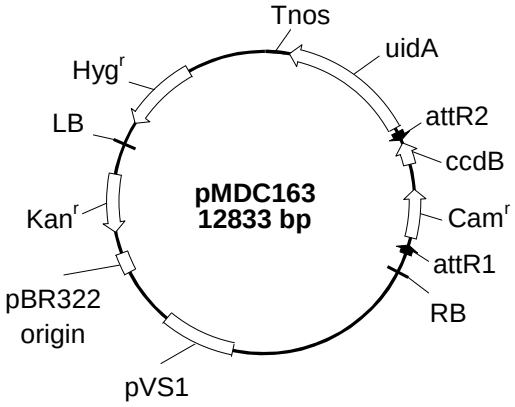

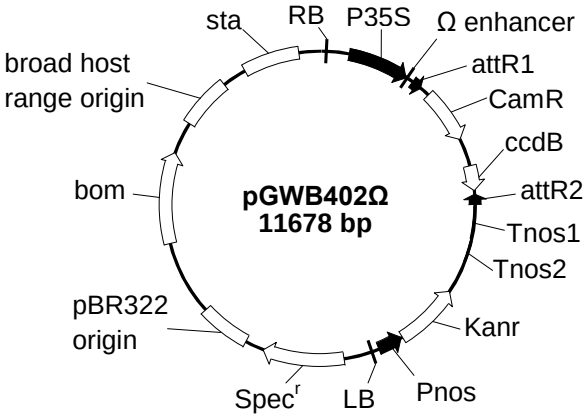

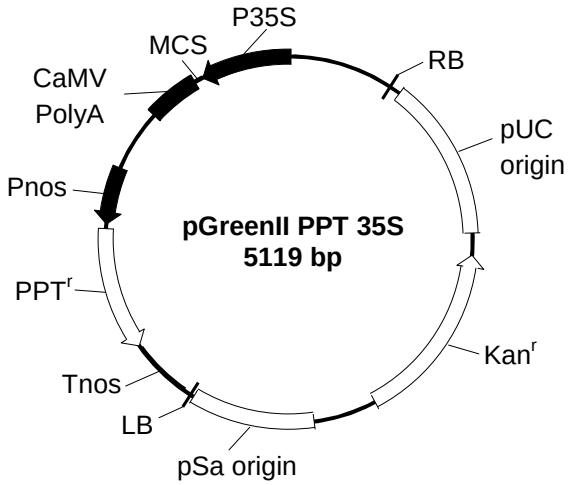
P35S
MCS
CaMV
PolyA
RB
pUC
origin
Pnos
pGreenII PPT 35S
5119 bp
PPTr
Kanr
Tnos
LB
pSa origin

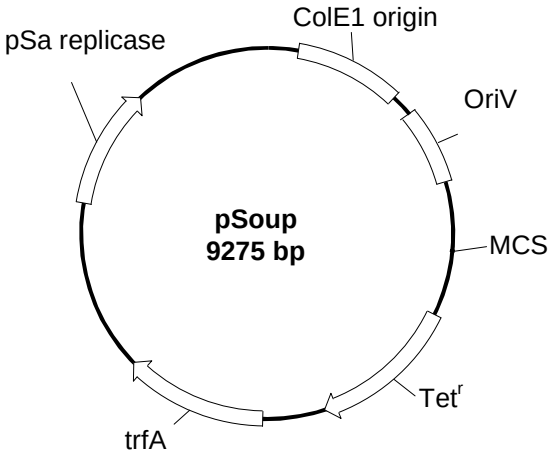
ColE1 origin
pSa replicase
OriV
pSoup
9275 bp
MCS
Tetr
trfA

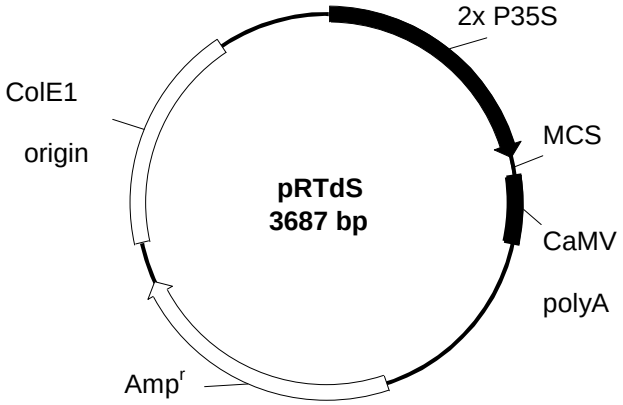
2x P35S
ColE1
origin
MCS
pRTdS
3687 bp
CaMV
polyA
Ampr

8 Declaration (Erklärung)

Hiermit erkläre ich, dass ich die vorgelegte Dissertation selbst verfasst und mich dabei keiner anderen als der von mir bezeichneten Quellen und Hilfen bedient habe.

Außerdem erkläre ich hiermit, dass ich an keiner anderen Stelle ein Prüfungsverfahren beantragt bzw. die Dissertation in dieser oder anderer Form bereits anderweitig als Prüfungsarbeit verwendet oder einer anderen Fakultät als Dissertation vorgelegt habe.

Bochum, 15.06.2012

(Stefan Reuscher)

9 Acknowledgments

An dieser Stelle möchte ich all den Menschen danke die mich in den letzten Jahren während meiner Promotion unterstützt haben.

Mein Dank gilt an erster Stelle Frau Professor Dr. Ute Krämer für die Aufnahme in ihre Arbeitsgruppe, die wissenschaftliche Betreuung und die fortwährende Diskussionsbereitschaft während dieser Zeit. Ich danke Herrn Professor Dr. Rüdiger Hell für seine Rolle als zweiter Gutachter und – zusammen mit Herrn Professor Dr. Marcus Koch – für die Bereitschaft als „thesis-advisory commitee“ zu fungieren.

Weiterhin danke ich Dr. Sergi Puig, meinem Kollaborationspartner für seine Unterstützung in Form von Resultaten und Plasmiden, die den Ablauf dieser Doktorarbeit wesentlich beschleunigt haben. Genauso danke ich Dr. Markus Fauth für seine Plasmide zur Ko-Lokalisierungs-Analyse.

Außderdem möchte ich noch allen gegenwärtigen und ehemaligen Mitarbeitern der AG Krämer danken. Besonders hervorheben möchte ich hier Dr. Mike Haydon der mir *Arabidopsis* Genetik beigebracht hat, sowie Vasantika Singh für ihre unverzichtbare Hilfe bei beiden „microarray“ Analysen. Havva Schäfer danke ich dafür, dass sie ihre Bachelor-Arbeit der hier beschriebenen *cth2-2* Mutante gewidmet hat. Zudem möchte ich Signore Michele Oliva danken für fünf Jahre gemeinsame Arbeit und Dr. Scott Sinclair für freie Unterkunft während der letzten Wochen als Doktorand. Klaus Hagemann danke ich dafür das ich nun endlich gelernt habe richtig mit Photoshop umgehen zu können.

An letzter Stelle möchte ich meinen Eltern Willibert und Monika Reuscher danken für ihre volle Unterstützung während immerhin schon 31 Jahren. Schön das es euch gibt !